

Nebraska Public Power District

Cooper Nuclear Station

# **PLANT UNIQUE ANALYSIS REPORT**

Mark I Containment Program

Revision 0

April, 1982

8205040337

## ABSTRACT

Nebraska Public Power District (NPPD) has completed the reevaluation of the Cooper Nuclear Station (CNS) Mark I containment system. This reevaluation was performed in response to the Nuclear Regulatory Commission's (NRC) requirements for resolving the "Unresolved Safety Issue" designation (pursuant to Section 210 of the Energy Reorganization Act of 1974) as it pertains to CNS. The NRC requirements resulted from the identification of suppression pool hydrodynamic loads not considered in the original boiling water reactor Mark I containment design.

This Plant Unique Analysis Report describes the evaluations performed by NPPD to demonstrate that the plant modifications installed at CNS in response to the NRC requirements are sufficient to restore the original margins of safety for the containment system. This report covers the CNS plant unique suppression pool hydrodynamic load definitions, the structural assessments for these load definitions, and the evaluation of the structural response against the Mark I Program Structural Acceptance Criteria. These evaluations consider the plant configuration after the installation of extensive modifications to upgrade the safety margins of the CNS containment for the newly defined loads.

The results of the plant unique containment evaluations indicate that the modifications installed at CNS are sufficient to satisfy the Mark I Long-Term Program criteria. Completion of these modifications by September 1982 thereby satisfies the requirements of the NRC for restoration of the original margins of safety for the CNS containment system.



## TABLE OF CONTENTS

	<u>Page</u>
Abstract	i
Table of Contents	ii
List of Tables	x
List of Figures	xi
 <u>SECTION 1 INTRODUCTION AND DESIGN CRITERIA</u>	
1.1 INTRODUCTION	1-1
1.1.1 Objective and Scope	1-1
1.1.2 Problem Definition	1-2
1.1.3 Short-Term Program	1-3
1.1.4 Long-Term Program	1-5
1.2 DESIGN CRITERIA	1-6
1.2.1 Design Specifications	1-6
1.2.1.1 Original Specifications	1-6
1.2.1.2 Specifications for Modifications	1-7
1.2.2 LTP Design Requirements	1-7
1.2.2.1 New Design Requirements	1-7
1.2.2.2 Exceptions to Design Requirements	1-9
1.3 CONTAINMENT AND MODIFICATION DESCRIPTION	1-10
1.3.1 General	1-10
1.3.1.1 Drywell	1-10
1.3.1.2 Wetwell	1-11
1.3.1.3 Vent System	1-11
1.3.2 Structural Components	1-12
1.3.2.1 Torus Shell and Supports	1-12
1.3.2.2 Vent System and Supports	1-16
1.3.2.3 Miscellaneous Torus Internals	1-19
1.3.3 Piping Systems	1-20
1.3.3.1 S/AV Discharge Piping	1-20
1.3.3.2 Torus Attached Piping	1-23
1.3.3.3 Torus Internal Piping	1-25

TABLE OF CONTENTS (Continued)

	<u>Page</u>
1.3.4 Miscellaneous System Modifications	1-27
1.3.4.1 Drywell/Wetwell Pressure Differential	1-27
1.3.4.2 S/RV Low-Low Set Relief Logic	1-29
1.3.4.3 Level I MSIV Trip Set Point	1-30
1.3.4.4 Torus Temperature Monitoring System	1-31
1.3.5 Modification Summary	1-32
1.4 SUMMARY OF RESULTS	1-33
1.4.1 Results and Conclusions	1-33
1.4.2 Conformity with Project Requirements	1-33

TABLE OF CONTENTS (Continued)

	<u>Page</u>
<u>SECTION 2 LOADS AND LOAD COMBINATIONS</u>	
2.1 INTRODUCTION	2-1
2.2 PLANT THERMAL-HYDRAULIC PARAMETERS	2-1
2.3 ORIGINAL DESIGN LOADS	2-3
2.4 LOCA-RELATED LOADS	2-4
2.4.1 Containment System Pressure and Temperature Response	2-6
2.4.1.1 Design Basis Accident	2-7
2.4.1.2 Intermediate Break Accident	2-7
2.4.1.3 Small Break Accident	2-7
2.4.2 Vent System Thrust Loads	2-8
2.4.2.1 Analysis Methods and Results	2-8
2.4.2.2 Load Application	2-8
2.4.3 Loads Associated With Pool Swell	2-9
2.4.3.1 Torus Net Vertical Loads	2-10
2.4.3.2 Torus Shell Pressure Histories	2-12
2.4.3.3 Impact, Drag, and Fallback Loads	2-12
2.4.3.4 Froth Impingement and Froth Fallback Loads	2-15
2.4.3.5 LOCA Water Jet-Induced Loads	2-16
2.4.3.6 LOCA Air Bubble-Induced Drag Load	2-17
2.4.3.7 Interference Effects	2-18
2.4.4 Loads Associated with Condensation Oscillation	2-19
2.4.4.1 Torus Shell Loads	2-20
2.4.4.2 Vent System Loads	2-21
2.4.4.3 Downcomer Lateral Loads	2-21
2.4.4.4 Submerged Structure Loads	2-22
2.4.5 Loads Associated with Chugging	2-24
2.4.5.1 Torus Shell Loads	2-25
2.4.5.2 Vent System Loads	2-26
2.4.5.3 Downcomer Lateral Loads	2-27
2.4.5.4 Submerged Structure Loads	2-28

## TABLE OF CONTENTS (Continued)

	<u>Page</u>
2.5 S/RV DISCHARGE-RELATED LOADS	2-29
2.5.1 S/RVDL Clearing Transient Loads	2-31
2.5.2 S/RVDL Reflood Transient	2-34
2.5.3 Thrust Loads on T-Quencher Arms	2-35
2.5.4 Torus Shell Pressures	2-36
2.5.5 Loads on Submerged Structure	2-39
2.5.5.1 T-Quencher Water Jet-Induced Drag Loads	2-40
2.5.5.2 T-Quencher Air Bubble-Induced Drag Loads	2-41
2.5.5.3 T-Quencher Air Bubble Differential Loads	2-42
2.5.5.4 Interference Effects	2-42
2.6 OTHER LOADS	2-42
2.6.1 Other Operating Loads	2-43
2.6.2 Other Secondary Loads	2-43
2.6.3 Steam Discharge Condensation Loads	2-44
2.7 LOAD COMBINATIONS	2-44
2.7.1 Torus Shell	2-45
2.7.2 Vent System	2-45
2.7.3 Internal Structures Above Pool	2-45
2.7.4 Submerged Structures	2-46
2.7.5 S/RVD Piping	2-46
2.7.6 Torus Attached Piping Systems	2-46
2.7.7 Fatigue Design Basis	2-46

## TABLE OF CONTENTS (Continued)

	<u>Page</u>
SECTION 3 <u>TORUS SHELL AND SUPPORTS</u>	
3.1 INTRODUCTION	3-1
3.2 TORUS SHELL	3-1
3.2.1 Design Load Combinations	3-1
3.2.2 Design Allowables	3-2
3.2.2.1 Shell Stress Intensity Allowables	3-2
3.2.2.2 Buckling Allowables	3-2
3.2.3 Analysis Methods and Results	3-4
3.2.3.1 Torus Mathematical Models	3-4
3.2.3.2 Analysis Procedures and Results	3-6
3.2.4 Code Evaluation	3-12
3.2.4.1 Shell Stress Intensities	3-12
3.2.4.2 Fatigue Evaluation	3-13
3.3 TORUS SUPPORT SYSTEM	3-13
3.3.1 Design Load Combinations	3-13
3.3.2 Design Allowables	3-14
3.3.2.1 Support Columns	3-14
3.3.2.2 Anchorage Assembly	3-14
3.3.2.3 Seismic Ties	3-15
3.3.2.4 Ring Girder Saddle	3-15
3.3.3 Analysis Methods and Results	3-15
3.3.3.1 Column and Anchorage Evaluation	3-15
3.3.3.2 Seismic Tie Evaluation	3-17
3.3.3.3 Ring Girder Saddle Evaluation	3-18
3.3.3.4 Nonlinear Support Assessment	3-20
3.3.4 Code Evaluation	3-20
3.3.4.1 Column and Anchorage	3-20
3.3.4.2 Seismic Ties	3-21
3.3.4.3 Ring Girder Saddle	3-21
3.3.4.4 Fatigue Evaluation	3-21

TABLE OF CONTENTS (Continued)

	<u>Page</u>
3.4 RING GIRDER	3-21
3.4.1 Design Load Combinations	3-22
3.4.2 Design Allowables	3-22
3.4.2.1 Ring Girder Web and Flange	3-22
3.4.2.2 Ring Girder-to-Shell Weld	3-22
3.4.3 Analysis Methods and Results	3-23
3.4.3.1 Ring Girder In-Plane Loading	3-23
3.4.3.2 Ring Girder Lateral Loading	3-23
3.4.3.3 Ring Girder Attachments	3-24
3.4.4 Code Evaluation	3-25
3.4.4.1 Ring Girder Web and Flange	3-25
3.4.4.2 Ring Girder-to-Shell Weld	3-25
3.4.4.3 Fatigue Evaluation	3-25
3.5 TORUS SHELL PENETRATIONS AND ATTACHMENTS	
3.5.1 Design Load Combinations	3-26
3.5.2 Design Allowables	3-26
3.5.3 Analysis Methods and Results	3-26
3.5.3.1 Torus Attached Piping Penetrations	3-27
3.5.3.2 Monorail Supports	3-27
3.5.3.3 ECCS Piping Supports	3-27
3.5.4 Code Evaluation	3-28
3.5.4.1 Torus Attached Piping Penetrations	3-29
3.5.4.2 Torus Shell Stress Intensities at Attachments	3-29
3.5.4.3 Fatigue Evaluation	3-29

TABLE OF CONTENTS (Continued)

	<u>Page</u>
<u>SECTION 4 VENT SYSTEM AND SUPPORTS</u>	
4.1 INTRODUCTION	4-1
4.2 VENT HEADER AND MAIN VENT	4-1
4.2.1 Design Load Combinations	4-1
4.2.2 Design Allowables	4-2
4.2.2.1 Vent Header and Main Vent	4-2
4.2.2.2 Vent Header and Main Vent Penetrations	4-2
4.2.2.3 Drywell Penetration	4-3
4.2.2.4 Main Vent Bellows	4-3
4.2.3 Analysis Methods and Results	4-3
4.2.3.1 Vent System Mathematical Models	4-4
4.2.3.2 Vent Header and Main Vent	4-7
4.2.3.3 Vent Header and Main Vent Penetrations	4-16
4.2.3.4 Drywell Penetration	4-17
4.2.3.5 Main Vent Bellows	4-18
4.2.4 Code Evaluation	4-18
4.2.4.1 Main Vent	4-19
4.2.4.2 Vent Header	4-19
4.2.4.3 Main Vent/Vent Header Intersection	4-20
4.2.4.4 Vent Header and Main Vent Penetrations	4-21
4.2.4.5 Drywell Penetration	4-22
4.2.4.6 Main Vent Bellows	4-22
4.2.4.7 Shell Buckling Assessment	4-22
4.2.4.8 Fatigue Evaluation	4-23
4.3 DOWNCOMERS AND TIEBARS	4-24
4.3.1 Design Load Combinations	4-25
4.3.2 Design Allowables	4-25
4.3.2.1 Downcomer/Vent Header Intersection	4-25
4.3.2.2 Downcomers	4-25
4.3.2.3 Downcomer Tiebar	4-26
4.3.3 Analysis Methods and Results	4-26
4.3.3.1 Downcomer/Vent Header Intersection	4-26
4.3.3.2 Downcomers	4-29
4.3.3.3 Downcomer Tiebar	4-31



TABLE OF CONTENTS (Continued)

	<u>Page</u>
4.3.4 Code Evaluation	4-32
4.3.4.1 Downcomer/Vent Header Intersection	4-32
4.3.4.2 Downcomers	4-32
4.3.4.3 Downcomer Tiebar	4-32
4.3.4.4 Fatigue Evaluation	4-33
4.4 VENT DRAIN LINE	4-33
4.4.1 Design Load Combinations	4-34
4.4.2 Design Allowables	4-34
4.4.3 Analysis Methods and Results	4-34
4.4.4 Code Evaluation	4-34
4.5 VENT HEADER DEFLECTOR	4-35
4.5.1 Design Load Combinations	4-35
4.5.2 Design Allowables	4-35
4.5.3 Analysis Methods and Results	4-35
4.5.4 Code Evaluation	4-35
4.6 VENT HEADER SUPPORT SYSTEM	4-36
4.6.1 Design Load Combinations	4-36
4.6.2 Design Allowables	4-36
4.6.3 Analysis Methods and Results	4-36
4.6.4 Code Evaluation	4-36

TABLE OF CONTENTS (Continued)

	<u>Page</u>
SECTION 5 <u>S/RV DISCHARGE PIPING</u>	
5.1 INTRODUCTION	5-1
5.2 DRYWELL S/RVD PIPING	5-1
5.2.1 Design Load Combinations	5-1
5.2.2 Design Allowables	5-2
5.2.2.1 Piping Stress Allowables	5-2
5.2.2.2 Support Allowables	5-2
5.2.3 Analysis Methods and Results	5-3
5.2.3.1 S/RVD Piping Models	5-3
5.2.3.2 Piping Analysis Procedures and Results	5-4
5.2.3.3 Drywell Piping Support Evaluation	5-7
5.2.4 Code Evaluation	5-10
5.2.4.1 S/RV Back Pressure	5-10
5.2.4.2 S/RVD Piping	5-11
5.2.4.3 Drywell Pipe Supports	5-11
5.2.4.4 Drywell Liner	5-12
5.2.4.5 Drywell Steel Framing	5-12
5.3 WETWELL S/RVD PIPING	5-13
5.3.1 Design Load Combinations	5-14
5.3.2 Design Allowables	5-14
5.3.2.1 Piping Stress Allowables	5-14
5.3.2.2 Support Allowables	5-14
5.3.2.3 Fatigue Considerations	5-15
5.3.3 Analysis Methods and Results	5-15
5.3.3.1 S/RVD Piping Models	5-15
5.3.3.2 Piping Analysis Procedures and Results	5-16
5.3.3.3 T-Quencher Evaluation	5-22
5.3.3.4 Wetwell Piping Support Evaluation	5-23
5.3.4 Code Evaluation	5-25
5.3.4.1 S/RVD Piping	5-25
5.3.4.2 T-Quencher Assembly	5-25
5.3.4.3 Wetwell Pipe Supports	5-25
5.3.4.4 T-Quencher Supports	5-25
5.4 S/RVDL VACUUM REAKERS	5-26
5.4.1 Design Criteria	5-26
5.4.2 Analysis Methods and Results	5-26

TABLE OF CONTENTS (Continued)

	<u>Page</u>
<u>SECTION 6 TORUS ATTACHEL PIPING AND TORUS INTERNAL STRUCTURES</u>	
6.1 INTRODUCTION	6-1
6.2 PIPING SYSTEMS EXTERNAL TO TORUS	6-1
6.2.1 Design Load Combinations	6-2
6.2.2 Design Allowables	6-2
6.2.2.1 Piping Stress Allowables	6-2
6.2.2.2 Support Allowables	6-4
6.2.2.3 Fatigue Considerations	6-4
6.2.3 Analysis Methods and Results	6-5
6.2.3.1 Piping Models	6-5
6.2.3.2 Coupling of Torus and Piping System	6-7
6.2.3.3 Analysis Procedures and Results	6-9
6.2.3.4 External Piping Support Evaluation	6-12
6.2.3.5 Branch Line Evaluations	6-13
6.2.3.6 Torus Attached Piping Valve Evaluations	6-14
6.2.3.7 ECCS Pump and Turbine End Load Evaluations	6-15
6.2.4 Code Evaluation	6-16
6.2.4.1 External Piping	6-16
6.2.4.2 External Piping Supports	6-16
6.2.4.3 Branch Lines	6-17
6.2.4.4 Torus Attached Piping Valves	6-17
6.2.4.5 ECCS Pumps and Turbines	6-17
6.3 PIPING SYSTEMS INTERNAL TO TORUS	6-17
6.3.1 Design Load Combinations	6-18
6.3.2 Design Allowables	6-18
6.3.2.1 Piping Stress Allowables	6-18
6.3.2.2 Support Allowables	6-19
6.3.2.3 Fatigue Considerations	6-19
6.3.3 Analysis Methods and Results	6-19
6.3.3.1 Piping Models	6-19
6.3.3.2 Analysis Procedures and Results	6-20
6.3.3.3 Internal Piping Support Evaluation	6-24

TABLE OF CONTENTS (Continued)

	<u>Page</u>
6.3.4 Code Evaluation	6-25
6.3.4.1 Internal Piping	6-25
6.3.4.2 Internal Piping Supports	6-26
6.4 TORUS INTERNAL STRUCTURES	6-26
6.4.1 Design Load Combinations	6-26
6.4.1.1 Platform System	6-27
6.4.1.2 Monorail Beam	6-27
6.4.2 Design Allowables	6-27
6.4.3 Analysis Methods and Results	6-28
6.4.3.1 Platform System	6-28
6.4.3.2 Monorail Beam	6-29
6.4.4 Code Evaluation	6-29
6.4.4.1 Platform System	6-29
6.4.4.2 Monorail Beam	6-30

TABLE OF CONTENTS (Continued)

	<u>Page</u>
SECTION 7 <u>POOL TEMPERATURE EVALUATION</u>	
7.1 INTRODUCTION	7-1
7.2 DESIGN TRANSIENTS AND INITIAL CONDITIONS	7-1
7.3 MODEL DESCRIPTION	7-3
7.3.1 Coupled Reactor and Suppression Pool Model	7-3
7.3.2 Local Pool Temperature Model	7-3
7.4 POOL TEMPERATURE EVALUATION RESULTS	7-4
7.5 POOL TEMPERATURE MONITORING SYSTEM	7-5

TABLE OF CONTENTS (Continued)

Page

Section 8 APPENDICES AND REFERENCES

APPENDICES

Appendix A:	Adaptation of the SRSS Method for Combined Torus Shell Pressures Following Multiple S/RV Actuations	A-1
Appendix B:	Descriptions of Major Computer Programs	B-1
Appendix C:	Modeling of Fluid-Structure Interaction Effects Using EDS-SNAP	C-1
Appendix D:	Combination of Dynamic Structural Responses	D-1

REFERENCES

R-1

LIST OF TABLES

<u>TABLE NO.</u>	<u>TITLE</u>
1.1	S/RVD Lines in the Drywell - Summary of Support Modifications/Additions
1.2	Torus Pipe Penetrations
1.3	Summary of Pipe Support Modifications for Torus Attached (External) Piping
1.4	Torus Internal Piping Systems
1.5	Proposed Low-Low Set Safety/Relief Valve System
1.6	S/RV Load Case Analysis Results
1.7	MSIV Water Level Trip
2.1	Containment Hydrodynamic Data
2.2	Safety/Relief Valve System
2.3	Plant Conditions at Instant of DBA Pipe Break
2.4	Plant Conditions at Instant of IBA/SBA Pipe Break
2.5	Structures Subjected to Pool Swell Impact, Drag, and Fallback Loads
2.6	Structures Subjected to Froth Impingement and Froth Fallback Loads
2.7	Structures Subjected to LOCA Water Jet-Induced Drag Loads
2.8	Structures Subjected to Submerged Structure Drag Loads and Interference Factors
2.9	Condensation Oscillation Baseline Rigid Wall Pressure Amplitudes on Torus Shell Bottom Dead Center
2.10	Condensation Oscillation Onset and Duration
2.11	Vent System Load Amplitudes and Frequencies for Condensation Oscillation
2.12	Vent System Downcomer Lateral Load Due to Condensation Oscillation
2.13	Chugging Onset and Duration
2.14	Post-Chug Rigid Wall Pressure Amplitudes on Torus Shell Bottom Dead Center
2.15	Vent System Load Amplitudes and Frequencies for Chugging
2.16	Distribution of Downcomer Lateral Load Reversals Due to Chugging



LIST OF TABLES (Continued)

<u>TABLE NO.</u>	<u>TITLE</u>
2.17	Structures Subjected to T-Quencher Water Jet Loads
2.18	Fatigue Design Basis Including DBA Event
2.19	Fatigue Design Basis Including IBA/SBA Event
3.1	Design Load Combinations and Service Limits for Class MC Components and Internal Structures
3.2	Bounding Load Combinations for Torus Shell Evaluations
3.3	Allowable Stress Intensities for the Torus Shell
3.4	Bounding Load Combinations for Torus Support Column Evaluations
3.5	Bounding Load Combinations for Torus Saddle Evaluations
3.6	Bounding Load Combinations for Ring Girder Evaluation
3.7	Bounding Load Combinations for Torus Shell Penetrations and Attachments
3.8	Local Stress Intensities of Torus Attached Piping Penetrations
4.1	Design Load Combinations and Corresponding Service Level Limits for the Vent Header and Main Vent
4.2	Allowable Stress Intensities for Vent System Class MC Components
4.3	Vent System Design Temperatures
4.4	Frequencies and Mode Shapes of 1/16 Vent System Model
4.5	Modified Downcomer Sway Mode Frequencies Accounting for Gusset Reinforcement
4.6	Maximum Compressive Membrane Stresses in Vent System Components due to Pool Swell Loads
4.7	Vent System Downcomer Lateral Load due to Condensation Oscillation
4.8	S/RV Discharge-Related Drag Loads on Vent System Components
4.9	Equivalent Static Loads on Downcomers due to S/RV Discharge Bubble Drag
4.10	Bounding Load Combinations and Corresponding Service Level Limits for Downcomers and Tiebars
4.11	Design Stress Allowables for Downcomer Tiebars

LIST OF TABLES (Continued)

<u>TABLE NO.</u>	<u>TITLE</u>
4.12	Maximum Stresses at the Downcomer/Vent Header Intersection for Unit Load Analyses
4.13	Summary of Downcomer Lateral Loads
4.14	Condensation Oscillation Pressure Amplitudes in the Downcomers
4.15	Stress Intensity Allowable for Design Load Combinations for Main Vent Drain Line
4.16	Stress Intensity Allowables for the Vent Header Deflector
4.17	Design Loads and Load Combinations for Vent System Support Columns
5.1	Event Combinations and Service Levels for Class 2 and 3 Piping
5.2	Bounding Load Case Combinations for S/RVD Lines in the Drywell
5.3	S/RV Discharge Piping Stress Allowables
5.4	Maximum Pipe Stresses Due to S/RVD Thrust Loading in Drywell Routing of S/RVDs
5.5	S/RVDs in the Drywell - Maximum Stress as a Percentage of Allowable for Bounding Load Combination
5.6	Results of Code Evaluation - Maximum Interaction Ratios
5.7	Bounding Load Combination for S/RVD Lines in the Wetwell
5.8	Representative Maximum Pipe Stress for the Wetwell Routing of the S/RVD Lines
6.1	Bounding Load Case Combinations for Torus Attached External Piping
6.2	Torus Attached Piping Stress Allowables
6.3	Torus Pipe Penetrations and Associated Analysis Models for External Piping

LIST OF TABLES (Continued)

<u>TABLE NO.</u>	<u>TITLE</u>
6.4	Large Bore Torus Attached External Piping - Representative Maximum Stresses
6.5	Scale Factors to be Used on Coupled S/RV Responses to Obtain all S/RV Load Cases
6.6	Large Bore Torus Attached External Piping - Maximum Stress as a Percentage of Allowables for Bounding Load Combinations
6.7	Bounding Load Combination for Torus Attached Internal Piping
6.8	Torus Pipe Penetrations and Associated Analysis Models for Internal Piping
6.9	Design Load Cases for Platform Support Columns
7.1	Summary of Results Cooper Pool Temperature Response
7.2	Environmental Requirements for Devices to be Mounted in Harsh Environments
A.1	Summary of Peak Pressure Comparison
D.1	Non-Exceedance Probabilities

## LIST OF FIGURES

<u>FIGURE NO.</u>	<u>TITLE</u>
1.1	Cross Section - Composite Plant Layout
1.2	Cross Section - Wetwell
1.3	Torus Support Column
1.4	Torus Saddle
1.5	Section - Vent System
1.6	Partial Plan - Vent System
1.7	Elevation - Downcomer Reinforcement
1.8	Section - Vent Header Deflector
1.9	Vent Header Support Columns
1.10	Drywell/Wetwell Vacuum Breaker Reinforcement
1.11	Plan - Service Platform
1.12	Elevation - Service Platform
1.13	Cross Section - Service Platform
1.14	Wetwell Routing of S/RVDLs
1.15	T-Quencher Support Structure
1.16	Elevation - RHR Pump Test Return Line Modification
1.17	HPCI Turbine Exhaust Line - Reroute and Resupport
1.18	RCIC Turbine Exhaust Line - Reroute and Resupport
1.19	Core Spray Pump Test Return Line Truncation
2.1	DBA Containment Pressure Response
2.2	DBA Containment Temperature Response
2.3	IBA Containment Pressure Response
2.4	IBA Containment Temperature Response
2.5	SBA Containment Pressure Response
2.6	SBA Containment Temperature Response
2.7	Vent System Load Application
2.8	Single Main Vent Forces (0-30 sec), Zero $\Delta P$
2.9	Vent Header Forces per Miter Bend (0-30 sec), Zero $\Delta P$
2.10	Single Downcomer Forces (0-30 sec), Zero $\Delta P$
2.11	Total and Net Vertical Forces (0-30 sec), Zero $\Delta P$
2.12	Net Torus Vertical Load, (Zero $\Delta P$ )
2.13	Corrected Torus Net Vertical Loads (NRC), Zero $\Delta P$
2.14	Corrected Average Submerged Pressure due to Pool Swell (NRC), Zero $\Delta P$

LIST OF FIGURES (Continued)

<u>FIGURE NO.</u>	<u>TITLE</u>
2.15	Corrected Torus Airspace Pressure due to Pool Swell (NRC), Zero $\Delta P$
2.16	Location of Impact/Drag Pressure Transients on Vent Header
2.17	Pool Swell Impact/Drag Load Transients on Main Vent, $\Delta P=1.0$ psid
2.18	Vent Header Deflector Loads
2.19	Definition of Froth Impingement Regions
2.20	Definition of Froth Load Applications and Transients
2.21	Torus Pressure Amplitude Distribution for Condensation Oscillation
2.22	Torus Asymmetric Circumferential Distribution for Pre-Chug Pressure Amplitude
2.23	Sectors Used to Define Directions of Lateral Loads on Downcomer End
2.24	Typical Torus Shell S/RV Pressure Time History
2.25	Torus Shell Load Combinations for LOCA-DBA
2.26	Torus Shell Load Combinations for LOCA-IBA
2.27	Torus Shell Load Combinations for LOCA-SBA
2.28	Vent System Load Combinations for LOCA-DBA
2.29	Vent System Load Combinations for LOCA-IBA
2.30	Vent System Load Combinations for LOCA-SBA
2.31	Load Combinations for Structures Above HWL for LOCA-DBA
2.32	Submerged Structures Load Combinations for LOCA-DBA
2.33	Submerged Structures Load Combinations for LOCA-IBA
2.34	Submerged Structures Load Combinations for LOCA-SBA
2.35	S/RV Discharge Loads on Submerged Structures
3.1	1/32 Section Torus Model
3.2	90° Section Torus Model
3.3	1/32 Section Torus Model with Detailed Ring Girder Saddle
3.4	Load Combinations Used in Saddle Evaluation

LIST OF FIGURES (Continued)

<u>FIGURE NO.</u>	<u>TITLE</u>
4.1	1/16th Finite Element Shell Model of Vent System
4.2	180° Vent System Beam Model
4.3	Vent System Pressurization Following a DBA
4.4	Vertical Thrust Load Transient on Main Vent End Cap ( $\Delta P = 0.0$ )
4.5	Sequence and Duration of Pool Swell Load
4.6	Vertical Displacement Time History at Main Vent S/RVDL Penetration
4.7	Vertical Acceleration Response Spectrum at the Vacuum Breaker Penetration
4.8	Possible Configurations of Downcomer Pressure Differential for Condensation Oscillation Downcomer Lateral Load
4.9	Chug Synchronization Loads
4.10	Development of Scale Factors Chug Synchronization Load
4.11	Typical S/RV Discharge Drag Load Transient for Submerged Downcomer Segment
4.12	Downcomer/Vent Header Gusset Reinforcement Design
4.13	Detailed Downcomer/Vent Header Intersection Model Including Gusset Plate Stiffeners
5.1	Representative Drywell S/RVD Line Model (Line 71G) Before and After Modifications
5.2	S/RVD Line Models (Wetwell Routing)
A.1	Suppression Pool Geometry and S/RV Discharge Lines
A.2	Typical Pressure Wave
A.3	Sequence of S/RV Discharge Events
A.4	Probability Density Distribution for the Reactor Pressure Rise Rate
A.5	Frequency Distribution of Combined Peak Pressure Ratios - 8 MVA
D.1	Illustration of CDF Computation
D.2	Typical CDF for Mark I Data



## LIST OF ABBREVIATIONS

ABSS	Absolute Sum
ADS	Automatic Depressurization System
AISC	American Institute of Steel Construction
ASME	American Society of Mechanical Engineers
BWR	Boiling Water Reactor
CDF	Cumulative Distribution Function
CNS	Cooper Nuclear Station
CO	Condensation Oscillation
CVA	Consecutive Valve Actuation
DBA	Design Basis Accident
DLF	Dynamic Load Factor
DOF	Degree of Freedom
ECCS	Emergency Core Coolant System
EPRI	Electric Power Research Institute
FSAR	Final Safety Analysis Report
FSI	Fluid Structure Interaction
FSTF	Full Scale Test Facility
GE	General Electric
HPCI	High Pressure Coolant Injection
HWL	High Water Level
Hz	Hertz
IBA	Intermediate Break Accident
Kip	Kilopound
Ksi	Kilopound Per Square Inch
Lbf	Pound Force
LDR	Load Definition Report
LOCA	Loss of Coolant Accident
LOOSP	Loss of Off-Site Power
LTP	Long-Term Program
MSIV	Main Steam Isolation Valves
MSL	Main Steam Lines
MVA	Multiple Valve Actuation
MWe	Megawatt Electric
MWt	Megawatt Thermal



LIST OF ABBREVIATIONS (Continued)

NEP	Non-Exceedence probability
NOC	Normal Operating Conditions
NPPD	Nebraska Public Power District
NPSH	Net Positive Suction Head
NRC	Nuclear Regulatory Commission
OBE	Operating Basis Earthquake
PAS	Pump Around System
Psi	Pounds Per Square Inch
Psia	Pounds Per Square Inch (Absolute)
Psid	Pounds Per Square Inch (Differential)
Psig	Pounds Per Square Inch (Gauge)
PSTF	Pressure Suppression Test Facility
PUAAG	Plant Unique Analysis Application Guide
PULD	Plant Unique Load Definitions
QSTF	Quarter Scale Test Facility
RCIC	Reactor Core Isolation Cooling
RHR	Residual Heat Removal
RPV	Reactor Pressure Vessel
SBA	Small Break Accident
SER	Safety Evaluation Report
SORV	Stuck-Open Relief Valve
SRSS	Square Root of the Sum of the Squares
S/RV	Safety/Relief Valve
S/RVD	Safety/Relief Valve Discharge
S/RVDL	Safety/Relief Valve Discharge Line
SSE	Safe Shutdown Earthquake
STP	Short-Term Program
SVA	Single Value Actuation
TAP	Torus Attached Piping
WRC	Welding Research Council

COOPER NUCLEAR STATION

PLANT UNIQUE ANALYSIS REPORT

SECTION 1

INTRODUCTION AND DESIGN CRITERIA

## 1.1 INTRODUCTION

### 1.1.1 Objective and Scope

The objective of the Plant Unique Analysis Report (PUAR) is to document compliance with Mark I Containment Program requirements for the Cooper Nuclear Station (CNS) containment system and associated piping. These requirements involve demonstration that the originally intended design safety margins are restored for hydrodynamic loads which were not explicitly included in the original design. This reassessment was made using conservative load definitions, analysis methodologies, and structural acceptance criteria that are both consistent with applicable codes and standards and appropriate for the life of the facility.

Submittal of this report is Nebraska Public Power District's (NPPD) response to the Nuclear Regulatory Commission's (NRC) letters transmitted in February and April 1975 (References 1 and 2) relating to hydrodynamic loadings associated with Safety/Relief Valve (S/RV) discharges and the Loss of Coolant Accident (LOCA) events. The report also satisfies the NPPD's commitment to the Commission as a member of the Mark I Owners Group. Review and approval of this report will eliminate the "Unresolved Safety Issue" designation (pursuant to Section 210 of the Energy Reorganization Act of 1974) assigned to this program as it pertains to CNS.

The report consists of eight major sections:

Section 1 includes the design criteria, the containment description (including recent modifications), and a summary of the requalification results;

Section 2 includes thermal-hydraulic parameters, original design loads, LOCA and S/RV discharge-related load definitions, and load combinations for the major containment system components;

Sections 3 through 6 describe the design load combinations, allowable stresses, analysis methods and results, and ASME Boiler and Pressure Vessel Code evaluations for the torus shell and supports, vent system, S/RV discharge piping, torus attached piping, and torus internal structures;

Section 7 discusses the suppression pool temperature evaluation;

Section 8 includes references and appendices.

The PUAR summarizes more than five years of complex analysis and design work using state-of-the-art analytical tools and techniques. Thousands of manhours were expended in response to NRC concerns with containment integrity. The primary objective was to enhance the performance of the pressure suppression system and improve design safety margins through component modifications or the addition of new systems.

#### 1.1.2 Problem Definition

The original design of the CNS Mark I containment system considered postulated accident loads previously associated with a LOCA, seismic loads, dead loads, jet-impingement loads, hydrostatic loads due to water in the suppression chamber (torus), overload pressure test loads, and construction loads. However, since the establishment of the original design criteria, additional loading conditions associated with the pressure-suppression concept utilized in the Mark I containment system design have been identified. These additional loads result from dynamic effects of drywell air and steam being rapidly forced into the suppression pool during a postulated LOCA and from suppression pool response to S/RV operation associated with plant transient operating conditions. Because these hydrodynamic loads were not explicitly considered in the original design of the containment system, NPPD received NRC requests in early 1975 that these loads be quantified and an assessment be performed of the

effects of these loads on the Cooper Station containment components.

Recognizing that these evaluation efforts would be similar for all Mark I Boiling Water Reactor (BWR) plants, NPPD joined an ad hoc Mark I Owners Group with General Electric (GE) as the lead technical organization. The objectives of the Owners Group were to determine the magnitude and significance of these dynamic loads and to identify courses of action needed to resolve outstanding safety concerns. The Mark I Owners Group divided this task into two programs: a Short-Term Program (STP) for early assessment of critical components and a Long-Term Program (LTP) for final resolution of the issues.

#### 1.1.3 Short-Term Program

The objectives of the Short-Term Program were to verify that the CNS Mark I containment system would maintain its integrity and functional capability when subjected to the most probable loads induced by a postulated design-basis LOCA and to verify that continued plant operation was not inimical to the health and safety of the public. The STP justified interim plant operation while further tests and evaluations were conducted during the comprehensive LTP.

The STP evolved into two areas of investigation: (1) an evaluation of loads on structures within the torus, and (2) an evaluation of the integrated loads on the torus structure which are transmitted to its supports. The loads on the structures within the torus were based on impact data developed from Mark III containment tests conducted at the GE Pressure Suppression Test Facility (PSTF) coupled with pool swell velocity data derived from scaled Mark I test facilities. The loads on the torus structure and its external supports were based on series of tests performed in a 1/12-scale facility representing a segment of a typical Mark I torus.

The STP task of evaluating the integrity of the torus internal structures for Mark I BWR facilities is documented in a five volume report which was submitted to the NRC in September 1975 (Reference 3). On December 2, 1975, GE submitted Addendum 1 (Reference 4) to this report, which addressed potential pool swell impact on S/RV discharge piping and the vent system bellows assembly within the torus. Additional information was provided in response to NRC questions on the STP Final Report. These responses were compiled in a letter to the NRC dated September 9, 1976 (Reference 5) which was submitted by GE on behalf of the Mark I Owners Group.

During the STP review, structural safety margins were increased by implementation of procedures to maintain a differential pressure of at least one pound per square inch between the drywell and the torus during reactor operation. These procedures currently remain in effect. In addition, during the course of the STP review, NPPD performed modifications to the containment support system to provide additional design safety margins.

As a result of differences in the design of the torus support systems at Mark I BWR facilities and due to the sensitivity of the predicted structural response of the torus support system to variations in applied loads, the NRC required that NPPD perform a plant unique analysis of the torus support system and piping attached to the torus. In April 1976, GE submitted a summary of the actions being taken by the Mark I Owners Group to complete the STP evaluations, including a description of the program for the plant unique analyses of the torus support system and external torus attached piping (Reference 6). Subsequently, this report and its associated acceptance criteria were revised to incorporate the results of discussions held in several meetings between the Mark I Owners Group and the NRC staff. As revised, the plant unique analysis Structural Acceptance Criteria require a factor of safety against failure of two for each component of the torus support and piping systems.



The STP analysis work and evaluations were performed in mid-1976, using loads and methodology defined in Addendum 2 (Reference 7) and Addendum 3 (Reference 8) to the STP Final Report. The STP report was submitted to the NRC in July 1976 (Reference 9). The staff concluded that a sufficient margin of safety had been demonstrated to assure the functional performance of the containment system and, therefore, any undue risk to the health and safety of the public was precluded (Reference 10). Subsequently, the staff granted NPPD exemptions relating to the design margin requirements of 10 CFR 50.55(a). These exemptions were granted for an interim period while the more comprehensive LTP was being conducted and modifications to the containment and piping systems were completed.

#### 1.1.4 Long-Term Program

The Long-Term Program activities were initiated in June 1976. The objectives of the LTP were to establish design basis loads that are appropriate for the life of each Mark I BWR facility and to restore the originally intended design safety margins for each Mark I containment system. These objectives were satisfied through extensive testing and analytical programs that led to the development of generic methods for the definition of suppression pool hydrodynamic loading events and the associated structural assessment techniques. The program also included establishment of structural acceptance criteria and evaluations of both load mitigation devices and system modifications to improve margins of safety.

The generic aspects of the LTP were completed with submittal of Revision 0 of the Load Definition Report (LDR) by GE in December 1978 (partial) and in March 1979. In July 1979, the structural acceptance criteria and plant unique analysis applications guidelines were submitted to the NRC for review. The staff reviewed the experimental and analytical programs, assessment procedures, and acceptance criteria. The NRC documented their



findings and modifications to this material in the Safety Evaluation Report (SER) for the LTP (Reference 11). With very few exceptions, the requirements resulting from the staff evaluation were used to perform the plant unique reassessment of the CNS containment and piping systems and to design plant modifications which satisfy all LTP criteria.

## 1.2 DESIGN CRITERIA

This subsection reviews the design criteria established for the Mark I containment LTP and used in the CNS structural reevaluation. Deviations from these criteria are also summarized in this subsection.

### 1.2.1. Design Specifications

#### 1.2.1.1 Original Specifications

The original design of the drywell, wetwell, and vent system was performed in accordance with the ASME Boiler and Pressure Vessel Code, Section III (Reference 12). The original code of record included the latest addenda as of June 1967 and included Code Cases 1330-1 and 1177-5.

Piping systems were designed using USAS B31.1 (1967) and USAS B31.7 (Feb. 1968) Power Piping Codes (References 13 and 14). As-built verification of these piping systems as required by IE bulletins 79-02 and 79-14 was considered separate from any Mark I program design criteria. Completion of the 79-02 and 79-14 programs on the torus attached piping systems preceded the reanalysis and modification of these systems for LTP requirements. Original design requirements for pipe supports and other structural members were obtained from the AISC Code (Reference 15).

Design information regarding containment and ECCS performance was obtained from the CNS Final Safety Analysis Report (FSAR)

(Reference 16). Technical Specification requirements through Amendment 77 were used in the containment evaluations. Changes to CNS Technical Specifications either resulting from the Mark I LTP studies or occurring simultaneously with the studies were factored into the design basis.

#### 1.2.1.2 Specifications for Modifications

Modifications to containment components and supports were designed, fabricated, and installed in accordance with the requirements of the ASME Boiler and Pressure Vessel Code, Section III (including Summer 1977 Addenda). Modifications involving new structural components (including new pipe support installations) were also designed, fabricated and installed to these requirements.

Modifications to existing structural components were designed, fabricated and installed to the requirements of the original code of record. This code of record was typically the latest edition of the AISC Code.

#### 1.2.2 LTP Design Requirements

Design criteria for the Mark I Long-Term Program include both the definition of the newly-identified hydrodynamic loads and the code evaluation requirements for containment components. These criteria are summarized in this subsection. Any alternative approaches or interpretations of these criteria used in the CNS reevaluations are summarized in this subsection.

##### 1.2.2.1 New Design Requirements

The load definition procedures for suppression pool hydrodynamic loads used in the CNS containment reevaluations were taken from the Load Definition Report (LDR), Revision 2, November 1981 (Reference 17). In cases where the NRC concluded that the LDR procedures were unacceptable, the requirements of the NRC

Acceptance Criteria (Reference 18) were followed. This acceptance criteria is provided as an appendix to the Safety Evaluation Report (NUREG-0661) which provides the bases for these requirements. The NRC Acceptance Criteria used in the CNS containment reevaluations was Revision 1, dated February 1980. These revisions of the SER and Acceptance Criteria did not address the final downcomer lateral load definition for condensation oscillation (CO) nor did they address the final Full Scale Test Facility (FSTF) tests for CO. The CNS reevaluations used design loads developed by the Mark I program in response to NRC concerns as referenced in this report. This approach anticipates NRC acceptance of these load definitions in the final revision of the SER to be issued by the NRC at a later date.

These criteria address only those events or event combinations which involve suppression pool hydrodynamic loads. Other loads in the event combinations were reviewed and approved by the NRC in the FSAR for CNS. However, these loads are discussed in the SER because improved analysis techniques have evolved since the time the FSAR was reviewed. Unless otherwise specified, any loading condition or structural analysis technique not addressed in the SER are defined in accordance with the approved FSAR for CNS.

The structural and mechanical acceptance criteria and the general analysis techniques were obtained from the Mark I LTP Structural Acceptance Criteria Plant Unique Analysis Application Guide (PUAAG) (Reference 19). The PUAAG was also reviewed by the NRC and accepted for use without modification in plant unique analyses. The ASME Boiler and Pressure Vessel Code, Division 1, Section III, including Summer 1977 Addenda is generally used in demonstrating the margins of safety required for steel structures and piping. This criteria is referred to as "the Code" throughout this report.

#### 1.2.2.2 Exceptions to Design Requirements

In several cases, direct application of the LTP design requirements resulted in unusual hardship without a compensating increase in plant safety margins. Alternate analytical approaches or interpretations were used in these cases. These approaches have already been identified to the NRC in Reference 20. These approaches are summarized again below.

- (1) In the analyses of structures for CO loads, the 50 individual load harmonics were combined using a realistic phasing technique. This phasing procedure has already been justified through both analytical and empirical studies, and in combination with other conservatisms in the CO analysis procedure, still produces a conservative design basis for evaluating containment components. (Subsection 3.2.3.2.4)
- (2) In the calculation of torus shell pressure loads due to multiple S/RV actuations, a modified SRSS technique using a 1.2 multiplier has been used instead of the absolute sum combination method. Plant unique statistical studies show that the modified SRSS method bounds peak pressures with an appropriate confidence level (Appendix A).
- (3) For piping analyses, dynamic responses due to S/RV discharge and LOCA loads were combined by a modified SRSS method with a multiplier of 1.1 on the SRSS of the response of the two loads. This approach is an extension of the CDF procedure allowed by the Structural Acceptance Criteria and is supported by further statistical studies (Appendix D).
- (4) ASME code allowables for shell buckling were not used in the evaluation of the torus shell. Generic analyses performed in the Mark I program have demonstrated that

torus buckling will not occur as a result of LOCA and S/RV discharge dynamic loads. Since the CNS torus shell geometry has a lower diameter/thickness ratio than the torus shell considered in the generic study, the results of this study can be conservatively applied to the CNS configuration. This approach is in accordance with the intention of the ASME code (Subsection 3.2.2.2).

- (5) The LDR procedure for defining torus shell pressure loads following an S/RV actuation assumes that pure air mass is in the S/RVDL prior to the valve opening. For S/RV discharge load cases involving ADS actuation during an IBA/SBA event, torus shell pressure loads were defined using an initial 30% relative humidity in the S/RVDL (Subsection 2.5.4).

The appropriate subsections of this report where further description and justification for each approach can be found are shown above in parentheses following each approach.

### 1.3 CONTAINMENT AND MODIFICATION DESCRIPTION

#### 1.3.1 General

Cooper Nuclear Station is a BWR 4 Mark I operating power plant owned by NPPD. It was built in the early 1970's, has a net generating capacity of 778 MWe. CNS has been in operation since July 1974. The primary containment components are the drywell, wetwell, and an interconnecting vent system which are typical of a GE Mark I BWR containment design. A composite of the containment system is shown in Figure 1.1.

##### 1.3.1.1 Drywell

The drywell is a steel pressure vessel supported in concrete, with a spherical lower section and a cylindrical upper portion. The



shell is fabricated of SA-516 Grade 70 steel and has a nominal shell thickness of 3/4 to 1-1/2 inches. The drywell houses the biological shield wall, reactor, reactor pedestal, reactor coolant recirculation system and other piping, valves, and equipment essential to system functions.

#### 1.3.1.2 Wetwell

The wetwell is a toroidal cylindrical shell located below the drywell containing a large pool of water for pressure suppression during postulated LOCAs and S/RV discharges. The torus is fabricated from sixteen mitered cylindrical segments and has a centerline elevation of 876 feet 7-1/2 inches. The torus is constructed of SA-516 Grade 70 steel and has a shell thickness of 0.616 and 0.688 inches at the top and bottom half, respectively. The shell is stiffened by sixteen internal ring girders located at each miter joint of the torus. The torus is supported by saddle assemblies which transmit operational, accident, and seismic loads to the reinforced concrete foundation slab of the reactor building. These supports consist of a pair of columns connected by saddles at each miter joint. In addition to its pressure suppression functions, the torus houses S/RV discharge devices, vent system components, protective structural members, Emergency Core Coolant System (ECCS) suction nozzles, turbine exhaust piping, coolant recirculation piping, monitoring accessories, and other non-essential structures. The basic geometry and components internal to the torus are shown in Figure 1.2.

#### 1.3.1.3 Vent System

In the event of a LOCA, the vent system provides a flow path to the wetwell suppression pool for condensation of steam released in the drywell. At the end of a LOCA transient, when ECCS water spills out of the break and rapidly reduces the drywell pressure, vacuum breakers installed on the vent system equalize the pressure between the two vessels, thereby protecting the drywell and vent

system from negative pressures in excess of design values. The eight S/RV discharge lines (S/RVDLs) are also routed through the main vent and terminate in a quencher discharge device located in the suppression pool. The vent system provides a contained path for the maintenance of a pressure differential between the drywell and the wetwell.

The vent system consists of eight main vents connecting the drywell air space to the wetwell. These vent lines extend to the approximate centerline of the torus, where they are connected to a common vent header located above the suppression pool. The vent header is supported by a pair of hangers at each ring girder location. The vent system includes forty pairs of partially submerged downcomers connected to the vent header. The vent system also has twelve vacuum breaker valves, two each at six of the main vent intersections on the vent header. The vent header is protected from LOCA-related pool swell impact loads by a deflector device suspended below the header.

### 1.3.2 Structural Components

#### 1.3.2.1 Torus Shell and Supports

The torus has an inside radius of 14 feet 4-1/2 inches and a toroidal centerline radius of 50 feet 10-1/2 inches from the centerline of the reactor. The original construction of the torus support system consisted of two columns at each miter joint. Each column was fabricated from a W14x136 rolled shape of A-36 material, except for a short upper portion interfacing with the torus shell. This upper section was fabricated plate, equivalent to a W14x136 of SA-516 Grade 70 material. The upper end of the columns was welded to the torus shell. The column base plates bear on lubrite plate assemblies which allow for thermal expansion of the torus. The base of the column was stabilized by means of diagonal bracing of double angles connected to the shell. As a



result of torus requalification for new loading conditions, three major modifications were made to the original torus support system. These modifications are:

- (1) Reinforcement of the column support configuration to improve safety margins for LOCA and S/RV discharge loads.
- (2) Addition of saddles connecting the two columns at sixteen ring girder locations to enhance the response characteristics of the torus structure during dynamic events.
- (3) Stiffening of the ring girder web to achieve a load transfer mechanism for LOCA and S/RV discharge drag loads.

#### 1.3.2.1.1 Torus Support Column Modifications

The torus support columns were modified to increase their original capacity for new design loads. Basically, the modifications consisted of the following:

- (1) Reinforcement of the basic column section to increase its structural strength.
- (2) Addition of base anchorage assemblies to provide resistance against uplift forces.
- (3) Reinforcement to the weldment connecting the column to the torus shell.

The strength of the outside columns was increased by means of welding two 1-inch x 16-inch A-36 reinforcing plates between the opposite flanges, such that a box section was formed. The inside columns were reinforced with two 3/4-inch x 16-inch A-36 plates in an identical manner. The bottom edge of the reinforcing plates was connected to the base plate for an effective transfer of the column tensile load. As a result of this reinforcement, the

cross-sectional area of the columns was increased by 80% and 60% for the outside and inside column, respectively.

The base anchorage assembly at each column location consisted of four 2-inch diameter A-615 Grade 75 anchor bolts grouted in core-drilled holes in the reinforced concrete foundation mat. A box beam assembly or a bracket arrangement of various configurations was installed on top of the base plate and around the column, to transfer the column tension reaction to the anchor bolts. The anchor bolt nuts were torqued "snug-tight" and backed off  $\frac{1}{2}$  turn to allow the columns to translate in a radial direction as a result of torus thermal expansion. The variations in the configuration of the box beam assemblies and the anchor bolt locations at each column base were due to limitations on the cutting of reinforcing steel in the foundation slab during the core drilling process.

The weldment connecting the support columns to the torus shell was reinforced by means of additional full penetration weld over an arc length of  $23\frac{1}{2}$  inches. The outside column web interfacing with the torus shell was reinforced with two  $\frac{3}{4}$ -inch SA-516 Grade 70 plates to provide the additional weldment. The web reinforcement for the inside column consists of two  $\frac{1}{2}$ -inch SA-516 Grade 70 plates. Details of a typical reinforced torus support column are shown in Figure 1.3.

#### 1.3.2.1.2 Torus Saddles

As part of the torus support modifications, saddle supports were installed at each of the sixteen ring girder locations. The primary reason for installing the saddles was the inadequacy of the original support configuration to inhibit the tendency of the torus shell to ovalize at frequencies close to the predominant frequencies of the new hydrodynamic loads. The addition of the saddles alters the stiffness characteristics of the torus, thereby inhibiting this ovaling mode of response. This reduced

ovalization results in a significant reduction in shell stresses. Additionally, the torus saddle shares the overall compression reaction loads with the torus columns, relieving the highly stressed region at the column connection to the shell.

Figure 1.4 shows a typical saddle configuration consisting of a contoured saddle web plate, a 20-inch-wide flange plate, and stiffener plates at various locations. The saddle is fabricated from 1½-inch thick SA-299 plate, has two intermediate bearings located on the foundation slab, and connects to the torus support column at the edges. The web of the saddles is aligned with the web of the internal ring girder and is connected to the torus shell by a partial penetration weld with fillet reinforcement. Prior to welding, a weld overlay was applied to the torus shell to protect the shell plate material. Connection of the saddle web to the torus column flange is by means of two ¾-inch fillet welds. The intermediate bearings consist of a 1/2-inch self-lubricating bearing plate installed between a base plate and a sole plate. The base plate is a 1-1/2 x 29 x 36-inch plate anchored to the foundation slab for seismic resistance. The sole plate is a 3-1/2 x 22 x 42-inch plate with a machined surface that bears on the lubricated plate. Each bearing location has three stiffener plates for load distribution and web stabilization.

#### 1.3.1.2.3 Ring Girder Modifications

The ring girders were strengthened to resist additional reaction loads from miscellaneous pipe supports inside the torus. Web stiffeners were added between the top flange of the ring girder and the torus shell. Also, the existing weld connecting the ring girder web to the torus shell was locally reinforced with additional fillet welds at the platform support column locations. Web stiffeners were added at eight locations on each ring girder to resist various drag loads and to transfer the ring girder reactions to the saddles.

### 1.3.2.2 Vent System and Supports

The major components of the vent system are the main vent, bellows assembly, vent header and downcomers, deflector, vent supports, and drywell/wetwell vacuum breakers. A description of these components and Mark I program modifications are provided below.

#### 1.3.2.2.1 Main Vent

There are eight main vents equally spaced around the base of the drywell. Figure 1.5 shows an elevation of a typical main vent (one of four with S/RV discharge line penetrations). The 5-foot 11-inch inside-diameter main vent is constructed of SA-516 Grade 70 steel with a nominal thickness of 1/2-inch inside the torus and 3/8-inch external to the torus (the four main vents without the S/RV discharge line penetrations have a nominal thickness of 1/4 inch inside the torus). The bottom section of the main vent in the region of the two S/RV discharge piping penetrations is 1-inch thick.

#### 1.3.2.2.2 Bellows Assembly

An expansion bellows is installed on each main vent at the torus penetration to isolate the two components thereby preventing interaction during differential thermal movements and dynamic excitation. The bellows are approximately 39 inches long and 80 inches in diameter, and consist of two stainless steel sections, each having four convolutions (1 ply, 1-1/2-inch pitch, 2-inch height) protected by a 1/8-inch thick carbon steel cover plate. The bellows assembly has the following design characteristics:

- Ply thickness 0.078 inch
- Axial extension 0.375 inch
- Axial compression 0.875 inch
- Lateral displacement  $\pm$  0.625 inch
- Axial spring rate 8,770 pounds/inch
- Lateral spring rate 75,700 pounds/inch

#### 1.3.2.2.3 Vent Header and Downcomers

A plan view of a typical vent header segment is shown in Figure 1.6. The figure shows the details of the transition from the 4-foot 2-inch diameter vent header to the 5 foot 11-inch diameter main vent intersection, including the T junction and associated Y stiffeners. The vent header circumscribes the torus at a center-line elevation of 880 feet 11 inches (5 feet 9 inches above the pool high-water level) as shown in Figure 1.2.

Forty downcomer pairs are located on the vent header as shown in Figure 1.6. A typical elevation of a downcomer pair is shown in Figure 1.7. Each downcomer has been modified with reinforcing pads and stiffener plates (5/8-inch SA-516 Grade 70 plate) to reduce stresses at the intersection. The original downcomer tie angle and connection rings have been replaced with the new tiebar configuration shown in the figure. In addition, the original downcomer maximum submergence of 4 feet 4-1/2 inches has been reduced to 3 feet 4 inches by truncating the downcomer legs.

#### 1.3.2.2.4 Vent Header Deflector

A vent header deflector device was installed to protect the 1/4-inch-thick vent header from pool swell impact loads resulting from a design basis LOCA. The underside of the deflector pipe is approximately 4 inches above the suppression pool (at maximum water level). Details of the deflector and the support arrangement are shown in Figure 1.8. The deflector supports are welded to the clevis assembly at the top of the original pipe support columns.

#### 1.3.2.2.5 Vent System Supports

The original vent header supports consisted of two 6-inch diameter schedule 80 pipes connecting the vent collar to the web extension plate at each ring girder location. The top and bottom of the



support columns were connected by means of a clevis and pin arrangement which allowed column rotation to accommodate thermal expansion of the vent system. In their original location, these columns were subjected to high submerged structure drag loads. Reinforcement for these loads would increase the severity of the loads due to the larger submerged surface area. Therefore, the vent header support system was modified by removing the columns and suspending the vent header from each ring girder. Figure 1.9 shows the modified support system geometry. The modification consists of two 6-inch diameter schedule XXS pipes suspended by means of a 2-3/4-inch diameter pin connection at the top and bottom. The original upper clevis connection to the vent header collar was retained as part of the support for the deflector pipe.

#### 1.3.2.2.6 Vent System Vacuum Breakers

The vent system is equipped with twelve 18-inch GPE vacuum breakers. These check valves (normally closed) are located in pairs at six of the eight main vent/vent header intersections. The vacuum breakers maintain the wetwell pressure at a value less than or equal to the drywell pressure by permitting air flow from the wetwell to the drywell when the wetwell is pressurized and the drywell is slowly depressurized. This vacuum relief function prevents pool water from entering the vent system and limits the negative pressure differential on the drywell and vent system.

Since the vacuum breaker valves are cantilevered from the vent system and located near the center of a vent bay, they are subjected to high pool swell impact and froth impingement loads during a DBA. The valves were modified by installing vertical stiffener and vent pad plates as shown in Figure 1.10. The stiffeners were fabricated from 5/8-inch thick SA-516 Grade 70 steel plate. The valve modifications were necessary to satisfy the Code pressure boundary requirements at the vent penetrations.

#### 1.3.2.3 Miscellaneous Torus Internals

This subsection addresses only torus internal structural components; other piping and nonstructural internals are described in Subsection 1.3.3.

##### 1.3.2.3.1 Service Platform

The service platform is a 3-foot wide catwalk installed above the pool surface inside the torus. It has an extended work area at six locations in the vicinity of the main vent/vent header intersection for access to the drywell/wetwell vacuum breakers. The platform is fabricated from structural channels and angles, and supported from below by angle posts connected to the ring girders or torus shell. An analysis to evaluate safety margins of the various platform components for LOCA pool swell impact and drag loads indicated unacceptable levels of deformation for these components. Accordingly, modifications were made to restore structural safety margins to an acceptable level. In summary, the modifications consisted of replacement of the angle posts and channel support framing at the ring girders, installation of stronger and additional supports, platform horizontal bracing, and provisions for additional anchorage of the grating to the channel framing members.

The existing angle posts were replaced by a 4-inch-diameter schedule XXS pipe welded to a pipe sleeve connected to the ring girder flange. The existing channel cross-beam was replaced by a 4x10x $\frac{1}{2}$ -inch tubular section at each ring girder. The stringer channels were braced with 2x2x $\frac{1}{4}$ -inch tubular sections for lateral stability. Also, these channels were supported by additional diagonal supports of 3- or 4-inch diameter schedule XXS pipe at the approximate third points to reduce the span length and to transfer the upward pool swell impact reaction to the ring girder. The existing grating was further secured by installing a 2- $\frac{1}{2}$  x 2 x 6-inch-long angle piece welded to the grating and the existing toe plate. This tie-down installation was repeated at 12-inch



intervals around the perimeter of the platform. Figures 1.11, 1.12, and 1.13 show the typical modified platform arrangement and its various components.

#### 1.3.2.3.2 Monorail

The 360° monorail beam is located approximately 11 feet above and 5 feet outward from the centerline of the torus. The original construction consists of an S12x31.8 rolled shape supported by two welded connections to the shell in every torus bay. During a postulated LOCA, some of the rising water, after impacting the vent header deflector, gets detached from the bulk pool surface and forms into froth. When evaluated for the froth impingement load, the monorail was found to be structurally overstressed. Modifications were made to reduce the unsupported span length of the beam. The modification consists of an additional support at the midpoint of the monorail beam in each bay. The support was fabricated from a 4-inch diameter pipe (SA-106, Grade B) with a 6-inch diameter sleeve, and was connected to the torus shell with a 1-1/2 x 18-inch diameter reinforcing pad plate (SA-299).

#### 1.3.3 Piping Systems

##### 1.3.3.1 Safety/Relief Valve Discharge Piping

The S/RV discharge piping consists of eight 10-inch lines routed from the S/RVs in the drywell, through penetrations in the main vents to the wetwell, where they are terminated at the steam quencher devices in the suppression pool. The original line configuration consisted of schedule 40 piping, with the exception of a short schedule 80 segment through the main vent penetration, and included a ramshead steam discharge device.

S/RVDL configurations are often designated by the number of the S/RV from which the line is routed. The S/RVs are designated as

-71A through -71H. This terminology should not be confused with the designation of the wetwell piping configurations as discussed below.

Extensive modifications were made to the S/RVD lines in order to accommodate the newly defined S/RV discharge and LOCA-related hydrodynamic loadings. These modifications were:

(1) Drywell routing

- (a) Addition of two 10-inch vacuum relief valves on each S/RVDL in order to reduce the amount of water reflood in the lines following S/RV closure.
- (b) Addition of pipe supports, as well as relocation and reinforcement of existing supports, in order to accommodate S/RVD thrust loads or loads transmitted to the S/RVDLs by motion of the main vent. Table 1.1 provides a line-by-line summary of the pipe support modifications in the drywell.
- (c) Portions of the drywell framing were reinforced for reactions from S/RVD piping supports. A W12x27 lateral member spanning between the upper level radial beams at azimuths 212 and 240 degrees required minor axis bracing. Four end brackets supporting lower level radial beams at the reactor pedestal between azimuths 189 and 212 degrees were also reinforced.

(2) Wetwell routing

- (a) Rerouting of the piping to minimize load effects from pool swell impact and submerged structure drag loads. The modified pipe routing in the wetwell is shown in Figure 1.14.

After rerouting of the wetwell portion of S/RVDL, two distinct wetwell piping configurations exist at CNS. One configuration routes directly to the T-quencher discharge device in the same bay as the main vent penetration. This configuration is referred to as the short S/RVDL (or S/RVDL "A"). The second configuration routes from the main vent penetration, through the torus airspace of the adjacent non-vent bay and into the next vent bay where it descends into the submerged T-quencher discharge device. This configuration is referred to as the long S/RVDL (or S/RVDL "B"). This terminology for the wetwell portion of the S/RVDL should not be confused with the line designations based on the S/RV number (as discussed above). When designating the line by S/RV number, the number 71 will always precede the letter designation.

- (b) Replacement of all schedule 40 piping with schedule 80.
- (c) Addition of T-quencher discharge devices.

The T-quencher discharge device and support configuration are shown in Figure 1.15. The design is based upon the standard T-quencher assembly developed for the Mark I Owners Group. The T-quencher arms are stainless steel TP316L 12-inch schedule 80 pipes capped at the end with 794 holes per arm. On one end cap 40 holes are located while the other end cap is closed. The end cap holes are intended to provide better thermal mixing during extended S/RV blowdown. The T-quencher arms are connected to the S/RVDL by a ramshead component and a 12 x 10 reducer component.

The T-quencher support arrangement is shown in Figure 1.15. The support consists of a 24-inch diameter schedule 100 pipe extending across each vent bay at bottom dead center. A 10-inch schedule 80 pipe is provided in each non-vent bay to act as a brace for the large support pipe. An extension plate on the ring girder was installed to accommodate the 24-inch diameter pipe attachment above the ring girder flange. Support plates act as guides for the T-quencher arms. Axial restraint is provided by the shear key attached to the lower gusset plate on the ramshead. All eight T-quencher discharge devices have the same support configuration.

(d) Addition of pipe supports.

Three supports were installed on each long S/RVDL in the wetwell. A normal restraint was located below the bend in the piping slightly below the torus high water level. This restraint was tied to a 16-inch diameter support pipe which spanned between the two ring girders in the bay. An axial restraint and a guide are provided at the ring girder location above the high water level. No supports are provided on the short S/RVDL between the main vent and the T-quencher.

1.3.3.2 Torus Attached Piping

A total of 19 large bore (greater than 6 inches) and 25 small bore (less than or equal to 6 inches) pipes penetrate the torus shell. The torus attached piping systems are listed by penetration number and function in Table 1.2. The large bore lines have primarily ECCS functions while the small bore lines have instrumentation and vacuum breaker actuation functions.

Modifications were made to the torus attached piping systems to ensure that the originally intended design safety margins were restored under the new hydrodynamic loads transmitted to the piping through the torus shell vibrations.

The modifications are:

- (1) Addition of new pipe supports or reinforcement of existing supports were performed on nearly all torus attached piping systems. For the large bore lines, a total of 14 new supports were added and 137 of the existing 239 supports were reinforced for the new increased loads. Existing dead weight supports of the rod hanger type were typically replaced by sway struts to accommodate dynamic, reversing loads. For the small bore torus attached piping, a total of 60 new and modified supports were installed. A summary of these pipe support modifications is presented in Table 1.3.
- (2) The major portions of the torus liquid level indicator piping was rerouted to isolate the piping from the torus motion effects. This isolation was accomplished by installing in-line anchors to the reactor building wall. Expansion loops were added between the anchors and the torus shell to accommodate the torus shell displacements.
- (3) One torus drain line and one atmospheric instrumentation line were rerouted.
- (4) 25 new or modified supports on branch piping (less than four inch diameter) were installed.
- (5) 13 valves on large bore piping systems were stiffened in the valve yoke area. These modifications consist of a 3/8" bent plate bolted to the operator flange at the existing bolt and at the available bolt below the yoke leg.



- (6) Three torus attached piping penetrations were reinforced. These penetrations are for the two core spray pump test return lines (X-223A and X-223B) and one core spray pump suction line (X-227B). Four 5/8 inch gusset plates were located around each penetration with welding pads included between the gussets and the piping and torus shell.
- (7) The supports on the four RHR pumps were reinforced for high shear loads on the baseplate bolts. For each pump, four 4" x 7" x 1" angle brackets were welded to the edge of the baseplate and then fit over the edge of the pump foundation.

#### 1.3.3.3 Torus Internal Piping

The torus internal piping systems are listed by function and penetration number in Table 1.4.

With the exception of the containment spray header, which extends around the top of the torus and penetrates the torus at two locations, the torus internal piping consists exclusively of short, submerged suction strainers and partially submerged discharge pipes.

Structural modifications performed on the torus internal piping are summarized below:

- (1) The discharge configuration of the Residual Heat Removal (RHR) pump test return line was modified. The existing 10-inch discharge elbow is replaced by a 14-inch elbow with its discharge oriented  $67.5^{\circ}$  below a horizontal plane in the torus. The existing 18" x 10" reducer and support located on the 10-inch portion of the piping is also replaced with components which accommodate the 14-inch elbow (Figure 1.16). The increased elbow size is intended to improve thermal mixing in the suppression pool.

A guide is also located near the elbow to reduce pipe stresses due to submerged structure drag loads.

- (2) The High Pressure Coolant Injection (HPCI) and Reactor Core Isolation Cooling (RCIC) turbine exhaust piping were rerouted and resupported close to the ring girders to minimize their exposure to submerged structure drag loads (Figures 1.17 and 1.18).
- (3) The two 10-inch diameter core spray pump test lines are truncated to discharge into the suppression pool at elevation 872' - 7-3/4". This modification involves removal of a 2' - 6" portion of the line between the existing discharge outlet and the specified elevation (Figure 1.19). The existing 45° elbow located at the discharge outlet is to be relocated at the new discharge elevation. Truncation of these lines reduces reaction loads at the torus penetration due to drag loads on the submerged portion of the line. The discharge outlet is still two feet below the suppression pool low water level.
- (4) The 2-inch condensate drain lines for the HPCI and RCIC systems are cantilevered from the torus penetrations (X-221 and X-222) into the suppression pool. V-type guides consisting of 2-inch diameter struts bracing back to the torus shell are to be located at torus elevation 875' - 3 1/4". These guides reduce pipe stresses due to submerged structure drag loads.
- (5) The 16 existing U-shaped hangers provided at each ring girder for the 4-inch diameter containment spray header are to be reinforced. A 1,2-inch gusset plate is to be welded from the existing support to the ring girder flange on the inboard side of each support. The reinforced supports are designed for reactions due to differential thermal motion between the piping and torus shell.



#### 1.3.4 Miscellaneous System Modifications

##### 1.3.4.1 Drywell/Wetwell Pressure Differential

To maintain a pressure differential of 1.0 psid between the drywell and wetwell as a limiting condition for plant operation, a Pump Around System (PAS) was installed. The purpose of this pressure differential is to reduce the water level within the submerged portion of the vent system downcomers, thereby reducing LOCA-generated loads on torus structural components.

The PAS consists of a piping loop between the drywell and torus. The piping loop includes dual motor-operated isolation valves at existing torus and drywell penetrations. The PAS is isolated from primary containment upon initiation of a Group II isolation signal from the Primary Containment Isolation System. Two air-cooled compressors, each with a capacity of 100 cfm at 7 psid, are located in series with the piping loop to provide the motive force for the gas. The compressors take suction from the torus and discharge to the drywell. To dampen compressor pulsations, a surge chamber is located in the compressor outlet piping.

All piping and valves in the PAS system are ASME Section III, Class II, with a Seismic Category I rating. The compressors were seismically qualified in conformance with IEEE Standard 344-1975 to the applicable response spectrum curve. The PAS is designed with sufficient redundancy so that no single active system component failure can degrade the Primary Containment Isolation System.

Electrical power for the PAS components is supplied from the critical power supply. The instrumentation automatically controls the differential pressure between the torus and the drywell. Pressure sensors convert the differential pressure between the torus and drywell into pneumatic signals to load and unload the compressors. Instrumentation is provided to measure the temperature, pressure, differential pressure (two monitoring

channels), recirculation flow rate, and the position of all isolation valves.

#### 1.3.4.1.1 Normal System Operation

Operation of the PAS is from the control room. System operation is initiated by the remote manual opening of isolation valves and starting the compressors. Recirculation begins when the low differential set point is reached. At this point, the pressure switches close, energizing the electrical solenoid valves supplying pneumatic pressure to the compressor unloader valves. Energizing the solenoid valves removes the pneumatic pressure from the compressor unloaders, and the compressors begin to pump from the torus to the drywell. When the high differential pressure set point is reached, the pressure switch opens and the solenoid valves are deenergized. Pressure is supplied to the compressor unloaders, thereby terminating circulation flow.

#### 1.3.4.1.2 Accident Operation

The occurrence of low reactor water level and high drywell pressure (Group 2 isolation signal) indicates the possibility of a LOCA requiring the isolation of the primary containment. The PAS suction line from the torus is isolated by the two motor-operated isolation valves upon receipt of the Group 2 isolation signal. The same signal also closes the two motor-operated valves on the compressor discharge line to the drywell. These valves remain closed until the Group 2 isolation signal clears and is reset, or the valves are opened manually for PAS operation.

The system would operate in the same manner during loss-of-off-site power since one valve in each pair of isolation valves is AC-powered from Bus 1-F, and one valve is powered by the 250 V DC bus.

#### 1.3.4.2 S/RV Low-Low Set Relief Logic

General Electric recently completed an evaluation of the LDR S/RV Load Cases C3.1, C3.2, and C3.3 (defined in Subsection 2.5) for Cooper Nuclear Station (Reference 21). The purpose of this evaluation was to identify design changes that will mitigate S/RV subsequent actuation-induced loads during postulated Intermediate Break Accident/Small Break Accident (IBA/SBA) LOCA events. The primary concerns are the potential high thrust loads on the discharge piping (Load Cases C3.1 and C3.3), and the high frequency pressure loading on the containment (Load Case C3.2). GE concluded that delayed isolation achieved by means of a Level 1 Main Steam Isolation Valve (MSIV) water level trip set point (Subsection 1.3.4.3), combined with a 100 psi low-low set relief logic, produced the maximum potential benefit. The planning and procurement necessary for installation of these design changes is currently in progress.

The proposed low-low set relief logic system is shown in Table 1.5. When the logic is armed by actuation of any S/RV and a high reactor pressure scram signal, the logic will lower the opening and closing set points of valves D and H to new preset pressures which are sufficiently below the set points of the remaining valves. The opening and closing set points for valves 71D and 71H will be separated by 100 psi as indicated in the table. Thus, more energy will be released each time an S/RV actuates and more energy will be required for repressurization before an S/RV opens. If the amount of energy release is sufficient to prevent reactor repressurization to a level where the low-low set valve reopens, then subsequent S/RV actuations can be prevented. If the amount of energy release is insufficient to prevent subsequent actuation, the low-low set relief logic will delay S/RV reopening by virtue of the longer time required to repressurize the reactor.

For an anticipated operational transient event, such as a 3-second MSIV closure, the relief logic extends the minimum time between

actuations to approximately 36 seconds. If there is no loss of offsite power (LOOSP) or early MSIV isolation during a LOCA event, subsequent S/RV actuations will not occur for any break size. If LOOSP does occur, the relief logic extends the minimum time between actuations to approximately 31 seconds for break sizes smaller than 0.20 ft<sup>2</sup>. No subsequent actuations will occur for breaks of 0.20 ft<sup>2</sup> or larger (see Table 1.6). The time intervals described above effectively mitigate the S/RV discharge loading conditions of concern (Subsection 2.5.2).

A more detailed description of the low-low set relief system can be found in Reference 21. Also included in this reference is an evaluation of the design changes with respect to plant operations and other safety systems, as well as analysis results for S/RV system performance with the low-low set relief logic.

#### 1.3.4.3 Level 1 MSIV Trip Setpoint

The proposed new MSIV trip set point is shown in Table 1.7. The lower trip setpoint will mitigate subsequent S/RV actuation load cases because of the slower repressurization rate due to the lower reactor decay heat rate after delayed isolation. In order to obtain the maximum benefit of this change, the water level trip is to be lowered to reactor vessel Level 1. However, this maximum benefit can be realized only if early isolation due to LOOSP does not occur. Nevertheless, the Level 1 MSIV trip does reduce S/RV challenges, increase plant availability, and mitigate S/RV load case C3.3.

Lowering the MSIV trip set point to Level 1 will potentially eliminate S/RV actuations for break sizes of 0.15 ft<sup>2</sup> or larger, if earlier isolation due to LOOSP does not occur. When combined with the low-low set relief logic, transient analysis results indicate that subsequent S/RV actuations will not occur for any break size. Although a significant amount of energy is released from the vessel without heating the suppression pool by imple-

menting both of these design changes, it is ADS initiation that prevents the future subsequent S/RV actuations. If ADS were not initiated, the time interval between subsequent actuations would be approximately 51 seconds for a break size approaching zero. This interval is more than sufficient to mitigate the S/RV discharge load cases of concern. Additional information on S/RV system performance with the Level 1 MSIV trip, installed independently or in combination with the low-low set relief logic, can be found in Table 1.6 (summary) and Reference 21.

#### 1.3.4.4 Torus Temperature Monitoring System

To comply with the requirements of the NRC described in the SER, a new torus temperature monitoring system was installed at CNS. This monitoring system replaces the previous (water) torus temperature monitoring system which consisted of six sensors, three for water and three for air, monitored in panel VBD-J in the control room.

Although not required by the SER, the new temperature monitoring system is designed as IE qualified. This allows the system to be upgraded to a safety related system should NRC regulations require this at a later date.

This new system consists of sixteen qualified Pyco resistance thermometers (RTDs), eight qualified Foxboro Spec 200 input converters, eight qualified Foxboro Spec 200 isolated output buffers and one Leeds and Northrup Speedomax 250 series recorder.

The RTDs are housed in thermowells installed at 16 separate locations on the drywell side of the torus. The thermowells are located in pairs at a location which is approximately at the middle of the T-quencher arm hole pattern on the downstream arm of the quencher (Downstream refers to the bulk flow direction in the pool created by T-quencher discharge). The thermowells are located approximately five feet below the suppression pool minimum water level.



The power for the RTDs is supplied from the input converters, which produce a 0 to 10 volt signal to represent the temperature reading of the RTD. This signal is then fed to the isolated output buffers, which produce a 4 to 20mA signal. This signal is then taken to panel VBD-J and connected to the recorder. Also, the capability of connecting a computer at a later date is provided with the addition of the appropriate dropping resistor to the signal current loop.

System operation is continuous with the multipoint recorder sequentially stepping through each of the sixteen RTD inputs and plotting its measured temperature. When any of these temperatures exceeds the alarm setpoint on the recorder, an annunciator point on panel VBD-J is energized. The recorder will continue to plot all of the sixteen RTD inputs.

Bulk pool temperatures, which will be calculated by the future plant process computer, will allow the operator to anticipate local pool temperatures and to take actions to keep them below Technical Specification limits.

#### 1.3.5 Modification Summary

The containment, piping, and system modification descriptions discussed in the previous paragraphs include the majority of the Mark I containment program modifications installed (or to be installed) at Cooper Nuclear Station. Table 1.8 summarizes the complete CNS modification program. The table provides a brief description, including the purpose or primary load event dictating the change, and the completion time frame for the modifications. All the modification work is scheduled for completion by September 1982 with the exception of the low-low set relief logic and reduced MSIV trip setpoint, which will be installed in 1983.

## 1.4 Summary of Results

### 1.4.1 Results and Conclusions

The objective of the Mark I containment LTP for CNS is the restoration of originally intended design safety margins for the new suppression pool hydrodynamic loads. These margins are identified through the application of the design loads to the CNS plant unique containment configuration and comparison of the resulting responses against established structural and mechanical acceptance criteria. The required evaluations have been completed for CNS. The results indicate that the CNS containment configuration as of September 30, 1982, will satisfy all established design criteria (with the exceptions noted in Subsection 1.2.2.2).

To meet the objectives of the LTP, NPPD has performed extensive modification work on CNS containment components. This work has been performed over the last three years during scheduled plant outages and, in several instances, during plant operation. This modification program has been responsive to NRC concerns on containment integrity by providing timely improvements in safety margins without adversely impacting normal plant operation. This responsiveness is further illustrated by the fact that NPPD will be the first Mark I containment owner to complete the installation of all LTP-related modifications.

In conclusion, the CNS containment system has been shown through analysis, including the necessary modification work, to meet the objectives of the Mark I containment LTP.

### 1.4.2 Conformity with Project Requirements

The PUAR for CNS is submitted in partial fulfillment of the requirements of the NRC for the Mark I LTP. The PUAR summarizes the work which demonstrates that with the containment



modifications identified in Subsection 1.3 all established design criteria are satisfied. Therefore, completion of these modifications will result in conformity with the requirements of the NRC-issued Order for Modification of License and Grant of Extension of Exemption to NPPD as holder of Facility Operating License DPR-46 for CNS. As required by this order, all modifications are to be installed by September 30, 1982.

Subsequent review and approval of this report will eliminate the "Unresolved Safety Issue" designation (pursuant to Section 210 of the Energy Reorganization Act of 1974) as it pertains to CNS.

Table 1.1

S/RVD LINES IN THE DRYWELL  
SUMMARY OF SUPPORT MODIFICATIONS/ADDITIONS

<u>Line No.</u>	<u>Number of Supports</u>	
	<u>New/Added</u>	<u>Modified</u>
71A	9	6
71B	11	6
71C	4	5
71D	4	4
71E	3	4
71F	4	3
71G	5	6
71H	9	6

Table 1.2

TORUS PIPE PENETRATIONS

Penetration Number	Line Size (in)	Description
X-203A	1	Oxygen Analyzer
X-203B	1	Oxygen Analyzer
X-205	20	Vacuum Relief from Bldg. and Vent Purge Inlet
X-206A	1	Liquid Level Indicator
X-206B	1	Liquid Level Indicator
X-206C	1	Liquid Level Indicator
X-206D	1	Liquid Level Indicator
X-209A	1	Air and Water Temperature
X-209B	1	Air and Water Temperature
X-209C	1	Air and Water Temperature
X-209D	1	Air and Water Temperature
X-210A	18	RHR Pump Test Line
X-210B	18	RHR Pump Test Line
X-211A	6	Containment Cooling to Spray Header
X-211B	6	Containment Cooling to Spray Header
X-212	12	RCIC Turbine Exhaust
X-213A	8	Torus Drain
X-213B	8	Torus Drain
X-214	24	HPCI Turbine Exhaust
X-215	1	Atmospheric Pressure Instrumentation
X-220	16	Vent Purge Outlet
X-221	2	RCIC Condensate Drain
X-222	2	HPCI Condensate Drain
X-223A	10	Core Spray System Pump Test Line
X-223B	10	Core Spray System Pump Test Line
X-224	6	RCIC Pump Suction
X-225A	20	RHR Pump Suction
X-225B	20	RHR Pump Suction
X-225C	20	RHR Pump Suction
X-225D	20	RHR Pump Suction
X-226	16	HPCI Pump Suction
X-227A	16	Core Spray Pump Suction
X-227B	16	Core Spray Pump Suction
X-228	10	Demineralized Water Inlet
X-229A	1	Vacuum Breaker Actuating Air
X-229B	1	Vacuum Breaker Actuating Air
X-229C	1	Vacuum Breaker Actuating Air
X-229D	1	Vacuum Breaker Actuating Air
X-229E	1	Vacuum Breaker Actuating Air
X-229F	1	Vacuum Breaker Actuating Air
X-229G	1	Vacuum Breaker Actuating Air
X-229H	1	Vacuum Breaker Actuating Air
X-229J	1	Vacuum Breaker Actuating Air
X-229K	1	Vacuum Breaker Actuating Air
X-229L	1	Vacuum Breaker Actuating Air
X-229M	1	Vacuum Breaker Actuating Air

Table 1.3

SUMMARY OF PIPE SUPPORT MODIFICATIONS  
FOR TORUS ATTACHED (EXTERNAL) PIPING

<u>Lines</u>	<u>Number of Supports</u>	
	<u>New</u>	<u>Modified</u>
X-205	1	6
X-206A/B	11	0
X-206C/D	13	0
X-209	6	0
X-210A, X-211A	2	10
X-210B, X-211B	1	7
X-212	0	3
X-213A, X-213B	0	0
X-214	2	15
X-215, X-203	7	0
X-220	1	1
X-221	5	0
X-222	12	0
X-223A	2	12
X-223B	0	17
X-224	0	15
X-225A, X-225B	4	12
X-225C, X-225D	1	18
X-226	0	7
X-227A, X-227B	0	14
X-229	6	0
Branch Lines	8	17

Table 1.4

TORUS INTERNAL PIPING SYSTEMS

<u>Penetration Number</u>	<u>Line Size (in)</u>	<u>Description</u>
X-210A	18	RHR Pump Test Line
X-210B	18	RHR Pump Test Line
X-211A	6	Containment Cooling to Spray Header
X-211B	6	Containment Cooling to Spray Header
X-212	12	RCIC Turbine Exhaust
X-214	24	HPCI Turbine Exhaust
X-221	2	RCIC Condensate Drain
X-222	2	HPCI Condensate Drain
X-223A	10	Core Spray Pump Test Line
X-223B	10	Core Spray Pump Test Line
X-224	6	RCIC Pump Suction
X-225A	20	RHR Pump Suction
X-225B	20	RHR Pump Suction
X-225C	20	RHR Pump Suction
X-225D	20	RHR Pump Suction
X-226	16	HPCI Pump Suction
X-227A	16	Core Spray Pump Suction
X-227B	16	Core Spray Pump Suction
X-228	10	Demineralized Water Inlet

Table 1.5

PROPOSED LOW-LOW SET SAFETY/RELIEF VALVE SYSTEM

	S/RV							
	A	B	C	D	E	F	G	H <sup>(1)</sup>
Pressure Relief Function	X	X	X	X	X	X	X	X
ADS Function	X	X	X	-	X	X	X	-
Low-Low Set Relief Function	-	-	-	X	-	-	-	X
Valve Group	III	III	II	I	II	II	III	I
Steam Pilot Opening Set Point (psig)	1125	1125	1115	1105	1115	1115	1125	1105
Steam Pilot Closing Set Point (psig)	1091	1091	1082	1072	1082	1082	1091	1072
Low-Low Set Open (psig)	-	-	-	1045	-	-	-	1075
Low-Low Set Close (psig)	-	-	-	945	-	-	-	975

Note:

- (1) Valve H is currently designated as an ADS valve. Since it is necessary to separate ADS valves from low-low set valves, and since it is desirable to use the lowest group valves for low-low set, the ADS function for valve H will be assigned to valve F.



Table 1.6

S/RV LOAD CASE ANALYSIS RESULTS

Suction Line Break Area (ft <sup>2</sup> )	MSIV Trip Level	Low-Low Set $\Delta P$ (psid)	Isolation (1) Mechanism	Subsequent Actuation Time (sec)	Remarks
0.0	2	Not Used	L	14	As-is Case
0.01	2	Not Used	L	13	As-is Case
0.05	2	Not Used	L	14	As-is Case
0.10	2	Not Used	L	16	As-is Case
0.15	2	Not Used	L	22	As-is Case
0.20	2	Not Used	L	26	As-is Case
0.0	1	Not Used	L	22	Level 1 Trip
0.01	1	Not Used	L	21	Level 1 Trip
0.05	1	Not Used	L	22	Level 1 Trip
0.10	1	Not Used	L	20	Level 1 Trip
0.15	1	Not Used	L	$\infty$	Level 1 Trip
0.0	2	100	L	31	2-Valve Low-Low Set
0.01	2	100	L	33	2-Valve Low-Low Set
0.05	2	100	L	39	2-Valve Low-Low Set
0.10	2	100	L	46	2-Valve Low-Low Set
0.15	2	100	L	56	2-Valve Low-Low Set
0.20	2	100	L	$\infty$	2-Valve Low-Low Set
0.0	2	100	L	35	1-Valve Low-Low Set
0.01	2	100	L	34	1-Valve Low-Low Set
0.0	1	100	L	$\infty$	Level 1 + Low-Low Set
0.01	1	100	L	$\infty$	Level 1 + Low-Low Set
0.0	1	100	L	51	Level 1 + Low-Low Set ADS Off
0.0	1	100	M (2.0)	34	LOOSP + 2-Valve Low-Low Set
0.0	1	100	M (6.0)	33	LOOSP + 1-Valve Low-Low Set

Note:

(1) L = Isolation due to water level trip.

M = Isolation due to loss of reactor protection system MG set.  
Assumed time of isolation in parentheses.

Table 1.7

MSIV WATER LEVEL TRIP

<u>Reactor Vessel Levels</u>	<u>Inches Above Vessel Zero</u>	<u>Description of Trips</u>
8	575.25	Reactor Feed Pump Trip Close Main Steam Turbine Stop Valves Trip RCIC and HPCI Turbines
7	559.25	High Water Level Alarm
5, 6		Normal Water Level
4	554.25	Low Level Alarm
3	529.25	Scram Reactor
2	479.75	Initiate HPCI, RCIC Close MSIV Trip Recirculation Pumps
1	371.25	Initiate RHR and Core Spray Systems Contribute to ADS PROPOSED AS NEW MSIV TRIP
-	352.5	Top of Active Fuel

Table 1.8

SUMMARY OF CONTAINMENT AND PIPING MODIFICATIONS

COMPONENT NAME	NATURE OF MODIFICATION	PRIMARY LOAD OR PURPOSE	COMPLETION DATE
<u>STRUCTURAL COMPONENTS</u>			
<u>Torus Shell and Supports</u>			
Torus Support Column	Plate reinforcement to column web and flanges	Increase column capacity	Spring 77
Column Anchorage	Installed anchor bolts, brackets, and box beam assemblies	Resist LOCA uplift forces	Spring 77
Column-to-Torus Connection	Additional full penetration weldment	Increase connection capacity	Spring 76
Torus Saddle	Full saddles connecting torus support columns	Improve dynamic response	Summer 81
Column Anchorage Reinforcement	Reinforcement of box beams and bracket weldments	Resist LOCA uplift forces	Spring 82
Ring Girder	Web stiffeners; local reinforcement of weld to shell	Pool drag loads; attachment loads	Fall 81
<u>Vent System</u>			
Vent Header/Downcomer Intersection	Reinforced 80 penetrations with stiffener plates and pads	Chugging & S/RV discharge loads	Fall 81
Downcomers	Reduced downcomer submergence by truncation	Mitigate DBA blowdown load	Spring 80
Downcomer Ties	Installed tie bar and ring assembly at each downcomer pair	CO and chugging lateral loads	Spring 80
Vent Header Deflector	Installed deflector assembly in all torus bays	Pool swell impact load	Spring 80
Vent Header Supports	Removed existing supports; resupported from girder above	Pool drag loads	Spring 81
DW/WW Vacuum Breakers	Reinforced 12 vacuum breaker penetrations	Pool swell/froth impact loads	Fall 81
<u>Miscellaneous Torus Internals</u>			
Monorail	Installed midbay supports in all torus bays	Froth impingement load	Spring 81
Service Platform	Replaced existing supports; added new supports, bracing and grating tie-down	Pool swell impact/drag loads	Spring 82
<u>Drywell Steel Framing</u>	Reinforcement of beam seat connections and framing members	S/RV pipe support loads	Spring 82
<u>MISCELLANEOUS SYSTEM MODIFICATIONS</u>			
Drywell/Wetwell Pressure Differential	Installed Pump Around System	Mitigate LOCA blowdown vent clearing	Spring 76
Torus Temperature Monitoring System	Installed monitoring system and instrumentation	Monitor pool temperature	Summer 82
S/RV Low-Low Set Logic	Will install control logic and instrumentation for safety relief valves	Mitigate/eliminate S/RV subsequent actuation loads	Spring 83
MSIV Trip Set Point	Will lower set point to reactor level 1	Reduce S/RV Challenges	Spring 83

Table 1.8 (Cont'd)

SUMMARY OF CONTAINMENT AND PIPING MODIFICATIONS

COMPONENT NAME	NATURE OF MODIFICATION	PRIMARY LOAD OR PURPOSE	COMPLETION DATE
<u>PIPING SYSTEMS</u>			
<u>S/RV Discharge Piping</u>			
Wetwell Piping	Rerouted with stronger pipe; added 12 new supports	Pool swell impact/drag loads	Spring 80
T-Quencher Discharge Device	Installed T-quencher device on each S/RV line	Mitigate water/air clearing loads	Spring 80
T-Quencher Support	Installed quencher support assembly in 8 bays	Support quencher device	Spring 80
Quencher Support Bracing	Installed quencher support bracing in 8 bays	Distribute quencher reactions	Spring 80
Vacuum Breakers	Installed two, 10-inch vacuum breakers on each line	Prevent excessive reflood in line	Spring 80
Pipe Supports and Restraints	Installed 89 new or modified supports in drywell	S/RV blowdown thrust loads	80, 81 & 82
<u>Torus Attached Piping</u>			
Large Bore Supports	Installed 151 new or modified supports	Torus motions due to LOCA & S/RV loads	Summer 82
Small Bore Supports	Installed 54 new supports	Torus motions due to LOCA & S/RV loads	Summer 82
Small Bore Rerouting	Rerouted 5 lines	Torus motions due to LOCA & S/RV loads	Spring 82
Branch Line Supports	Installed 25 new or modified supports	Torus motions due to LOCA & S/RV loads	Summer 82
Torus Penetrations	Reinforced three large bore torus penetrations	Pipe reactions from LOCA & S/RV loads	Spring 82
Valve Operator Supports	Reinforced 13 valve yokes	Torus motions due to LOCA & S/RV loads	Summer 82
Pump Anchors	Modified anchorage of 4 RHR pumps	Pipe reactions at nozzles	Summer 82
<u>Torus Internal Piping</u>			
HPCI Turbine Exhaust	Rerouted and resupported HPCI sparger	Pool drag loads	Fall 81
RCIC Turbine Exhaust	Rerouted and resupported RCIC sparger	Pool drag loads	Fall 81
Core Spray Return Test Line	Truncated test lines	Pool drag loads	Spring 82
RHR Return Test Line	Installed reducer, discharge elbow, and new supports	Pool thermal mixing	Spring 82
Spray Header	Reinforced existing supports	Thermal loads	Spring 82
Vent Drain Line	Rerouted lines and installed supports	Pool drag loads	Spring 80

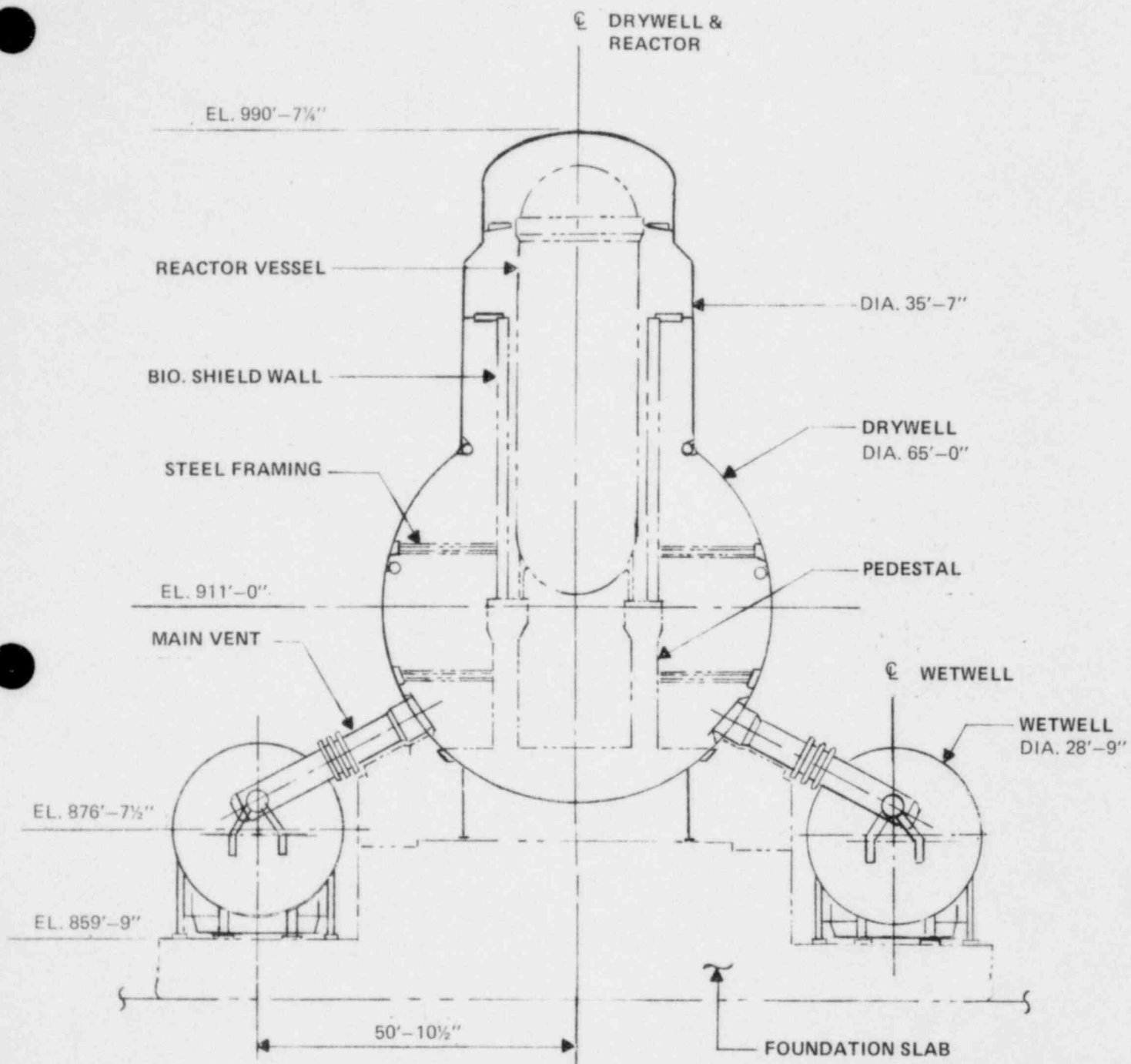


FIGURE 1.1

CROSS SECTION - COMPOSITE PLANT LAYOUT

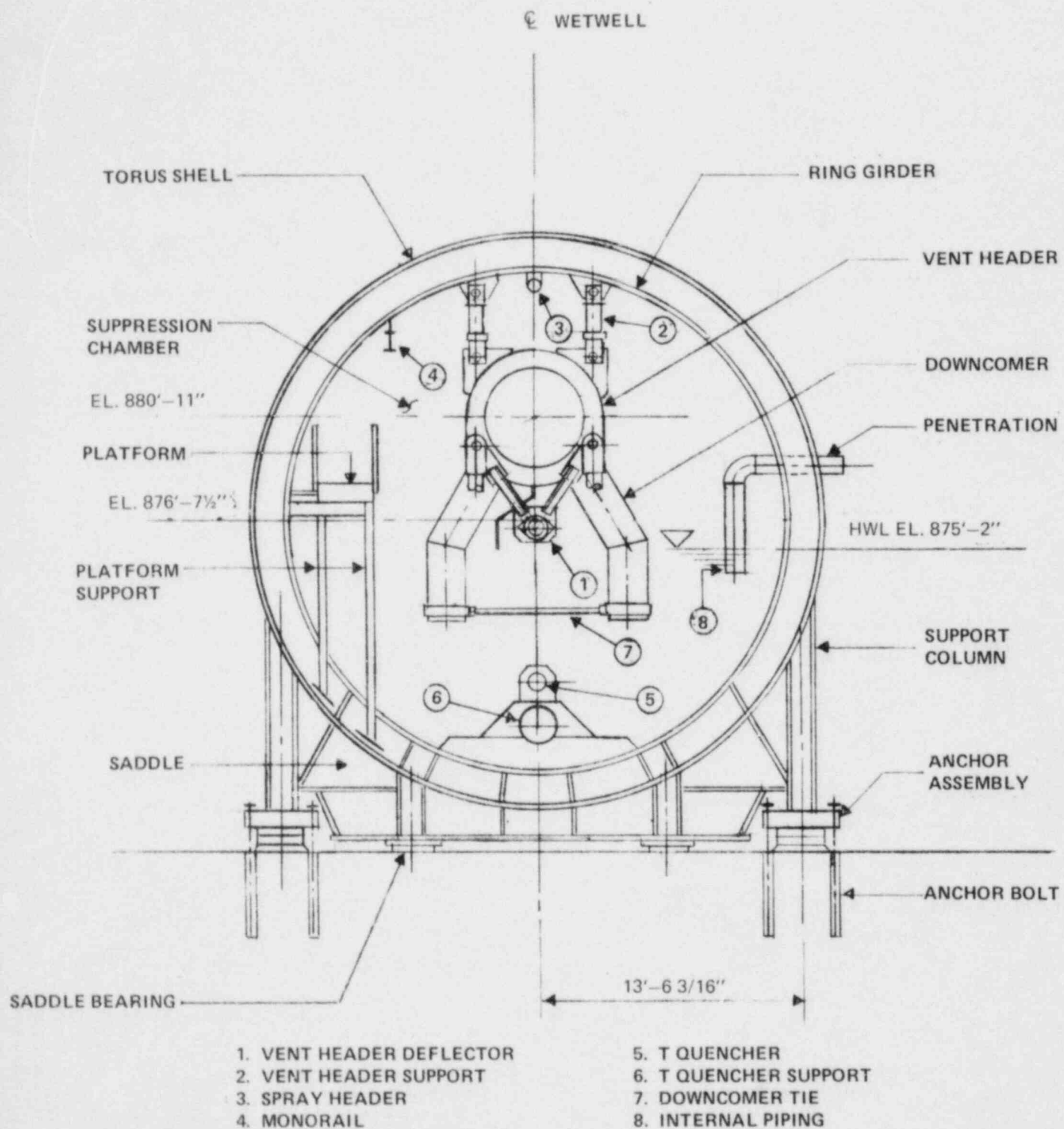


FIGURE 1.2  
CROSS SECTION - WETWELL



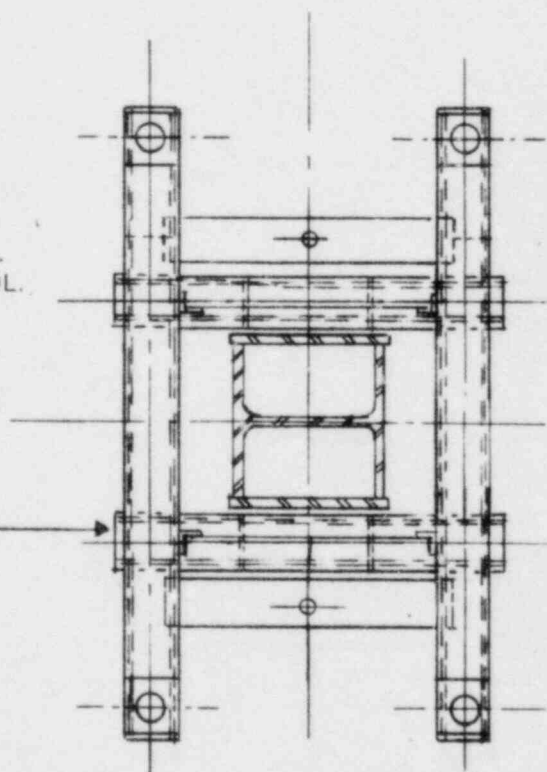
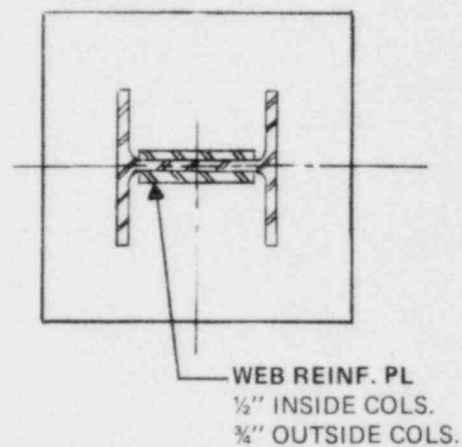
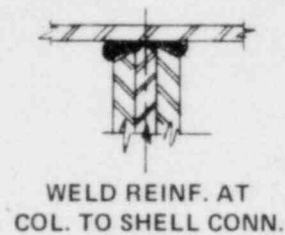
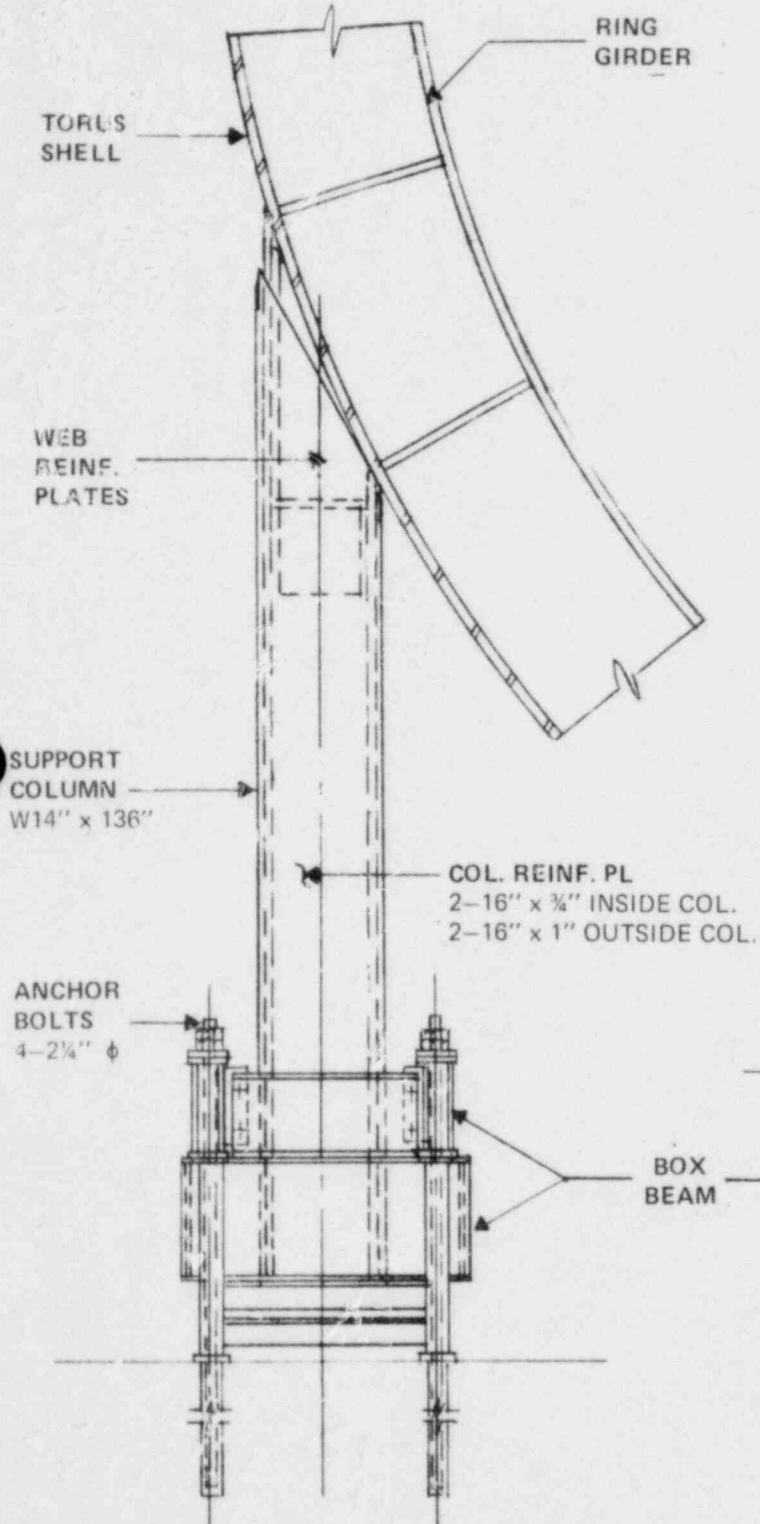


FIGURE 1.3  
TORUS SUPPORT COLUMN

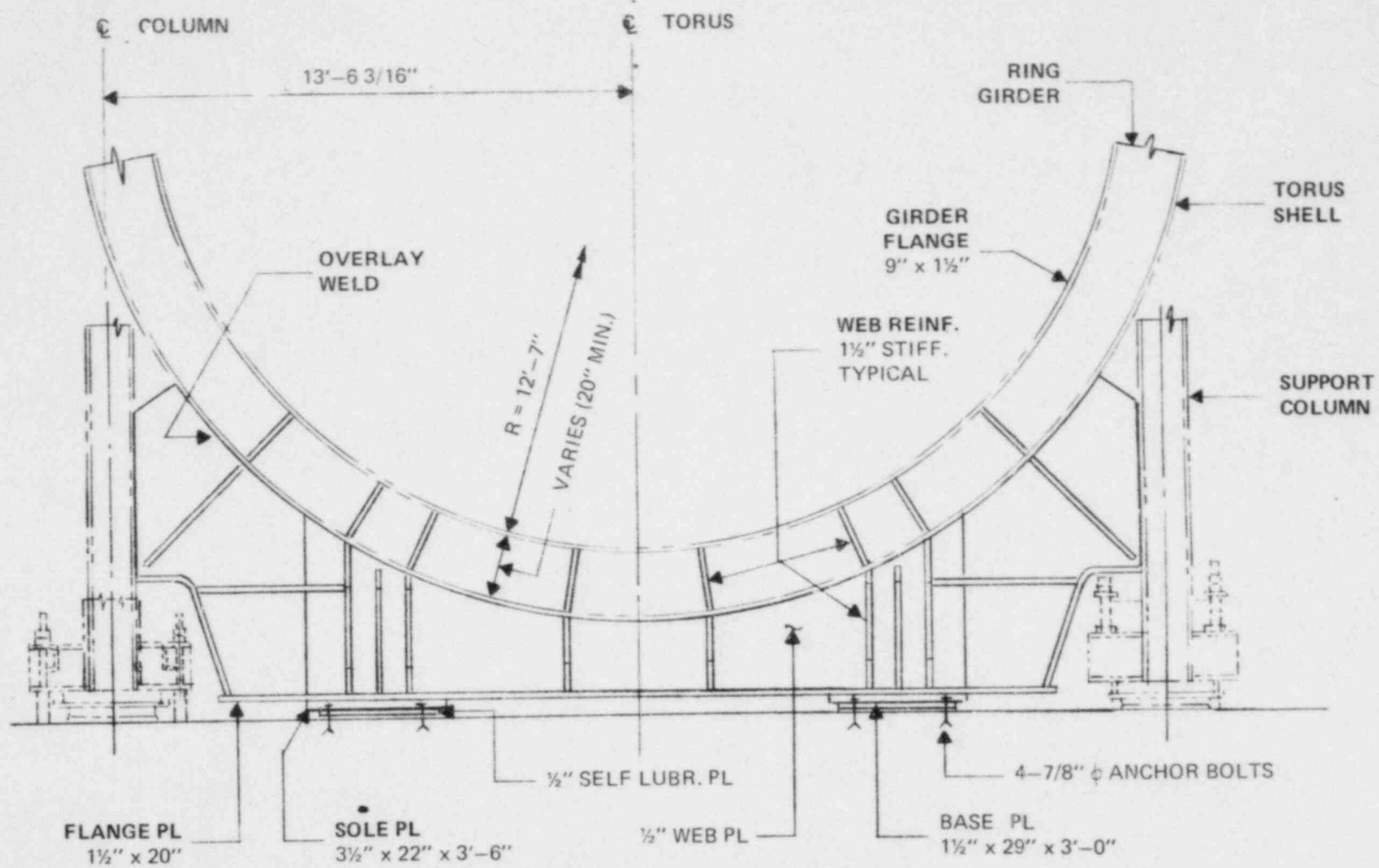


FIGURE 1.4  
 TORUS SADDLE

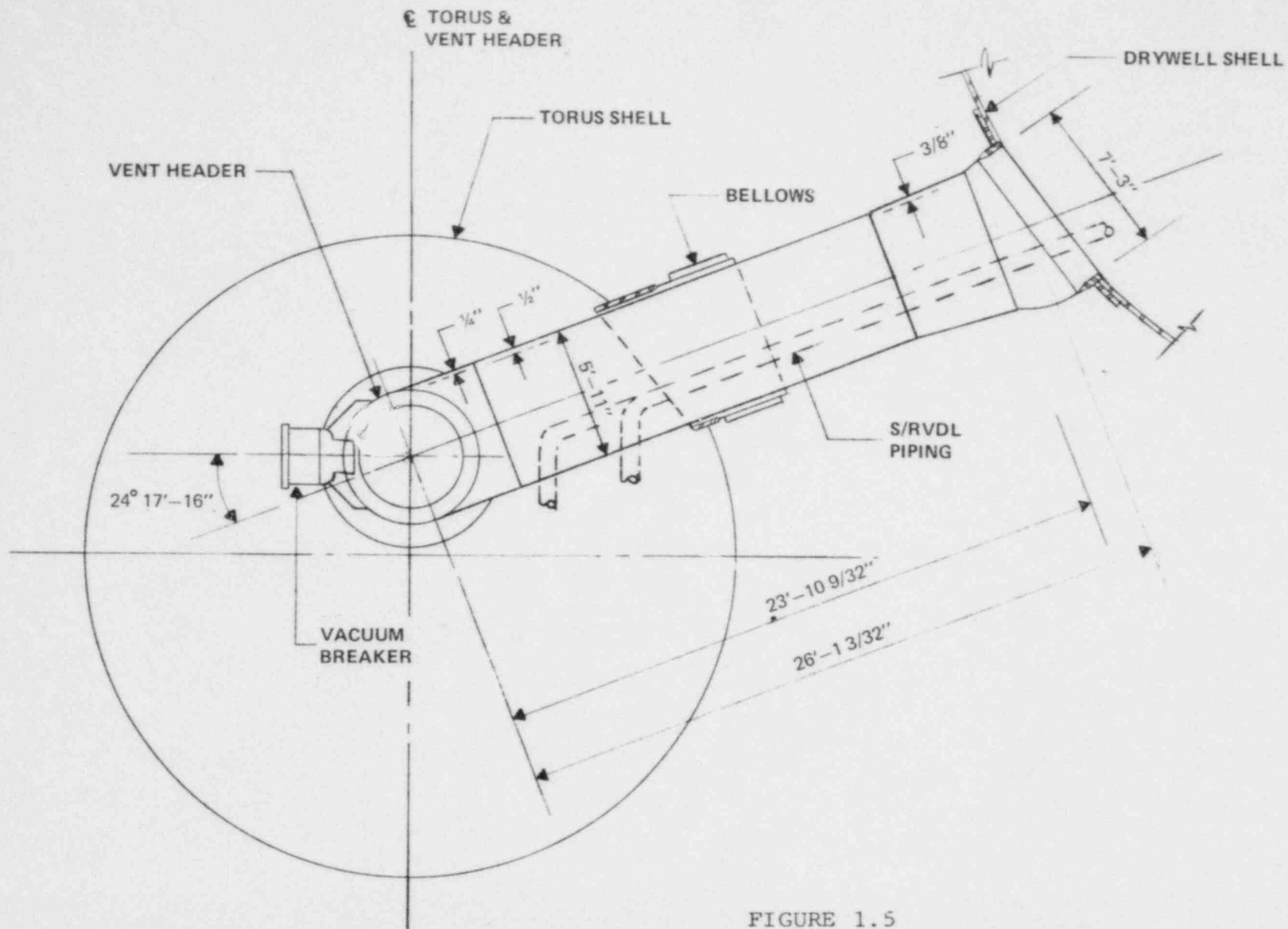


FIGURE 1.5  
 SECTION - VENT SYSTEM

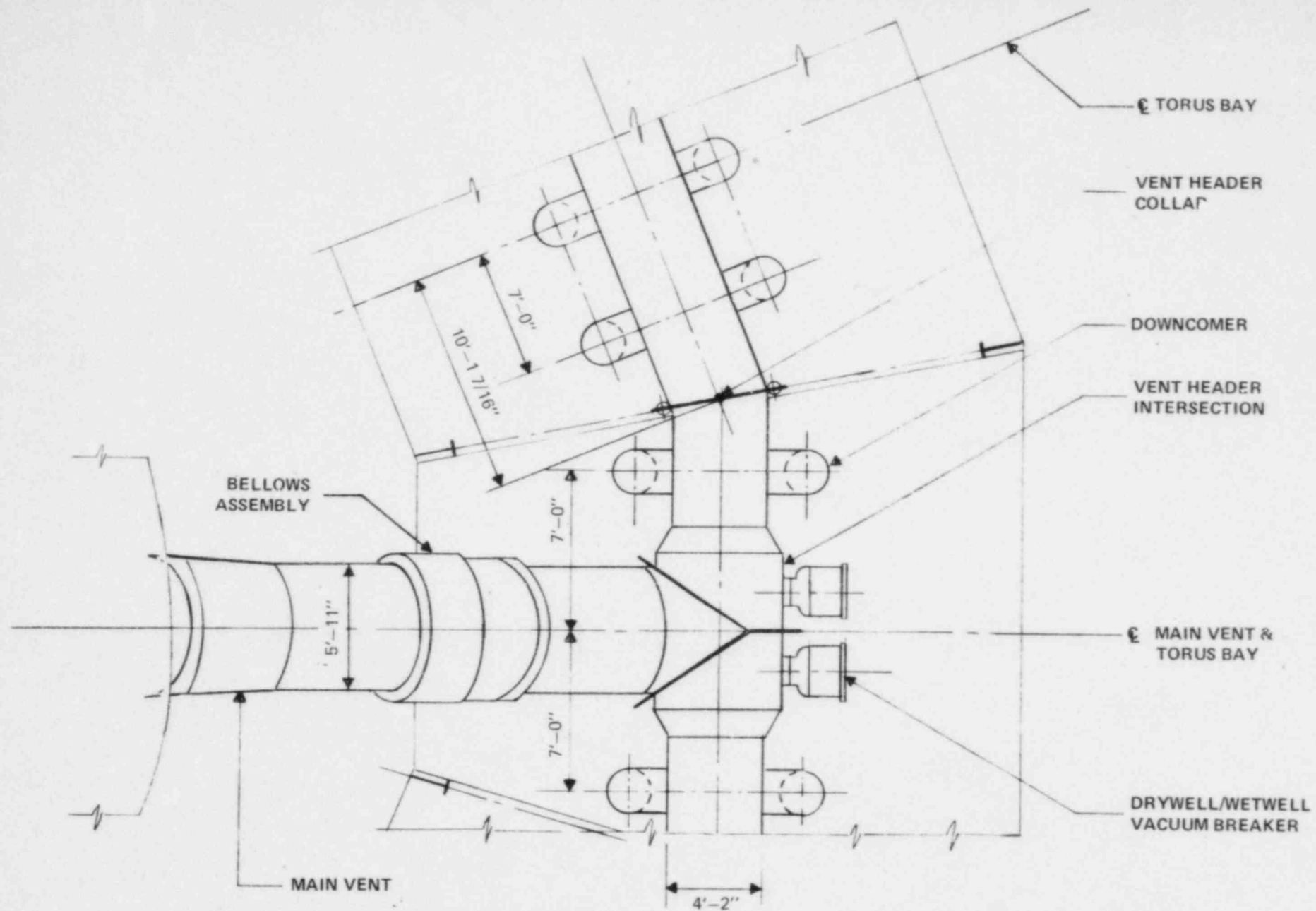


FIGURE 1.6

PARTIAL PLAN - VENT SYSTEM

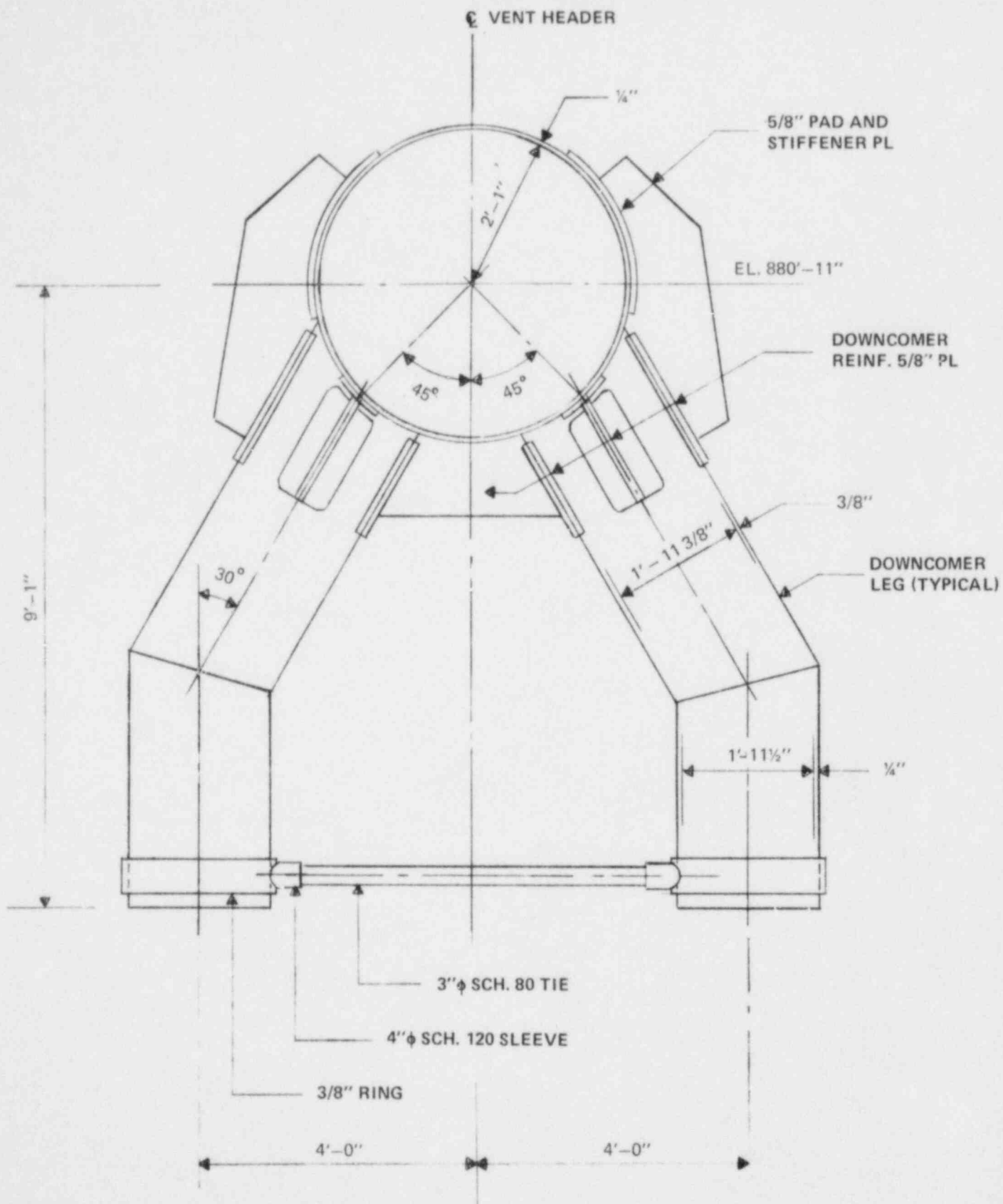


FIGURE 1.7

ELEVATION - DOWNCOMER REINFORCEMENT

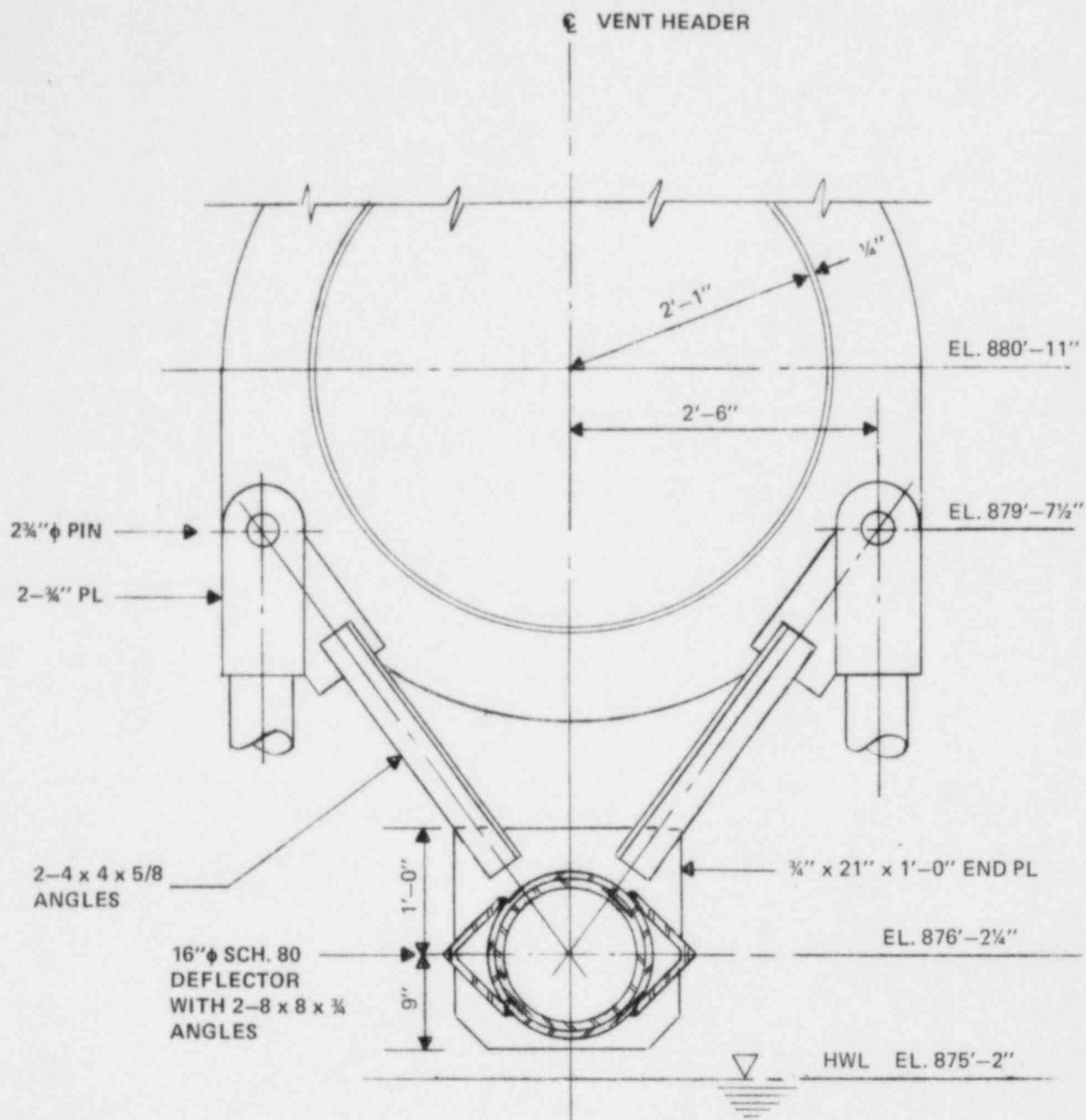


FIGURE 1.8

SECTION - VENT HEADER DEFLECTOR



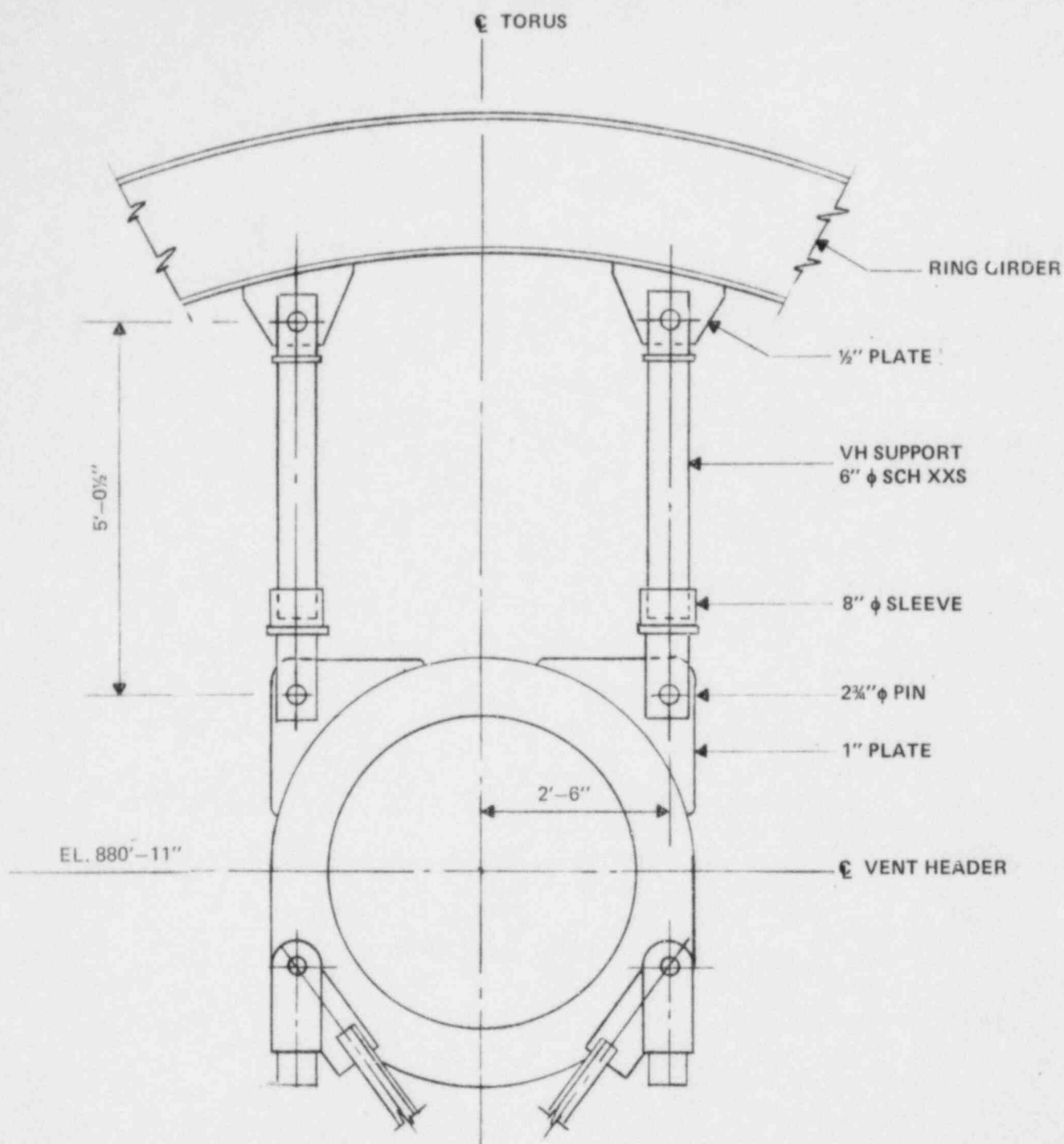


FIGURE 1.9

VENT HEADER SUPPORT COLUMNS

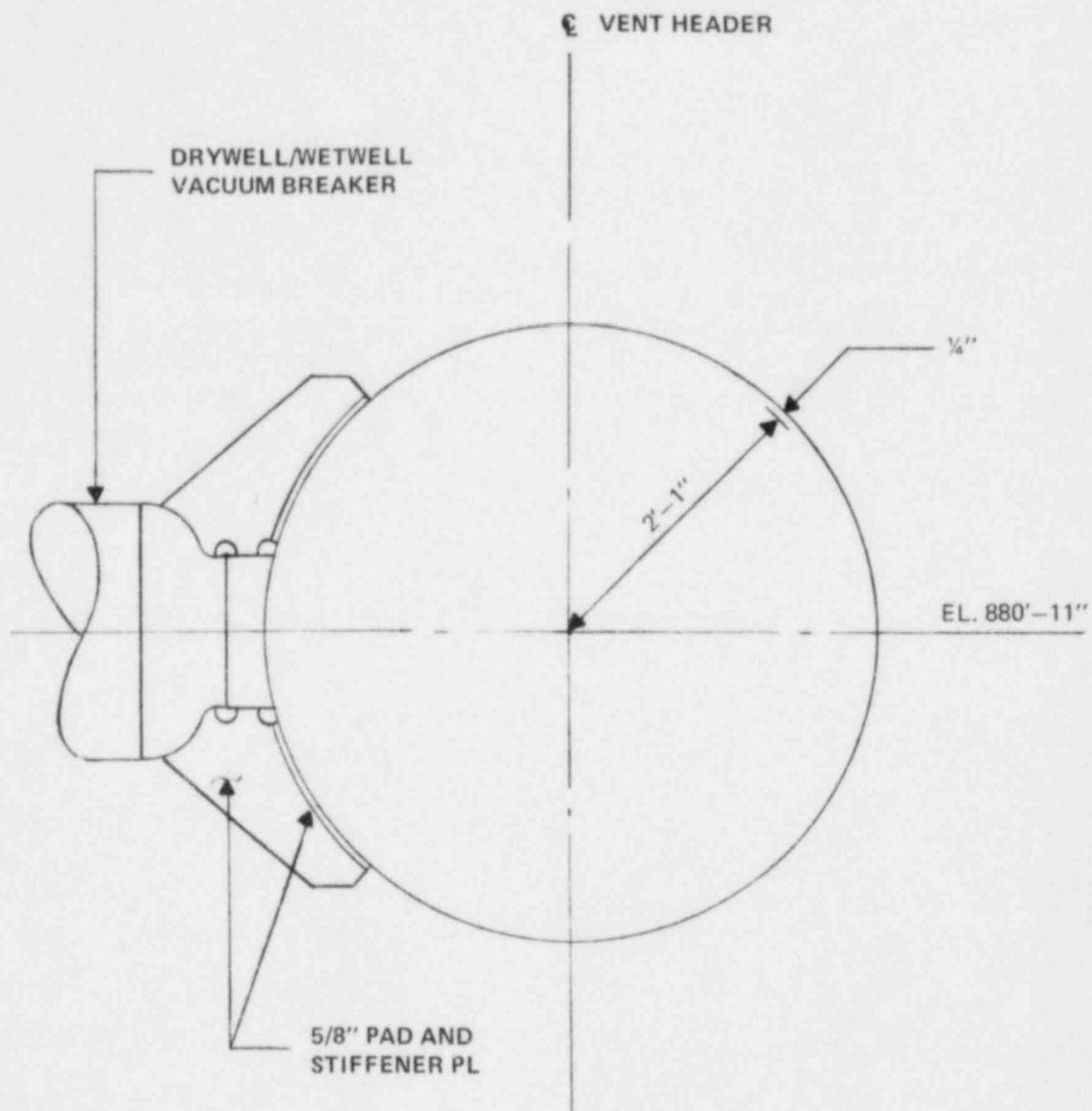


FIGURE 1.10  
 DRYWELL/WETWELL VACUUM BREAKER REINFORCEMENT

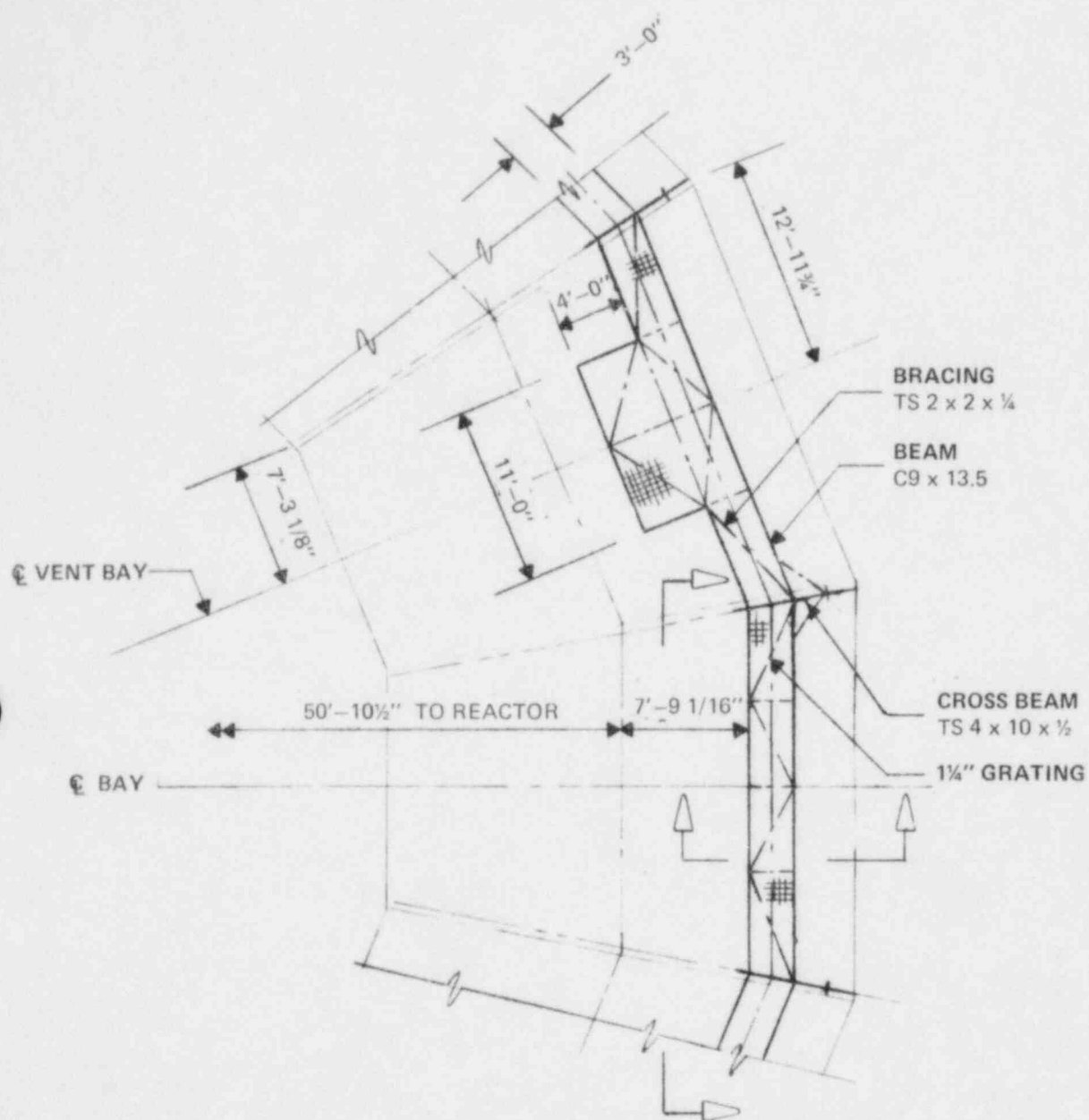


FIGURE 1.11

PLAN - SERVICE PLATFORM

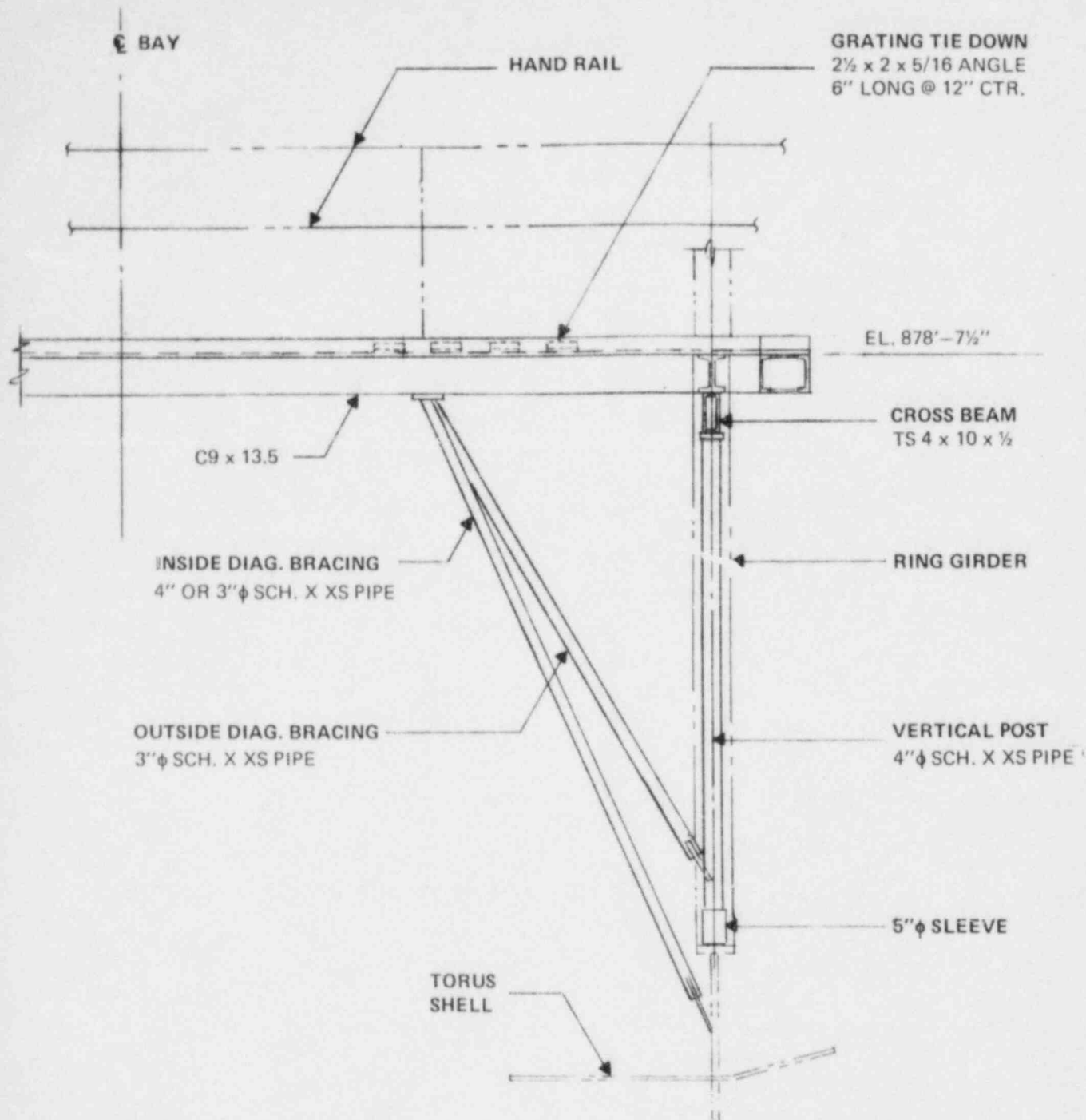


FIGURE 1.12  
 ELEVATION - SERVICE PLATFORM

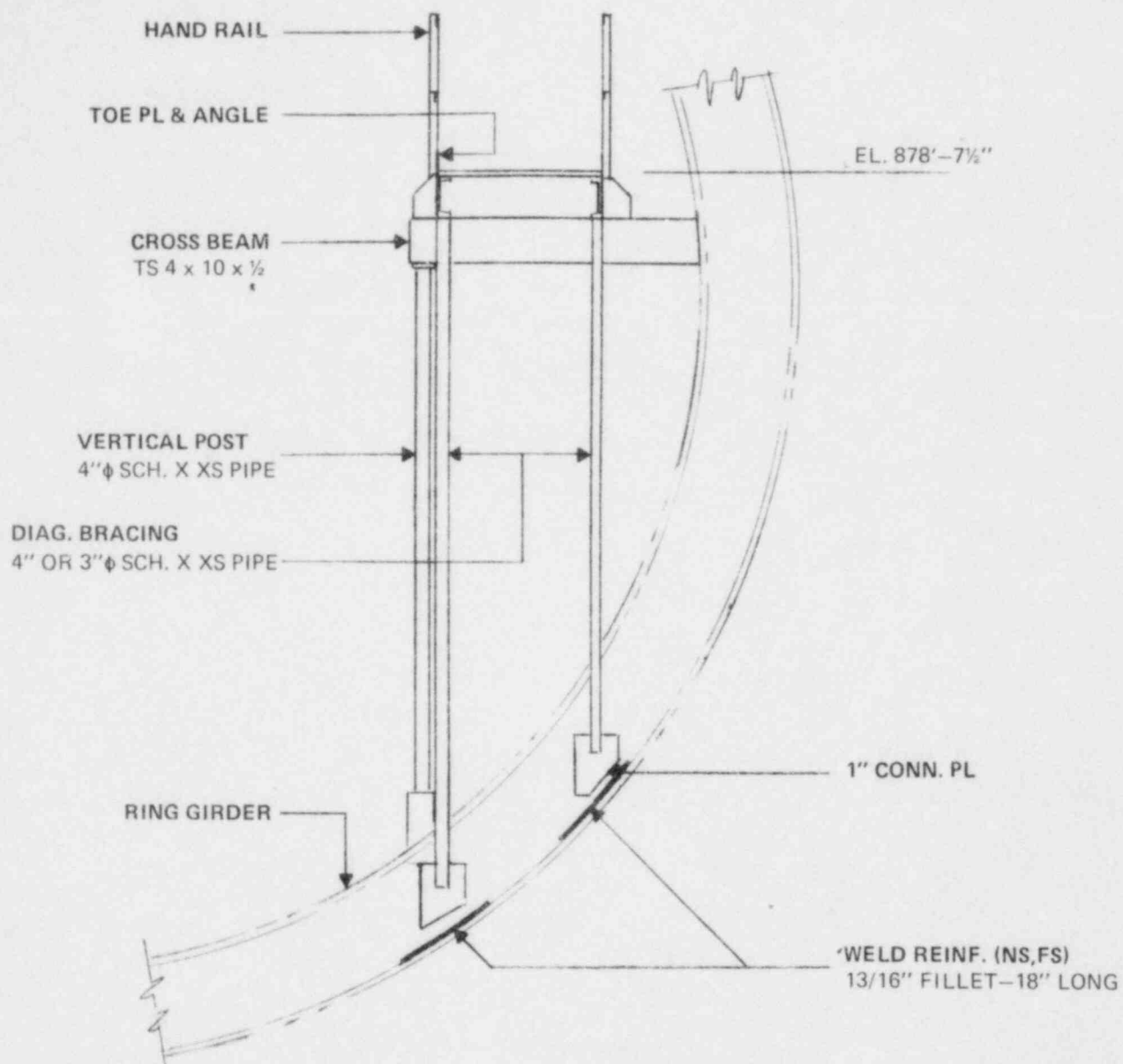


FIGURE 1.13

CROSS SECTION - SERVICE PLATFORM

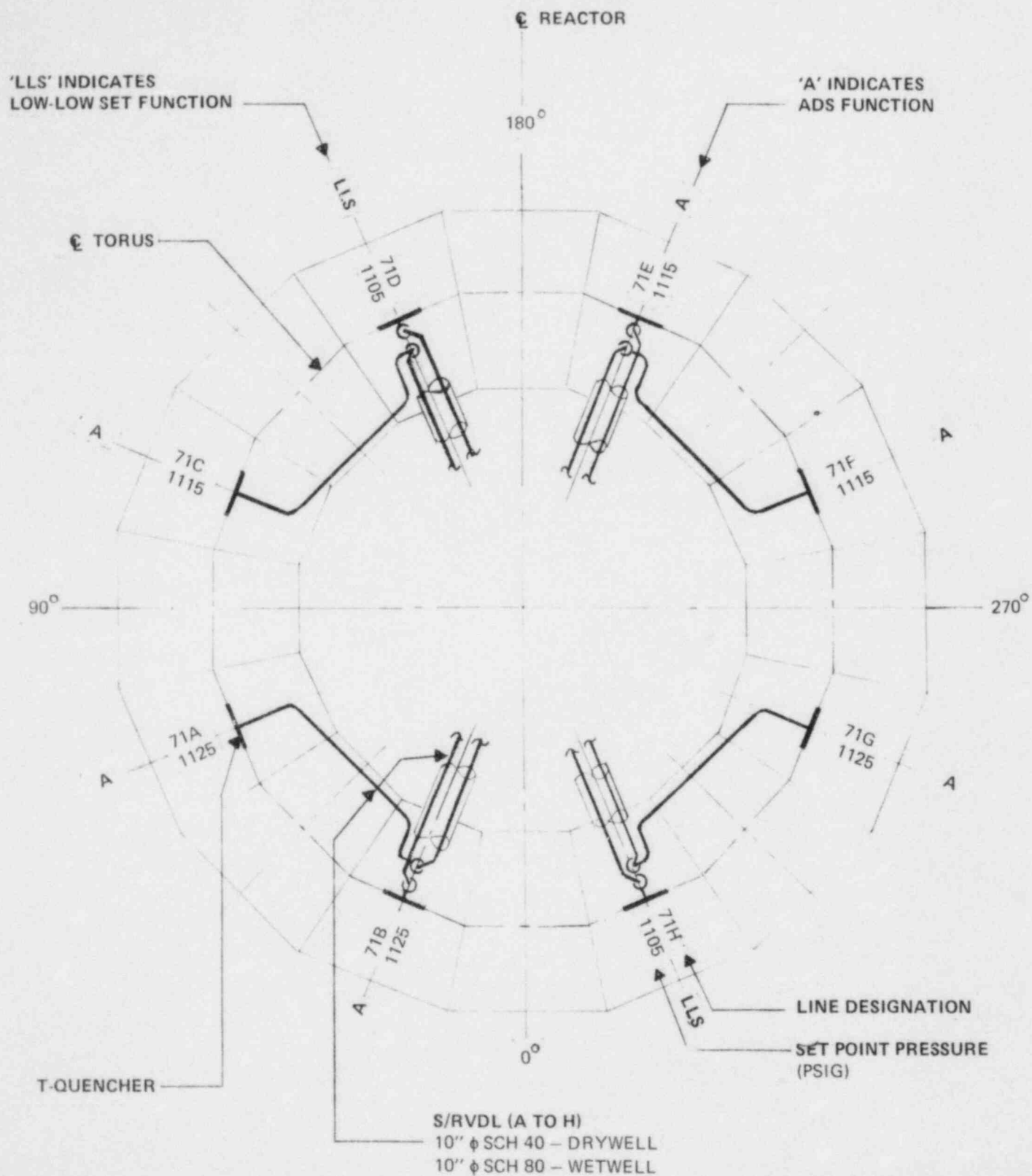


FIGURE 1.14

WETWELL ROUTING OF S/RVDLS



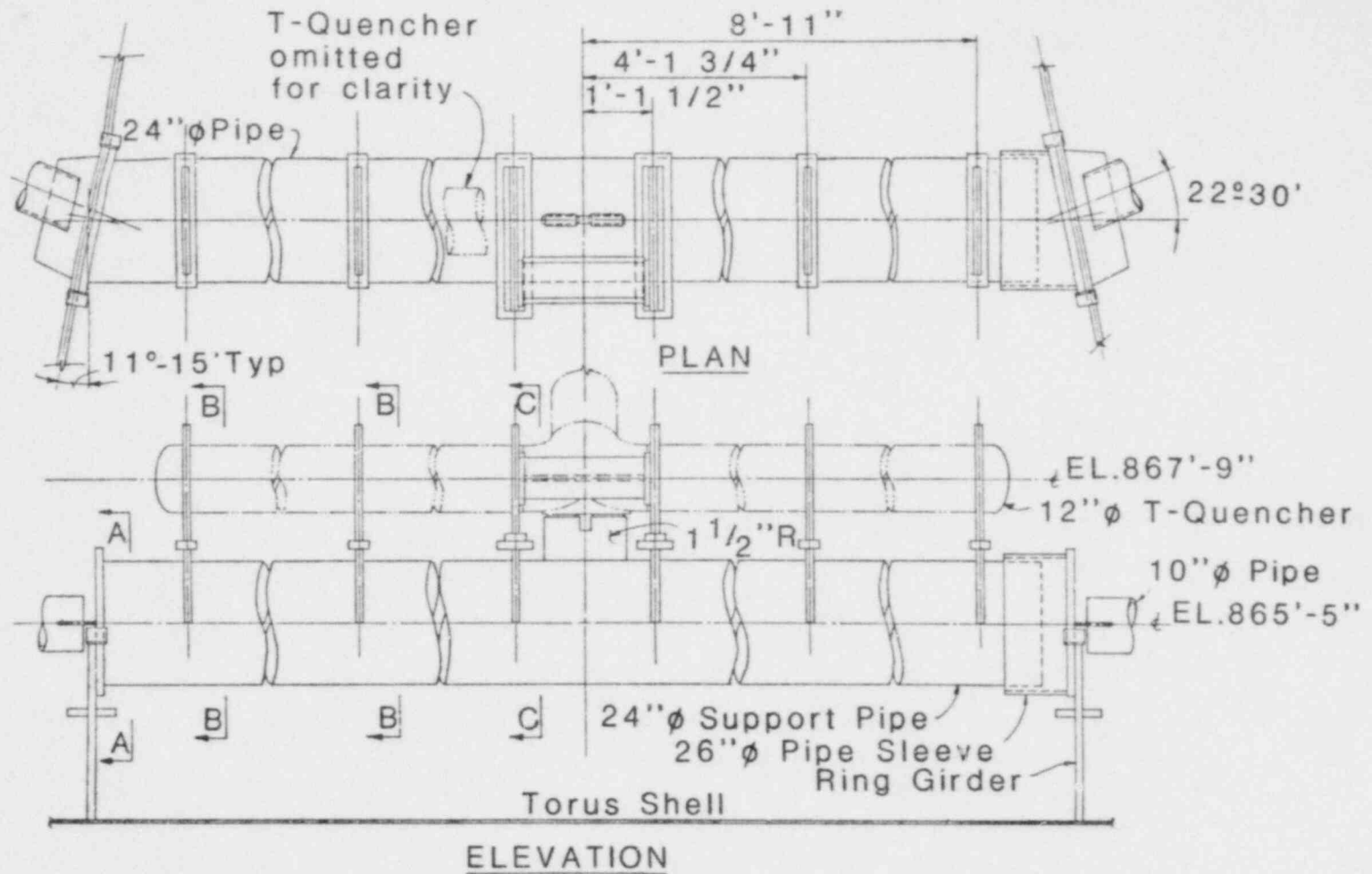


FIGURE 1.15

T-QUENCHER SUPPORT STRUCTURE

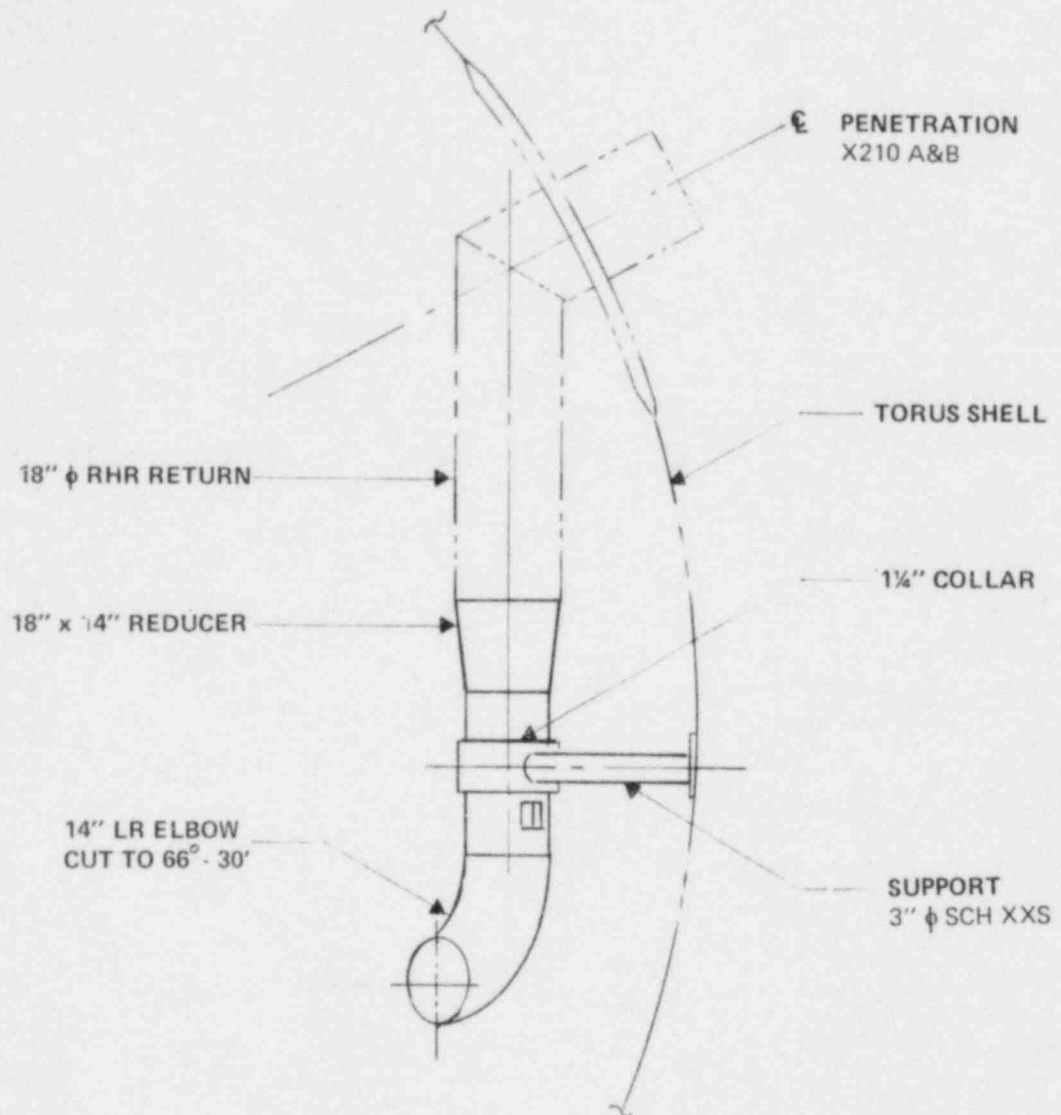


FIGURE 1.16

ELEVATION - RHR PUMP TEST RETURN LINE MODIFICATION

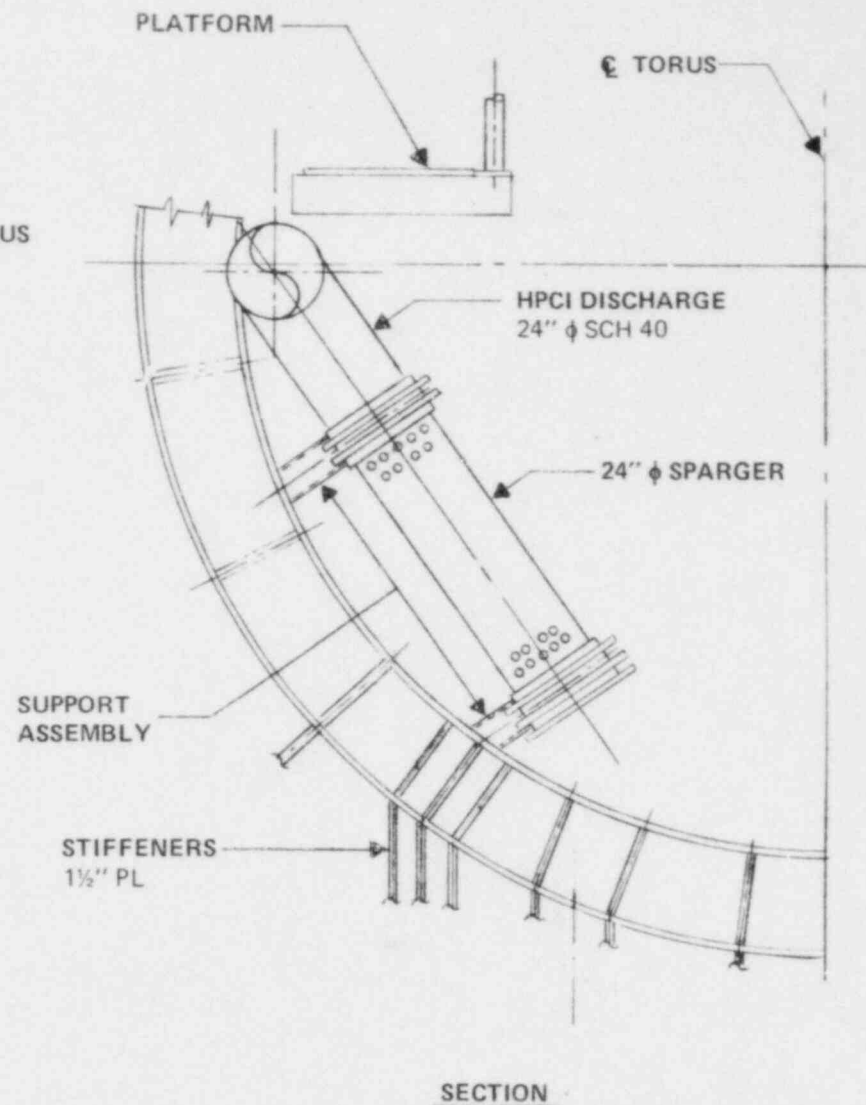
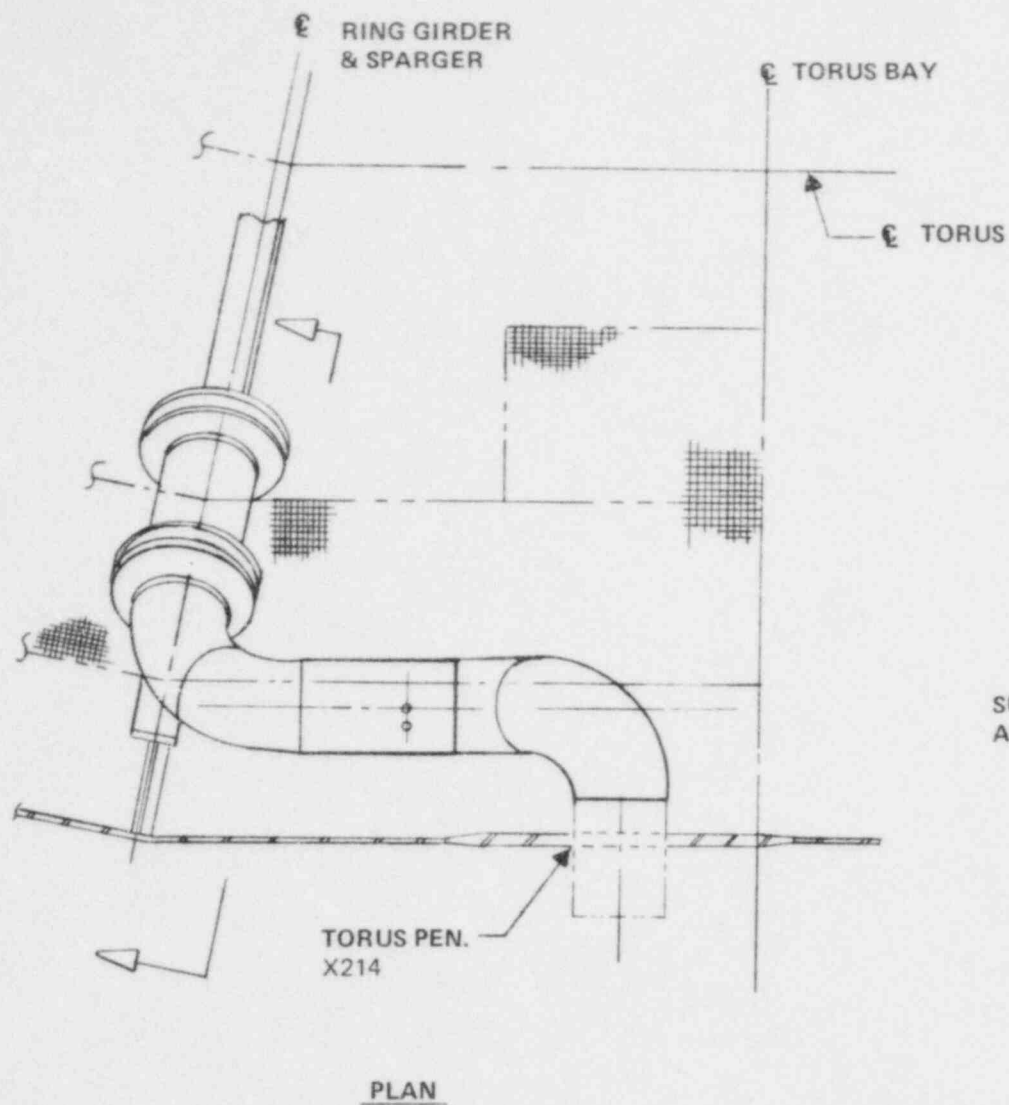
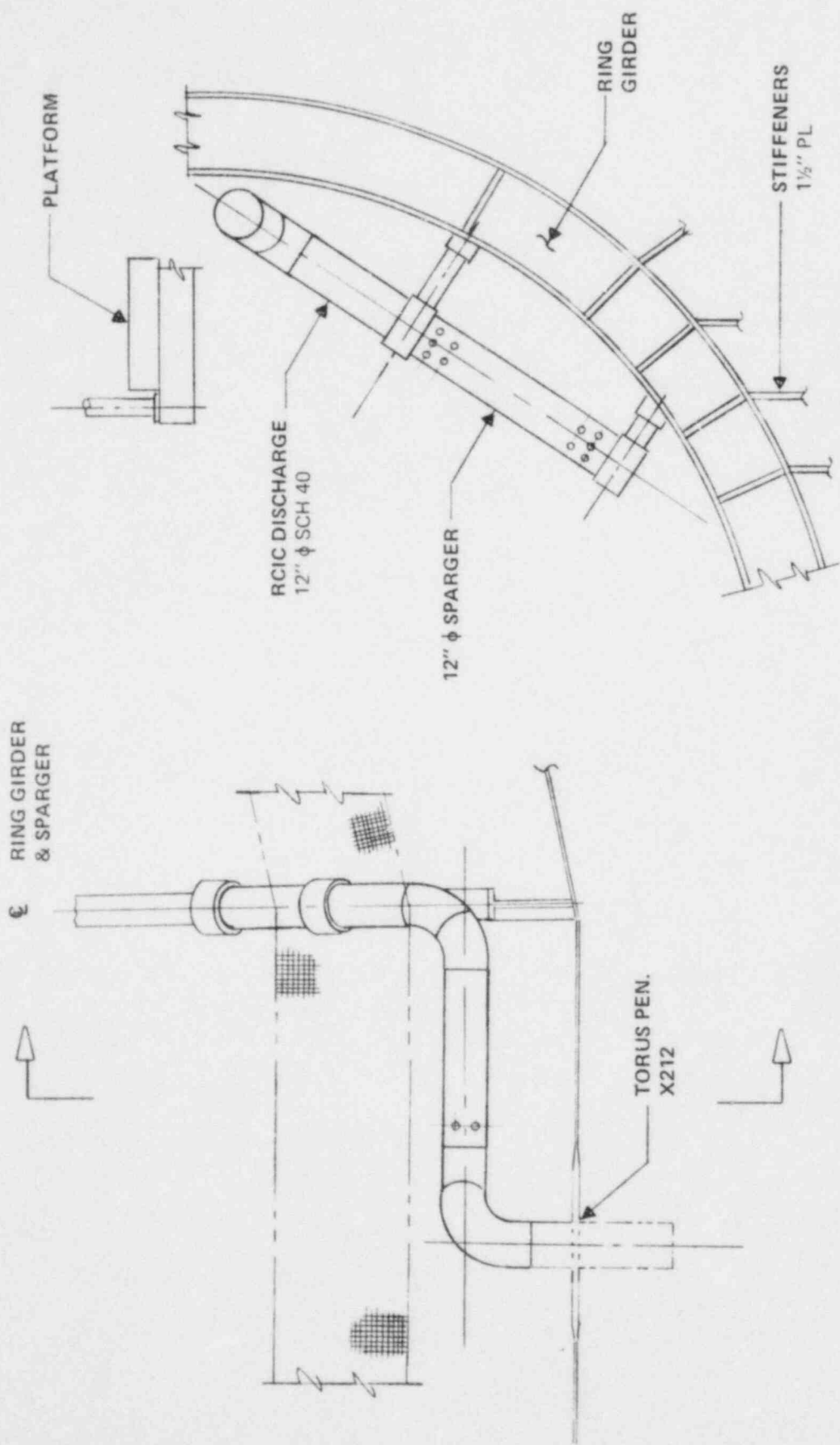


FIGURE 1.17

HPCI TURBINE EXHAUST - REROUTE RESUPPORT



SECTION

PLAN

FIGURE 1.18

RCIC TURBINE EXHAUST - REROUTE AND RESUPPORT

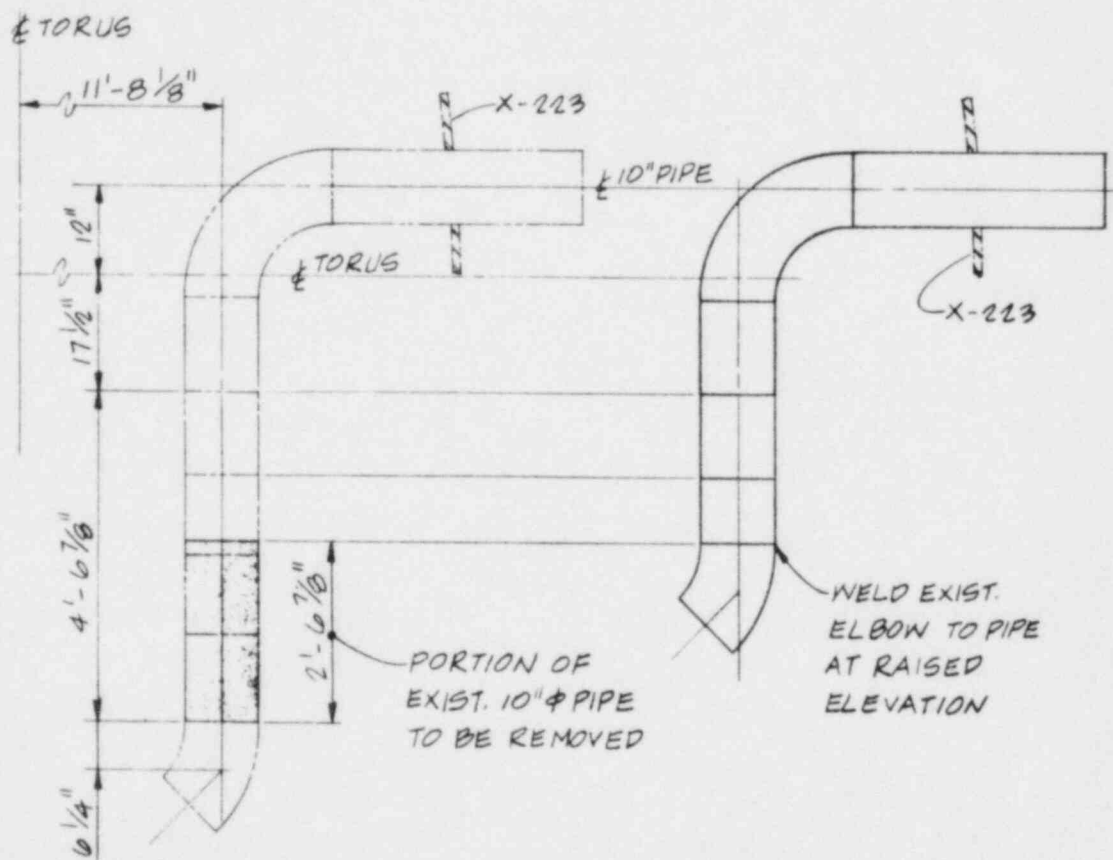


FIGURE 1.19

CORE SPRAY PUMP TEST RETURN TRUNCATION

COOPER NUCLEAR STATION

PLANT UNIQUE ANALYSIS REPORT

SECTION 2

LOADS AND LOAD COMBINATIONS



## 2.1 INTRODUCTION

This section describes the design loads and load combinations used in performing the Mark I containment reevaluation for Cooper Nuclear Station. These loads are determined using the criteria established in the NRC Safety Evaluation Report (SER) (Reference 11). These criteria are based on the General Electric Load Definition Report (LDR) for the Mark I program (Reference 17), the Mark I Containment Program Plant Unique Analysis Application Guide (PUAAG) (Reference 19), and the NRC Acceptance Criteria for the Mark I Containment Long-Term Program (Reference 18). The latest available revisions of each of these documents were used in determining design loads and load combinations.

The information in this section relates to the procedures used to apply the load definition criteria to plant unique thermal-hydraulic parameters and structural configurations at Cooper Nuclear Station. Where direct application of these criteria resulted in the need for excessive structural modifications, alternative criteria were developed. These alternative criteria are summarized in Subsection 1.2.2.2; justification is provided where appropriate in this section. Important results are summarized to indicate load magnitudes on selected structures.

This section is divided into a description of plant thermal-hydraulic parameters related to containment load definitions, design loads used in the original containment design, hydrodynamic loads associated with LOCA and S/RV discharge events, and load combinations used in the structural evaluations. All load definitions pertain to the final modified structural configurations.

## 2.2 PLANT THERMAL-HYDRAULIC PARAMETERS

Cooper Nuclear Station is a 778 Mwe boiling water reactor (BWR 4) with a Mark I containment system. Containment hydrodynamic data is summarized in Table 2.1.

CNS is currently operating with an initial drywell-to-wetwell pressure differential ( $\Delta p$ ) of 1.00 psid (nominal). However, all loads used in the containment structural evaluations are defined for both zero  $\Delta p$  and the current  $\Delta p$ . Structural evaluations are performed for the initial conditions associated with the higher loads.

The FSAR design temperature for the wetwell is 281°F. However, plant unique transient analyses have demonstrated that suppression pool temperatures remain below 200°F for all LOCA and S/RV discharge transients. Therefore, design temperature for the wetwell reevaluation was taken as 200°F.

The plant is equipped with eight pilot-operated Target Rock Safety/Relief Valves (S/RVs). The valves are divided into three groups according to the opening set points. The opening and closing set points for each valve are shown in Table 2.2. In addition to the safety and relief function, six of the eight S/RVs at CNS also serve as Automatic Depressurization System (ADS) valves. These valves are in all three groups. The ADS function for each S/RV is performed by a solenoid pilot valve connected to a 90-psi air supply. Electrical power for the ADS is supplied by two separate d-c power stations with switchover capabilities in case of loss of power. The ADS valves will actuate when the preset delay time expires after receiving a high drywell pressure signal and a low reactor water level signal (Level 1). The present delay time is nominally 120 seconds maximum.

The two Group I low-low set logic valves are indicated in Table 1.5 with their opening and closing set points. Low-low set logic and a reduced MSIV level trip set point are to be implemented as design changes to mitigate loads on the Mark I containment system (description provided in Section 1).

Each of the eight S/RVs at Cooper is connected to a discharge line (S/RVDL) which routes through the drywell, main vent, and into the

suppression pool. A T-quencher discharge device is located at the outlet in the suppression pool. Each S/RVDL is equipped with pressure sensors to detect S/RV opening. Two 10-in. diameter vacuum breakers are currently installed on each S/RVDL in the drywell close to the valve.

### 2.3 ORIGINAL DESIGN LOADS

Original design criteria for the containment system for normal operating and accident conditions included the following load cases:

- (1) Dead load of the vessel, attachments, and piping systems
- (2) Dead load of the suppression pool
- (3) Seismic: vertical and lateral loads
- (4) Design pressure (positive and negative)
- (5) Design temperature
- (6) Vent thrust loads
- (7) Jet forces on downcomer pipes.

For the structural reevaluation program, the first three load cases (dead loads and seismic) are considered with the newly defined loads. The remaining four load cases have been redefined in the GE LDR.

Seismic loads on containment system components are taken from the Cooper Station FSAR (Reference 16). Seismic loads are defined in the vertical and lateral directions for Operating Basis Earthquake (OBE) and Safe Shutdown Earthquake (SSE).

## 2.4 LOCA-RELATED LOADS

This subsection describes the loads on structures in the wetwell and vent system during a postulated LOCA. In the event of a postulated LOCA, reactor steam and water would expand into the drywell atmosphere. Three categories of a LOCA are considered:

- Design Basis Accident (DBA)
- Intermediate Break Accident (IBA)
- Small Break Accident (SBA).

The limiting loads for a particular containment component can be generated by combinations involving one of these categories and other containment loads. A detailed description of each category is provided in the LDR. A summary description is given below:

### (1) Design Basis Accident

The design basis accident for a Mark I BWR is the instantaneous double-ended guillotine break of the recirculation pump suction line at the reactor vessel. This break results in the maximum flow rate of primary system fluid and energy into the drywell, through the vent system and into the suppression chamber (wetwell). The event sequence is divided into three phases, which are identified as follows:

- (a) Pool Swell, results from the air in the vent system being forced into the suppression pool at a sufficiently high rate that the upper water volume of the pool is displaced upward, later falling back to its original position;
- (b) Condensation Oscillation, results from a steam or a steam-and-air mixture flowing through the vent system

at a high rate, and forming discharge bubbles at the end of the downcomers which oscillate in size and pressure;

- (c) Chugging, is a result of intermittent flow of nearly pure steam through the downcomer exits and into the suppression pool, forming large bubbles which expand and then rapidly collapse.

At the end of the LOCA, when ECCS water spills out of the break and rapidly reduces the drywell pressure, the suppression chamber is vented to the drywell through vacuum breakers to equalize the pressure between the two vessels. The ECCS cools the reactor core and transports the heat to the water in the suppression chamber, thus providing a continuous path for the removal of decay heat from the primary system.

## (2) Intermediate Break Accident

The intermediate break accident (IBA) for a Mark I BWR is defined to be a liquid break equal to  $0.1 \text{ ft}^2$ . This break is large enough such that the High Pressure Coolant Injection System (HPCI) cannot maintain the coolant level in the reactor vessel, but the reactor pressure is not substantially reduced. The break is of sufficient magnitude that operation of the ADS will occur soon after the break and will result in reactor depressurization.

Following the break, the drywell pressure transient is sufficiently slow that the clearing of air from the vent system does not lead to pool swell. As the flow of air, steam, and water continues from the drywell to the wetwell, the wetwell airspace pressure increases. Following the purge of air from the drywell, the flow through the vent system becomes steam, which is quenched in the pool.



The initiation of the ADS vents steam from the reactor vessel directly into the suppression pool through the S/RVDL. ADS operation continues until the reactor vessel is depressurized. The energy added to the pool via the ADS results in a heating of the suppression pool and a small additional increase in wetwell and drywell pressure. When the reactor is sufficiently depressurized such that the low-pressure ECCS water floods the vessel, liquid spills out the break and condenses steam in the drywell. This causes the drywell-to-wetwell vacuum breakers to open and equalizes the drywell and wetwell pressures.

(3) Small Break Accident

The small break accident (SBA) for a Mark I BWR is defined to be a  $0.01 \text{ ft}^2$  steam break in the primary system. Following the break, the drywell pressure slowly increases, depressing the water level in the vents until drywell air and steam pass to the suppression pool. The steam is condensed and the air rises to the free airspace, resulting in wetwell pressurization. Flow through the vent system and into the pool is sufficiently slow that no significant bubble or fluid dynamic loading occurs. At 10 minutes after the break, the operator initiates the ADS, allowing primary system fluid to flow directly to the pool. When the reactor pressure is sufficiently low, the ECCS is used to circulate suppression pool water into the reactor and cool the pool water.

The sequencing of the LOCA phenomena for each category, and the duration of each LOCA phenomenon, is provided in Subsection 2.7.

2.4.1 Containment System Pressure and Temperature Response

Containment pressure and temperature transients for each LOCA category were taken from the Plant Unique Load Definition (PULD)



for CNS (Reference 22). The procedure used to determine these transients is given in the LDR and has previously been reviewed by the NRC in the Safety Evaluation Report.

#### 2.4.1.1 Design Basis Accident

Initial conditions for evaluating DBA drywell and wetwell pressure and temperature transients are shown in Table 2.3. Transients were determined for both  $\Delta p=0$  and  $\Delta p=1.0$  psid. The initial conditions maximize the initial drywell pressurization rate and the vent system thrust loads. To utilize a bounding wetwell pressure response, 1.0 psi was added to the calculated pressure transient for the time period less than 30 seconds, and 2.0 psi was added to the wetwell pressure calculated at 30 seconds for the time period beyond 30 seconds.

Figures 2.1 and 2.2 show the DBA pressure and temperature transients (prior to being corrected for bounding wetwell pressure response) for initial condition  $\Delta p=1$  psid.

#### 2.4.1.2 Intermediate Break Accident

Initial conditions for evaluating IBA drywell and wetwell pressure and temperature transients are shown in Table 2.4. Figures 2.3 and 2.4 show the IBA pressure and temperature transients for initial condition  $\Delta p=1$  psid. Reducing the initial drywell-to-wetwell  $\Delta p$  produces insignificant changes in the transients. Peak containment pressures, containment temperatures at the end of reactor pressure vessel (RPV) blowdown, and containment pressures and temperatures at the time of ADS initiation are identified on the figures.

#### 2.4.1.3 Small Break Accident

Initial conditions for evaluating SBA containment transients are the same as those used for the IBA transients (Table 2.4). SBA transients are insensitive to  $\Delta p$ ; no significant changes are observed for  $\Delta p=0$ .

Figures 2.5 and 2.6 show the SBA pressure and temperature transients. Peak containment pressures, containment temperatures at the end of RPV blowdown, and containment pressures and temperatures at the time of ADS initiation are identified on the figures.

#### 2.4.2 Vent System Thrust Loads

Vent system thrust loads were defined for DBA conditions only. These conditions involve the most rapid pressurization of the containment system, the largest vent system mass flow rate, and, therefore, the most severe vent system thrust loads.

##### 2.4.2.1 Analysis Methods and Results

The procedure for evaluating vent system thrust loads is described in Section 4.2 of the LDR. The procedure uses thrust equations which consider forces due to both pressure distribution and momentum, to define horizontal and vertical thrust forces on the main vents, vent header, and downcomers as shown in Figure 2.7.

Initial conditions are the same as those used to predict DBA containment transients (Table 2.3). Analyses were performed for the bounding case of  $\Delta p = 0$ . The transients were taken from the PULD and are shown in Figures 2.8 to 2.10.

##### 2.4.2.2 Load Application

The horizontal and vertical main vent thrust transients shown in Figure 2.8 represent the resolution of the thrust loads which act on the end cap of the main vent. This loading is actually distributed over the end cap area.

The vertical and horizontal vent header thrust transients shown in Figure 2.9 represent the vent header loading per miter joint. Vertical loading is due to the contributions of individual downcomer pairs, which were assumed to be equal.

The horizontal and vertical thrust transients shown in Figure 2.10 are loads for a single downcomer, and are the resultant forces due to a change in momentum of the flow through the downcomer miter joint.

Total vertical thrust loads and net vertical thrust loads exist for the entire vent system and are defined as follows:

$F_{1VT}$  = Main vent end cap vertical force multiplied by the number of main vents.

$F_{2VT}$  = Vent header vertical force per miter joint, multiplied by the number of vent header miter joints.

$F_{3VT}$  = Downcomer miter joint vertical force multiplied by the number of downcomers.

$F_{NETV} = F_{1VT} + F_{2VT} + F_{3VT}$

Figure 2.11 shows the total net vertical thrust loads over a time period of 30 seconds.

#### 2.4.3 Loads Associated with Pool Swell

Immediately following a postulated DBA rupture, the pressure rapidly increases in the drywell and vent system, resulting in the water leg in the downcomers being injected into the suppression pool. When this clearing process is completed, the air behind the downcomer water slug produces a bubble at the end of the downcomer. The water above the bubble is accelerated upward as the bubble expands. As the bubble expansion continues, the pool water rises in the torus and compresses the airspace above the pool surface. Eventually, the bubble "breaks through" to the torus airspace, and the displaced pool liquid settles back to its original level.

Pool swell phenomena are associated only with a DBA event. Loads are generated on the torus shell boundary and all containment components located within the torus. Plant unique loads associated with pool swell are described in this section.

#### 2.4.3.1 Torus Net Vertical Loads

In the postulated LOCA-DBA event, the downcomer air, which is initially at drywell pressure, is injected into the suppression pool, producing a downward reaction force on the torus. The subsequent bubble expansion causes the pool water to swell in the torus, compressing the airspace above the pool and producing an upward reaction force on the torus. These vertical loads create a dynamic imbalance of forces on the torus, which act in addition to the weight of the water into the torus.

The torus net vertical dynamic loads are defined as load time histories. The static loads (i.e., water and structural weights) are not included in these load histories. The net dynamic load is defined as an equivalent pressure acting on the projected plan area of the torus.

The torus net vertical loads, based on plant-specific Quarter Scale Test Facility (QSTF) data, are determined by spatial integration of the pressure transducers located on the QSTF torus shell. These load histories are corrected for water mass inertia. The assumptions used in modeling the actual plant in the QSTF facility and calculation of net torus load histories are given in Section 4.3.1 of the LDR.

The net torus load history for  $\Delta p=0$  is given in Figure 2.12. This transient is taken from the PULD.

In accordance with Section 2.3 of the NRC Acceptance Criteria, the following margins were applied to each loading phase:

$$UP = UP_{mean} + 0.215 (UP_{mean})$$

$$DOWN = DOWN_{mean} + 2 \times 10^{-5} (DOWN_{mean})^2$$

Where "UP" and "DOWN" indicate the peak upward and peak downward torus net vertical pressures (in lbf) with the additional NRC margins included, and "mean" refers to the average of QSTF test results (lbf). These margins were applied to the QSTF "mean" load function prior to scaling the load function to full-scale equivalent conditions. The margin for the downward loading function was derived in terms of a fraction of the load at the time of the peak downward load, and that fraction was applied to the entire downward loading phase.

The pool swell transient with the margins applied is shown in Figure 2.13 for  $\Delta p=0$ .

The plant unique QSTF test series for pool swell showed that the net vertical upforce applied to the torus exceeded the weight of the torus and its contents, and a net upward pressure was measured. To evaluate this event, it was necessary to account for the reduction in pool mass due to the mass of water "in flight" at the time of maximum upforce on the torus. The reduced pool mass does not affect the torus forces presented above, since these were referenced to the full water weight. The effective mass simply provides an estimate of the vertical inertial force resisting upward displacement of the torus.

From the QSTF test data, the resultant weight fraction of the pool in flight was found to be 59% for  $\Delta p=0$  psid.

All torus shell evaluations were performed for the initial condition  $\Delta p=0$ . The analyses are therefore conservative since they take



no credit for the mitigating effects of the drywell-to-wetwell pressure differential.

#### 2.4.3.2 Torus Shell Pressure Histories

Torus shell structural evaluations were performed using local torus shell pressure time histories. When integrated over the torus shell inside surface, these local pressure transients result in the net torus vertical load due to pool swell. Torus shell pressure histories were obtained from the CNS PULD based on plant unique QSTF tests with  $\Delta p=0$ . Pressure histories for the wetted portion of the shell and the airspace are shown in Figures 2.14 and 2.15, respectively. The initial static pressure was subtracted so that only the dynamic pressure histories are shown.

In accordance with the NRC Acceptance Criteria, these averaged submerged and airspace pressure histories were modified to contain specified margins for the torus net vertical downward and upward loading phases. Figures 2.14 and 2.15 include this modification.

The pool swell airspace pressure transients shown in Figure 2.15 are the same at all points on the unwetted portion of the torus shell. The submerged pressure history transients in Figure 2.14, however, vary along the longitudinal and circumferential directions. The longitudinal variation of the average submerged pressure is based on 1/12 scale, three-dimensional (3-D) test results (Section 4.3.2.2 of the LDR), and the circumferential variation is based on 1/4 scale, two-dimensional (2-D) test results. These variations are given as multipliers to be applied to the average submerged pressure histories.

#### 2.4.3.3 Impact, Drag, and Fallback Loads

During the LOCA-DBA pool swell transient, the rising pool will impact structures above the initial pool surface. As the pool surface rises and impacts the structures, loads are generated due



to both the impact and drag. The timing and amplitude of the loading on a particular structure depends on the velocity of the pool surface as it impacts and flows past the structure.

Following the pool swell transient, the pool water falls back to its original level, and in the process generates fallback loads on structures inside the torus which are located between the maximum bulk pool swell height and the downcomer exit level. The fallback load starts as soon as the pool swell reaches its maximum height and ends when the pool surface falls past the structure of concern.

#### 2.4.3.3.1 Vent System

The load definition for the vent system impact and drag is specified in a different form for each of the three major components of the vent system, e.g., the main vent, vent header, and downcomers.

The CNS plant unique, quarter-scale 2-D pool swell tests, the EPRI impact data, and the 1/12 scale, 3-D test data provide the primary basis for the vent system impact and drag load definition. Vent system loads are provided in the PULD. Loads associated with  $\Delta p=0$  initial condition were used in the structural evaluations, with the exception of the main vent impact and drag loads where the bounding initial condition of  $\Delta p=1$  psid was used.

##### (1) Downcomers

The impact and drag loading on the downcomers was generically defined from the 1/4 scale tests. The downcomer pressure transient with an amplitude of 8.0 psid as defined in the LDR is to be applied uniformly over the bottom 50° sector of the angled portion of the downcomer perpendicular to the local downcomer surface. The impact pressure transient begins as soon as the rising pool reaches the lower end of the angled portion of the downcomer (0.20 sec), and ends at the time of maximum pool swell (0.72 sec).

(2) Vent Header

The local impact and drag pressure transients were obtained from the QSTF measured impact and drag pressures. The general form of the vent header local impact and drag pressure transient is a triangular pulse load with a duration of approximately 0.1 sec.

The impact and drag pressure transient corresponds to an average downcomer spacing impact and drag velocity. Since the impact and drag velocity varies along the length of the vent header, the local impact and drag pressure transients are adjusted for impact and drag velocity.

Impact and drag pressure transients were developed for CNS at the vent header locations shown in Figure 2.16. The maximum pressure is 17.7 psi at 60° from bottom dead center and at a longitudinal location  $z/l$  of 0.92.

(3) Main Vent

Main vent impact and drag loads were determined using the QSTF results and the procedure outlined in Section 4.3.3.2 of the LDR. A three-foot section of the main vent experiences impact and drag loads. The net impact load transient is shown in Figure 2.17.

2.4.3.3.2 Vent Header Deflector

The pool swell load transient for the vent header deflector is provided in the PULD based on QSTF measured impact and drag loads. This transient is shown in Figure 2.18 for the bounding case of  $\Delta p=0$ .

#### 2.4.3.3.3 Other Structures Above the Pool

Impact, drag, and fallback loads on structures other than the vent system above the pool surface were determined using the following procedure:

- (1) Pool swell impact velocity at any point in the airspace was determined. This velocity is based on velocity profiles provided in the PULD as a result of QSTF and 1/12-scale 3-D tests. The results of the EPRI main vent orifice tests were included in this data.
- (2) Impact and drag forces were calculated using the procedure described in Section 2.7 of the NRC Acceptance Criteria.
- (3) Pool fallback loads were calculated using the procedure described in Section 4.3.6 of the LDR. Fallback loads are applied uniformly over the upper projected surface of the structure in the most critical direction.

All loads were defined for both initial conditions  $\Delta p=0$  and  $\Delta p=1$  psid. The bounding loads were used in the structural evaluations.

Impact, drag, and fallback loads were determined in this manner for the structures indicated in Table 2.5.

#### 2.4.3.4 Froth Impingement and Froth Fallback Loads

Froth impingement loads were defined for structures above the pool in two regions:

Region I - Froth formed by the rising pool striking the bottom of the vent header and/or the vent header deflector.

Region II - Froth formed by the water above the expanding pool and detached from the bulk pool surface.

These regions are shown in Figure 2.19 for CNS.

Froth impingement loads were defined using the procedure given in Section 4.3.5.2 of the LDR, as modified by Section 2.8 of the NRC Acceptance Criteria. Pool surface displacement and velocity profiles from the QSTF and EPRI tests were given in the PULD. The Region I froth impingement loads were determined from the QSTF plant-specific high-speed films, as described in Section 2.8 of the NRC Acceptance Criteria.

Froth impingement and fallback loads are specified as rectangular load pulses of 80, 100, and 1000 milliseconds for Region I, Region II, and fallback loads, respectively. Figure 2.20 shows the load transients and directions of load application for these loads.

All loads were defined for both initial conditions  $\Delta p=0$  and  $\Delta p=1$  psid. The bounding load was used in the structural evaluation. Table 2.6 indicates the structures in the torus for which froth impingement and fallback loads were defined. This table includes all structures located in either Region I or II.

#### 2.4.3.5 LOCA Water Jet-Induced Loads

As the drywell pressurizes during a postulated LOCA-DBA, the water slug initially standing in the submerged portion of each downcomer is accelerated downward into the suppression pool. As the water slug enters the pool, it forms a water jet which induces drag loads on submerged structures.

The methodology to determine the LOCA water jet loads on the structures intercepted by the jet is given in Section 4.3.7 of the LDR. In accordance with the NRC Acceptance Criteria, the load definition was extended to all submerged structures which are within four downcomer diameters below the downcomer exit elevation, even if the structure is not intercepted by the jet. The extended methodology defines the LOCA water jet-induced loads on submerged

structures by generating a flow field in the suppression pool induced by expanding and moving hemispherical caps which represent the jet front and contain the same amount of water volume as the jet at each downcomer exit.

A comparison of the QSTF results for zero and operating drywell-to-wetwell pressure differentials shows that the  $\Delta p=0$  case results in a longer jet penetration than the  $\Delta p=1$  psid case. Therefore, only the  $\Delta p=0$  case was analyzed.

There are no submerged structures experiencing direct jet impact loads; however, drag loads have been derived in accordance with the NRC Acceptance Criteria. Table 2.7 lists the structures for which loads were defined. All other submerged structures are outside of the jet load zone.

Interference effects on all LOCA water jet-induced loads were included as multipliers on the loads determined by the procedure described above (Subsection 2.4.3.7).

#### 2.4.3.6 LOCA Air Bubble-Induced Drag Loads

During the initial phase of a postulated LOCA-DBA, the drywell air space is pressurized rapidly by flashing steam discharging from the ruptured pipe. Air is purged from the drywell and vent system and is discharged through the downcomers into the suppression pool. The charging, expanding bubbles at the end of the downcomers create velocity and acceleration fields in the pool, thus inducing drag forces on structures initially submerged in the pool.

The computer code LOCAFOR, developed by GE, was used to calculate the drag loads due to air discharge on submerged structures. The bases of the flow model and the assumptions used in the load evaluation for LOCA air bubble-induced drag loads are described in Section 4.3.8.1 of the LDR.



The drag load formulation starts by considering an infinitesimal bubble (point source) in an infinite liquid pool. The mass/energy conservation equation and the bubble-dynamics equation are solved simultaneously, to obtain the radius of the bubble as a function of time. The velocity and acceleration at any time and location in the infinite pool are calculated from the time-history of the bubble radius. The equivalent velocity and acceleration at any point in the idealized rectangular pool with a free surface is obtained by using the method of images. Drag loads due to the velocity and the acceleration are calculated. The two components are added to obtain the total drag force.

The calculation is continued at every time step until the bubble touches the structure under consideration or until the bubbles coalesce. When the bubble touches the structure, the structure will not experience any more load. After the bubbles coalesce, the pool swell flow field above the downcomer exit elevation is derived from the QSTF plant unique test.

The analyses were done for both initial conditions  $\Delta p=0$  and  $\Delta p=1$  psid. Table 2.8 lists the structures for which LOCA air bubble drag loads were defined.

Interference effects on all LOCA air bubble drag loads were included as multipliers on the loads determined by the procedure described above (Subsection 2.4.3.7).

#### 2.4.3.7 Interference Effects

In evaluating submerged structure drag loads, consideration of interference effects is required by the NRC Acceptance Criteria (Section 2.14.2). Interference effects are applicable to structures whose submerged fluid loads may be influenced by other nearby structures. Interference effects are generally caused by the production of turbulent water flow on the downstream side of a structure. Such effects are highly dependent on the location and



orientation of nearby structures with respect to the target structures. Table 2.8 summarizes the factors used in the load definitions. The interference effects for the submerged structures were usually evaluated according to the procedure in the NRC Acceptance Criteria. Situations existed where interference effects must be considered but the techniques specified by the NRC were not applicable. Such situations arise when two structures are less than three average diameters apart, but are not within  $30^{\circ}$  of being parallel. In these cases, as required by the NRC, a detailed interference effects analysis was performed. The computer analysis, using a finite element calculation technique, determined the increase of the loads due to the presence of another nearby structure.

#### 2.4.4 Loads Associated with Condensation Oscillation

Following the pool swell transient of a postulated LOCA, there is a period during which condensation oscillations (CO) occur at the downcomer exits.

Condensation oscillation loads on the torus shell, submerged structures, and in the vent system are caused by periodic pressure oscillations. These pressure oscillations are associated with the pulsating movement of the steam-water interface of the downcomer water slug caused by variations in the condensation rate.

As discussed in Section 4.4 of the LDR, the loads specified for CO are based on results from the Full Scale Test Facility (FSTF). It was observed that the CO loads with the largest amplitude occurred during the DBA event. CO loads during the IBA are bounded by chugging loads. Chugging loads are typically used in the structural evaluations in lieu of IBA CO loads (see Subsection 2.4.5).

#### 2.4.4.1 Torus Shell Loads

The CO load on the submerged portion of the torus shell is an oscillating load caused by periodic pressure oscillations superimposed upon the prevailing local static pressures. The load is defined as a rigid wall load which is to be used in conjunction with a flexible wall coupled fluid-structure model in the structural evaluations.

The values of pressure amplitude versus frequency for the baseline rigid wall DBA CO load definition are given in Table 2.9. This load definition is taken directly from the LDR (Section 4.4.1.2.1) and is based on FSTF test data which was corrected to remove effects of the FSTF wall flexibility (Reference 23). This CO load definition includes the results of the supplemental FSTF tests required by the NRC (Reference 24).

Three alternative sets of spectral amplitudes are provided in the range from 4 to 16 Hz, and the alternate which maximizes the response is to be used. For all structural evaluations, these alternative amplitudes were enveloped, resulting in a conservative torus shell loading.

The DBA CO load is spatially distributed uniformly along the torus centerline and has a linear hydrostatic variation with depth as shown in Figure 2.21. Also shown in Figure 2.21 is a graphical representation of the DBA CO data contained in Table 2.9. The total spectrum from 0 to 50 Hz was considered.

Since the dimensions of the torus and the number of downcomers for CNS are different from those of the FSTF, the magnitude of the condensation oscillation loads given in Table 2.9 were modified using a multiplication factor which accounts for the effect of the pool-to-vent area ratio. The plant unique CO load on the torus shell is obtained by multiplying the amplitudes of the baseline rigid wall load given in Table 2.9 by a factor of 0.91. The

resulting load is applied to the prevailing local static pressures on the wetted portion of the torus shell at the appropriate times given in Table 2.10.

#### 2.4.4.2 Vent System Loads

Oscillating loads on the vent system during the condensation oscillation phenomenon are caused by harmonic pressure oscillations superimposed on the prevailing local static pressures in the vent system. The vent system components subjected to these loads include the main vents, the vent header, and downcomers.

Table 2.11 gives the magnitudes and frequencies of this pressure load for both DBA and IBA CO. These loads are based on the data from FSTF test M8 (large liquid break), as described in Section 4.4.4.1 of the LDR.

The CO pressure load specified for the downcomers was used only to calculate the circumferential structural response (i.e., hoop stress) of the downcomer, not the vent system responses to lateral, thrust, or other loads which are transmitted through the downcomers to other components.

#### 2.4.4.3 Downcomer Lateral Loads

Downcomer lateral loads due to CO were defined in accordance with the procedure in the LDR. These loads are based on FSTF test measurements correlated with results from a structural model of the FSTF vent system (Reference 25). NRC review of this load definition will be included in the SER supplement to be issued.

Net lateral loads on the submerged portions of the downcomers during CO arise due to differential pressure between two downcomers of a downcomer pair. Additionally, an oscillating internal pressure is simultaneously added to both downcomers in the pair to produce net vertical loads on the downcomer pair. Both the uniform

internal and differential pressures are defined in the frequency domain, as summarized in Table 2.12. In specifying the differential pressures in a number of downcomer pairs, the load application which maximizes the vent system response must be considered, as discussed in Subsection 4.2.3.2.4.

#### 2.4.4.4 Submerged Structure Loads

Steam condensation begins after the vent is cleared of water and the drywell air has been carried over into the suppression chamber. The CO phase induces bulk water motion and creates drag loads on structures submerged in the pool. Submerged structure drag loads due to CO are defined on all structures listed in Table 2.8.

##### 2.4.4.4.1 Drag Loads

The computer code CONDFOR, developed by GE, was used to determine the CO loads on submerged structures. The program CONDFOR defines loads in the frequency domain similar to the torus shell wall pressure load definition (Subsection 2.4.4.1). The load magnitude at 5 Hz is determined, then the remaining frequency components are scaled according to the CO source function amplitudes at corresponding frequencies.

Drag loads were defined in accordance with the LDR methodology as modified by Section 2.14.5 of the NRC Acceptance Criteria. Two conditions were considered:

- (1) CO assuming the average source strength at all downcomers (oscillating in phase).
- (2) CO assuming the maximum source strength (twice the average source strength) applied at the downcomer nearest to the structure of concern.

#### 2.4.4.4.2 FSI Effects

As required by the NRC Acceptance Criteria, fluid structure interaction (FSI) effects were included for all structural segments for which the local fluid acceleration is less than twice the torus boundary acceleration effects. The FSI effects were incorporated using the following procedure:

- (1) Generation of the torus shell acceleration spatial distribution due to CO loads at 1 Hz frequency intervals from 0 to 50 Hz.
- (2) Determination of fluid accelerations at all points in the pool due to the boundary accelerations determined in Step 1, using the methodology in Reference 26. This step is done for each 1 Hz frequency interval.
- (3) If the acceleration determined in Step (2) at a given frequency interval at a structure location is greater than one-half the acceleration at that location predicted by CONDFOR for that frequency interval, the two accelerations are summed absolutely.
- (4) Calculation of the total drag load from the combined acceleration using the procedure in the LDR as modified by the NPC Acceptance Criteria.

FSI effects are included for both CO load cases (maximum and average source strength) and for all submerged structures. The FSI effects determined in this manner typically result in increased submerged structure loads by factors of 10 over those predicted by CONDFOR. It can be shown from energy considerations that the FSI effects are of the same order of magnitude as the loads producing this effect. Thus, any FSI effect which increases the CONDFOR load by anywhere near a factor of 10 is unrealistic. Therefore, an upper bound factor of 10 on FSI effects was used. This approach still provides a rather conservative treatment of FSI effects.



#### 2.4.4.4.3 Interference Effects

Interference effects were included in all CO submerged structure drag loads as multipliers on the loads. These multipliers were applied to the drag loads after FSI effects were included. Interference factors for the structures are tabulated in Table 2.8.

#### 2.4.5 Loads Associated with Chugging

Chugging occurs during a postulated LOCA when the steam flow through the vent system falls below the rate necessary to maintain steady condensation at the downcomer exit. The corresponding flow rates for chugging are less than those of the CO phenomenon discussed previously. During chugging, steam bubbles form at the downcomer exit, oscillate as they grow to a critical size, and begin to collapse independently in time. The chugging load definitions, as discussed in Section 4.5 of the LDR, are based upon FSTF test data.

During the chugging regime of a postulated LOCA, the chugging loads occur as a series of chug cycles, each of which can be broken down into a pre-chug and a post-chug portion. The pre-chug portion occurs during the initiation of the chug. As the steam-water interface enters the pool, a relatively low-frequency pressure loading occurs. The interface eventually becomes unstable and breaks up, producing a rapid underpressure as the chug occurs. The post-chug portion of the cycle is a system response to the rapid underpressure caused by the breakup of the steam-water interface.

Chugging loads are observed during three LOCA categories: DBA, IBA, and SBA. Table 2.13 indicates the onset time and duration of chugging loads for all three break sizes.



#### 2.4.5.1 Torus Shell Loads

The pre-chug and post-chug torus shell load definitions, as given by the LDR (Section 4.5.1.2) are provided below:

##### (1) Pre-Chug Load

Both a symmetric and an asymmetric load distribution were evaluated independently. The symmetric distribution has an amplitude of  $\pm 2.0$  psi uniformly distributed axially along the torus centerline at bottom dead center. The asymmetric distribution has a maximum pressure amplitude of  $\pm 2.0$  psi and a spatial distribution as shown in Figure 2.22. Both load distributions have a linear hydrostatic variation with depth, similar to the CO load, and are to be applied at the frequency producing the maximum response between 6.9 and 9.5 Hz. The pre-chug cycle duration is 0.5 seconds every 1.4 seconds for the appropriate total duration defined in Table 2.13.

##### (2) Post-Chug Load

The post-chug rigid wall pressure amplitudes are defined over a 0 to 50 Hz range in 1 Hz increments as given in Table 2.14. Similar to the symmetric pre-chug load, the post-chug load varies uniformly along the torus centerline and has a linear hydrostatic variation with depth. The post-chug cycle duration is 0.5 seconds every 1.4 seconds for the appropriate duration defined in Table 2.13.

Similar to the CO load definition, the structural response effects unique to the FSTF data, including FSI effects, are eliminated by defining the chugging load as a rigid wall load. The load can then be used in conjunction with a flexible wall, plant unique torus model, which includes inertial effects due to the torus fluid. Also similar to

the CO load definition, the chugging load on the submerged portion of the torus shell was superimposed on the local static pressures.

#### 2.4.5.2 Vent System Loads

Pressure loadings are experienced by the vent system as a result of chugging. These vent system loads can be separated into the following three components:

- (1) A gross vent system pressure oscillation consisting of pressurization during the pre-chug portion and depressurization during the post-chug portion of each chug cycle.
- (2) An acoustic vent system pressure oscillation which is excited as a result of the pressurization and depressurization of the vent system.
- (3) An acoustic downcomer pressure oscillation which is excited as a result of the rapid depressurization at the downcomer exits.

The first component of pressure loading is applied over a relatively long loading cycle which corresponds to the time between chug cycles. The second and third pressure load components are related to the acoustic response frequencies in the vent system and downcomer, and are defined as a periodic load with components at the acoustic frequencies of the vent system (including the downcomers) and of the downcomers themselves.

The vent system chugging load definition was taken from Section 4.5.4.2 of the LDR and is summarized in Table 2.15. The loads were applied individually about the local pressures at the appropriate times in the blowdown, depending on the size of the break, as shown in Table 2.13.

The chugging load specified for the downcomers in Table 2.15 was used only to calculate circumferential structural response (i.e. hoop stress) and not the vent system responses to lateral, thrust, or other loads which are transmitted through the downcomers to other components.

#### 2.4.5.3 Downcomer Lateral Loads

A net lateral load also exists on the submerged portions of the downcomers due to chugging. This loading is caused by vapor bubbles, forming at the downcomer end, which collapse suddenly and intermittently. From chugging tests in the FSTF, this load was determined to be 3,046 lbs. This load is applied randomly at the downcomer end to maximize the stresses at the downcomer/vent header intersection.

This load was applied as an equivalent static force at the ends of the downcomers. The magnitude of this load was determined using the ratio of downcomer frequency to FSTF downcomer frequency as described in Reference 27 and modified by Section 2.12.2.1 of the NRC Acceptance Criteria. This evaluation is described in Subsection 4.2.3.2.5.

Additionally, the following aspects of the chugging downcomer lateral load were considered in the vent system analysis:

##### (1) Chug Synchronization

The potential for a number of downcomers experiencing a lateral load in the same direction at the same time results in a chug synchronization load on the vent system and its supports. This load was based on the procedure in the LDR. The exceedance probability used to calculate the load on a single downcomer was  $10^{-4}$ , as specified in the NRC Acceptance Criteria.

(2) Fatigue

For fatigue considerations, histograms of load reversals for chugging were determined at the downcomer end from the FSTF test data, as described in the LDR. These load reversals were applied over the time durations specified in Table 2.13. These load reversals were applied as shown in Table 2.16 and Figure 2.23.

(3) Downcomer Tiebar Load

Dynamic forces in the downcomer tiebar were calculated using the procedure defined in the NRC Acceptance Criteria (Section 2.12.2.2). These forces were used to evaluate the tiebar when only one downcomer of a tied downcomer pair is loaded.

2.4.5.4 Submerged Structure Loads

Steam chugging at the downcomers creates bulk water motion, and therefore induces drag loads on structures submerged in the pool. The submerged structure load definition method for chugging parallels that used to predict induced drag forces caused by CO (Subsection 2.4.4.4). Submerged structure drag loads due to chugging were defined on the structures listed in Table 2.8.

2.4.5.4.1 Drag Loads

The computer code CONDFOR was used to determine the chugging loads on submerged structures. The method is the same as that for CO loads (Subsection 2.4.4.4.1) except that the source function amplitude versus frequency spectrum is proportional to the torus wall load measurement corresponding to chugging. For chugging drag loads, CONDFOR determines the load magnitude at 26 Hz and then the remaining frequency components are scaled according to the chugging source function amplitudes at corresponding frequencies.

Drag loads were defined in accordance with the LDR methodology as modified by Section 2.14.6 of the NRC Acceptance Criteria. Three conditions are considered for each structure:

- (1) Pre-chug,
- (2) Post-chug, using the maximum source strength applied at the nearest downcomers (oscillating in phase), and
- (3) Post-chug, using the maximum source strength applied at the two nearest downcomers (oscillating  $180^\circ$  out of phase) maximizing the local acceleration in either of the in-plane directions.

#### 2.4.5.4.2 FSI Effects

FSI effects due to chugging loads on submerged structures were defined using the procedure outlined in Subsection 2.4.4.4.2 for CO drag loads. Torus shell accelerations due to chugging loads were used in lieu of CO accelerations for this effect.

#### 2.4.5.4.3 Interference Effects

Interference effects were included in all chugging submerged structure drag loads as multipliers on the loads. These multipliers were applied to the drag loads after FSI effects were included. Interference factors for the structures are tabulated in Table 2.8.

### 2.5 S/RV DISCHARGE-RELATED LOADS

Cooper Nuclear Station is equipped with S/RVs to control primary system pressure transients. For these transients, the S/RVs actuate to divert part or all of the generated steam to the suppression pool. The S/RVs will either self-actuate at a pre-set pressure or actuate by an external signal. Six of the S/RVs are



used for the ADS, which is designed to reduce the reactor system pressure during an IBA or SBA. The ADS performs this function by automatically actuating the specified S/RVs, following the receipt of specific signals from the reactor protection system.

Prior to the initial actuation of an S/RV caused by a normal operational transient, the S/RVDLs contain air and water in the submerged portion of the piping and within the discharge device. Following S/RV actuation, steam enters the S/RVDL, compressing the air and expelling the water slug into the suppression pool.

Following water clearing, the compressed air is accelerated into the suppression pool and forms high-pressure air bubbles. These bubbles expand and contract a number of times before they rise to the suppression pool surface. The associated transients create drag loads on submerged structures, as well as pressure loads on the submerged boundaries. These loads are referred to as S/RV air-clearing loads.

Following the air-clearing phase, essentially pure steam is injected into the pool. As long as the local pool temperature is low, steam condensation proceeds in a stable manner and no significant loads are experienced. Continued steam blowdown into the pool will increase the local pool temperature. To preclude the possibility of unstable steam condensation, pool temperature limits are established.

This subsection describes the procedures used to calculate loads on containment components related to S/RV discharge events. These loads include line loads on the S/RVDL piping, pressures on the torus shell boundary, and loads on structures submerged in the pool.

The magnitude and nature of the S/RV discharge loads depend upon the initial conditions used in the analyses. Load case numbers will



be used to describe these initial conditions. The following load cases are defined:

<u>S/RV Load Case</u>	<u>Initial Conditions</u>
A1.1	Actuation of one S/RV resulting from normal operational transients
A1.2	Actuation of one S/RV during an IBA/SBA event
A1.3	Actuation of one S/RV during a DBA event
A2.2	ADS actuation (6 S/RVs) during an IBA/SBA event
A3.1	Actuation of all 8 S/RVs resulting from normal operational transients
A3.2	Actuation of all 8 S/RVs during an IBA/SBA event (unrelated to ADS actuation)
C3.1	Subsequent actuation of all 8 S/RVs resulting from normal operational transients
C3.2	Subsequent actuation of all 8 S/RVs during an IBA/SBA event - S/RVDL atmosphere 100% air
C3.3	Subsequent actuation of all 8 S/RVs during an IBA/SBA event - S/RVDL atmosphere 100% steam

For load case A1.3, significant containment loads are considered only during the pool swell event. Although S/RV actuations can occur later in the event, the resulting loads are negligible since the air and water initially in the line will be cleared as the drywell-to-wetwell  $\Delta p$  increases during the DBA transient.

S/RV discharge-related loads are dependent on the initial drywell-to-wetwell  $\Delta p$ . The initial conditions producing the bounding load were used in all structural evaluations.

#### 2.5.1 S/RVDL-Clearing Transient Loads

When an S/RV opens, the pressure within the S/RVDL undergoes a transient prior to reaching a steady-state value. A transient

pressure wave travels back and forth in the line as the pressure continues to increase, until the inertia of the water slug in the submerged portion of piping is overcome. During the water-clearing transient, the pressures within the discharge pipe and the T-quencher reach their maximum values. Following expulsion of the water slug, the peak pressure in the discharge pipe decreases to a quasi-steady-state value which is a function of the S/RV steam flow rate and friction along the line upstream of the entrance to the T-quencher. Similarly, the T-quencher internal pressure increases and then decreases to a quasi-steady-state value which is a function of the steam flow rate and pressure losses resulting from flow through the holes in the T-quencher.

During the early portion of this transient, a substantial pressure differential exists across the pressure wave. Therefore, when the wave is within an S/RV pipe segment between a pair of elbows, there exists a substantial difference in the pressure applied to the interior surface of the elbows on each end of the segment. This pressure differential, plus momentum effects from steam (or water in initially submerged pipe runs) flowing around elbows in the line, results in transient thrust loads on the S/RV discharge pipe segments. These loads were considered in the design of S/RVDL pipe restraints, the connection of the S/RV to the main steam line, and the T-quencher support system.

S/RVDL transient loads were defined using the procedure described in Section 5.2.1 of the LDR. This procedure and the assumptions in calculating the loads have been reviewed by the NRC in the SER. The computer code RVFORO4 was used to predict S/RVD line-clearing transient loads. RVFORO4 was developed by GE for determining these loads, using the analytical model described in Reference 28. The following conservative assumptions were made in defining these loads:

- (1) The S/RV flow rate is assumed to be 1.225 times the ASME-rated S/RV flow.

- (2) The S/RV main disk-stroke time is assumed to be 0.02 seconds. The S/RV loading most significantly affected by the main disk stroke time is the transient wave thrust load. Shorter stroke times result in higher loading. The value of 0.02 seconds represents a lower bound of main disk stroke times measured during performance testing of S/RVs of similar design to those installed in Mark I plants.
- (3) The suppression pool water level is at the maximum value allowed by technical specifications. This assumption results in the maximum initial water leg in the S/RV discharge line, which, in turn, results in the highest water-clearing loads on the S/RVDL and discharge device.
- (4) The S/RVDL vacuum breaker does not leak. By assuming the vacuum breaker does not leak, a lower value of S/RVDL to wetwell pressure differential is calculated, which results in a longer initial water leg in the discharge line.

From the RVFOR04 analyses, the following loads and response quantities were obtained:

- S/RVDL internal pressure transient
- S/RVDL pipe segment wave thrust transient
- S/RVDL water-clearing thrust transient
- Water-clearing time
- Water-clearing velocity and acceleration
- T-Quencher internal pressure
- S/RVDL wall temperature

Loads were obtained for all 8 S/RVDLs including all piping from the S/RV in the drywell through the T-quencher discharge device. S/RV discharge Load Case A1.2 (actuation during ISA/SBA) was identified as the bounding load cases for the S/RVD piping (both drywell and wetwell portions) based on a study of the longest S/RVDL for all S/RV load cases.

#### 2.5.2 S/RVDL Reflood Transient

Following closure of an S/RV, the steam pressure in the S/RVDL decreases rapidly as the steam flows out into the pressure suppression pool. At a sufficiently low steam pressure, pool water reenters the S/RVDL, causing a rapid depressurization of the line. The water may then rise through the S/RVDL to a level somewhat above its initial level before equilibrium is reestablished. The actual reflood level depends primarily on the ability of the S/RVDL vacuum breakers to allow a rapid depressurization of the line. At some minimum time interval after closure of the S/RV, a second actuation may occur. Loads are developed on the S/RVDL during this actuation. These loads (wave thrust, water-clearing thrust, and S/RVD pipe and T-quencher pressures) depend on the water level and/or the gas properties in the line.

In the case of a consecutive S/RV actuation, the necessary input data for the line-clearing transient load was obtained from the computer code RVRIZO2, which predicts the water reflood transient into the S/RVDL after the valve closure. This computer code was developed by GE and is incorporated as part of the LDR load definition (Section 5.2.3) for S/RVDL-clearing transient loads (as described above).

Sufficient sensitivity studies were conducted to identify the highest water reflood heights, which determine the maximum line-clearing transients. A plant unique transient evaluation was also performed to identify the minimum time between S/RV actuations for

both normal operating and LOCA conditions (Reference 21). This transient analysis is based on the low-low set relief logic to be installed on the S/RVs.

For all anticipated operational transient events, the low-low set relief logic extends the minimum time between actuations to approximately 36 seconds, which is enough to pass all significant reflood peaks for Load Case C3.1. Therefore, the loads associated with Load Case C3.1 were not governing for design. If there is no loss of off-site power (LOOSP) or early MSIV isolation during a LOCA event, S/RV subsequent actuations would not occur for any break size. If LOOSP occurs, the low-low set relief logic extends the minimum time interval between two consecutive actuations to approximately 31 seconds for breaks smaller than  $0.2 \text{ ft}^2$ , which will be enough to pass the first peak water reflood for Load Case C3.3. Predicted second peak reflood levels are below the initial water level in the line; therefore, line-clearing loads associated with Load Case C3.3 were not governing for design.

#### 2.5.3 Thrust Loads on T-Quencher Arms

Following an S/RV actuation, the pressurization of the discharge line causes the water initially in the T-quencher and piping to be accelerated and expelled through the T-quencher arm holes into the suppression pool. The redirection of flow of the fluid in the arms (90 degrees out the holes) and the internal pressure of the arms results in thrust loads on the arm and endcaps. Since the T-quencher discharge devices in the Cooper Station suppression pool have endcap holes on one arm only, and due to uneven water-clearing between the two arms of the T-quencher, a net thrust load acts along the axis of the T-quencher device. Following the water and air clearing, there are net thrust loads along the axis of the T-quencher device due to steam discharging. Uneven water clearing between the two sides of an arm results in a thrust load perpendicular to the T-quencher arms. All of these loadings were calculated for the S/RVDL were calculated with the bounding loads.



The procedure used to calculate these thrust loads is the procedure specified in Section 5.3.6 of the LDR. Water-clearing velocities and accelerations from RVFOR04 analyses were used in determining these loads. Loads were defined for the bounding S/RV Load Case C3.1 for the line with the highest thrust loads. The following uneven thrust load cases were defined:

- (1) Thrust loads along axis of the T-quencher based on endcap forces.
- (2) Thrust loads perpendicular to the T-quencher arms due to uneven water-clearing. The signs of the end loads on each T-quencher arm were arranged to consider all possible combinations, i.e. to result in the maximum turning moment on the discharge device and the maximum bending moment at the center of the discharge device.

#### 2.5.4 Torus Shell Pressures

When an S/RV actuates, the expulsion of water and then air into the suppression pool through the discharge device results in pressure loads on the submerged portion of the torus shell and induces drag loads on submerged structures.

Prior to the initial actuation of an S/RV, the S/RVDL contains air and suppression pool water in the submerged portion of the piping. Following S/RV actuation, steam enters the S/RVDL, compressing the air within the line, expelling the water slug, and discharging the air into the suppression pool. The compressed air bubbles expand, resulting in an outward motion of the suppression pool water. The outward momentum of the suppression pool water causes the pressure within the bubbles to drop below the local hydrostatic pool pressure. The negative bubble pressure slows and reverses the bubble expansion, and the suppression pool water begins to move inward. The inward momentum of the water results in a compression



of the air bubbles to a pressure above the local hydrostatic pool pressure. The expansion and compression of the air bubbles continues until the bubbles rise and break through at the suppression pool water surface. The positive and negative dynamic pressures developed within these bubbles result in an oscillatory pressure loading on the torus wall.

The load definition used to analyze the torus shell for S/RV discharge pressures is based on the procedure described in Section 5.2.2 of the LDR. A computer code (QBUBSO2), developed by GE, was used for analytically predicting the torus shell pressure distribution resulting from an S/RV discharge through a T-quencher device. The maximum torus shell pressure occurs at the torus bottom dead-center, and remains constant approximately 6.5 ft. on both sides from the discharge device centerline along the torus longitudinal axis. Then the pressure attenuates to a minimum value. The computer code also calculates pressures at selected cross-sectional locations. These pressures attenuate from the bottom dead-center to the water surface.

The pressure waveform predicted by QBUBSO2 was also used in all torus shell structural evaluations. A typical pressure waveform, showing very low attenuation with time, is shown in Figure 2.24. All assumptions described in LDR Section 5.2.2 (with the exception of one) were included in the load definition.

The modifications to the S/RVDL air clearing shell pressure loads required in Section 2.13.3 of the NRC Acceptance Criteria were also incorporated in the torus shell load definition. The modifications to the LDR procedure required by the NRC include:

- Limiting water leg length in the S/RVDL to 13.5 ft. for predicting bubble pressure.
- Limiting line volumes to 65 ft<sup>3</sup> for prediction of bubble pressure.

- Limiting torus shell pressures to 1.65 times the peak bubble pressure for multiple valve actuation cases.
- Use of recommended uncertainty margins (25% for first actuation; 40% for subsequent actuation) on predicted upper and lower frequency ranges.
- Use of first actuation pressure with subsequent actuation frequency for defining all subsequent actuation load definitions.

Two exceptions to the LDR and NRC Acceptance Criteria procedures were taken:

- (1) For multiple valve actuation events, the NRC Acceptance Criteria requires linear superposition (ABSS method) of bubble pressure spatial distributions due to single valve actuations. For CNS, a plant unique evaluation was performed to justify a modified square root of the sum of the squares (SRSS) method for combining spatial pressure distributions. The modified SRSS procedure was developed by generating CNS plant unique Cumulative Distribution Functions (CDFs) for combined peak torus shell pressures. These CDFs account for variations in reactor pressure rise rate, S/RV set point, and S/RV opening time. The combined peak pressures in these CDFs were determined through algebraic addition of the pressure waveforms analytically predicted for each valve. The studies indicated that a 1.2 multiplier on the SRSS combination of peak pressures provides an 84% NEP on the CDF with a 90% confidence level. This plant unique study is described in Appendix A to this report.
- (2) The LDR procedure for defining initial conditions for QBUBSO2 assumes that pure air mass is in the S/RVDL prior to valve opening. As discussed by the NRC in Section

3.10.2.6 of the SER, this is a conservative assumption for LOCA events when an air/steam mixture exists in the drywell. For load case A2.2 only (ADS actuation during an IBA/SBA event), torus shell pressure loads were defined using an initial 30% relative humidity in the S/RVDL. Reduced torus shell pressures and increased pressure waveform frequencies result from this assumption. The design ADS actuation event occurs 300 seconds into an IBA and 600 seconds into an SBA. Since these S/RVD pressure loads are to be combined with the high wetwell pressure obtained by assuming all air in drywell is purged into wetwell before ADS actuation, the results are still conservative.

Torus shell loads were calculated using the above procedure for the following load cases:

- A1.1 - NOC-SVA, First Valve Actuation
- A1.3 - LOCA-DBA, Single Valve Actuation
- A2.2 - LOCA-IBA/SBA, ADS Actuation
- C3.1 - NOC-8MVA, Subsequent Valve Actuation
- C3.2 - LOCA-SBA/IBA 8MVA, Subsequent Valve Actuation

Loads were defined for the S/RVDL configurations resulting in the highest shell pressures and the broadest pressure frequency ranges. Peak combined shell pressure for multiple valve cases was 20.5 psi; for the ADS event, the combined peak pressure was 14.5 psi. Frequency ranges were 5.8 to 15.4 Hz for subsequent actuation cases, and 4.5 to 9.4 Hz for first actuation cases.

#### 2.5.5 Loads on Submerged Structures

All structures submerged in the suppression pool are subjected to loadings following an S/RV discharge event. These loadings are due to either water jets following the water clearing from the S/RVDL or drag loadings due to the oscillating air bubbles expelled from the T-quencher.

#### 2.5.5.1 T-Quencher Water Jet-Induced Drag Loads

When an S/RV is actuated, water initially contained in the submerged portion of the S/RV discharge line is forced out of the T-Quencher arms through the arm holes. These T-quencher water jets will induce drag loads on nearby submerged structures which are within the jet path. T-quencher water jet loads were evaluated using a revised methodology based upon the procedure in Section 5.2.4 of the LDR. The main differences between LDR and the revised methodology and the major assumptions employed in revised methodology are:

- (1) In the LDR methodology, the jet velocity is assumed constant at its maximum value throughout the transient. However, the jet reaches its maximum velocity towards the end of the transient. The revised methodology defines the transient jet front location by taking into consideration the transient behavior of the jet velocity.
- (2) In the revised methodology, the velocity and position of each particle leaving the T-quencher arm are determined using steady jet characteristics. Actually, the decay of velocity in an unsteady jet will be much faster than steady jet; therefore, this assumption results in conservative jet penetration distances.
- (3) Conservatively, the loads are determined for the maximum velocity and the maximum loads are assumed to exist during the entire transient.

For the structures intercepted by the jet, the revised methodology gives higher loads. However, using the revised methodology, fewer structures are intercepted by the jet than would be intercepted if the LDR methodology is used. The loads on these structures, however, are very small in magnitude and are bounded by the

T-quencher air bubble-induced drag loads which immediately follow the T-quencher water jet loads.

A comparison of various load cases shows that S/RV Load Case C3.1 results in the longest jet penetration distances and highest jet velocities. Therefore, only Load Case C3.1 was analyzed to determine the T-quencher water jet loads.

The T-quencher water jet loads were determined using the revised methodology for the structures intercepted by the jet, which are tabulated in Table 2.17.

#### 2.5.5.2 T-Quencher Air Bubble-Induced Drag Loads

After actuation of the S/RV, high-pressure steam from the main steam line enters the S/RVDL and compresses the air-water vapor mixture initially inside the line. This process expels the water column and the air-vapor mixture into the suppression pool. Once inside the pool, the air-vapor mixture forms high-pressure bubbles which oscillate and rise toward the pool surface. The oscillation of these S/RV bubbles creates a three-dimensional flow field, and therefore induces standard and acceleration drag forces on the structures submerged in the suppression pool.

The computer program TQFORBF was developed by GE to calculate the drag forces induced by T-quencher air bubbles on submerged structures. The program is based upon the procedure described in Section 5.2.5 of the LDR, and includes all modifications required by Section 2.14.4 of the NRC Acceptance Criteria.

Submerged structure drag loads following S/RV actuations were defined for all structures listed in Table 2.8. Loads were conservatively estimated for the initial conditions producing the maximum drag load. These initial conditions correspond to first valve actuation during an SBA (Load Case A1.2). Thermal-hydraulic



parameters related to the longest S/RVDL (which results in the highest drag loads) were used in defining the loads for all structures regardless of location. The frequency ranges for the load transients correspond to an envelope of pressure waveform frequencies calculated for torus shell loads (see Subsection 2.5.4).

#### 2.5.5.3 T-Quencher Air Bubble Differential Loads

To account for uneven air-clearing loads on the T-quencher arms and supports, it is conservatively assumed that only two bubbles in phase are active.

To find the maximum lateral loads on the T-quencher arm and supports, it is assumed that two bubbles in phase on one side of the T-quencher arm are active and there are no bubbles on the other side of the arm.

To obtain the maximum moment-producing loading on the T-quencher arm and supports, it is assumed that there are two bubbles in phase on one diagonal side of the arm, and there are no bubbles on the other diagonal side.

With these assumptions, loads were then determined using the procedures and assumptions described in Subsection 2.5.5.2.

#### 2.5.5.4 Interference Effects

Interference effects were included in all S/RV discharge-related submerged structure loads as multipliers on the loads. Interference factors for structures are tabulated in Table 2.8.

### 2.6 OTHER LOADS

This section briefly discusses additional load cases not included in the original design basis and other LOCA-related or S/RV discharge-related hydrodynamic load definitions.



### 2.6.1 Other Operating Loads

In performing the structural evaluations, several load conditions not identified above were included in the evaluations. These loads are thrust forces at piping elbows due to momentum changes near discharge outlets. Additionally, for piping analysis of ECCS lines, consideration of design temperatures was included.

### 2.6.2 Other Secondary Loads

A number of suppression pool hydrodynamic-related phenomena which generate either secondary loads on the containment system and structures or other considerations to the load definitions were neglected. This conclusion is consistent with the NRC position in the SER. These secondary load considerations are:

- (1) Seismic slosh due to seismic motion of the suppression pool water.
- (2) Pressure loads on the torus walls due to post-pool swell waves.
- (3) Asymmetric pool hydrodynamic loading condition due to asymmetric vent system flow.
- (4) Downcomer air-clearing lateral loads due to LOCA air-clearing through the vents.
- (5) Differential pressure loading on submerged structures and the torus wall due to sonic and compression waves following a postulated LOCA-DBA.
- (6) Drag loads on submerged structures produced during the period of the S/RV steam discharge in the suppression pool through the T-quencher discharge device.

- (7) Effects of suppression pool thermal stratification for a minimum downcomer submergence of 3 feet.

### 2.6.3 Steam Discharge Condensation Loads

As discussed in Section 2.3 of the SER, S/RV actuation at elevated pool temperatures could result in severe vibratory pressure loads. To eliminate this concern, the current practice is to limit the pool temperature so that the "threshold" temperature for severe vibrations will not be achieved during operational and upset modes; e.g., a stuck-open S/RV event. Plant-unique transient evaluations of the Cooper Station suppression pool were performed to demonstrate that local pool temperatures remain below 200°F. Section 7 of this report describes this evaluation. Since the pool temperature limit is satisfied, S/RV discharge steam condensation loads were not considered in the requalification of CNS containment and piping systems.

## 2.7 LOAD COMBINATIONS

This subsection identifies the timing sequence of the loading conditions for containment components due to the hydrodynamic phenomena described throughout this section.

The timing sequence is illustrated in figures which identify the hydrodynamic loading conditions resulting from LOCA and from S/RV discharges. Seismic loadings, and structural and water deadweight loads, can act at any time during all transients. The lengths of the bars in the figures indicate the time periods during which a loading condition may exist. The loading conditions of CO and chugging were assumed to exist continually during the indicated time period. For S/RV discharge loads, the duration of the loading is short, but the loads may occur at any time during the indicated time period. Loads are considered to act simultaneously on a structure at a specific time if the loading condition bars overlap at that time.

### 2.7.1 Torus Shell

The torus shell load sequence for LOCA-DBA, -IBA, and -SBA cases are shown in Figures 2.25 through 2.27. Durations of the LOCA-related loads were based on the durations specified in the LDR with the exception of containment pressure and temperature transients which were based on plant unique transient evaluations (Subsection 2.4.1). Timing of S/RV discharge transients was also based on plant unique evaluations. In assessing the torus shell response to ADS actuations during a LOCA, containment pressures and temperatures at the time of ADS initiation were used in the load combinations.

The ring girder is also subjected to submerged structure load sequences (Subsection 2.7.4).

### 2.7.2 Vent System

The vent system load sequences for LOCA-DBA, -IBA, and -SBA are shown in Figures 2.28 to 2.30. These sequences are obtained from the LDR and plant unique transient evaluations of containment pressure and temperature.

The submerged portion of the downcomers, downcomer tiebars, and main vent drain line are also subjected to submerged structure load sequences (Subsection 2.7.4).

### 2.7.3 Internal Structures Above Pool

The load sequence for structures above the suppression pool high-water level during LOCA-DBA is shown in Figure 2.31. Structures above the pool surface are not subjected to hydrodynamic loading during either an IBA or SBA event.

#### 2.7.4 Submerged Structures

The load combinations for the submerged structures are shown in Figures 2.32 through 2.34 for LOCA-DBA, -IBA, and -SBA events. The loads following an S/RV actuation are illustrated in Figure 2.35.

#### 2.7.5 S/RVD Piping

S/RVD piping lines are subjected to line transient loads, submerged structure loads, and above-pool loads. The latter two load sequences are discussed in Subsections 2.7.4 and 2.7.3 respectively. For line transient events, loads associated with Load Case A1.2 were conservatively used for all S/RV discharge transients.

#### 2.7.6 Torus Attached Piping

Loadings on torus attached piping external to the torus shell are due to torus shell accelerations. Therefore, load sequencing for the torus shell (Subsection 2.7.1) applies to attached piping evaluations. Portions of attached piping systems inside the wetwell are also subject to submerged structure and above-pool loads (Subsections 2.7.4 and 2.7.3).

#### 2.7.7 Fatigue Design Basis

For components requiring evaluation for cyclic loads, a fatigue design basis was developed. The design basis assumes 40 years of plant operation with one LOCA over the design life. The postulated LOCA can be either a DBA, IBA, or SBA event. Tables 2.18 and 2.19 give the design basis for 40 years of normal operation followed by a DBA event or IBA/SBA event. In accordance with the PUAAG, pool swell is not considered as part of the fatigue design basis. For the fatigue evaluation of the downcomer/vent header intersection, the design basis for chugging is described in Subsection 2.4.5.3.

In developing the fatigue design basis, the number of cycles for each load combination was estimated by multiplying the duration of the load by the maximum significant structural response frequency (taken to be 30 Hz). Since the maximum stress for each load combination is unlikely to occur with this number of cycles, a reduced number of effective cycles was determined. This number of effective cycles was based on Mark I program studies which determined fatigue usage for actual response time histories. Calculation of fatigue usage assuming the maximum stress for the load combination applied over the number of effective cycles produces the same usage for the load combination as would be produced by considering the actual response time histories.

In determining the number of S/RV actuations over the 40-year plant life, operating records for CNS were reviewed. This review indicated that 63 S/RV actuations at full reactor power have occurred since start-up (i.e., over a period of roughly seven years). Therefore, the fatigue design basis of 500 valve actuations by each S/RV for a 40-year plant life is considered conservative.





Table 2.1

CONTAINMENT HYDRODYNAMIC DATADRYWELL

Free Air Volume	132,465 cu. ft.
Operating Pressure (High)	1.1 psig
(Low)	0.9 psig
Operating Bulk Temperature (Nominal)	135°F
Internal Design Pressure	58 psig
Design Temperature (FSAR)	281°F

VENT SYSTEM

Free Air Volume	13,540 cu. ft.
Number of Downcomers	80
Downcomer Submergence	
Maximum (High Water Level)	3.33 ft.
Minimum (Low Water Level)	3.00 ft.

WETWELL (SUPPRESSION CHAMBER)

Pool Volume	
Maximum (High Water Level)	91,100 cu. ft.
Minimum (Low Water Level)	87,650 cu. ft.
Free Air Volume	
Maximum (Low Water Level)	112,240 cu.ft.
Minimum (High Water Level)	106,850 cu.ft.
Water Level Distance to Torus Centerline	
Maximum (Low Water Level)	1.79 ft.
Minimum (High Water Level)	1.46 ft.
Pool Surface Area	9,115 sq. ft.
Operating Pool Temperature (Maximum)	95°F
Design Pressure	58 psig
Design Temperature (FSAR)	281°F

TABLE 2.2

PROPOSED LOW-LOW SET SAFETY/RELIEF VALVE SYSTEM

	S/RV							
	A	B	C	D	E	F	G	H <sup>(1)</sup>
Pressure Relief Function	X	X	X	X	X	X	X	X
ADS Function	X	X	X	-	X	X	X	-
Low-Low Set Relief Function	-	-	-	X	-	-	-	X
Valve Group	III	III	II	I	II	II	III	I
Steam Pilot Opening Set Point (psig)	1125	1125	1115	1105	1115	1115	1125	1105
Steam Pilot Closing Set Point (psig)	1091	1091	1082	1072	1082	1082	1091	1072
Low-Low Set Open (psig)	-	-	-	1045	-	-	-	1075
Low-Low Set Close (psig)	-	-	-	945	-	-	-	975

Note:

- (1) Valve H is currently designated as an ADS valve. Since it is necessary to separate ADS valves from low-low set valves, and since it is desirable to use the lowest group valves for low-low set, the ADS function for valve H will be assigned to valve F.

Table 2.3

PLANT CONDITIONS AT INSTANT OF DBA PIPE BREAK

102% Licensed Power (Mwt)	2429
Initial Suppression Pool Temperature (°F)	78.5
Downcomer Submergence (ft)	3.333
Airspace Volume (ft <sup>3</sup> ):	
Drywell	132,465
Wetwell	106,850
Airspace Pressure (psig)	
Drywell	1.10
Wetwell	0.1

Table 2.4

PLANT CONDITIONS AT INSTANT OF IBA/SBA PIPE BREAK

102% Licensed Power (Mwt)	2429
Initial Suppression Pool Temperature (°F)	90
Downcomer Submergence (ft)	3.333
Airspace Volume (ft <sup>3</sup> ):	
Drywell	132,465
Wetwell	106,850
Airspace Pressure (psig)	
Drywell	1.10
Wetwell	0.1

Table 2.5

STRUCTURES SUBJECTED TO POOL SWELL  
IMPACT, DRAG, AND FALLBACK LOADS

Vent System Components

- Main Vent
- Downcomer tiebar
- Vent deflector support struts
- Drywell-to-wetwell vacuum breakers
- Main vent drain line

S/RVDL Piping and Supports

- S/RVD line B (long line) piping
- S/RVD line B supports in airspace

Internal Piping and Supports

- RHR pump test line and supports
- RCIC turbine exhaust piping
- HPCI turbine exhaust piping
- Core spray pump test line
- RCIC condensate piping
- HPCI condensate piping
- Demineralized water inlet piping

Non-Essential Structures

- Platform grating, framing, and supports

Table 2.6

STRUCTURES SUBJECTED TO FROTH IMPINGEMENT  
AND FROTH FALLBACK LOADS

Vent System Components

- Main vent
- Vent system support columns
- Drywell-to-wetwell vacuum breakers
- Main vent drain line

S/RVD Piping and Supports

- S/RVD line B support in airspace

Internal Piping and Supports

- RHR pump test line
- Containment spray header

Non-Essential Structures

- Platform handrails and ladder
- Monorail beam



Table 2.7

STRUCTURES SUBJECTED TO LOCA  
WATER JET-INDUCED DRAG LOADS

Torus Shell Components

- Ring girder
- Ring girder gussets

S/RVD Piping and Supports

- S/RVD piping and T-quencher
- T-quencher support pipe assembly
- 16" support pipe for S/RVDL
- 10" stiffening pipe

Internal Piping and Supports

- RHR pump suction strainer
- RCIC pump suction strainer
- HPCI pump suction strainer
- Core spray pump suction strainer
- HPCI turbine exhaust piping and supports
- RCIC turbine exhaust piping and supports

Non-Essential Structures

- Platform support columns

Table 2.8

STRUCTURES SUBJECTED TO SUBMERGED STRUCTURE DRAG LOADS  
AND INTERFERENCE FACTORS

	<u>Interference Factors (1)</u>
<u>Torus Shell Components</u>	
- Ring girder	1.3 - 2.06
- Ring girder gussets	1.0 - 2.0
<u>Vent System Components</u>	
- Downcomer tie-bars	2.0
- Main vent drain line	1.0
- Downcomers (2)	1.0
<u>S/RVD Piping and Supports</u>	
- S/RVD line A piping and T-quencher	1.0 - 2.3
- S/RVD line B piping and T-quencher	1.0 - 2.3
- T-quencher support pipe assembly	1.2 - 2.2
- 16" support pipe for S/RVDL B	1.5 - 2.4
- 10" stiffening pipe	1.1 - 2.1
<u>Internal Piping and Supports</u>	
- RHR pump suction strainer	1.35
- RCIC pump suction strainer	1.35
- HPCI pump suction strainer	1.35
- Core spray pump suction strainer	1.35
- HPCI turbine exhaust piping and supports	1.71
- RCIC turbine exhaust piping and supports	1.76
- HPCI condensate piping	1.0
- RCIC condensate piping	1.0
- RHR pump test lines	1.0
- Core spray pump test lines	1.2 - 2.0
- Demineralized water inlet	1.0
<u>Non-Essential Structures</u>	
- Platform support columns	1.0 - 2.0

Notes:

- (1) For several structures, interference factors depend on location on the structure. Range of the factors is indicated in the table.
- (2) Submerged structure drag loads on downcomers are defined only for T-quencher bubble drag loads.

Table 2.9

CONDENSATION OSCILLATION BASELINE RIGID WALL PRESSURE  
AMPLITUDES ON TORUS SHELL BOTTOM DEAD CENTER

Frequency Range (Hz)	Amplitudes (1) to be Analyzed (PSI)	Alternate Amplitudes to be Analyzed (1) (PSI)		
		<u>1</u>	<u>2</u>	<u>3</u>
0-1	0.29			
1-2	0.25			
2-3	0.32			
3-4	0.48			
	↑			
4-5				
5-6		1.86	1.20	0.24
6-7		1.05	2.73	0.48
7-8		0.49	0.42	0.99
8-9		0.59	0.38	0.30
9-10		0.59	0.38	0.30
10-11		0.59	0.38	0.30
11-12		0.34	0.79	0.18
12-13		0.15	0.45	0.12
13-14		0.17	0.12	0.11
14-15		0.12	0.08	0.08
15-16		0.06	0.07	0.03
	↓	0.10	0.10	0.02
16-17	0.04			
17-18	0.04			
18-19	0.04			
19-20	0.27			
20-21	0.20			
21-22	0.30			
22-23	0.34			
23-24	0.33			
24-25	0.16			

SELECT ENTIRE SET  
OF VALUES FROM EITHER  
ALTERNATE 1, ALTERNATE  
2 OR ALTERNATE 3. SELECT ALTERNATE  
WHICH GIVES MAXIMUM  
RESPONSE.

↑  
NONE  
↓

↑  
NONE  
↓

Table 2.9 (Continued)

CONDENSATION OSCILLATION BASELINE RIGID WALL PRESSURE  
AMPLITUDES ON TORUS SHELL BOTTOM DEAD CENTER

<u>Frequency Range (Hz)</u>	<u>Amplitudes to be Analyzed (1) (PSI)</u>
25-26	0.25
26-27	0.58
27-28	0.13
28-29	0.19
29-30	0.14
30-31	0.08
31-32	0.03
32-33	0.03
33-34	0.03
34-35	0.05
35-36	0.08
36-37	0.10
37-38	0.07
38-39	0.06
39-40	0.09
40-41	0.33
41-42	0.33
42-43	0.33
43-44	0.33
44-45	0.33
45-46	0.33
46-47	0.33
47-48	0.33
48-49	0.33
49-50	0.33

NOTE

(1) Half range (= 1/2 of peak to peak amplitude)

Table 2.10

CONDENSATION OSCILLATION ONSET AND DURATION

<u>Break Size</u>	<u>Onset Time After Break</u>	<u>Duration After Onset</u>
DBA	5 seconds	30 seconds
IBA	5 seconds	900 seconds
SBA	Not Applicable	Not Applicable

Table 2.11

VENT SYSTEM LOAD AMPLITUDES AND FREQUENCIES  
FOR CONDENSATION OSCILLATION

	<u>DBA</u>	<u>IBA</u>
Forcing Function	Sinusoidal	Sinusoidal
Spatial Distribution	Uniform	Uniform
Frequency Range	4-8 Hz	6-10 Hz
Amplitude:		
Main Vent and Vent Header	<u>+2.5</u> psi	<u>+2.5</u> psi
Downcomer	<u>+5.5</u> psi	<u>+2.1</u> psi

Note:

These loads are used only to determine hoop stresses in vent system components.



Table 2.12

VENT SYSTEM DOWNCOMER LATERAL LOAD  
DUE TO CONDENSATION OSCILLATION

<u>Type</u>	<u>Pressure (psi)</u>		<u>Frequency Range (Hz)</u>	
	<u>Amplitude</u>		<u>DBA</u>	<u>IBA</u>
	<u>DBA</u>	<u>IBA</u>		
Internal	<u>+3.6</u>	<u>+1.1</u>	4-8	6-10
Differential	<u>+2.85</u>	<u>+0.2</u>		
Internal	<u>+1.3</u>	<u>+0.8</u>	8-16	12-20
Differential	<u>+2.6</u>	<u>+0.2</u>		
Internal	<u>+0.6</u>	<u>+0.2</u>	12-24	18-30
Differential	<u>+1.2</u>	<u>+0.2</u>		

Table 2.13

CHUGGING ONSET AND DURATION

<u>Break Size</u>	<u>Onset Time After Break</u>	<u>Duration After Onset</u>
DBA	35 seconds	30 seconds
IBA	5 seconds	900 seconds
SBA	300 seconds	900 seconds

Table 2.14

POST-CHUG RIGID WALL PRESSURE AMPLITUDES  
ON TORUS SHELL BOTTOM DEAD CENTER

<u>Frequency</u> <u>Range (Hz)</u>	<u>Amplitude (1)</u> <u>(PSI)</u>	<u>Frequency</u> <u>Range (Hz)</u>	<u>Amplitude (1)</u> <u>(PSI)</u>
0-1	0.04	25-26	0.04
1-2	0.04	26-27	0.28
2-3	0.05	27-28	0.18
3-4	0.05	28-29	0.12
4-5	0.06	29-30	0.09
5-6	0.05	30-31	0.03
6-7	0.1	31-32	0.02
7-8	0.1	32-33	0.02
8-9	0.1	33-34	0.02
9-10	0.1	34-35	0.02
10-11	0.06	35-36	0.03
11-12	0.05	36-37	0.05
12-13	0.03	37-38	0.03
13-14	0.03	38-39	0.04
14-15	0.02	39-40	0.04
15-16	0.02	40-41	0.15
16-17	0.01	41-42	0.15
17-18	0.01	42-43	0.15
18-19	0.01	43-44	0.15
19-20	0.04	44-45	0.15
20-21	0.03	45-46	0.15
21-22	0.05	46-47	0.15
22-23	0.05	47-48	0.15
23-24	0.05	48-49	0.15
24-25	0.04	49-50	0.15

NOTE:

(1) Half range (= 1/2 peak to peak amplitude)

Table 2.15

VENT SYSTEM LOAD AMPLITUDES  
AND FREQUENCIES FOR CHUGGING

<u>Load Type</u>	<u>Frequency (Hz)</u>	<u>Amplitude (psi)</u>		
		<u>Main Vents</u>	<u>Vent Header</u>	<u>Downcomers</u>
Gross Vent System Pressure Oscillation	Use wave form in LDR Figure 4.5.4-1 (0.7 Hz)	<u>+2.5</u>	<u>+2.5</u>	<u>+5.0</u>
Acoustic Vent System Pressure Oscillation	Sinusoidal with frequency varying between 6.9 to 9.5 Hz	<u>+2.5</u>	<u>+3.0</u>	<u>+3.5</u>
Acoustic Downcomer Pressure Oscillation	Sinusoidal with frequency varying between 40 to 50 Hz	N/A	N/A	N/A

Table 2.16

DISTRIBUTION OF DOWNCOMER LATERAL LOAD REVERSALS  
DUE TO CHUGGING

<u>Percent of Maximum Load Range</u>	<u>Group 1</u>	<u>Group 2</u>
5-10	4,706	3,168
10-15	2,696	1,104
15-20	1,399	709
20-25	676	452
25-30	380	255
30-35	209	139
35-40	157	86
40-45	113	48
45-50	83	32
50-55	65	14
55-60	51	11
60-65	44	5
65-70	32	7
70-75	19	11
75-80	26	4
80-85	12	2
85-90	11	0
90-95	9	2
95-100	7	2

Notes:

- (1) Group 1: Sectors 1, 2, 7, & 8  
Group 2: Sectors 3, 4, 5, & 6
- (2) Refer to Figure 2.23 for the sectors

Table 2.17

STRUCTURES SUBJECTED TO T-QUENCHER WATER JET LOADS

Torus Shell Components

- Ring girder

S/RVD Piping and Supports

- 16" support pipe for S/RVD

Internal Piping and Supports

- RCIC pump suction strainer
- HPCI pump suction strainer



Table 2.18

FATIGUE DESIGN BASIS INCLUDING DBA EVENT

<u>Combination Number</u>	<u>Load Combinations</u>	<u>Number of Effective Cycles at Maximum Stress (1)</u>
1	DBA CO + Containment Temp + Containment Pressure + SSE (2)	1
2	DBA CO + SSE	9
3	DBA CO	80
4	Post-Chug (3)	32
5	Pre-Chug (3)	100
6	NOC S/RV Discharge (4) + OBE (5)	50
7	NOC S/RV Discharge	2950

Notes:

- (1) Number of effective cycles is the equivalent number of cycles at maximum stress contributing to fatigue usage.
- (2) One SSE over 40 year plant life assumed to occur during DBA event (10 significant load cycles/SSE).
- (3) Chugging load duration divided into periods of Pre-chug and Post-chug as described in LDR Section 4.5.1.2.
- (4) 500 S/RV discharges during normal operating conditions (NOC) assumed based on plant operating data.
- (5) Five OBE events over 40 year plant life assumed to occur during S/RV discharge events (10 significant load cycles/OBE).
- (6) Cumulative usage determined by calculating usage for each combination and summing over all combinations.

Table 2.19

FATIGUE DESIGN BASIS INCLUDING IBA/SBA EVENT

<u>Combination Number</u>	<u>Load Combinations</u>	<u>Number of Effective Cycles at Maximum Stress (1)</u>
1	Post-Chug + 6 ADS S/RV Discharge + Containment Temp + Containment Pressure + SSE (2)	1
2	Post-Chug + 6 ADS S/RV Discharge + SSE	9
3	Post-Chug (3)	960
4	Pre-Chug (3)	3040
5	IBA CO	3040
6	NOC S/RV Discharge (4) + OBE (5)	50
7	NOC S/RV Discharge (4)	2950

Notes:

- (1) Number of effective cycles is the equivalent number of cycles at maximum stress contributing to fatigue usage.
- (2) One SSE over 40 year plant life assumed to occur during DBA event (10 significant load cycles/SSE).
- (3) Chugging load duration divided into periods of Pre-chug and Post-chug as described in LDR Section 4.5.1.2.
- (4) 500 S/RV discharges during normal operating conditions (NOC) assumed based on plant operating data.
- (5) Five OBE events over 40 year plant life assumed to occur during S/RV discharge events (10 significant load cycles/OBE).
- (6) Cumulative usage determined by calculating usage for each combination and summing over all combinations.

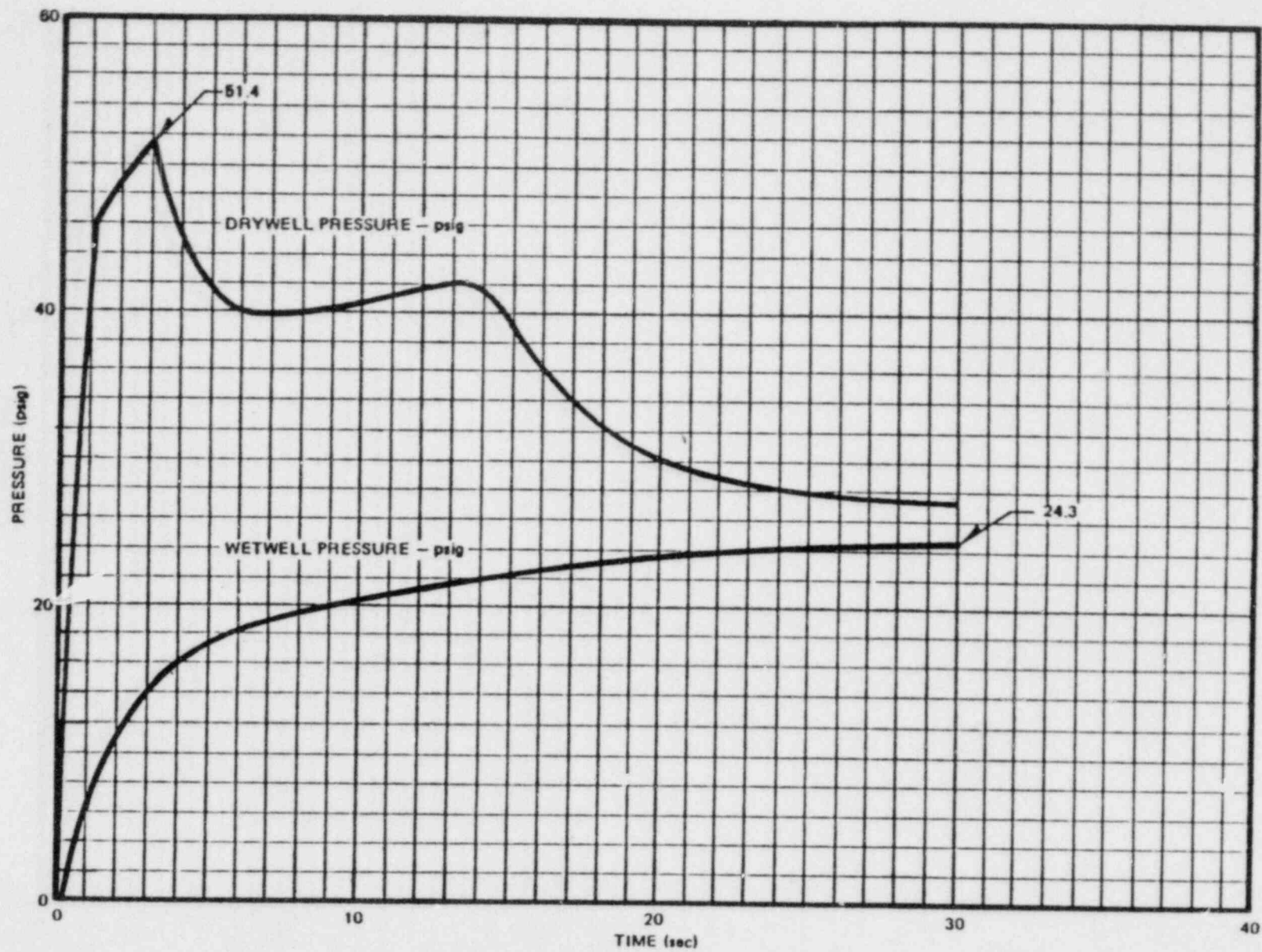


FIGURE 2.1

DBA CONTAINMENT PRESSURE RESPONSE

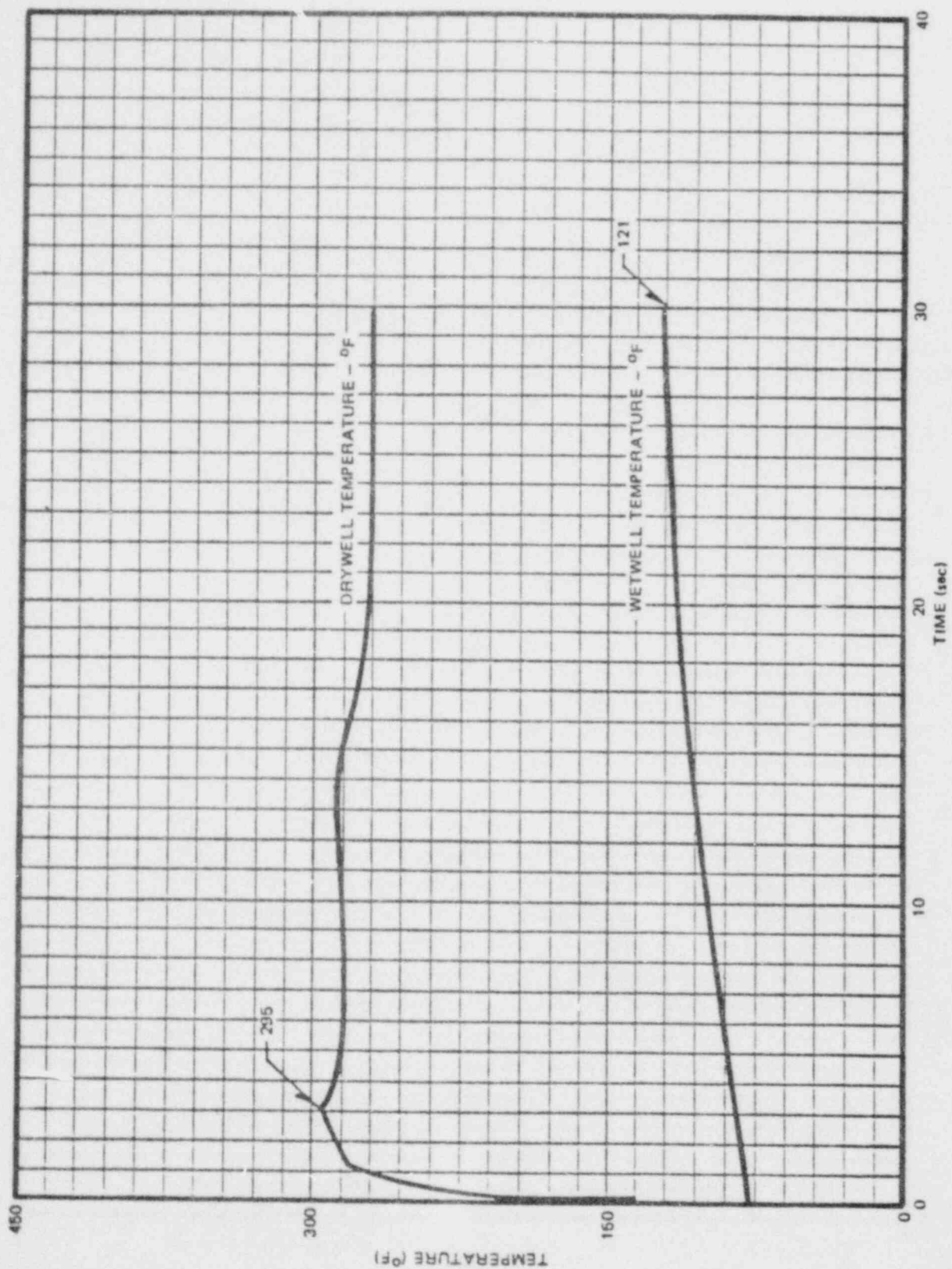


FIGURE 2.2  
DBA CONTAINMENT TEMPERATURE RESPONSE

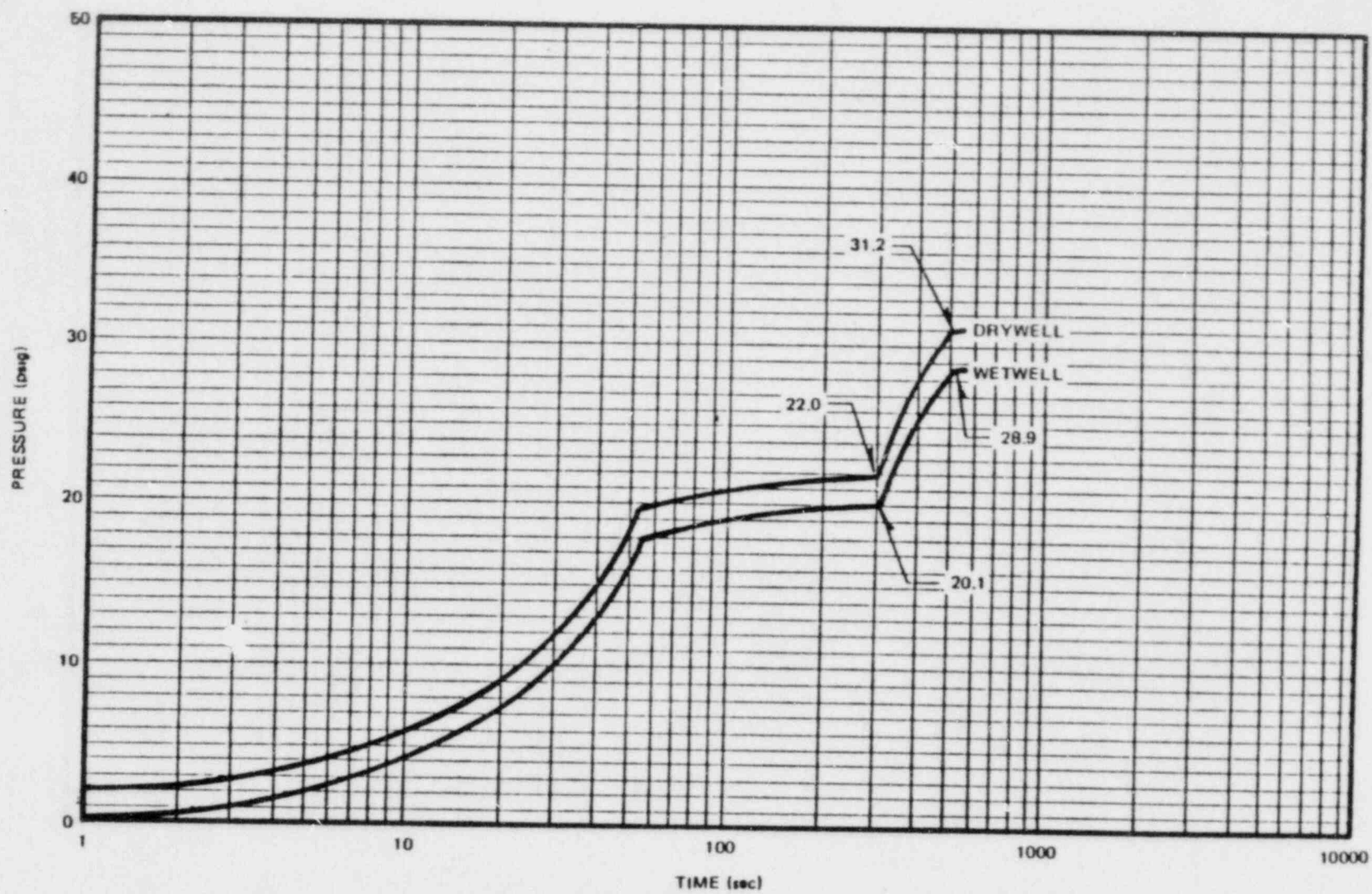


FIGURE 2.3

IBA CONTAINMENT PRESSURE RESPONSE



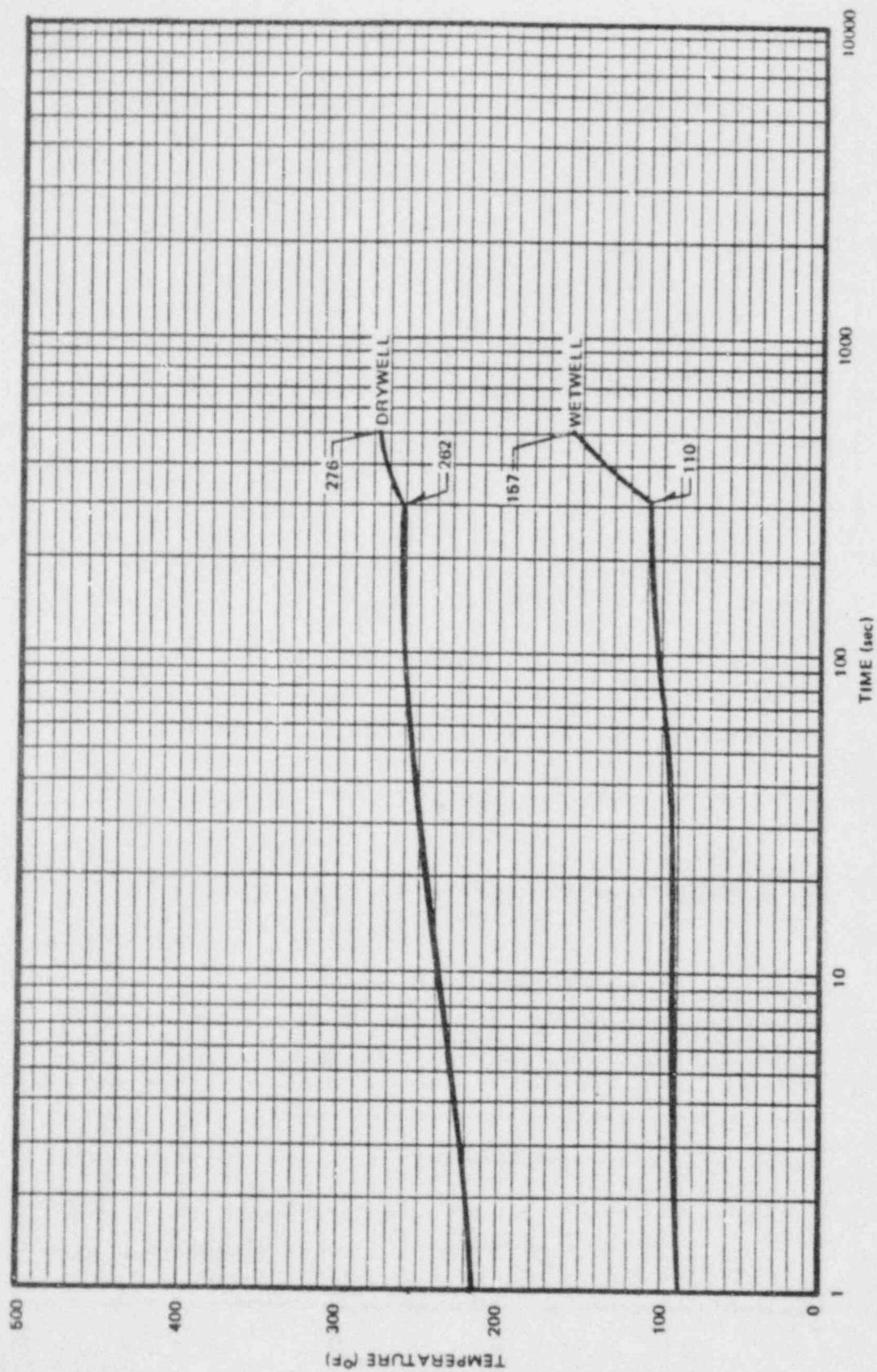


FIGURE 2.4  
IBA CONTAINMENT TEMPERATURE RESPONSE



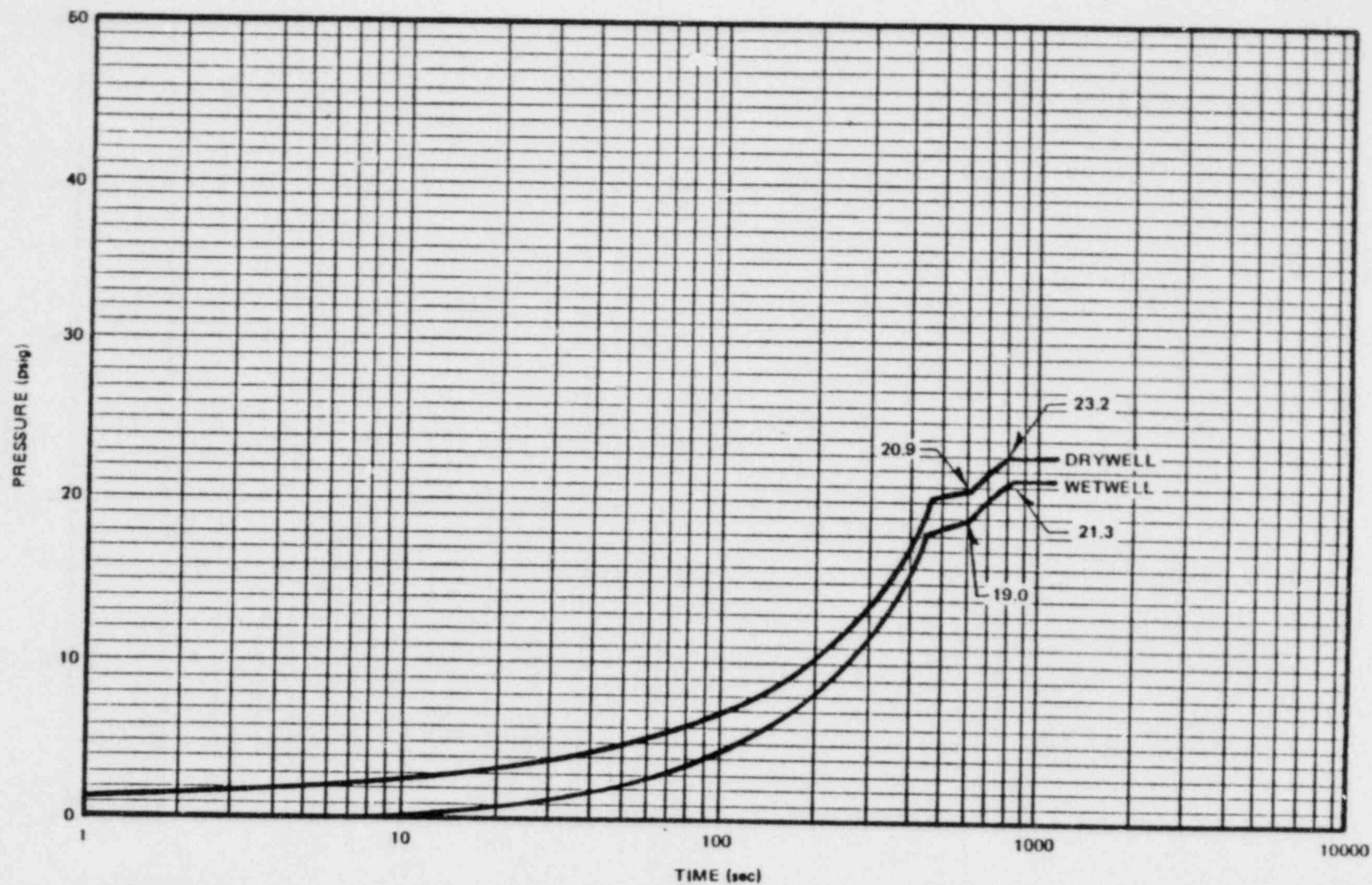


FIGURE 2.5

SBA CONTAINMENT PRESSURE RESPONSE

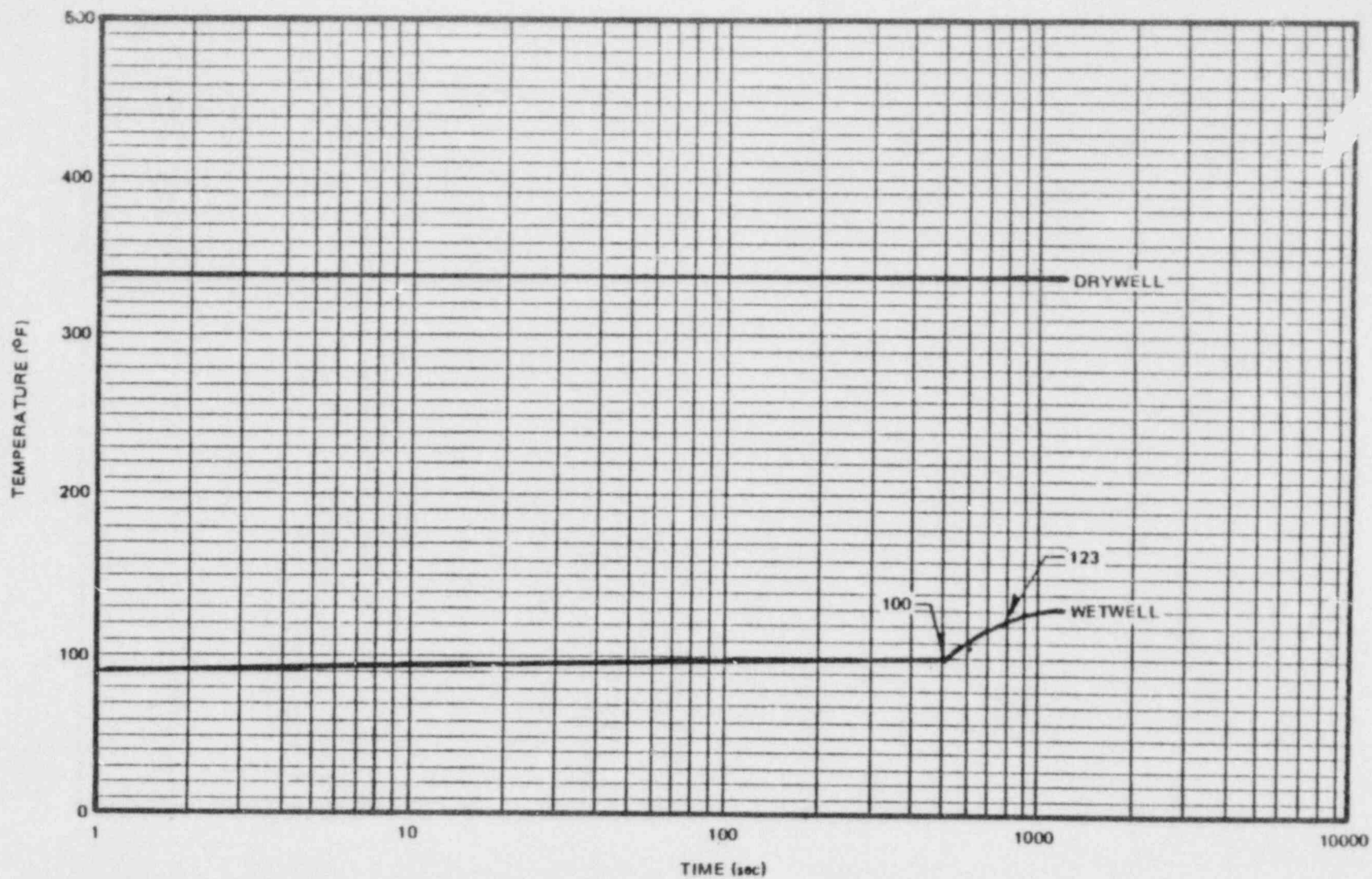
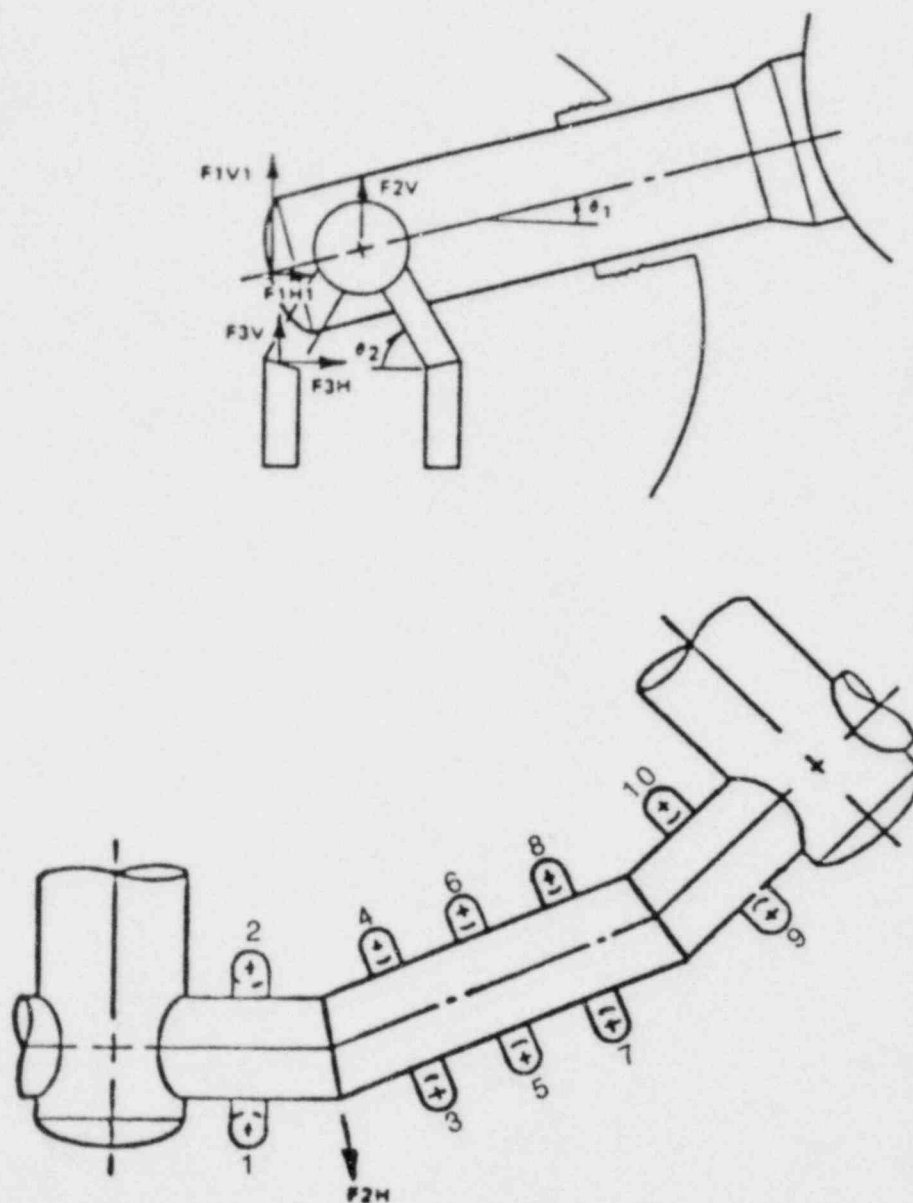


FIGURE 2.6

SBA CONTAINMENT TEMPERATURE RESPONSE



- F1V1 = VERTICAL FORCE ON MAIN VENT END CAP
- F1H1 = HORIZONTAL FORCE ON MAIN VENT END CAP
- F2V = VERTICAL FORCE ON VENT HEADER (PER MITRE BEND)
- F2H = HORIZONTAL FORCE ON VENT HEADER (PER MITRE BEND)
- F3V = VERTICAL FORCE ON DOWNCOMER MITRE BEND
- F3H = HORIZONTAL FORCE ON DOWNCOMER MITRE BEND

FIGURE 2.7

VENT SYSTEM THRUST LOAD APPLICATION

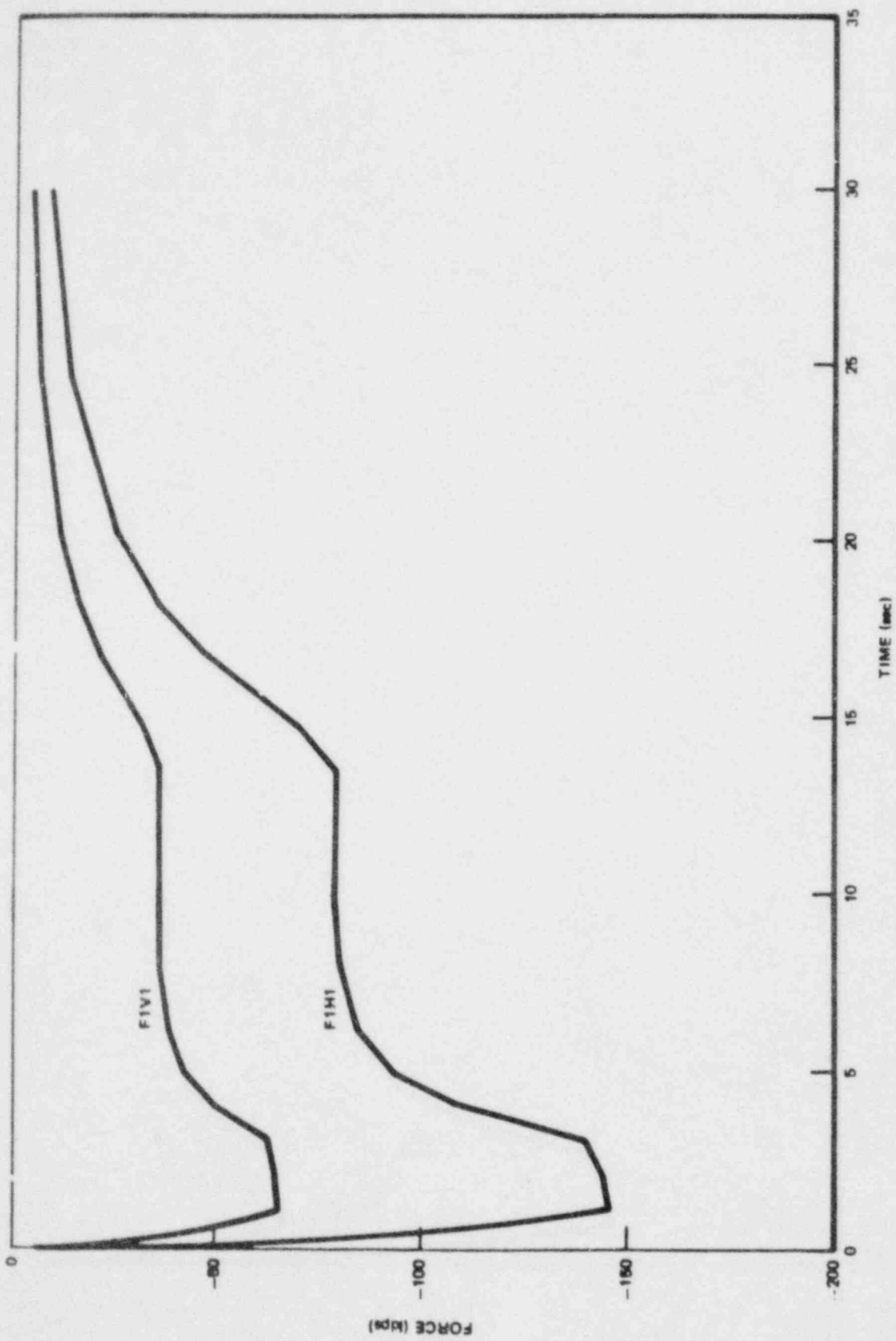


FIGURE 2.8  
SINGLE MAIN VENT FORCES (0-30 sec), ZERO  $\Delta P$

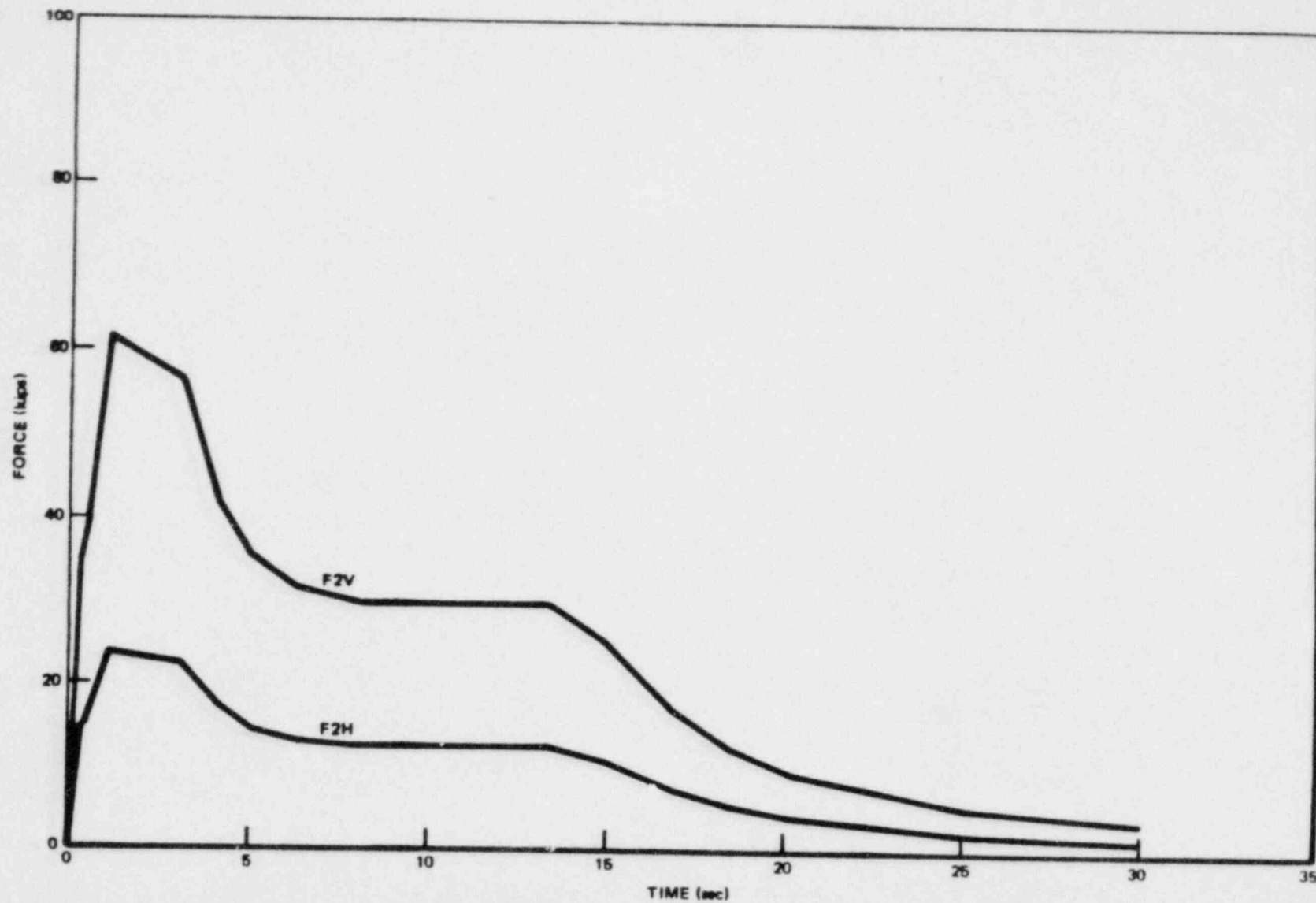


FIGURE 2.9

VENT HEADER FORCES PER MITER BEND (0-30 sec), ZERO  $\Delta P$

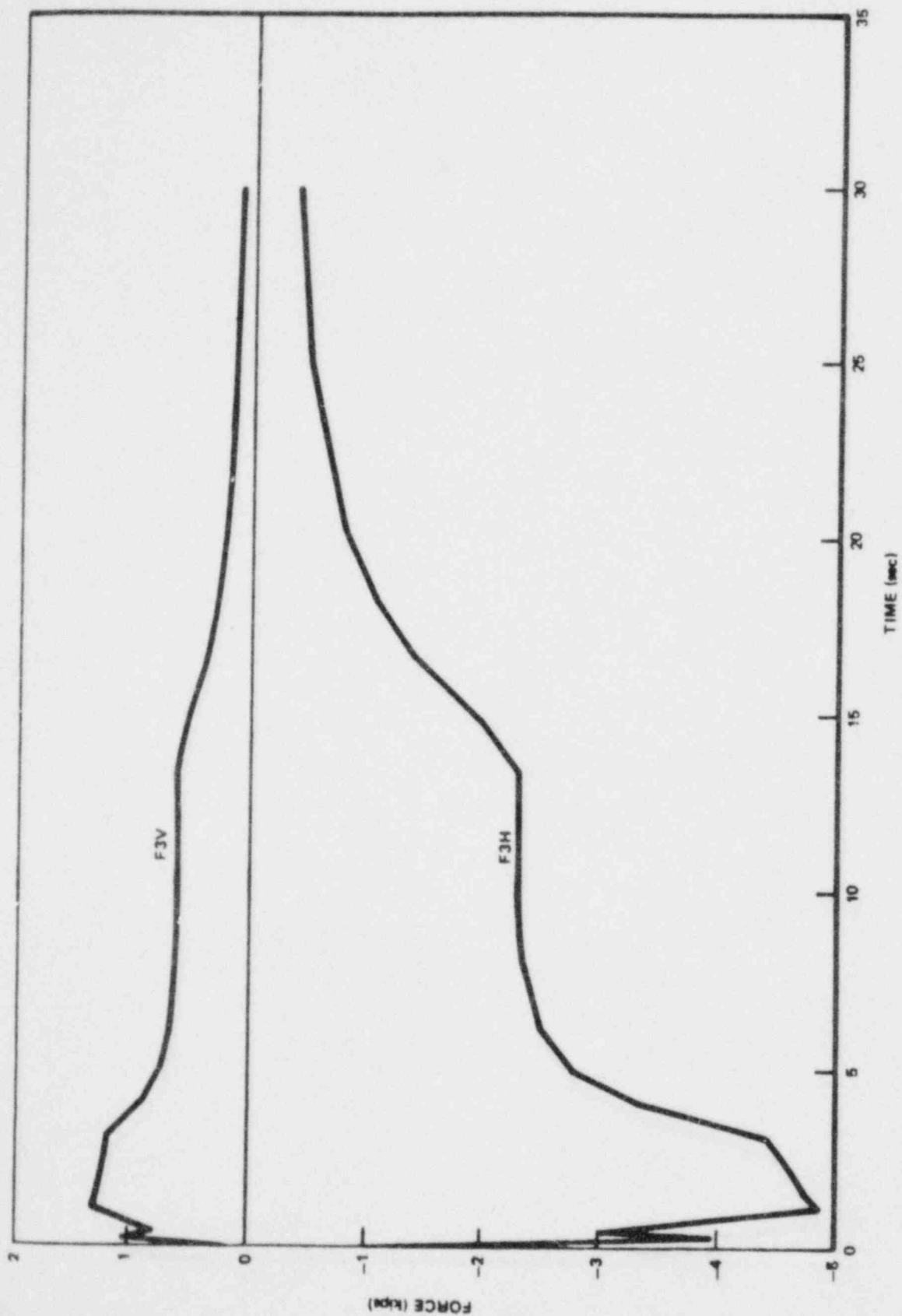


FIGURE 2.10  
SINGLE DOWNCOMER FORCES (0-30 sec), ZERO  $\Delta P$



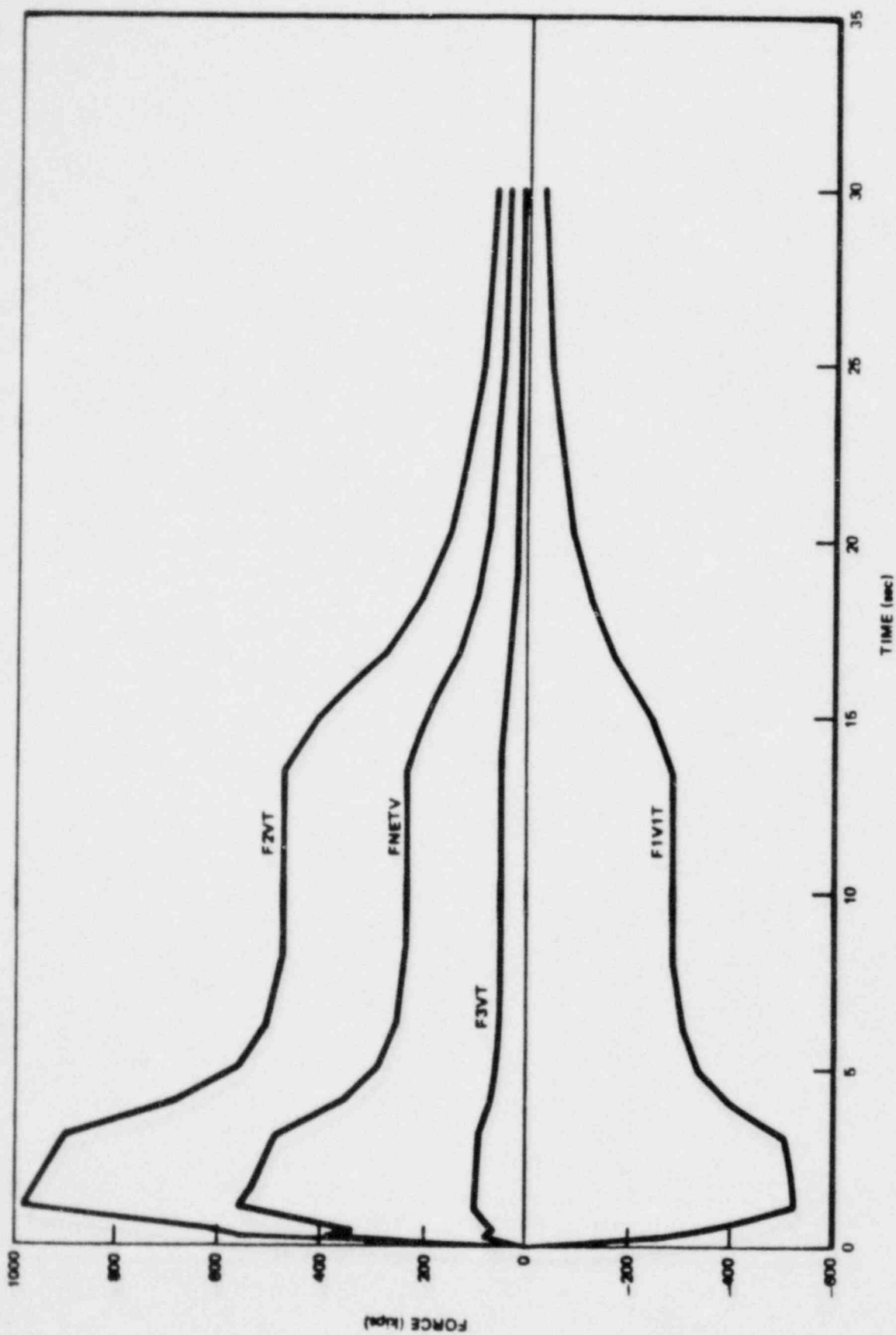


FIGURE 2.11  
TOTAL AND NET VERTICAL FORCES (0-30 sec), ZERO  $\Delta P$

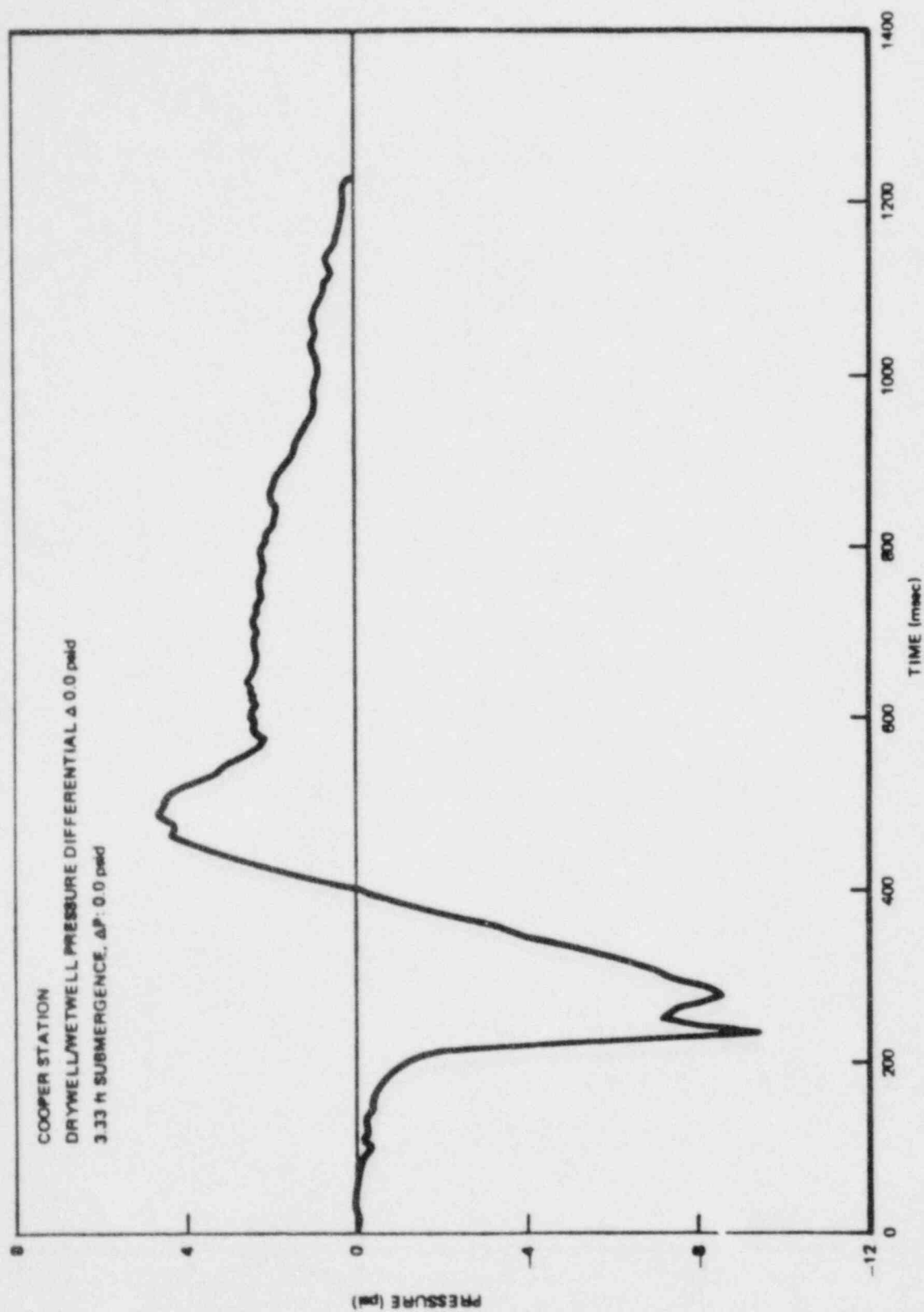


FIGURE 2.12  
NET TORUS VERTICAL LOAD, ZERO  $\Delta P$

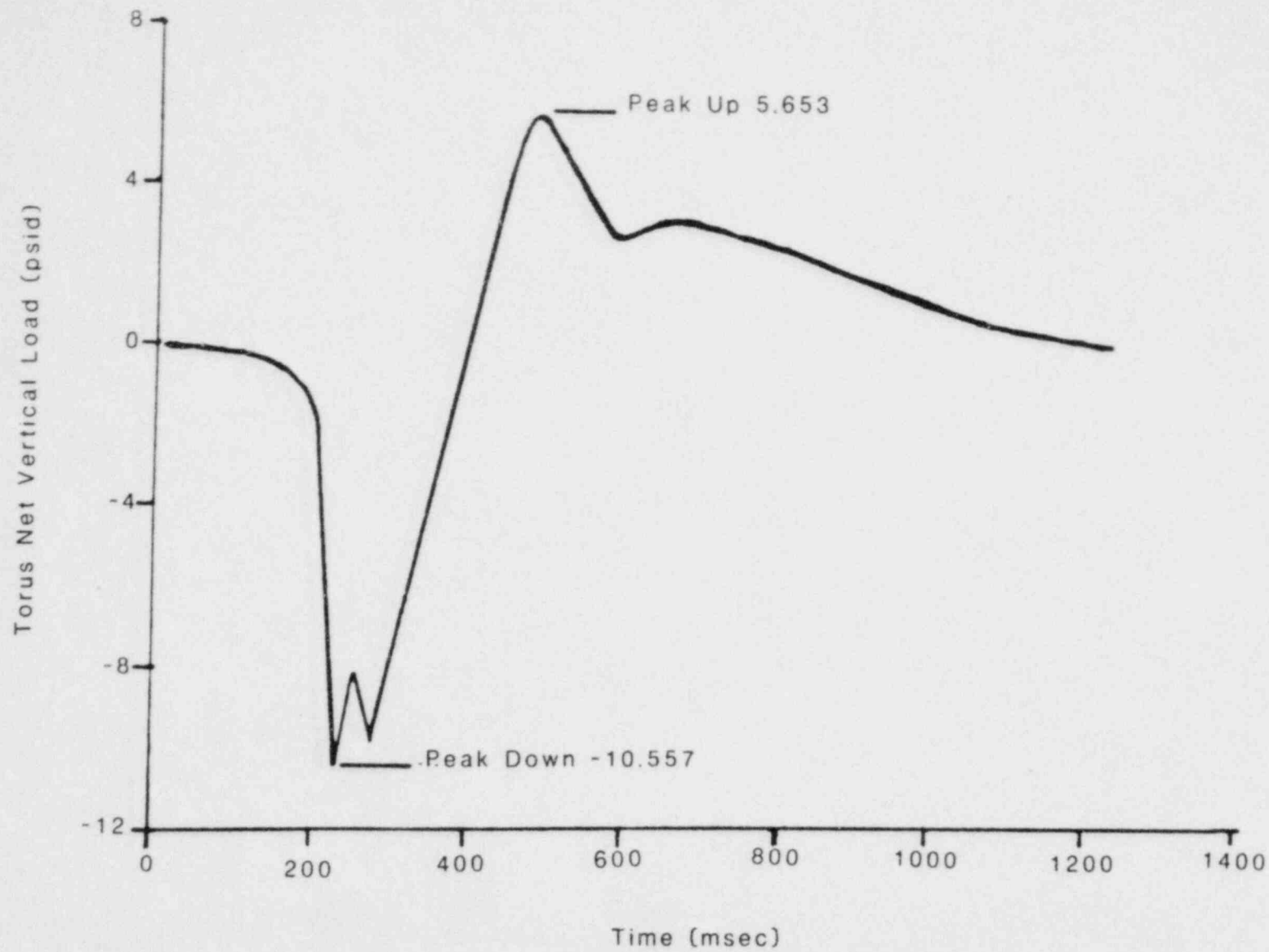


FIGURE 2.13

CORRECTED TORUS NET VERTICAL LOADS (NRC), (ZERO  $\Delta P$ )

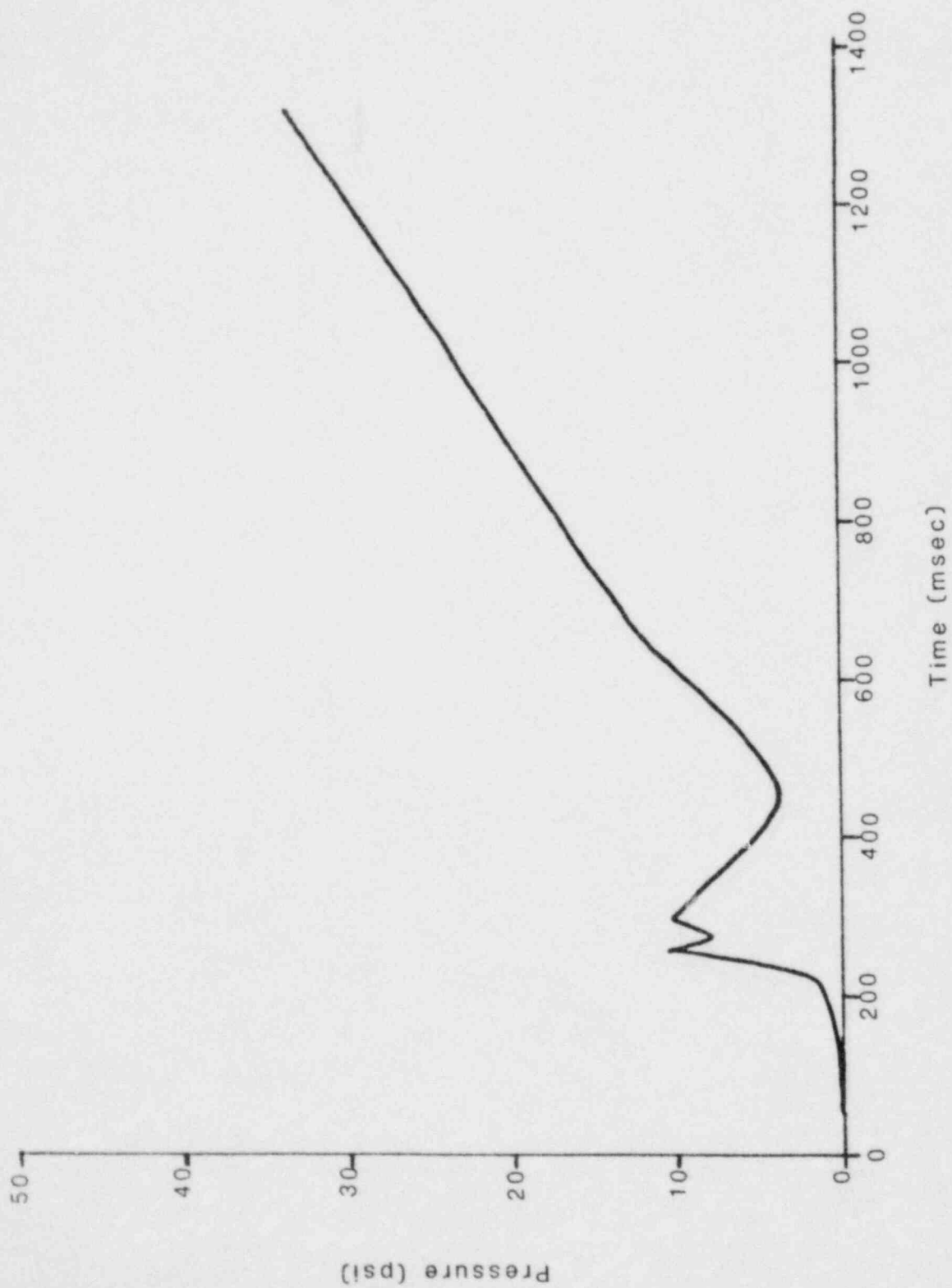


FIGURE 2.14  
CORRECTED AVERAGE SUBMERGED PRESSURE DUE TO POOL SWELL (NRC), ZERO  $\Delta P$

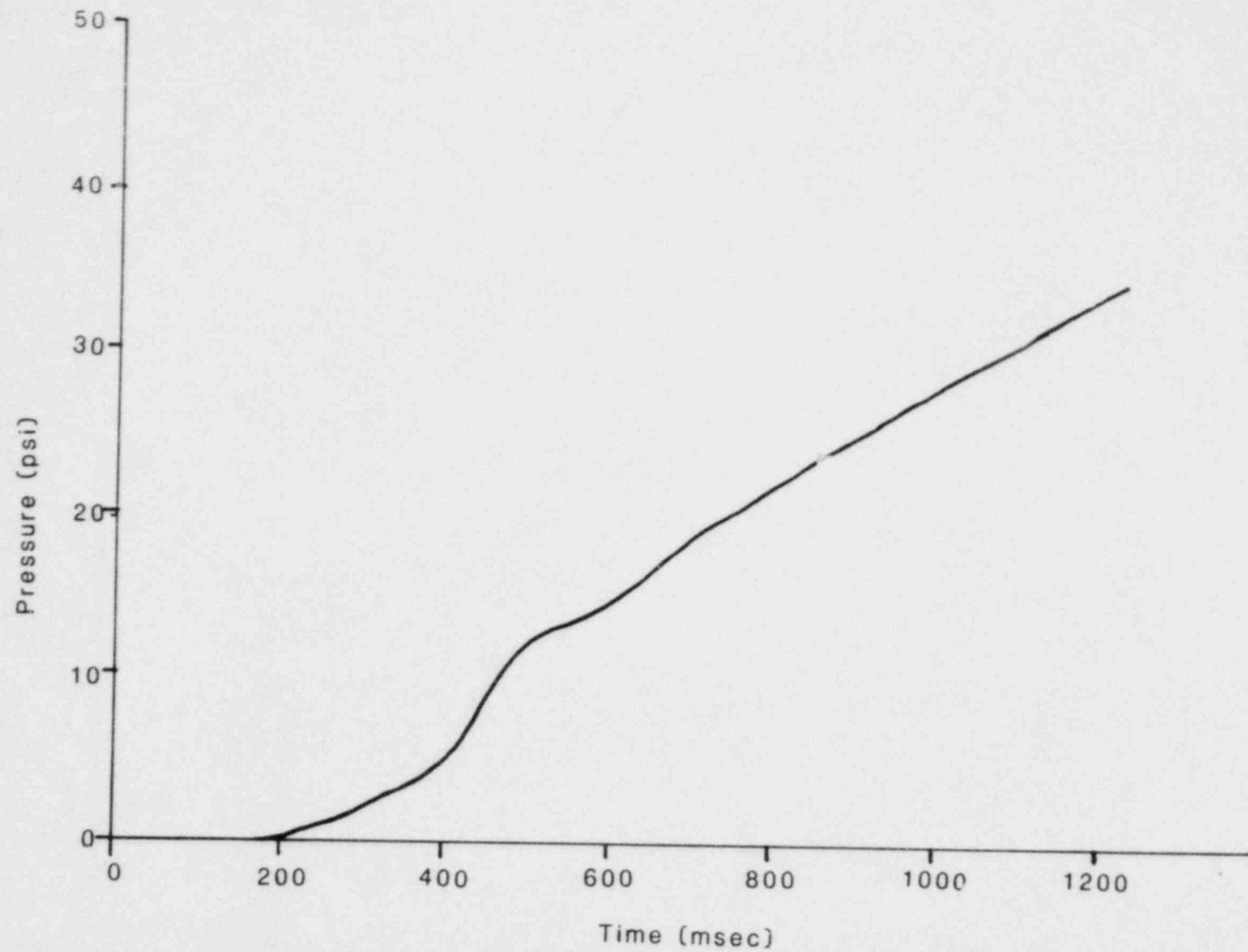
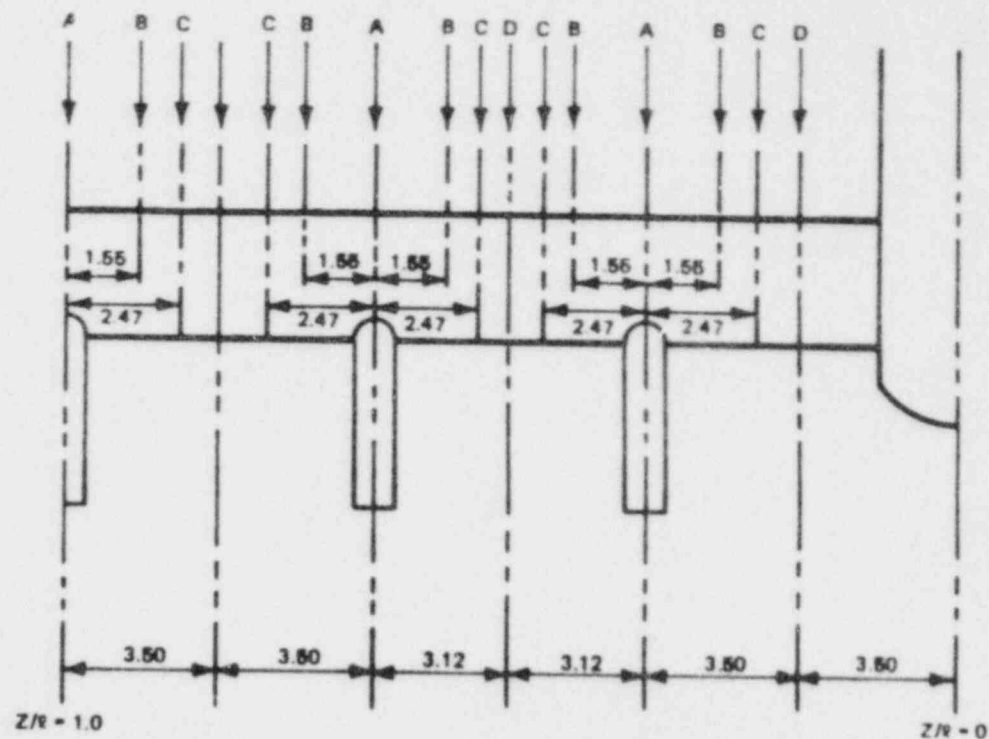
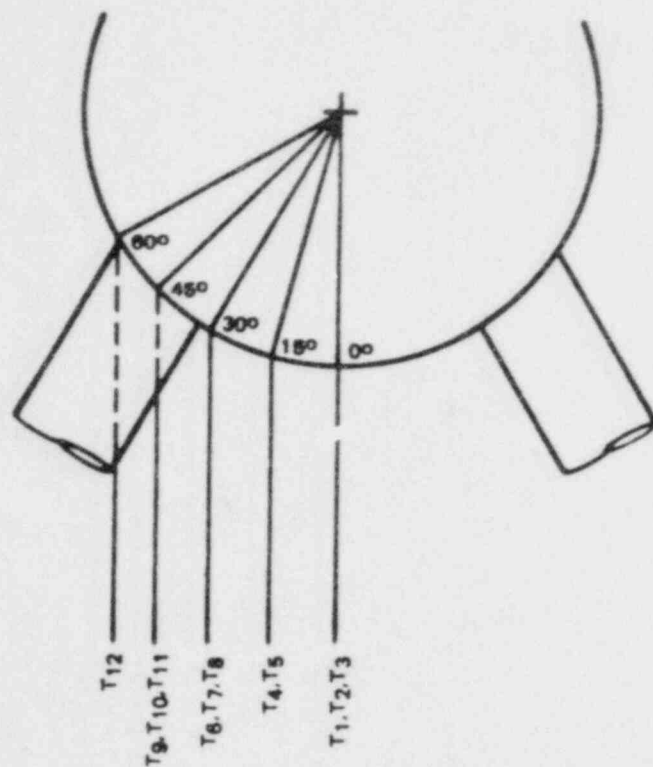


FIGURE 2.15

CORRECTED TORUS AIRSPACE PRESSURE DUE TO POOL SWELL (NRC) ZERO  $\Delta P$



ALL DIMENSIONS ARE IN FEET

A - TRANSIENTS T<sub>1</sub>

B - TRANSIENTS T<sub>2</sub>, T<sub>4</sub>, T<sub>6</sub>, T<sub>9</sub>

C - TRANSIENTS T<sub>7</sub>, T<sub>10</sub>, T<sub>12</sub>

D - TRANSIENTS T<sub>3</sub>, T<sub>5</sub>, T<sub>8</sub>, T<sub>11</sub>

FIGURE 2.16

LOCATION OF IMPACT/DRAG PRESSURE TRANSIENTS ON VENT HEADER



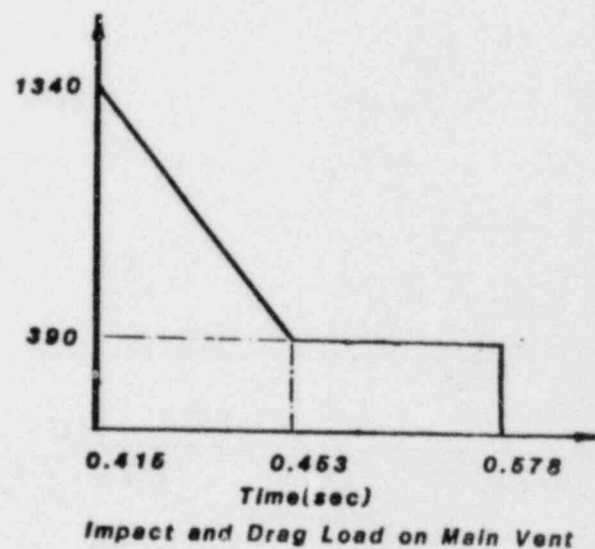
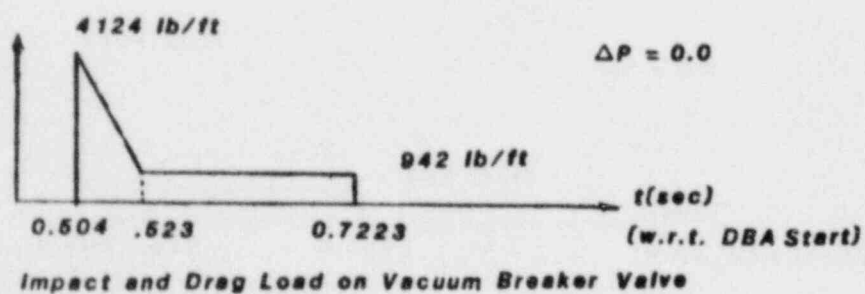
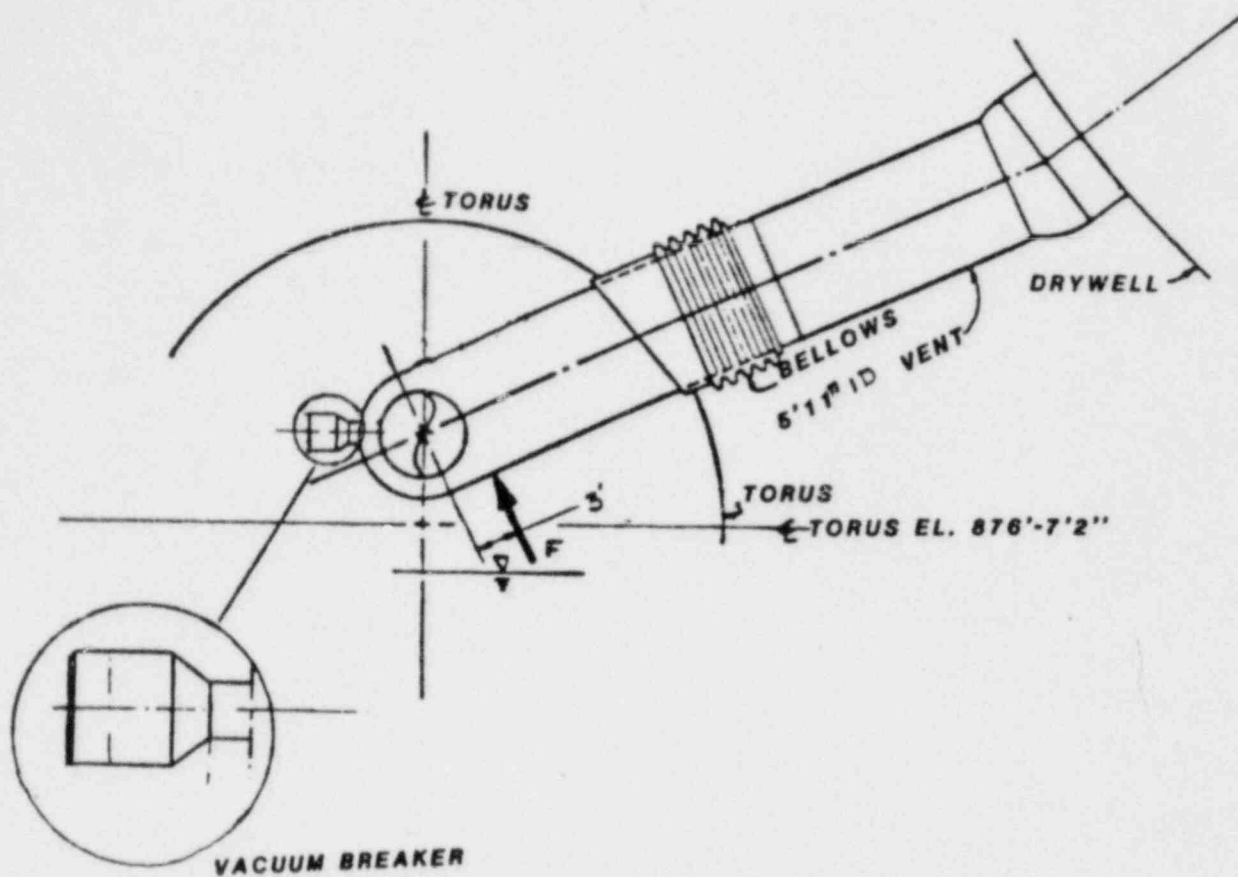


FIGURE 2.17

POOL SWELL IMPACT/DRAG LOAD TRANSIENTS  
ON MAIN VENT,  $\Delta P = 1.0$  psid

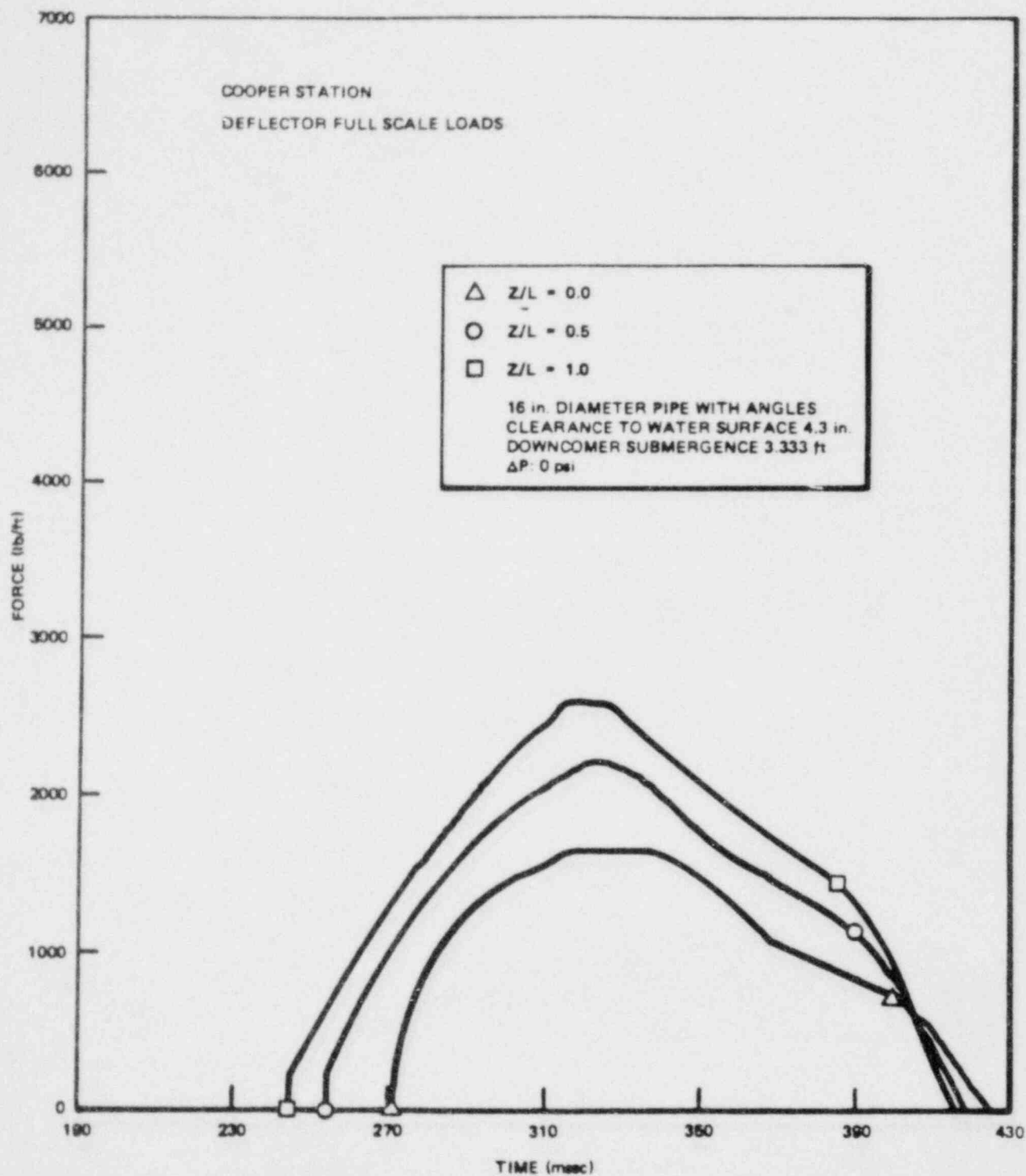
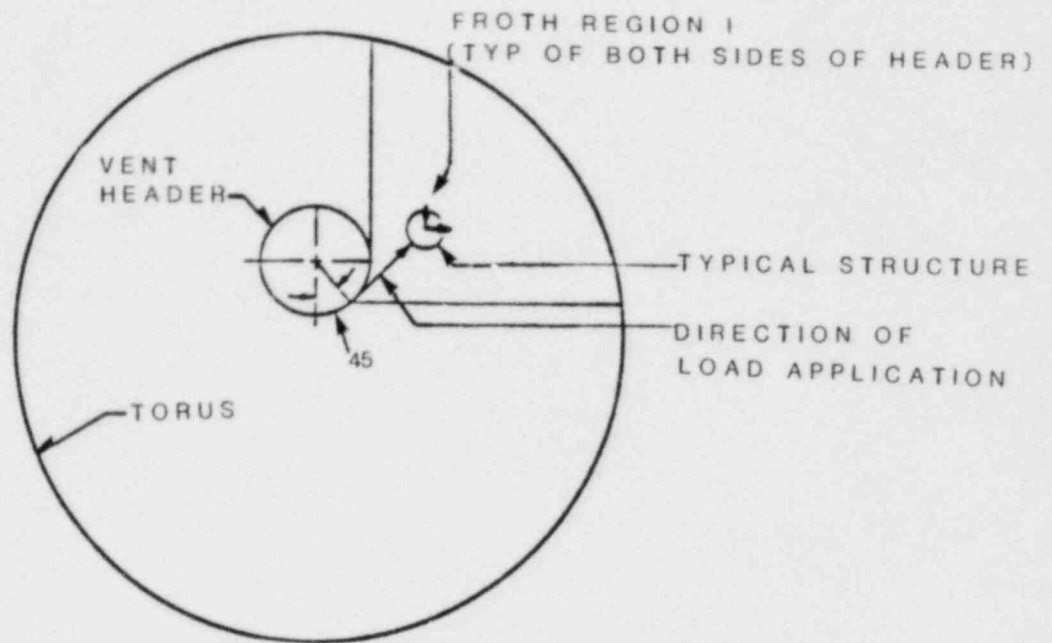
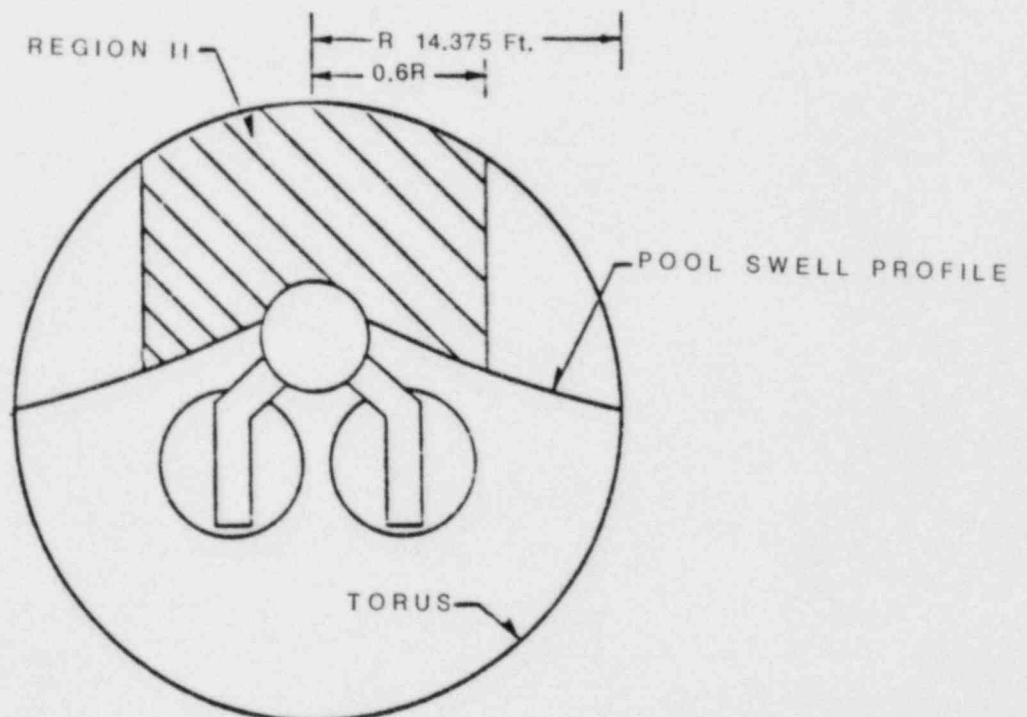


FIGURE 2.18  
VENT HEADER DEFLECTOR LOADS



Region I

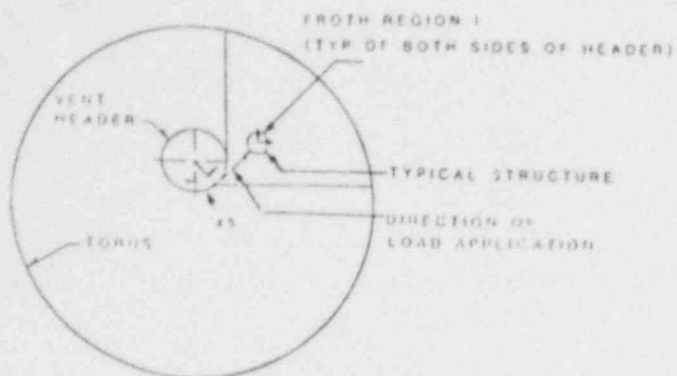


Region II

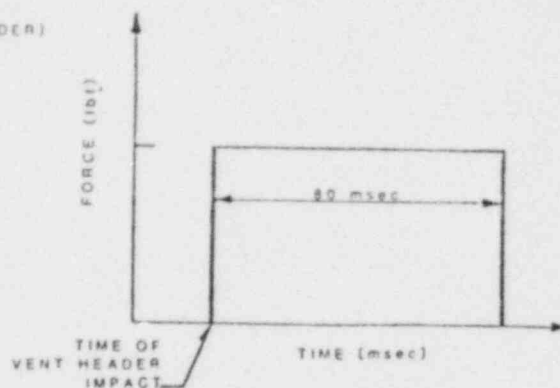
FIGURE 2.19

DEFINITION OF FROTH IMPINGEMENT REGIONS

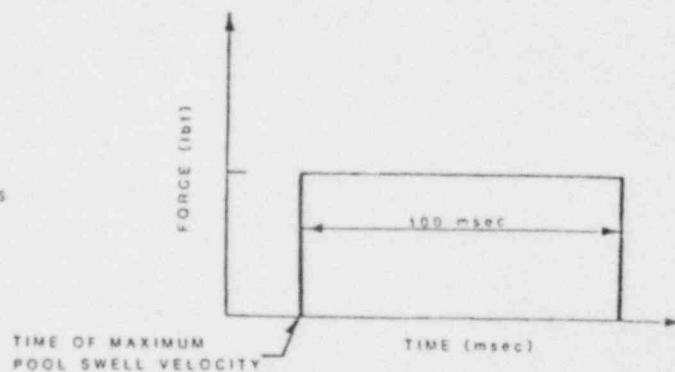
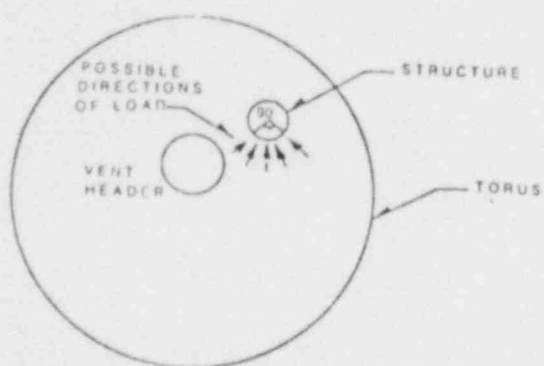
## DIRECTION OF LOAD APPLICATION



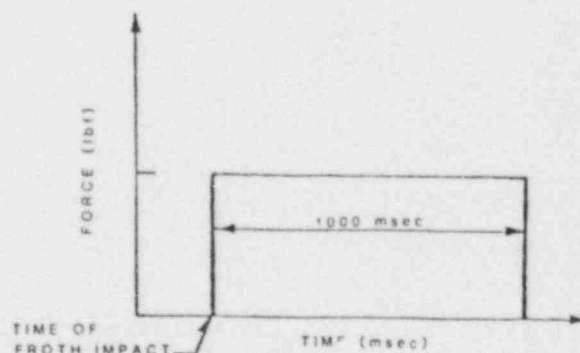
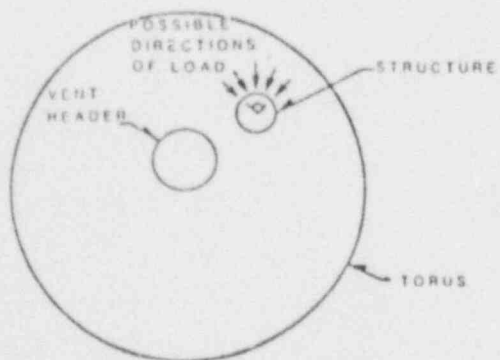
## LOAD TRANSIENT



Froth Impingement Region I



Froth Impingement Region II



Froth Fallback

FIGURE 2.20

DEFINITION OF FROTH LOAD APPLICATIONS AND TRANSIENTS

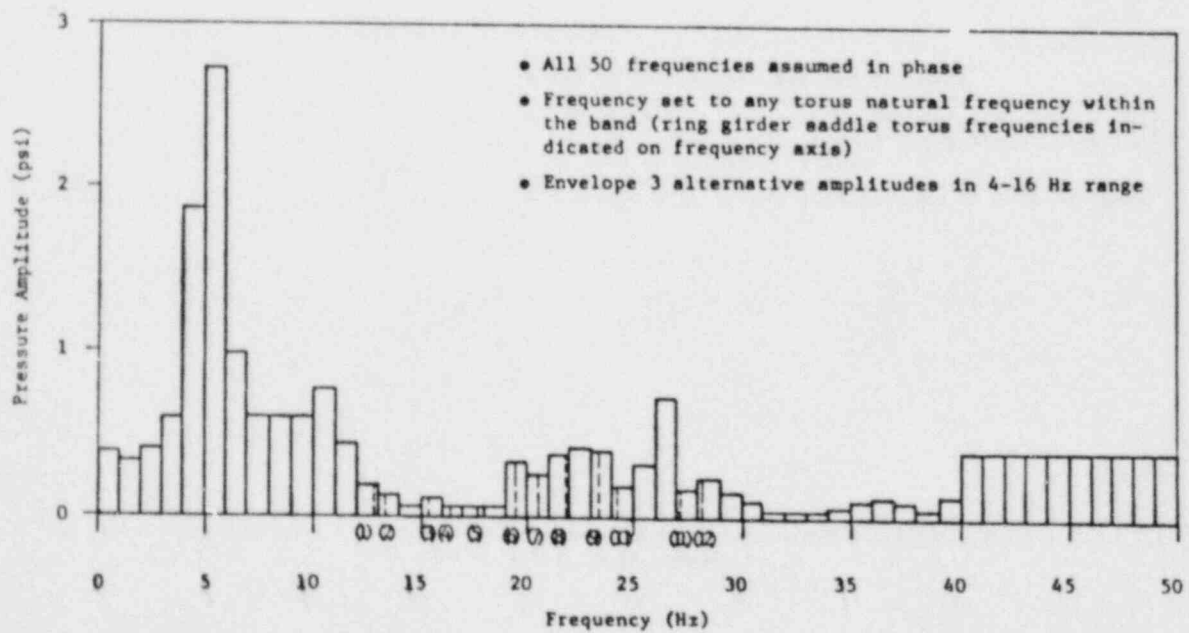
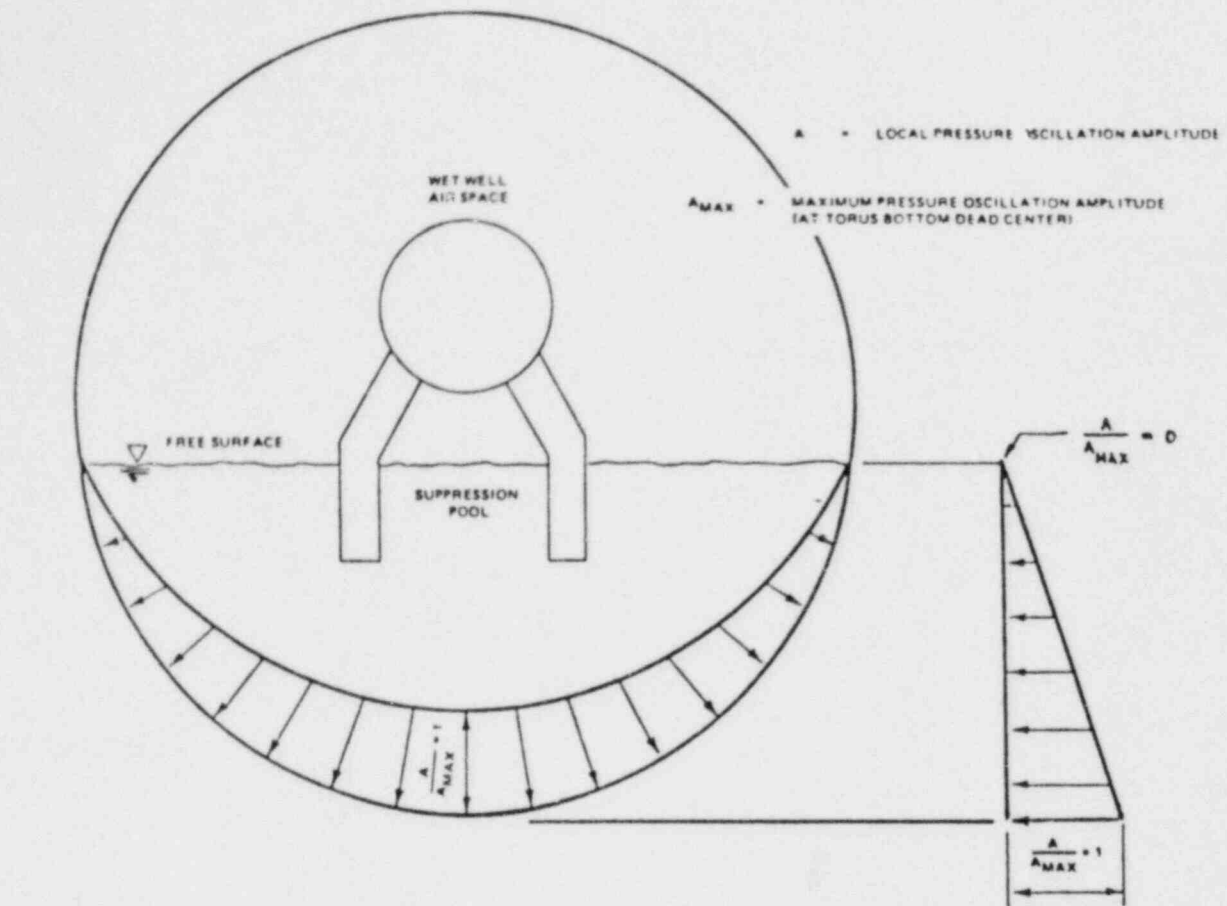


FIGURE 2.21

TORUS PRESSURE AMPLITUDE DISTRIBUTION FOR CONDENSATION OSCILLATION

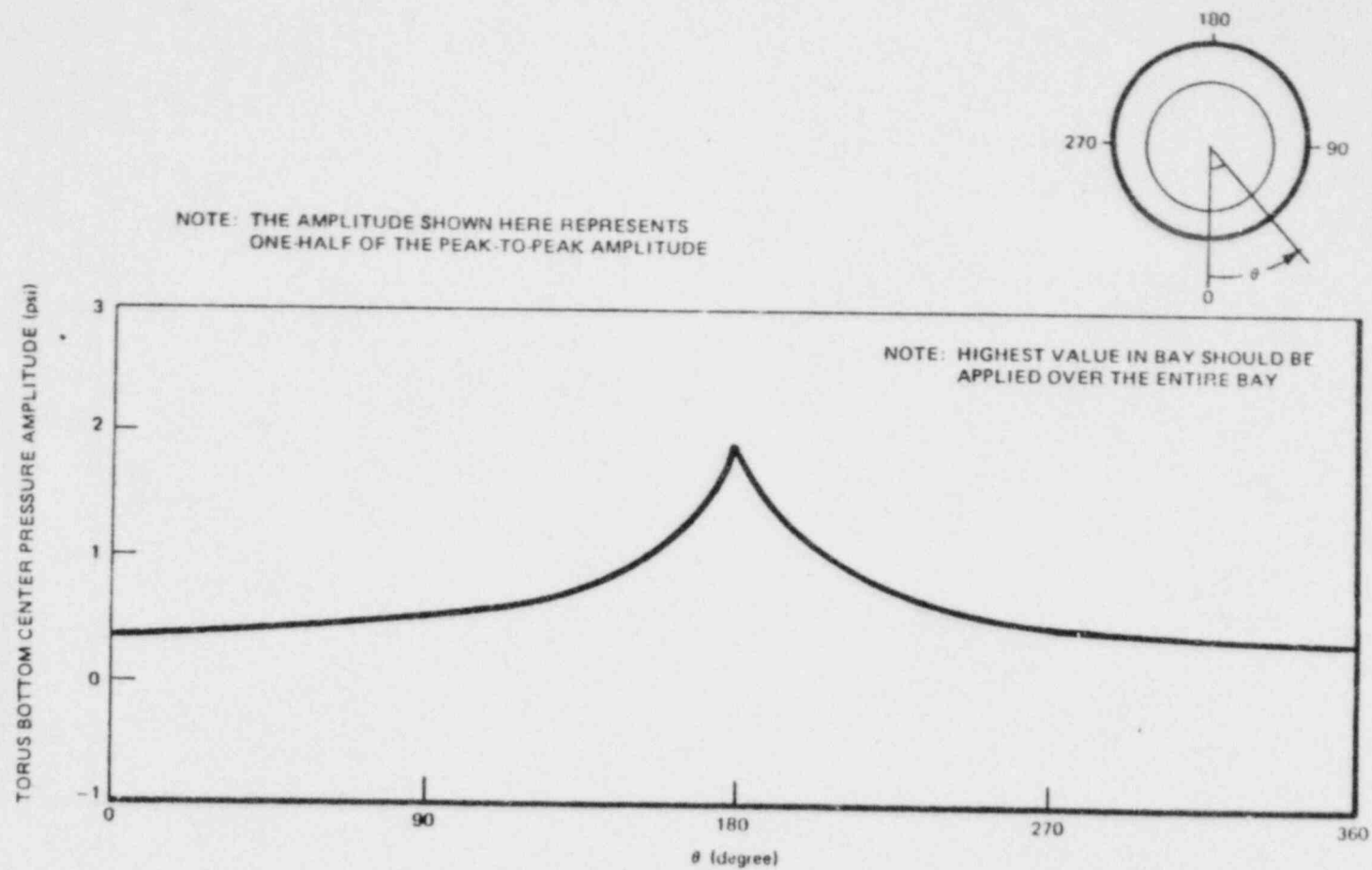


FIGURE 2.22

TORUS ASYMMETRIC CIRCUMFERENTIAL DISTRIBUTION FOR PRE-CHUG PRESSURE AMPLITUDE



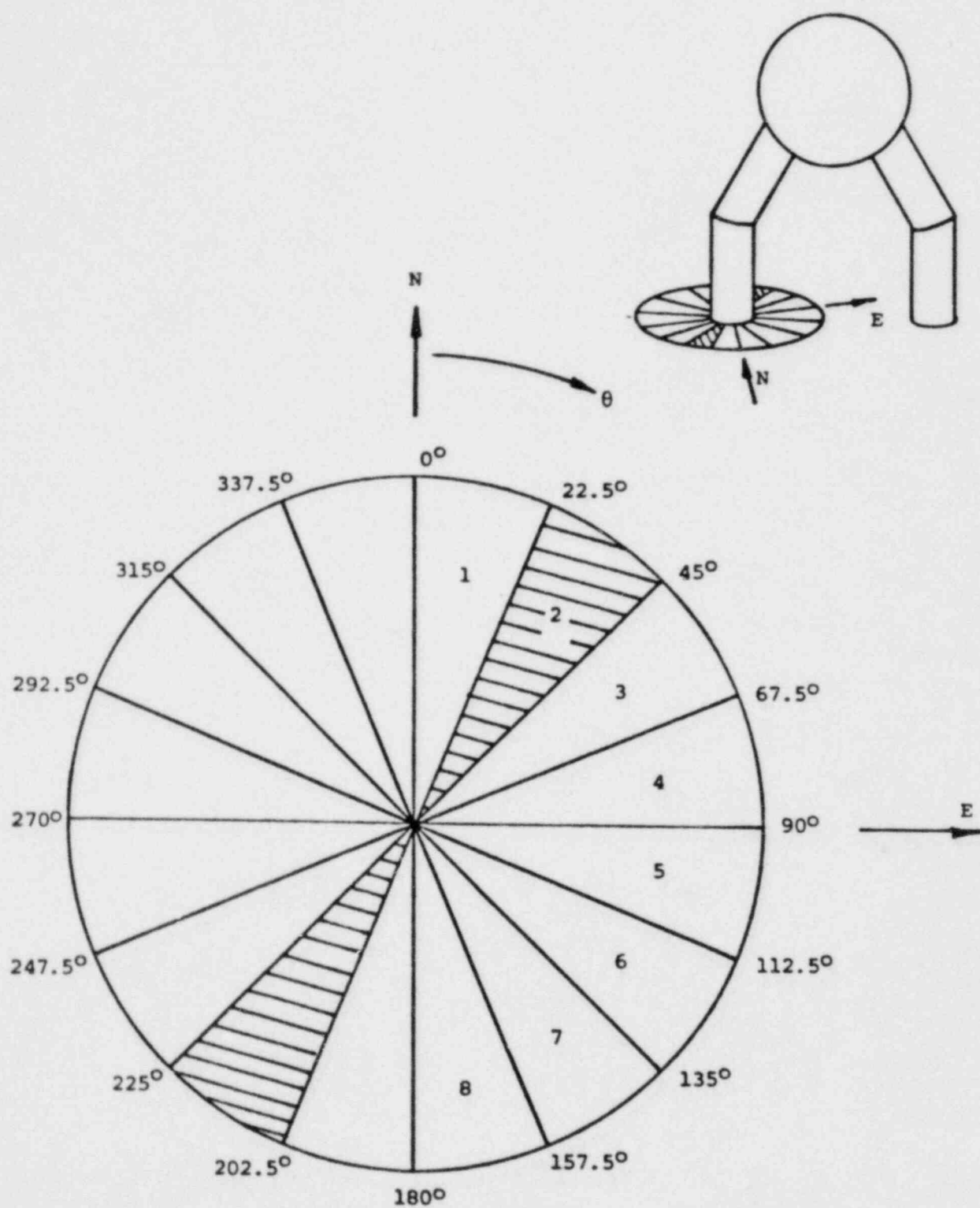


FIGURE 2.23  
SECTORS USED TO DEFINE DIRECTIONS OF LATERAL  
LOADS ON DOWNCOMER END

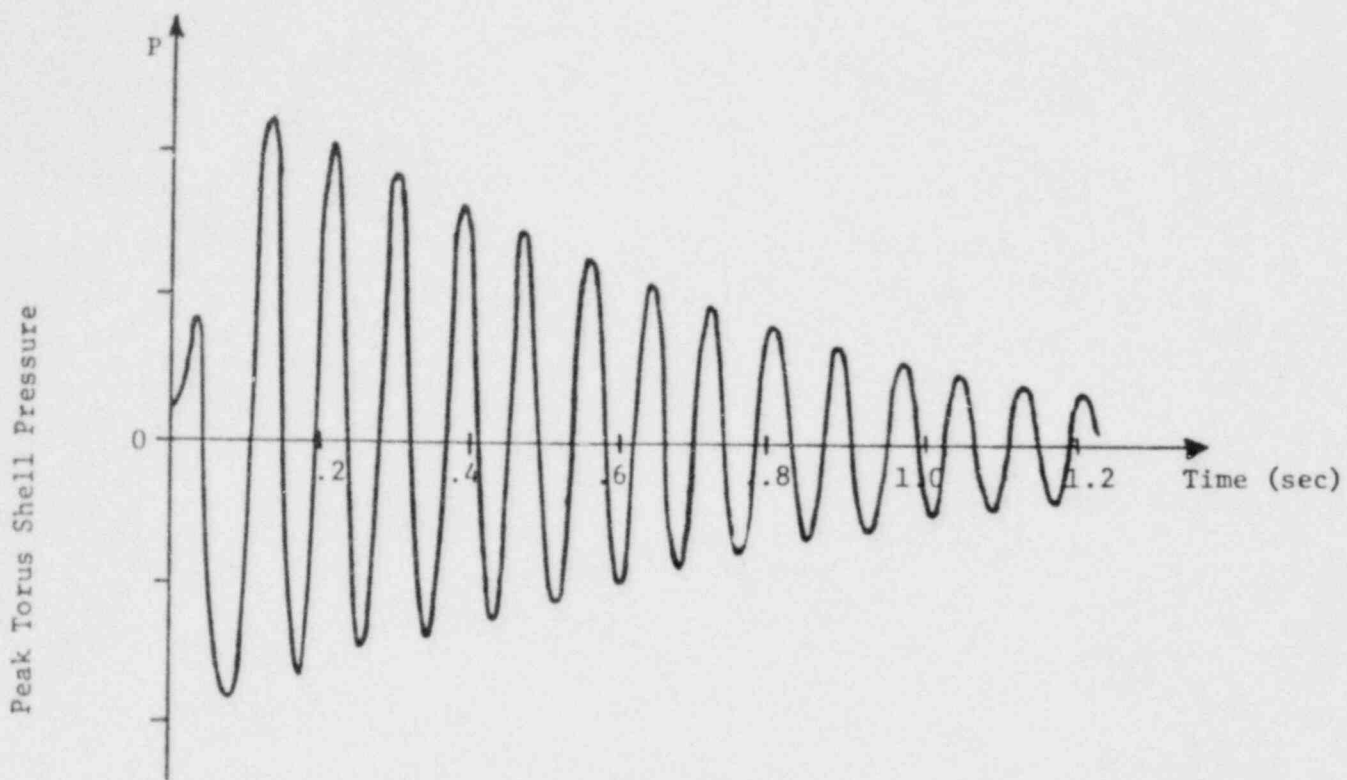


FIGURE 2.24

TYPICAL TORUS SHELL S/RV PRESSURE TIME HISTORY

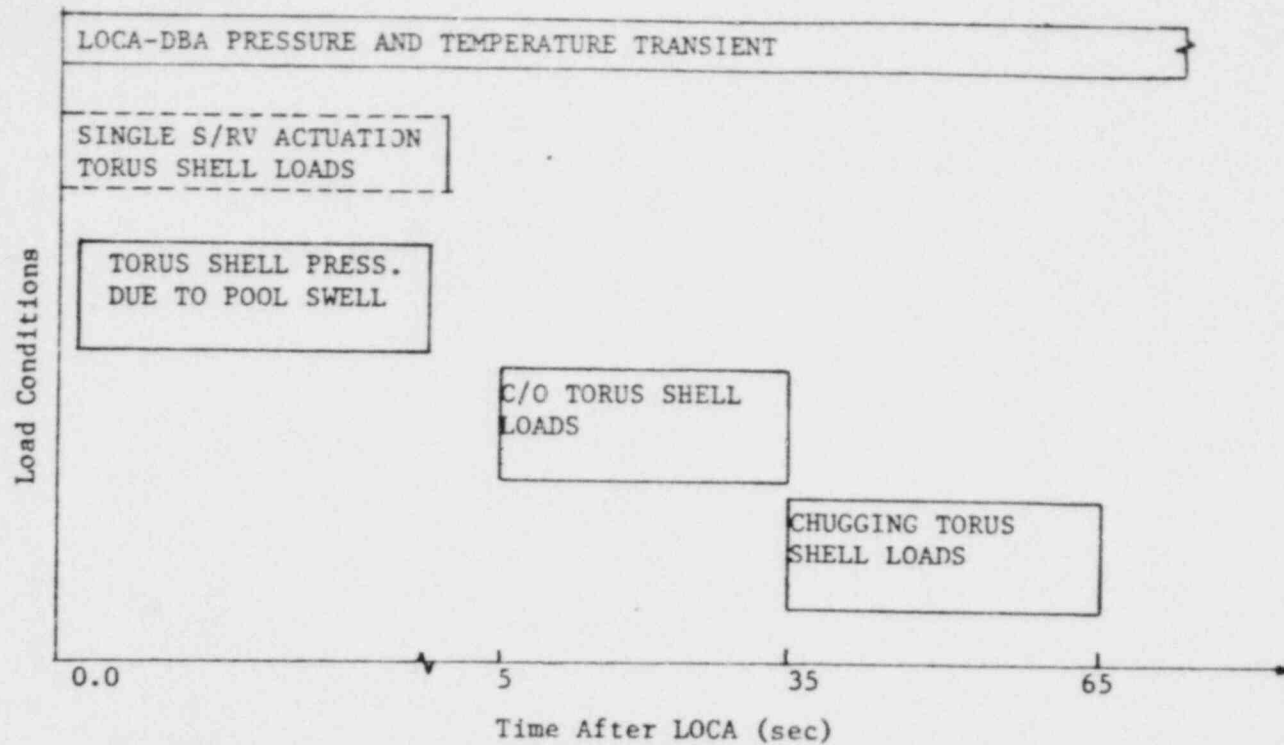
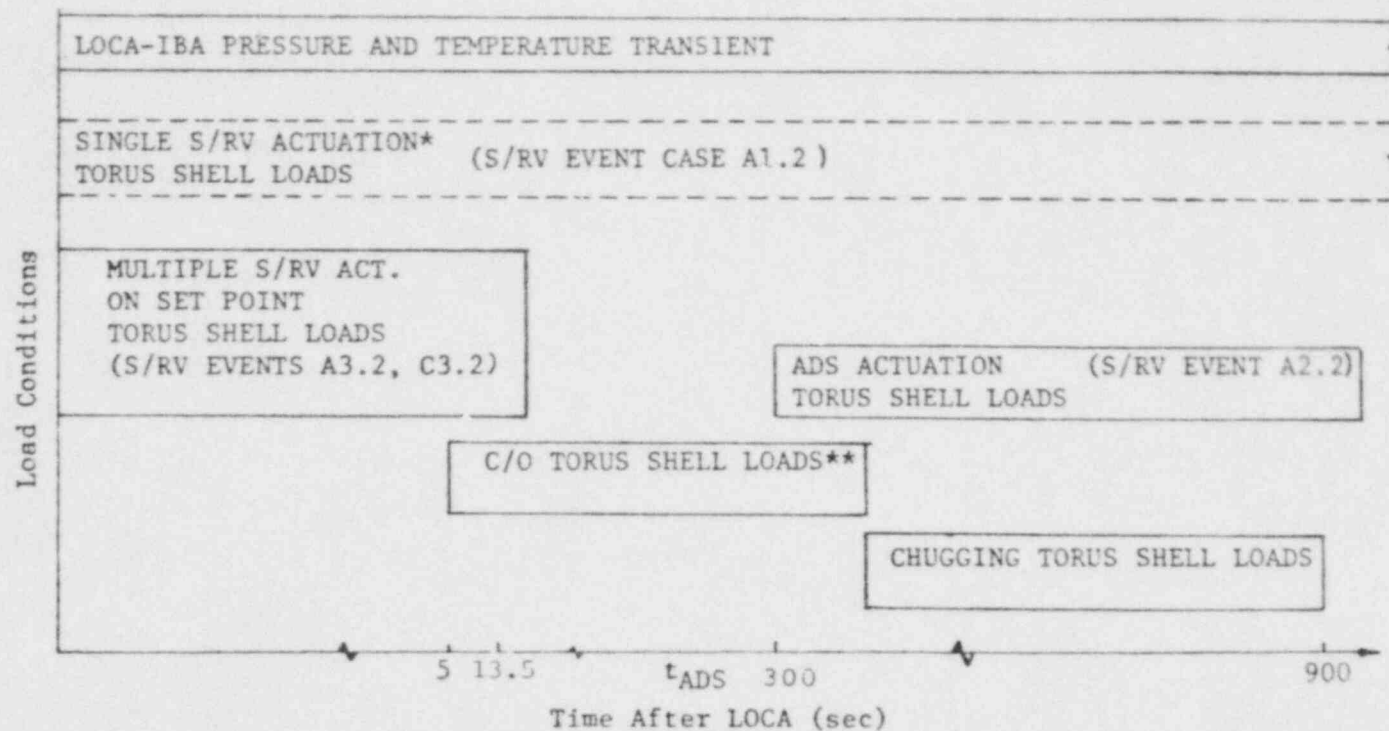


FIGURE 2.25

TORUS SHELL LOAD COMBINATIONS FOR LOCA-DBA

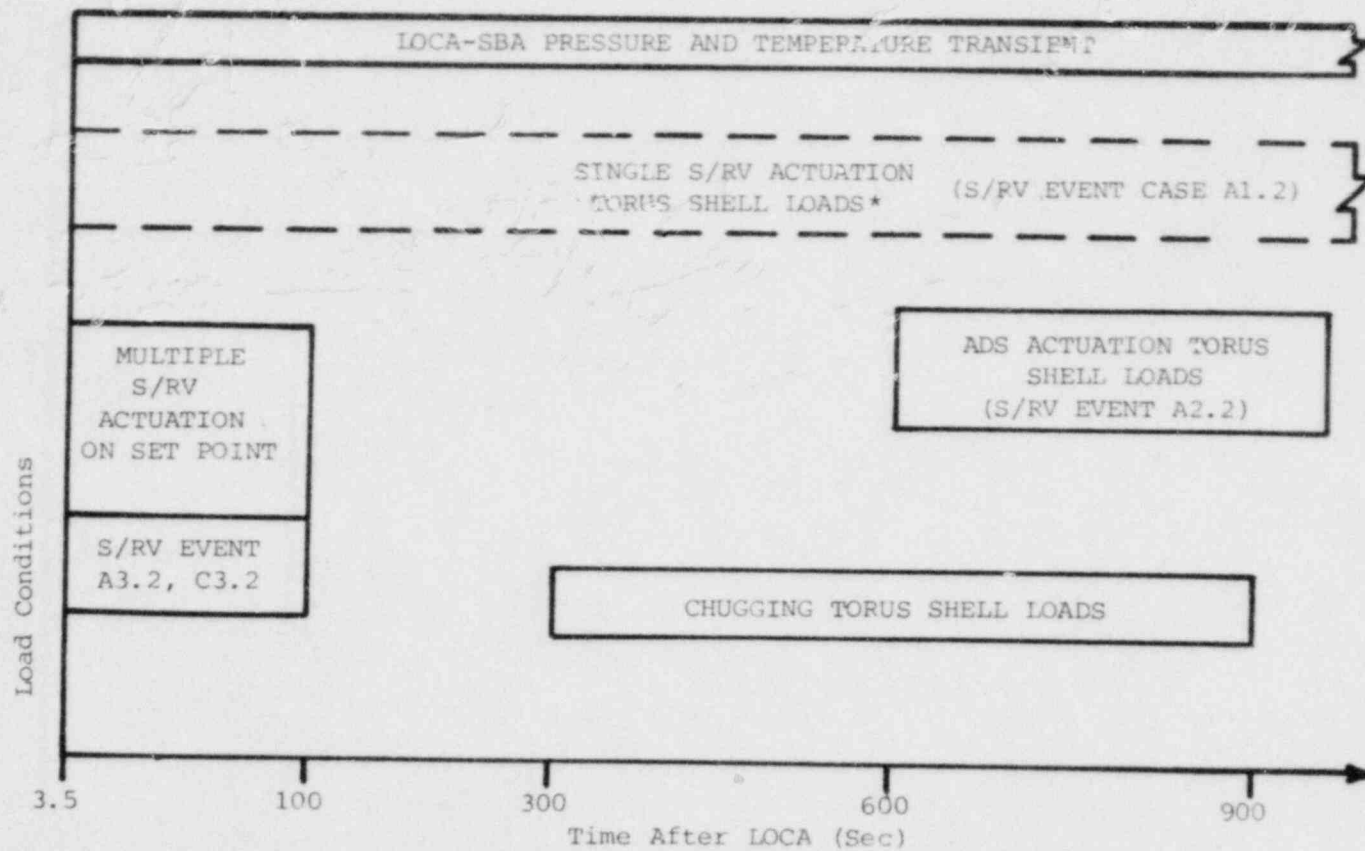


\*Loading does not combine with other S/RV cases.

\*\*Bounded by chugging loads.

FIGURE 2.26

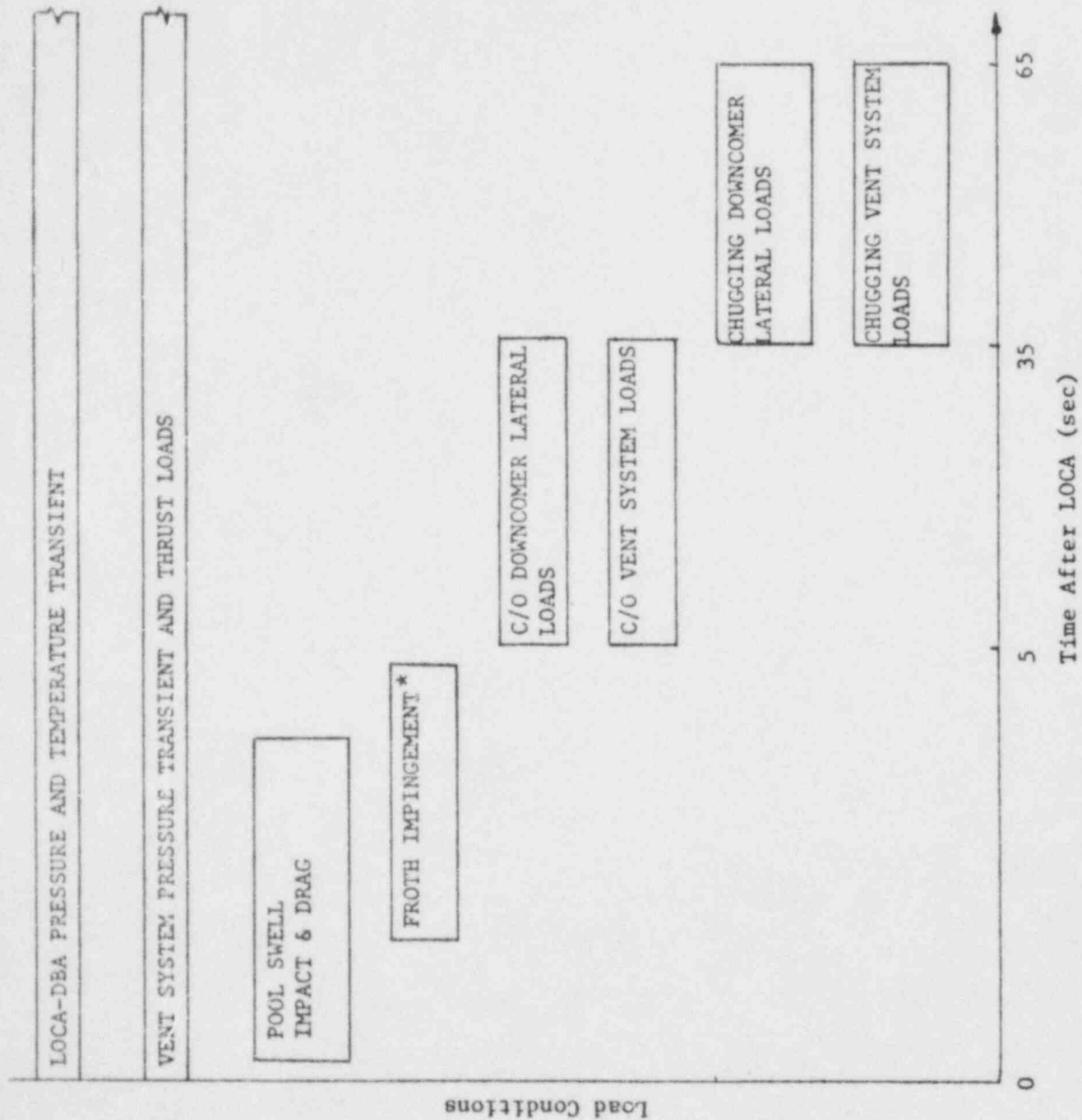
TORUS SHELL LOAD COMBINATIONS FOR LOCA-IBA



\*Loading does not combine with other S/RV cases.

FIGURE 2.27

TORUS SHELL LOAD COMBINATIONS FOR LOCA-SBA



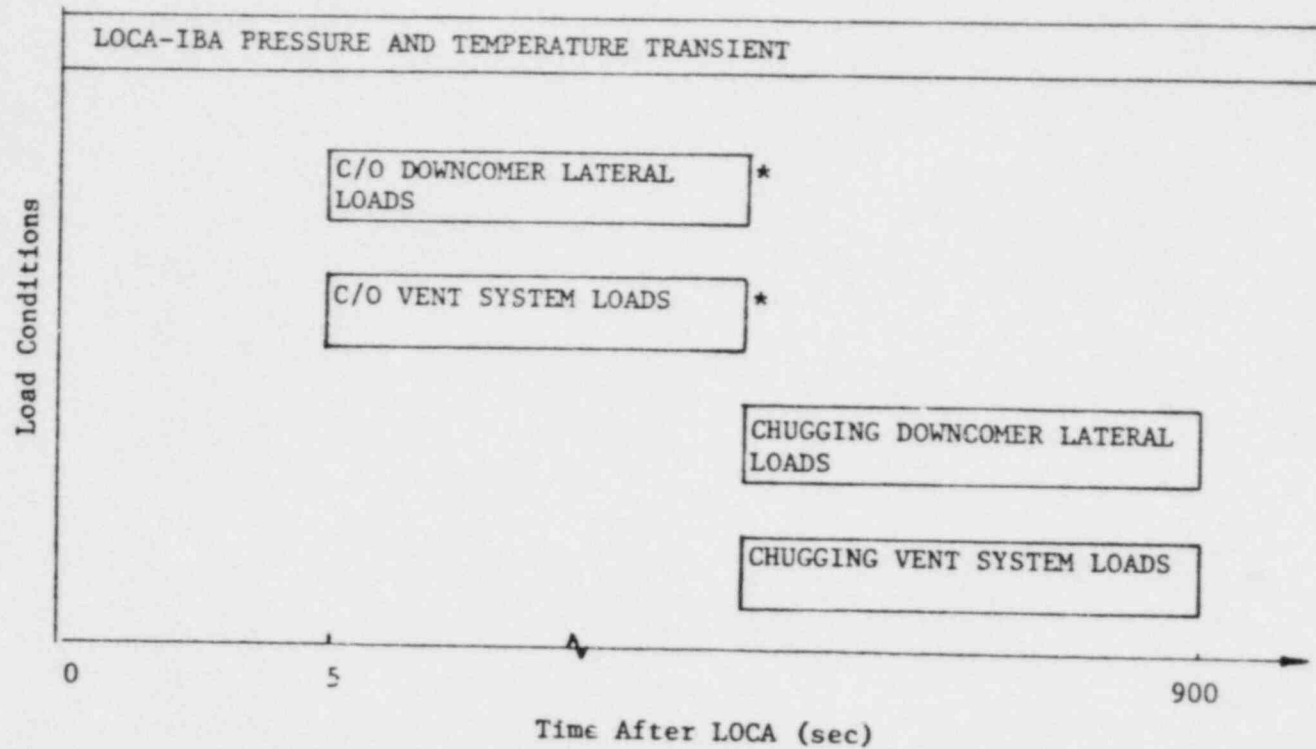
\*For main vent only.

\*\*For submerged portion of downcomers see also Figure 2.32

FIGURE 2.28

VENT SYSTEM LOAD COMBINATIONS FOR LOCA-DBA\*\*



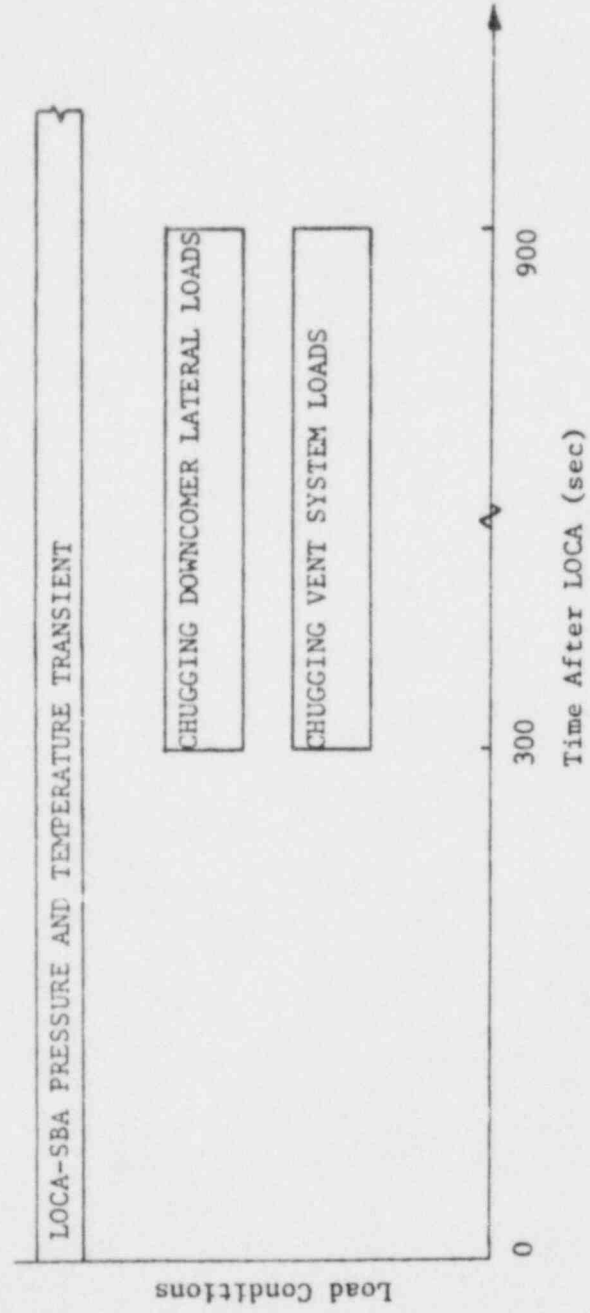


\*Bounded by chugging.

\*\*For submerged portion of downcomers see also Figure 2.33.

FIGURE 2.29

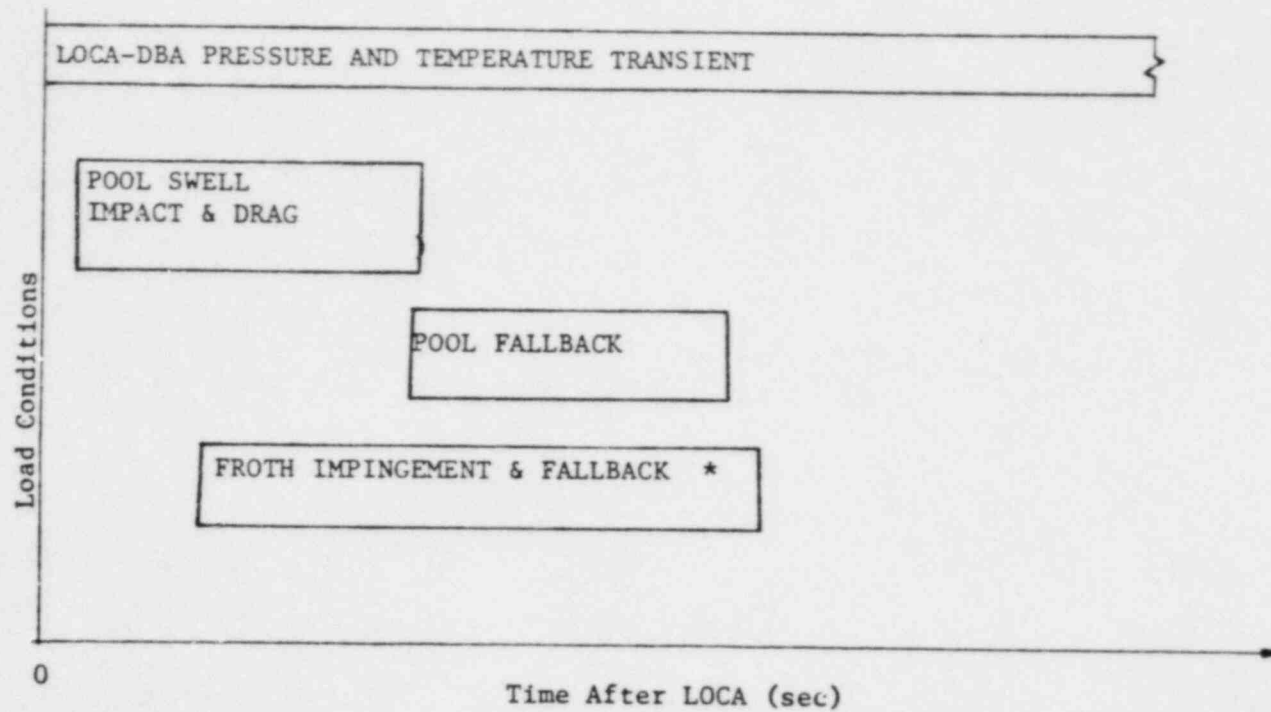
VENT SYSTEM LOAD COMBINATIONS FOR LOCA-IBA\*\*



\*\*For submerged portion of downcomers see also Figure 2.34.

FIGURE 2.30

VENT SYSTEM LOAD COMBINATIONS FOR LOCA-SBA\*\*



\*Froth fallback loads on structures in Region II only.

FIGURE 2.31

LOAD COMBINATIONS FOR STRUCTURES ABOVE HWL FOR LOCA-DBA

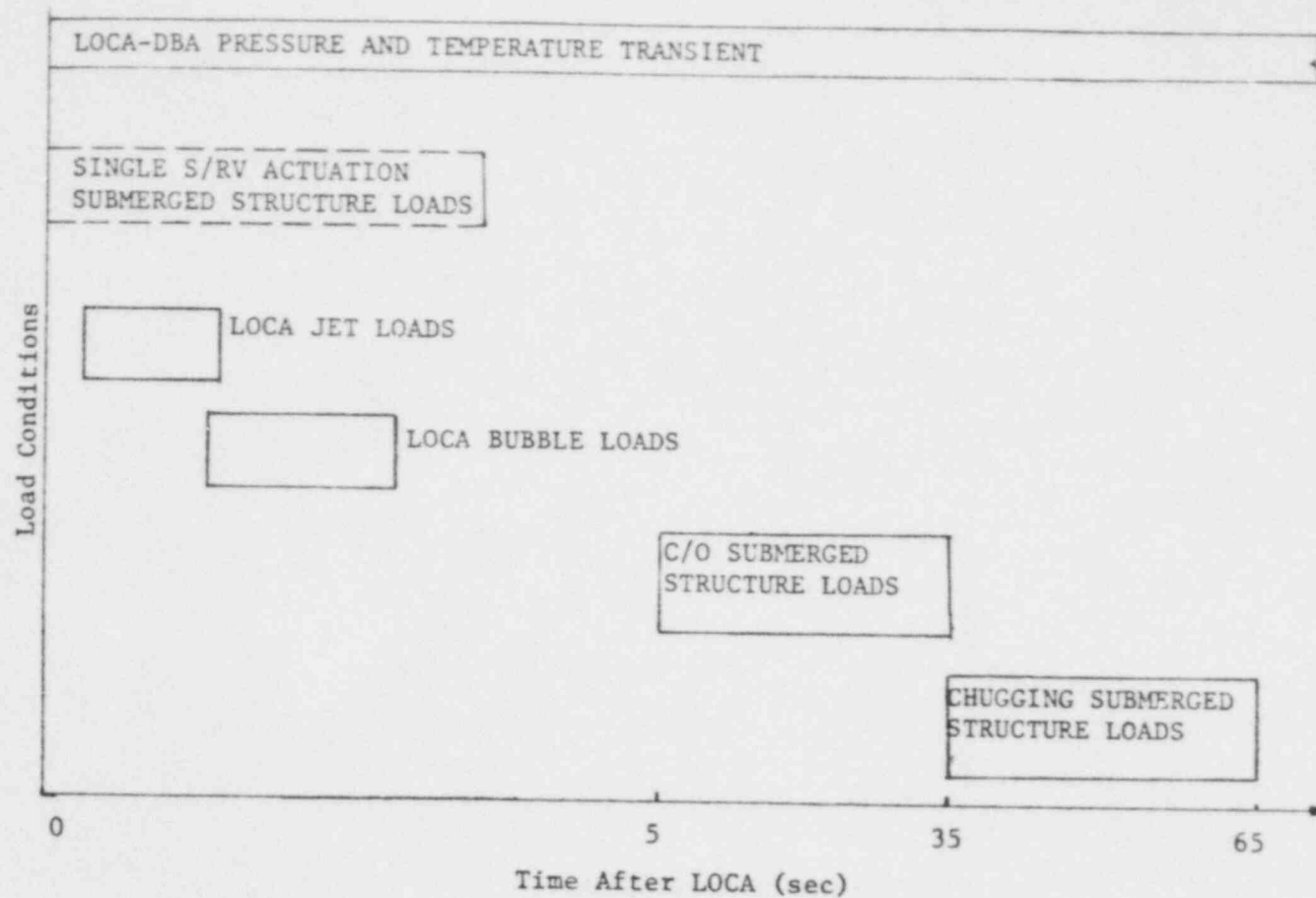
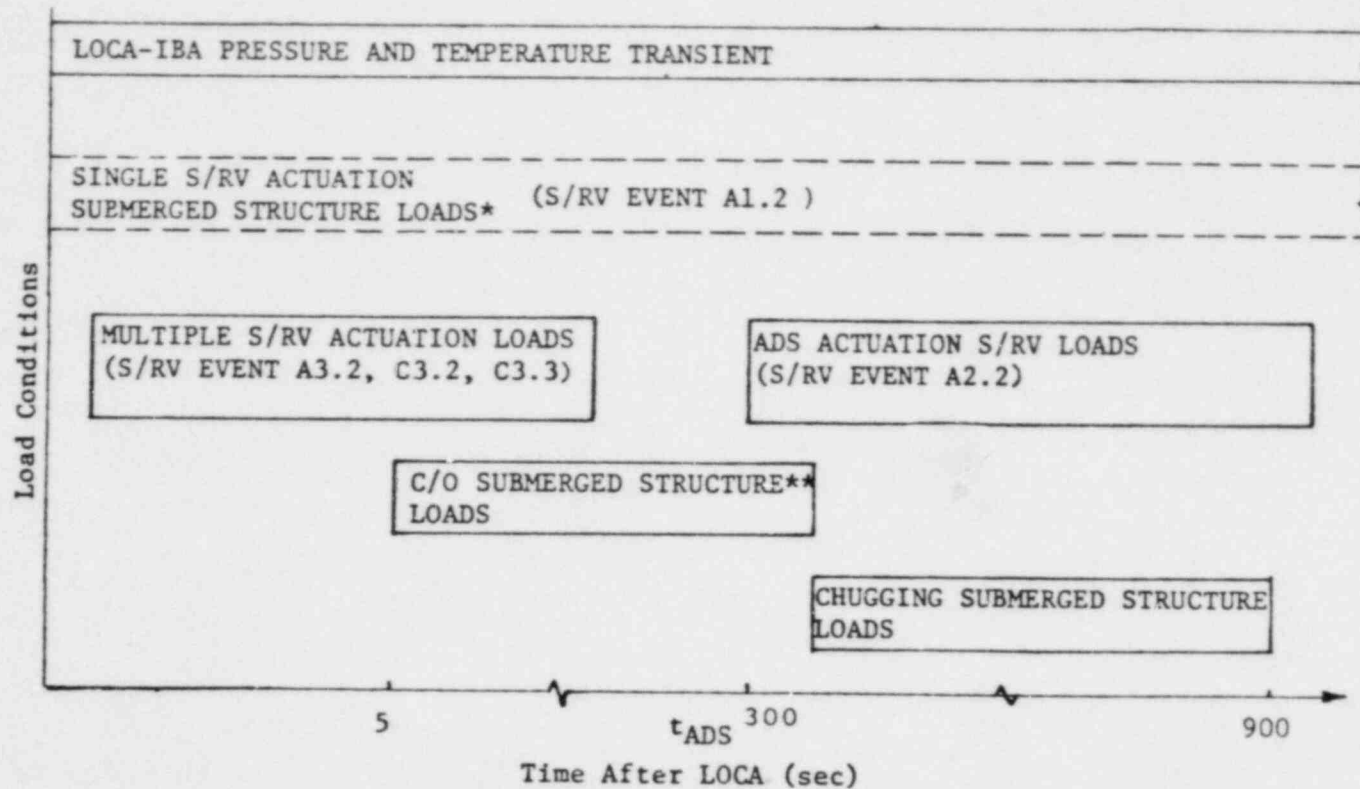


FIGURE 2.32

SUBMERGED STRUCTURES LOAD COMBINATIONS FOR LOCA-DBA



\*Loading does not combine with other S/RV events.  
 \*\*Bounded by chugging loads.

FIGURE 2.33

SUBMERGED STRUCTURES LOAD COMBINATIONS FOR LOCA-IBA

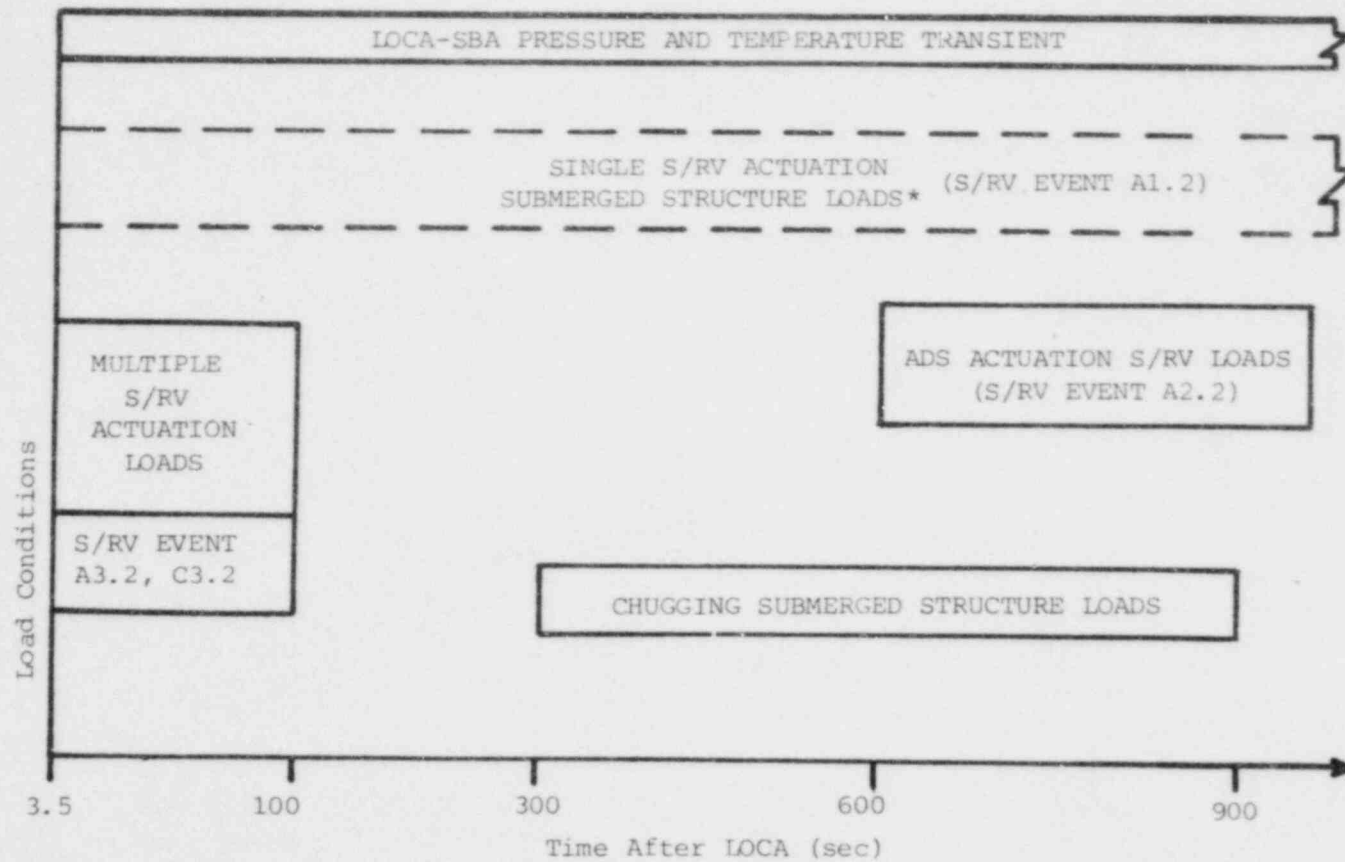
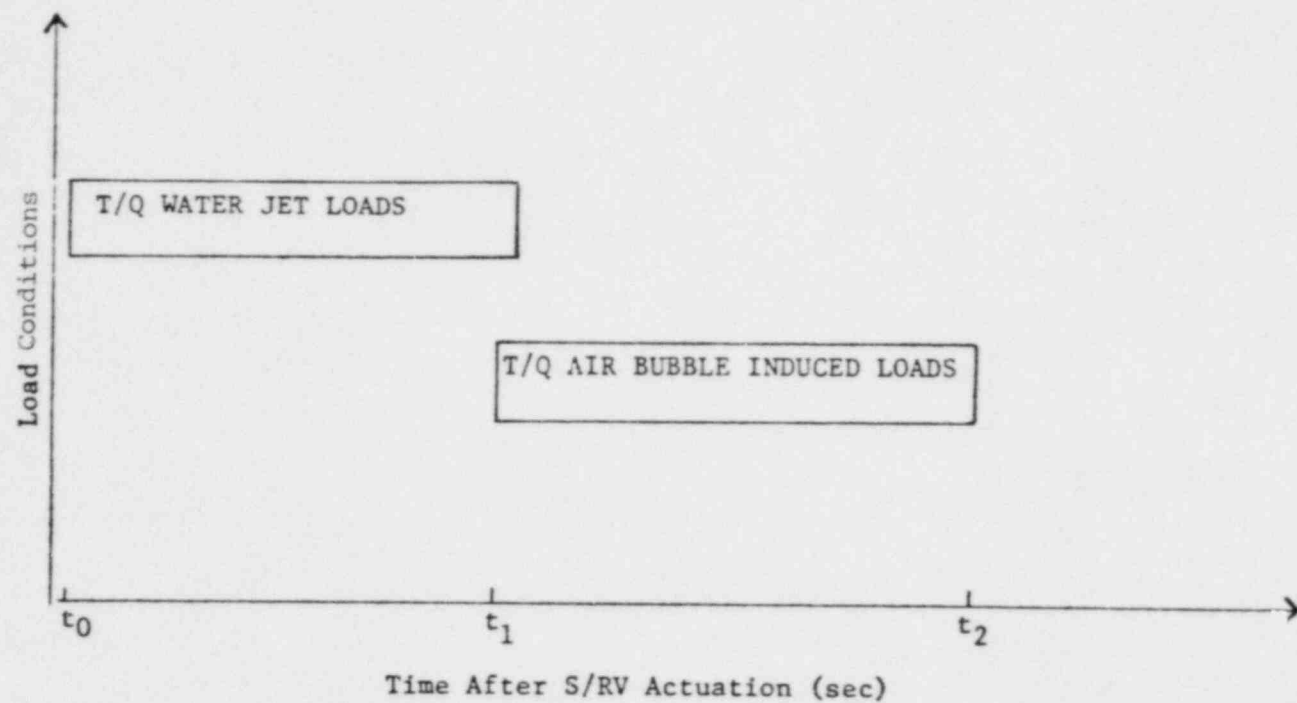


FIGURE 2.34

SUBMERGED STRUCTURES LOAD COMBINATIONS FOR LOCA-SBA





$t_0$  = S/RV actuation time

$t_1$  = S/RVDL water clearing time

$t_2$  = time at which S/RV bubbles reach pool surface

FIGURE 2.35

S/RV DISCHARGE LOADS ON SUBMERGED STRUCTURES

COOPER NUCLEAR STATION

PLANT UNIQUE ANALYSIS REPORT

SECTION 3

TORUS SHELL AND SUPPORTS

### 3.1 INTRODUCTION

This section describes the results of the structural evaluations of the CNS torus shell and support structures. Components included in these evaluations are the torus shell, the torus support system, the internal ring girder, and all attachments and penetrations on the torus shell pressure boundary.

Descriptions of these components and modifications made to these components are provided in Section 1 of this report. The thermal-hydraulic load definitions and load combinations are described in Section 2. This section provides a description of the design load combinations, design allowables, analysis methods and results, and code evaluations for all structural components listed above.

### 3.2 TORUS SHELL

This subsection discusses the results of the structural evaluations of the torus shell pressure boundary away from penetrations and attachments. Penetrations and attachments are addressed in Subsection 3.5.

#### 3.2.1 Design Load Combinations

Table 3.1 shows the 27 design load combinations applied to the torus shell. This table is taken directly from the Mark I Containment Program PUAAG. ASME Code Service level assignments for each event combination are also indicated in the table.

Of these 27 load combinations, potentially bounding load combinations were identified for the torus shell evaluations. These bounding combinations are shown in Table 3.2. Torus shell stresses were compared against allowables for these load combinations.

### 3.2.2 Design Allowables

The torus shell is classified as a Class MC vessel. Design allowables are taken from Subsection NE-3000 of the ASME Code (referred to as the Code).

#### 3.2.2.1 Shell Stress Intensity Allowables

Torus shell stress intensity values are calculated using the procedure in Subsection NE-3215 of the Code. Combined stress intensity values were required to satisfy the requirements of Subsection NE-3221 for all load combinations. The fatigue evaluation of the torus shell was also performed as required by Subsection NE-3221.5.

Stress intensity allowables are summarized in Table 3.3 for Level A, B, and C Service load combinations. Allowables are based on SA-516 Grade 70 material properties at 200°F (design torus temperature for Mark I containment loadings).

#### 3.2.2.2 Buckling Allowables

The LOCA and S/RV discharge-related loads are dynamic in nature. The ASME Code Section III analysis requirements for buckling apply static methods, using standard charts and equations that ignore the non-uniformity of the load and the inertial aspects of the structural response. This code solution indicates the typical Mark I containment torus shell does not meet the ASME buckling criteria of either Subsection NE-3133 or Code Case N-284 for the defined hydrodynamic loads. Therefore, the stability of the Mark I torus under these dynamic loads was demonstrated using both in-plant data and nonlinear dynamic analyses.

The potential torus instability cases investigated were the buckling of the bottom of the shell due to negative pressure, the buckling of the upper crown region due to beam-like bending, and the buckling of the inner equator region due to positive pressure.

The first two of these cases have been extensively evaluated using experimental data, and the last one has been eliminated as a design concern based on geometric considerations. The following conclusions were drawn from the evaluations of the experimental data (Reference 29):

- (1) The upper crown region of the torus will not experience any instability under the most unfavorable loading condition, which is combined LOCA and S/RV actuation.
- (2) The most unfavorable loading condition for the stability of the bottom of the shell is caused by S/RV actuation alone.
- (3) With the exception of Oyster Creek, the torus shells did not exhibit any instabilities in the eight in-plant S/RV discharge test results examined. The Oyster Creek torus was unstable for a short period of time during the tests, but it subsequently regained its stability without any damage. The Oyster Creek torus has the thinnest shell wall of all the Mark I plants and is nearly half as thick as the CNS torus shell.
- (4) S/RV discharge tests at Monticello, with pressure waveforms having frequencies nearly in resonance with torus shell frequencies, did not result in any instabilities.
- (5) Installation of T-quenchers provides a safety factor of 2.0 to 2.5 for the design conditions over the worst ramshead test case which was examined in the test data review.

To confirm the stability of a typical Mark I containment torus shell for bounding S/RV discharge transient loads, a nonlinear dynamic analysis was performed (Reference 29). For the design load case, a factor of safety of approximately seven against instability was observed. These conclusions can be directly applied to the CNS torus shell configuration for the following reasons:

- (a) The Cooper Station torus shell has a lower diameter/thickness ratio than the torus shell considered in the generic study.
- (b) The design torus shell S/RV discharge pressure for Cooper Station has a peak pressure value which is 70% of the peak pressure used in the generic study. The pressure waveforms used in both the CNS torus analysis and the generic study are both based on the GE computer code QBUBSO2, as described in Section 2.5.4.

In summary, an adequate margin of safety against instability of the CNS torus shell exists for all design load combinations and the provisions of Code Subsection NE-3222 are satisfied. Therefore, torus shell buckling was not considered as a design limitation.

### 3.2.3 Analysis Methods and Results

This subsection describes the analyses and key results of the torus shell evaluations. Analysis results from this subsection were also used in the evaluations of the torus support system, ring girder, penetrations, and attachments.

#### 3.2.3.1 Torus Mathematical Models

##### 3.2.3.1.1 Shell Models

Two finite element models of the torus shell and its support system were used in the structural evaluations:

- (1) Primary evaluations were performed using a coupled shell-fluid model representing a 1/32 section of the torus. This section extended from the centerline of a vert bay to the plane of the ring girder. The finite element model representing the torus is shown in Figure 3.1. The



general purpose program EDS-SNAP (described in Appendix B) was used to develop this model. Three-dimensional shell elements with mid-side nodes were used to represent the torus shell and ring girder web. These shell elements can accurately model a quadratic variation in displacement and allow the use of a coarser finite element mesh to represent a section of the torus. Linear beam elements were used to represent the torus support columns and ring girder flange. Modeling of fluid effects are discussed in Subsection 3.2.3.1.2.

- (2) Torus response to horizontal seismic loads was evaluated using a plate element model of a  $90^{\circ}$  section of the torus (Figure 3.2). Program EDSGAP (described in Appendix B) was used to develop this model. Fluid effects were included using the tributary mass method, assuming 100% of the fluid inertia is effective during horizontal seismic loading.

#### 3.2.3.1.2 Fluid-Structure Interaction Model

A three-dimensional consistent mass matrix formulation was used to model the structural and fluid mass characteristics of the 1/32 section torus model described above. The mass effects of the enclosed fluid were modeled by the added mass formulation, which uses a pressure-based fluid element to model the incompressible fluid and condenses the fluid inertia and fluid-structure interaction (FSI) effects into the structural consistent mass matrix. It has been demonstrated that added mass formulation produces a more accurate representation of the actual FSI effects (Reference 30) than provided by the conventional tributary mass methods. Appendix C describes this approach and its implementation. The fluid model used in the evaluations was developed to represent the enclosed fluid in a 1/32 segment of the torus, as shown in Figure 3.1. This model was developed based upon the high water elevation, which is approximately 1-1/2 feet below the torus centerline.

A second fluid model representing only 40% of the enclosed fluid was also developed for performing the pool swell dynamic analysis (Subsection 3.2.3.2.2).

### 3.2.3.2 Analysis Procedures and Results

The analyses described in this subsection were used in the qualification of the shell. All dynamic analyses were performed using the coupled shell-fluid model of 1/32-section of the torus described in Subsection 3.2.3.1.1. Damping was taken to be 2% of critical for all dynamic analyses.

#### 3.2.3.2.1 Static Analyses

Static analyses of the torus shell were performed using the 1/32 section torus model described in Subsection 3.2.3.1.1. The horizontal seismic analysis was performed using the 90° section model.

The following static load cases were analyzed:

##### (1) Containment Pressure

Analysis for a uniform internal pressure of 1 psi was performed. Results for other internal pressure values were determined by scaling these results by the ratio of the containment pressure to 1 psi.

##### (2) Containment Temperature

An analysis was performed for the worst case condition of the torus at maximum design temperature (200°F) and the reactor building at minimum design temperature (50°F). The torus support structure was assumed to be at the reactor building temperature except near the shell, where steady-state heat conduction methods were used to predict the temperature distribution.

(3) Gravity

An analysis was performed including the weight of the torus shell, enclosed suppression pool, and internal equipment (including vent system, T-quencher assembly, etc.). The saddle support was assumed to be inactive since installation of the saddle was performed while the torus was filled with water.

(4) Seismic

An equivalent static analysis was performed using design accelerations taken from the FSAR response spectra (Reference 16) using the lowest torus natural frequency. A separate analysis was done for vertical (using the 1/32 section model) and horizontal (using the 90° section model) seismic input. The analyses were performed for OBE loading and the SSE results were taken as twice the OBE results. Combined stress intensities for seismic loading were computed by taking the maximum stress intensity anywhere on the torus resulting from both the vertical and horizontal seismic analyses and combining them using the SRSS technique (in accordance with NRC Regulatory Guide 1.92). The maximum combined stress intensity was then used for all torus shell locations.

(5) Penetration and Attachment Reactions

See Subsection 3.5.3.

3.2.3.2.2 Torus Shell Dynamic Properties

Torus shell dynamic analyses were performed using torus natural frequencies and mode shapes determined through an eigensolution. The subspace iteration method was used for the eigensolution (Reference 31). The eigensolution was performed using the coupled

shell-fluid 1/32 section model described in Subsection 3.2.3.1.1. All torus model static degrees of freedom were retained as dynamic degrees of freedom in the eigensolution.

Eigensolutions were performed using two boundary conditions on the 1/32 section torus model:

- (1) Symmetric boundary conditions at both the ring girder plane and the midbay.
- (2) Anti-symmetric boundary conditions at the ring girder plane and symmetric boundary conditions at the midbay.

Consideration of both symmetric and anti-symmetric boundary conditions allows representation of the 1/16 section behavior under S/RV discharge loading. Torus mode shapes up to 50 Hz for the symmetric model and 40 Hz for the anti-symmetric model were computed. There are 50 torus natural frequencies in this range. The lowest torus natural frequencies are 9.8 Hz (anti-symmetric model) and 12.8 Hz (symmetric model).

#### 3.2.3.2.3 Pool Swell Dynamic Analysis

A time history analysis for pool swell loads was performed on the 1/32 section coupled shell-fluid model of the torus shell with symmetric boundary conditions. The pool swell load definition described in Subsection 2.4.3.2 was represented as a set of pressure surfaces which were directly applied to the finite element model. Direct time integration using the Newmark method was employed in the analysis. To model the water in flight during the upload portion of the pool swell event, the analysis was carried out to the start of the upload phase using a fluid model representing 100% of the enclosed pool volume. A restart analysis was then performed for the second half of the analysis, using a 40% fluid model to properly include the dynamic effects of the reduced pool mass (60% of the pool mass is in flight as discussed in Subsection 2.4.3.1). For the upload phase of the analysis, the

intermediate supports on the saddle were assumed to be inactive. Results from these two analyses were then sequenced to produce a time-history analysis of the entire pool swell event.

Only the bounding load case of zero initial drywell-to-wetwell pressure differential was considered in the torus shell evaluation. Maximum torus shell stress intensities due to pool swell were 7.1 ksi (membrane) and 9.5 ksi (surface).

#### 3.2.3.2.4 DBA CO Frequency Domain Analysis

For the DBA CO load case, a frequency domain analysis was performed on the 1/32 section coupled shell-fluid model of the torus shell with symmetric boundary conditions. In the frequency domain analysis procedure, torus shell response (stresses, accelerations, displacements, etc.) are determined for each of the 50 load harmonics in the DBA CO load definition (Subsection 2.4.4.1) assuming steady-state response. The responses to each load harmonic are then combined to obtain the total response to the load definition. The combination method used recognizes the random phasing of the individual load harmonics observed in the Full Scale Test Facility (FSTF) data. The combination method involves the determination of structural response to each of the individual load components, followed by the combination of these responses using the absolute sum of the four highest responses added to a SRSS combination of the remaining 46 responses.

Statistical studies have shown that this design rule provides an 84% Non-Exceedence Probability (NEP) on Cumulative Distribution Functions (CDFs) generated using random phase angles for the 50 load harmonics. These design rules were also used to analytically predict the response of the FSTF to DBA CO loading. Predicted results still conservatively bound the responses measured in all FSTF tests. These studies are documented in Reference 32.



For the DBA CO analysis, the envelope of the three LDR alternative load cases in the 4 to 16 Hz range was used. The load frequency for each harmonic band was set to the midpoint of the frequency band, except when a structural natural frequency fell within a band. In this case, the structural natural frequency was assigned to the pressure component. All 50 load harmonics were used in the analysis. All torus natural frequencies below 50 Hz were used to calculate the torus response. Maximum torus shell stress intensities due to DBA CO were 8.4 ksi (membrane) and 10.6 ksi (surface).

Analyses were performed only for DBA CO loading. IBA CO results were bounded by pre-chug loads (see below).

#### 3.2.3.2.5 Chugging Frequency Domain Analysis

The chugging frequency domain analysis was performed in a similar manner to the DBA CO analysis (described above). For chugging, no statistical studies on phasing of load components were available prior to preparation of this report; hence, responses to load harmonics were conservatively combined using absolute summation.

For post-chug loads, all 50 load harmonics (Subsection 2.4.5.1) were used in the analysis. All torus natural frequencies below 50 Hz were used to calculate the torus response. The load frequency for each harmonic band was set to the midpoint of the frequency band except when a structural natural frequency fell within a band. In this case, the structural natural frequency was assigned to this load component. Maximum torus shell stress intensities due to post-chug were 3.6 ksi (membrane) and 4.6 ksi (surface).

Evaluation of the torus for pre-chug loads indicated that all responses were bounded by post-chug responses. Therefore, post-chug results were conservatively used for all load combinations involving chugging. Pre-chug results were used for all load combinations involving IBA CO.



#### 3.2.3.2.6 S/RV Discharge Dynamic Analyses

For S/RV discharge load cases, time history analyses were performed on the 1/32 section coupled shell-fluid model of the torus shell. Since the spatial load distribution for S/RV discharge pressures is symmetric over a 1/16 section of the torus, the following analysis steps were employed:

- (1) The spatial load distribution for a 1/16 section (Subsection 2.5.4) was divided into two distributions: one symmetric about the ring girder plane and one anti-symmetric about the ring girder plane. The algebraic sum of these two distributions was equivalent to the S/RV discharge load definition for a 1/16 section.
- (2) The peak torus shell pressure waveform was identified by selecting the frequency of the waveform to be the value within the specified S/RV discharge frequency range which maximizes the torus response. This transient was extended over six significant load cycles, which was sufficient to generate the maximum torus response.
- (3) The 1/32 section coupled shell-fluid model with symmetric boundary conditions was analyzed for the symmetric load distribution and pressure waveform specified in step (2). Modal superposition time history analysis was performed with all symmetric torus modes up to 50 Hz included.
- (4) The 1/32 coupled shell-fluid model with anti-symmetric boundary conditions was analyzed for the anti-symmetric load distribution and pressure waveform in step (2). Modal superposition time-history analysis was performed with all anti-symmetric torus modes up to 40 Hz included.

- (5) To evaluate torus response in a typical vent bay, the results from steps (3) and (4) were algebraically added at each time step.
- (6) To evaluate torus response in a typical non-vent bay, results from step (4) were algebraically subtracted from the results of step (3) at each time step.

Torus analyses were performed in this manner for S/RV discharge Load Cases A2.2 and A1.1. Torus response to all other S/RV discharge load cases were obtained by scaling the results from these two analyses. See Subsection 2.5 for a discussion of S/RV discharge load cases and corresponding load definitions.

#### 3.2.4 Code Evaluation

This subsection describes the code evaluation of the torus shell for the design load combinations summarized in Table 3.2.

##### 3.2.4.1 Shell Stress Intensities

Torus shell stress intensities for the design load combinations were computed for all points on the torus shell. Absolute summation of the stress intensities from each load case in a combination was performed. For time history analyses, the maximum stress intensity over all time steps in the transient was used for the load combination.

The combined state of stress for all design load combinations meets the allowables of Table 3.3. Maximum combined stress intensities are 21.4 ksi (membrane) and 28.5 ksi (surface) for the Level B Service load combination IBA/SBA chugging plus S/RV discharge following ADS actuation. The combined membrane stress intensity is classified as a local primary membrane stress intensity according to the criteria of Code Subsection NE-3213.10. The maximum combined stress intensities are therefore 74% and 98%,

respectively, of the corresponding allowables. All other general primary membrane and membrane plus primary bending stress intensities are below allowables at all torus locations for all design load combinations.

#### 3.2.4.2 Fatigue Evaluation

Fatigue usage was checked at critical torus shell locations. The maximum stress intensity anywhere on the torus for each load case was conservatively used as the stress for each fatigue check. The fatigue design basis described in Subsection 2.7.7 was used for this evaluation. The highest torus shell usage factor was 0.51 at the butt weld between the torus shell plates of unequal thickness at the torus equator.

### 3.3 TORUS SUPPORT SYSTEM

This section describes the results of the structural evaluations of the torus shell support system, consisting of the support columns, saddle structure, and anchorage (tie-down) located at each of the sixteen miter joints. Also included as part of the support system are the four seismic ties designed to restrain net torus lateral movement.

#### 3.3.1 Design Load Combinations

The 27 design load combinations for the torus support system and the corresponding service limit assignments are shown in Table 3.1. An envelope of the load combinations producing the maximum net vertical reactions and bending moments was used in the evaluation of the torus support columns. The enveloping load cases are summarized in Table 3.4. In the saddle evaluation, the load combination producing the maximum net upload and download, summarized in Table 3.5, were used. For the seismic tie evaluation, the load combination horizontal SSE plus 8MVA S/RV discharge produces the maximum net lateral loads.

### 3.3.2 Design Allowables

The torus support system is classified as an integral Class MC component support. Design allowables are taken from Subsection NF-3000 of the Code, except for the portion of the supports within the limits of reinforcement from the torus shell (NE) boundary and the welds directly on the pressure boundary. These exceptions to the NF classification have design allowables specified in Section NE.

#### 3.3.2.1 Support Columns

The torus support columns are considered linear-type supports. Evaluation for axial and bending loads was performed in accordance with the procedure in Appendix XVII of the Code. Material allowables (based on a design temperature of 200°F) are 20.2 ksi in compression and 22.0 ksi in bending.

#### 3.3.2.2 Anchorage Assembly

The torus anchorage (tie-down) consists of four anchor bolts per column, connected to either a box beam or bracket assembly designed to transfer upload from the columns to the bolts. The box beam assemblies are considered linear type supports and have the same design allowables as the support columns. The bracket assembly is considered a plate-and-shell type support and is evaluated using the procedure in Subsection NF-3320. The allowable stress value for the bracket assembly is 13.9 ksi.

The anchor bolt allowables are based on the bolt material allowable and the pullout load for the bolt. The pullout load is based on the shear strength of the grout and the total shear area. The shear strength of the grout was based upon tests to determine the bond stress where the measured bond stress was divided by a factor of safety of 4. Based on the minimum of these two allowables, the allowable force per anchor bolt is 103 kips and 135 kips for the inner and outer columns, respectively.

#### 3.3.2.3 Seismic Ties

Seismic ties were considered as linear-type component supports since they act under a single component of direct stress. Material allowables are 12 ksi in shear and 18 ksi in bending. The welds connecting the seismic ties to the torus shell is within the NE jurisdiction and has an allowable force per unit length of 3.3 kip/in.

#### 3.3.2.4 Ring Girder Saddle

The ring girder saddle web is considered a plate-and-shell type support and is evaluated using the procedure in Subsection NF-3320. The allowable stress value is 20.6 ksi.

Stiffeners and flanges on the saddle web are considered linear-type component supports. The design allowable is 21.7 ksi in tension.

The portion of the ring girder saddle web within the NE limit of reinforcement (1-1/2") has the same design allowable stress intensities as the torus shell (see Subsection 3.2.2.1).

The weld attaching the saddle web to the torus boundary is also within the NE jurisdiction. The allowable force/unit length on this weld is 5.8 kip/in.

#### 3.3.3 Analysis Methods and Results

This Subsection describes the analysis procedure used to qualify the components of the torus support system. Results from the torus shell analyses (Subsection 3.2) are used in these evaluations.

##### 3.3.3.1 Column and Anchorage Evaluation

Design downloads on the torus support columns and the anchorage assembly were determined directly from the finite element analyses



of the 1/32 section torus model (Subsection 3.2.3). In determining the design uploads, the results of the 1/32 section torus model analyses required modification. The intermediate supports on the saddle are not tied down. However, the torus is modeled with these supports fixed. Any upload at these supports must be transferred to the column anchorages. In these cases, the uploads carried by the inner column and inner intermediate support were assigned to the inner column. A similar adjustment was performed for the outer column. At the anchorage, the load per bolt was determined by uniformly dividing the tensile reaction among the four anchor bolts.

Tensile and compressive reactions were determined in this fashion for all load cases. The weight of the torus and suppression pool is carried solely by the columns since the saddle was installed with the torus filled with water. For the S/RV discharge load cases, a knockdown factor of 0.6 was applied to the predicted column reactions. This knockdown factor is based on the factor used to bound global pressure loads on the torus from the Monticello in-plant test as specified by Section 2.13.3.2 of the NRC Acceptance Criteria.

Maximum combined uploads were 347 kips on the inner column and 494 kips on the outer column for the bounding Level B Service Service load combination. Maximum downloads were 407 kips (inner) and 460 kips (outer) for the bounding Level B Service Service load combinations (Table 3.4). In determining the column reactions for the chugging plus S/RV discharge load combination, the 1.1 SRSS combination method (Appendix D) was used to determine the combined reaction due to these two dynamic loads.

Evaluation of the column-to-shell connection, support column, anchor bolts, and box beam anchorage assemblies were performed using the procedures in Appendix XVII of the Code and the AISC manual (Reference 15). The bracket-type anchorage assembly was evaluated using a finite element model of this assembly (using program EDSGAP).



### 3.3.3.2 Seismic Tie Evaluations

Reactions at the seismic ties are a result of net torus lateral loads arising from the following load cases:

(1) Horizontal Seismic

Reactions were determined directly from the SSE analysis of the  $90^\circ$  section torus model for horizontal seismic loads (Subsection 3.2.3.2.1).

(2) Non-symmetric S/RV Discharges

S/RV discharge devices are located in alternate bays of the torus. If the torus is divided into two  $180^\circ$  segments, there will be four discharge devices located in each segment. The bounding net lateral load on the torus due to non-symmetric S/RV discharge is calculated assuming that the torus shell pressure waveforms acting on one  $180^\circ$  segment are out-of-phase with the pressure waveforms acting on the other  $180^\circ$  segment. The lateral load magnitude was determined by first calculating the horizontal reaction at one miter joint due to an 8MVA S/RV discharge event. The column load knockdown factor of 0.6 for S/RV discharge events was applied to this reaction. Then, this reaction was applied in an outward direction at eight consecutive miter joints and then applied in an inward direction at the remaining eight miter joints. This force distribution around the torus was integrated to give a conservative estimate of the net lateral load.

(3) Asymmetric Pre-Chug

Reactions from this load case are considered bounded by the previous two postulated load cases. This observation is based on the very low torus response to pre-chug loads as discussed in Subsection 3.2.3.2.5.

Lateral loads were divided equally among two of the four seismic ties. For the combination of load cases (1) and (2) above, the design reaction on one seismic tie is 300 kips. The procedure in Appendix XVII of the Code and AISC manual was used to evaluate the ties for this reaction.

#### 3.3.3.3 Ring Girder Saddle Evaluation

The ring girder saddle structure was evaluated using a finite element representation of the saddle and performing a series of static analyses, as described below.

##### 3.3.3.3.1 Saddle Model

A detailed model of the ring girder saddle support was developed for evaluating this component. The model was developed by modifying the 1/32 section shell model described in Subsection 3.2.2.2.1 to include a detailed representation of the saddle and its stiffeners and flanges. Figure 3.3 shows the basic saddle model. Program EDS-SNAP was used to develop this model. A second version of this saddle model was developed to evaluate the critical saddle cut-out (for piping) configuration.

##### 3.3.3.3.2 Static Analyses

A series of static analyses were performed on the saddle models to determine stresses and forces in the saddle elements. On both the basic saddle model and the cut-out configuration, the following static analyses were performed:

###### (1) Design Download

Maximum design download of 1600 kips for the Level C Service load case DBA pool swell plus SVA S/RV discharge (determined from the torus shell analyses and correcting for torus and suppression pool weight) was applied to the

support system. This load was applied by specifying a hydrostatic pressure distribution over the wetted portion of the torus shell as shown in Figure 3.4. The peak pressure for this distribution was determined to produce the design download. For the download analysis, the intermediate saddle supports are modeled as active.

(2) Design Upload

Maximum design upload of 1250 kips for the load case IBA/SBA chugging plus ADS S/RV discharge (determined from the torus shell analyses and correcting for torus and suppression pool weight) was applied to the support system. This load was applied as a negative hydrostatic pressure distribution over the wetted portion of the torus shell (Figure 3.4). The peak pressure for this distribution was selected to give the design upload. For the upload analysis, the intermediate saddle supports were modeled as inactive.

(3) Uniform Pressure

A uniform 30 psi positive pressure was applied over the torus shell to predict saddle stresses due to containment pressurization. Intermediate saddle supports were modeled as active.

(4) Design Temperature

The design uniform temperature distribution of the saddle at 50°F with the torus shell at 200°F was applied to the saddle model. To maximize the saddle stresses, the intermediate saddle supports were modeled as active.

Combined stresses and forces were determined for the cases of design down load plus pressure and design upload plus pressure

(Figure 3.4). Each of these two cases were considered with design temperature. Stresses and forces were combined algebraically.

From these combined stresses and forces, all saddle components were evaluated. These evaluations included design stresses in the saddle web, axial forces and bending moments in the stiffeners and flanges, forces per unit length along welds, and base plate stresses at the intermediate saddle supports. For either the cut-out configurations not explicitly modeled or variations in stiffener designs, evaluations were performed by hand calculations using the basic saddle load distributions predicted by these analyses.

#### 3.3.3.4 Nonlinear Support Assessment

For dynamic loading resulting in net tension on the intermediate saddle supports, the response of the torus support system will be nonlinear. This nonlinearity is due to the lack of anchorage at these intermediate locations. To assess this effect, a one-dimensional nonlinear model was developed, as discussed in Section 6.4 (c) of the PUAAG. Nonlinear time history analyses confirmed that for all design combinations, the linear analysis techniques provide a conservative estimate of torus shell and support response. Note that for pool swell loading, the nonlinear support behavior is included explicitly in the torus shell analysis (Subsection 3.2.3.2.3).

#### 3.3.4 Code Evaluation

This subsection describes the code evaluation of the torus shell support system for the design load combinations summarized in Table 3.4.

##### 3.3.4.1 Column and Anchorage

The column-to-shell connection, support columns, anchor bolts, and anchorage assemblies all meet design allowables for the design

load combinations. Torus tie-down capacity is 320 kips (inner column) and 430 kips (outer column) for the limiting anchorage assemblies. Design uploads are 97% (inner column) and 100% (outer column) of these capacities.

#### 3.3.4.2 Seismic Ties

The lateral load capacity of a seismic tie was determined to be 660 kips, which is greater than the design lateral load predicted by analysis (Subsection 3.3.3.2). Thus, the seismic ties and their welded connections to the torus shell meet design allowables.

#### 3.3.4.3 Ring Girder Saddles

Code evaluation of the ring girder saddle indicates that all components satisfy code allowables for the design load cases. This conclusion was determined for all saddle configurations. The maximum combined saddle web stress was 10.4 ksi (54% of allowable). The maximum force per length in the torus-to saddle web weld is 4.6 kips/in (79% of allowable).

#### 3.3.4.4 Fatigue Evaluation

Fatigue usage was checked at the welds connecting the torus to the columns, saddle web, and seismic ties. For the fatigue design basis described in Subsection 2.7.7, the cumulative usage at the torus to column intersection was 0.29. The cumulative usage at the other two locations was less than one percent. Therefore, all fatigue usage factors are within allowables.

### 3.4 RING GIRDER

This section discusses the results of the structural evaluations of the torus shell ring girder. The ring girder includes the ring girder web and flange, gusset stiffeners, and attachment to the torus shell.



### 3.4.1 Design Load Combinations

The ring girder is an integral part of the torus shell and therefore has the same 27 design load combinations as the torus shell (Table 3.1). In addition, the submerged portion of the ring girder is subjected to submerged structure drag loads. Concentrated reactions are also present at several attachment points on the ring girder.

Table 3.6 shows the bounding load cases considered in the evaluation of the ring girder. Where reactions at component attachment points are indicated, loads from these components were taken from the analysis results for these components.

### 3.4.2 Design Allowables

The ring girder is considered as an integral Class MC component support. Design allowables are taken from Subsection NF-3000 of the Code, except for the portion of the ring girder within the limits of reinforcement from the torus shell (NE) boundary. These exceptions to the NF classification have design allowables specified in Subsection NE.

#### 3.4.2.1 Ring Girder Web and Flange

The ring girder web is considered a plate-and-shell type support and is evaluated using the procedure in Subsection NF-3320. The allowable stress value is 19.3 ksi.

The ring girder flange and the gusset plates attached to the web are considered linear-type component supports. Design allowables are 20.2 ksi in tension and 13.5 ksi in shear.

The portions of the ring girder web within the NE limits of reinforcement (1-1/2" from the torus shell) have the same allowable stress intensities as specified for the torus shell (see Subsection 3.2.2.1).



#### 3.4.2.2 Ring Girder-to-Shell Weld

The double 5/16" fillet weld connecting the ring girder to the torus shell is within the NE jurisdiction. The allowable force/unit length on this weld is 3.3 kip/in. In the vicinity of the platform support attachments (where the weld is reinforced to 3/4" on each side), the allowable force/unit length is 8.9 kip/in.

#### 3.4.3 Analysis Methods and Results

This subsection describes the analysis procedures used to qualify the components of the ring girder. Results from the torus shell analyses (Subsection 3.2) are used in these evaluations.

##### 3.4.3.1 Ring Girder In-Plane Loading

Stresses in the ring girder web and flange were taken from the results of the 1/32 section coupled shell-fluid model analyses (Subsection 3.2.3.2). These results were also used to estimate the force/unit length on the ring girder-to-shell weld. The ring girder web and flange were explicitly modeled in these analyses. These analyses provided stress results for all load cases discussed in Subsection 3.2.3.2.

##### 3.4.3.2 Ring Girder Lateral Load

Stresses in the ring girder web and flange and reactions along the ring girder weld due to submerged structure drag loads were determined. The procedures described in Subsection 6.3.3.2 were used for these evaluations.

A finite element model of the longest submerged section of the web between gusset stiffeners was developed using program EDS-SNAP. Equivalent static analyses were then performed for all drag loadings acting on this section. The largest lateral load on any submerged section was uniformly applied to this model to conservatively consider the worst case loading. Stresses in the web and

reactions at the weld were then taken from this model. Forces in the ring girder gussets were also evaluated from this model. For the chugging plus S/RV discharge load combination, the 1.1 SRSS combination method (Appendix D) was used to determine the combined reaction on the ring girder weld due to these two dynamic lateral loads.

#### 3.4.3.3 Ring Girder Attachments

In addition to in-plane loading and lateral loads due to submerged structure drag, the ring girder was also analyzed for local reactions from torus internal structures and piping supports.

The local reactions considered were due to the following structures:

- (1) Vent system supports
- (2) 24-inch diameter T-quencher support pipe
- (3) 16-inch diameter S/RVDL B support pipe
- (4) 10-inch diameter T-quencher bracing pipe
- (5) S/RVDL B supports in the torus airspace
- (6) HPCI turbine exhaust sparger supports
- (7) RCIC turbine exhaust sparger supports
- (8) Containment spray header supports
- (9) Platform supports

The maximum reactions from each of these structures for all load cases were statically applied to calculate the ring girder and ring girder-to-shell weld stresses. These reactions were

determined from the individual analyses of each structure described throughout this report. Local stresses from the ring girder attachments were combined with the in-plane and lateral load-induced stresses prior to the code evaluation.

#### 3.4.4 Code Evaluation

This subsection describes the code evaluation for the Cooper Station ring girder for the design load combinations summarized in Table 3.6.

##### 3.4.4.1 Ring Girder Web and Flange

Stresses in the ring girder web are below allowables at all locations. The maximum web stress is 16.1 ksi (56% of allowable) away from any attachments due to pool swell plus S/RV discharge loads. At all attachments, local web stresses are also below the allowable. Loads on the ring girder flange and gusset stiffeners are all within allowables.

##### 3.4.4.2 Ring Girder-to-Shell Weld

The maximum force/length in the unreinforced ring girder-to-shell weld away from any ring girder attachments is 2.6 kip/in (79% of allowable). In the reinforced portion of the weld near the platform support attachments, the maximum force/length is 7.8 kip/in (97% of allowable). All ring girder-to-shell weld stresses at ring girder attachments are also within allowables.

##### 3.4.4.3 Fatigue Evaluation

Fatigue usage was checked at the ring girder-to-shell weld for the fatigue design basis described in Subsection 2.7.7. All cumulative fatigue usage factors at the critical locations were below one.

### 3.5 TORUS SHELL PENETRATIONS AND ATTACHMENTS

This subsection describes the results of the torus shell evaluations at both piping penetrations and other attachments (with the exception of the ring girder and saddle support). Piping penetrations are associated with the torus attached piping systems. Other attachments include supports for the monorail beam and ECCS piping inside the wetwell. Evaluations of these systems are covered in Section 6.

#### 3.5.1 Design Load Combinations

Evaluation of the torus shell penetrations and attachments involves the determination of local torus shell stresses. Therefore, the 27 design load combinations for the torus shell (Table 3.1) apply for these evaluations.

Table 3.7 shows the bounding load combinations for which the penetrations and attachments were evaluated.

#### 3.5.2 Design Allowables

Local stress intensities due to reactions at penetrations and attachments are determined using the procedure in Subsection NE-3215 of the Code. Since the torus shell is being evaluated, stress intensity limits established in Table 3.3 must be satisfied.

Local stress intensities due to penetrations and attachments are classified as primary local stresses for the membrane component and as secondary stresses for the surface stress intensity (see Code Subsection NE-3213). In comparison with allowables, stress intensities due to primary loads on the torus shell must also be included. Absolute summation of the local and primary stress intensities was performed. The combined stress intensity limits were summarized in Subsection 3.2.2.1.

### 3.5.3 Analysis Methods and Results

This subsection describes the analysis procedures used to determine local stress intensities at torus shell penetrations and attachments.

#### 3.5.3.1 Torus Attached Piping Penetrations

Torus shell attached piping penetrations are summarized in Table 1.2. Reactions at each penetration (3 forces and 3 moments) were obtained from the results of the torus attached piping analyses (Section 6). Where a piping system had both an internal and external portion (relative to the wetwell), reactions for a load case from each portion of the piping were conservatively summed absolutely to obtain the design reactions. Additionally, for dynamic load cases, the maximum reactions in all 6 directions are assumed to act on the penetration at the same time. Thus, the combined reaction load on each torus shell penetration was conservatively defined.

Combined reactions due to multiple dynamic load cases were determined by using a modified SRSS procedure. The reactions (in a given direction) from the two most significant dynamic load cases were combined by SRSS with a multiplier of 1.1 on the combination. Remaining dynamic and static load cases were then added absolutely to this combination. The modified SRSS method was justified for this application through the study summarized in Appendix D.

Local shell stresses at each nozzle were determined using the procedure in Welding Research Council (WRC) Bulletin No. 107 (Reference 33). For several 1 inch and 2 inch penetrations, the WRC procedure was not applicable. Stresses at these small-bore penetrations were calculated through modeling the penetration insert plate as a simply supported annular plate with concentrated forces and moments applied at the penetration.



Local shell stresses at the edge of each penetration insert plate were determined by considering the attenuation of the bending moment away from the nozzle. This attenuation was taken to be the same as that for a cylindrical shell under a concentrated radial ring load (Reference 34). A reduced bending moment was calculated at the end of the insert plate; then shell stresses were calculated considering the reduction in shell thickness going from the insert plate to the clean shell.

#### 3.5.3.2 Monorail Supports

Local torus shell stresses at the three monorail beam supports in each bay were computed using the WRC 107 method. Reactions from the monorail beam (resulting only from froth impingement loads) were determined using the procedure in Subsection 6.4.3.2.

#### 3.5.3.3 ECCS Piping Supports

Local torus shell stresses were computed at the torus shell attachment of several pipe supports for ECCS piping in the wetwell. These pipe supports are on the RHR pump test, HPCI condensate drain, and RCIC condensate drain lines. The WRC 107 method was used for these evaluations. Reaction loads on the shell were determined from the evaluations described in Subsection 6.3 and include both pipe reactions and hydrodynamic loads on the supports themselves.

#### 3.5.4 Code Evaluation

This subsection describes the code evaluation for the torus shell penetrations and attachments for the design load combinations summarized in Table 3.7.



#### 3.5.4.1 Torus Attached Piping Penetrations

The combined local and general torus shell stress intensities were compared against allowables for each penetration and each load combination. Stress intensities were checked at both the nozzle and the edge of the insert plate. All stress intensities (both primary local and secondary) were within allowables for all design load combinations. Table 3.8 shows the local stress intensity and the percentage of allowable for each penetration. The percentage of allowable is based on the combined local and general stress intensities.

#### 3.5.4.2 Torus Shell Stress Intensities at Attachments

Local torus shell stress intensities at all attachments (monorail supports and ECCS piping supports) are within the allowable reserve stresses for all load combinations.

#### 3.5.4.3 Fatigue Evaluation

Fatigue usage was checked at all penetrations (both at the nozzles and the edge of the insert plate), and at all attachments using the fatigue design basis in Subsection 2.7.7. In evaluating fatigue usage at penetrations subjected to reactions due to chugging loads from both internal and external piping, the local stress intensity was based on an SRSS of the internal and external reactions. For consideration of local stress intensity, absolute summation of internal and external reactions is a potential design concern. For fatigue evaluation, the assumption that the internal and external reactions add absolutely throughout an IBA, SBA, or D.A event is unnecessarily conservative. SRSS combination of these reactions for the fatigue evaluation only is therefore justifiable.

The cumulative usage factors at all torus shell penetrations and attachments are within allowables.



# DESIGN LOAD COMBINATIONS AND SERVICE LEVEL LIMITS FOR CLASS MC COMPONENTS AND INTERNAL STRUCTURES

[illegible]

Table 3.2

BOUNDING LOAD COMBINATIONS FOR  
TORUS SHELL EVALUATIONS

<u>Load Combination</u>	<u>Service Level</u>
IBA/SBA Chugging + 6 ADS S/RV + Gravity + Pressure + Thermal + OBE	B
DBA CO + Gravity + Pressure + OBE	B
DBA PS + Gravity + OBE	B
NOC 8MVA S/RV + IBA CO + Gravity + Pressure + OBE	B
DBA CO + Gravity + Pressure + SSE	C
IBA/SBA Chugging + 6 ADS S/RV + Gravity + Pressure + SSE	C
NOC 8MVA S/RV + IBA CO + Gravity + Pressure + SSE	C
DBA PS + SVA S/RV + Gravity + Pressure + SSE	C

TABLE 3.3

ALLOWABLE STRESS INTENSITIES FOR  
THE TORUS SHELL

<u>Type of Stress</u> <u>Intensity</u>	<u>Stress Intensity (ksi)</u>	
	<u>Service Level</u> <u>A/B</u>	<u>Service Level</u> <u>C</u>
$P_m$	19.3	33.7
$P_L$	29.0	50.6
$P_L + P_b$	29.0	50.6
$P_L + P_b + Q$	67.5	-

Notes:

- (1) Allowables are for SA-516 Grade 70 steel at 200° design temperature.

Table 3.4

BOUNDING LOAD COMBINATIONS FOR  
TORUS SUPPORT COLUMN EVALUATIONS

<u>Load Combination</u>	<u>Service Level</u>
DBA CO + Gravity + Pressure + OBE	B
DBA PS + Gravity + OBE	B
NOC 8 MVA S/RV + IBA CO + Gravity + OBE	B

Table 3.5

BOUNDING LOAD COMBINATIONS FOR TORUS SADDLE EVALUATIONS

<u>Load Combination</u>	<u>Service Level</u>
IBA/SBA Chugging + 6 ADS S/RV + Gravity + Pressure + OBE	B
IBA/SBA Chugging + 6 ADS S/RV + Gravity + Pressure + Thermal + OBE	B
DBA PS + SVA S/RV + Gravity + Pressure + SSE	C



Table 3.6

BOUNDING LOAD COMBINATIONS FOR  
RING GIRDER EVALUATION

<u>Load Combination</u>	<u>Service Level</u>
IBA/SBA Chugging + 6 ADS S/RV + Gravity + Pressure + OBE	B
IBA/SBA Chugging + 8 MVA S/RV + Gravity + Pressure + OBE	B
DBA CO + Gravity + Pressure + OBE	B
DBA PS + Gravity + OBE	B
DBA PS + SVA S/RV + Gravity + Pressure + SSE	C

Table 3.7

BOUNDING LOAD COMBINATIONS FOR  
TORUS SHELL PENETRATIONS AND ATTACHMENTS

<u>Load Combination</u>	<u>Service Level</u>
IBA/SBA Chugging + 6 ADS S/RV + Gravity + Pressure + OBE	B
IBA CO + NOC 8 MVA S/RV + Gravity + Pressure + OBE	B
DBA CO + Gravity + Pressure + OBE	B

Table 3.8

LOCAL STRESS INTENSITIES OF  
TORUS ATTACHED PIPING PENETRATIONS

PENETRATION	NOZZLE		EDGE OF INSERT PLATE	
	$P_L + P_b + Q$ (ksi)	Percent of Allowable	$P_L + P_b + Q$ (ksi)	Percent of Allowable
210A	66.2	98	59.6	88
210B	57.3	85	59.6	88
211A	12.4	92	(1)	(1)
211B	56.3	83	(1)	(1)
212	58.8	87	62.5	93
214	50.0	74	63.2	94
223A	N/A	N/A	60.6	90
223B	N/A	N/A	60.6	90
224	57.5	85	(1)	(1)
225A	65.0	96	(1)	(1)
225B	59.8	89	(1)	(1)
225C	65.6	97	(1)	(1)
225D	64.3	95	(1)	(1)
226	63.9	95	(1)	(1)
227A	67.5	100	(1)	(1)
227B	N/A	N/A	66.6	98

Notes:

- (1) Primary and secondary stress intensities at the edge of the insert plate were calculated to be less than those at the nozzle.
- (2) For penetrations 223A, 223B, and 227B maximum local stress intensities were determined at the edge of penetration reinforcement rather than at the nozzle.

TABLE 3.8 (Cont'd)

LOCAL STRESS INTENSITIES OF  
TORUS ATTACHED PIPING PENETRATIONS

PENETRATION	NOZZLE		EDGE OF INSERT PLATE	
	$P_L + P_b + Q$ (ksi)	Percent of Allowable	$P_L + P_b + Q$ (ksi)	Percent of Allowable
203A	36.9	55	34.9	52
203B	36.9	55	34.9	52
205	51.5	76	58.3	52
206A	36.9	55	34.9	52
206B	36.9	55	34.9	52
206C	36.9	55	34.9	52
206D	36.9	55	34.9	52
209A - D	36.9	55	34.9	52
215	36.9	55	34.9	52
220	48.5	72	66.5	98
221	48.8	72	38.9	58
222	48.8	72	38.9	58
228	60.0	89	65.0	96
229A - K	36.9	55	34.9	52
229L - M	36.9	55	34.9	52
213A	45.5	67	55.5	82
213B	45.5	67	55.5	82

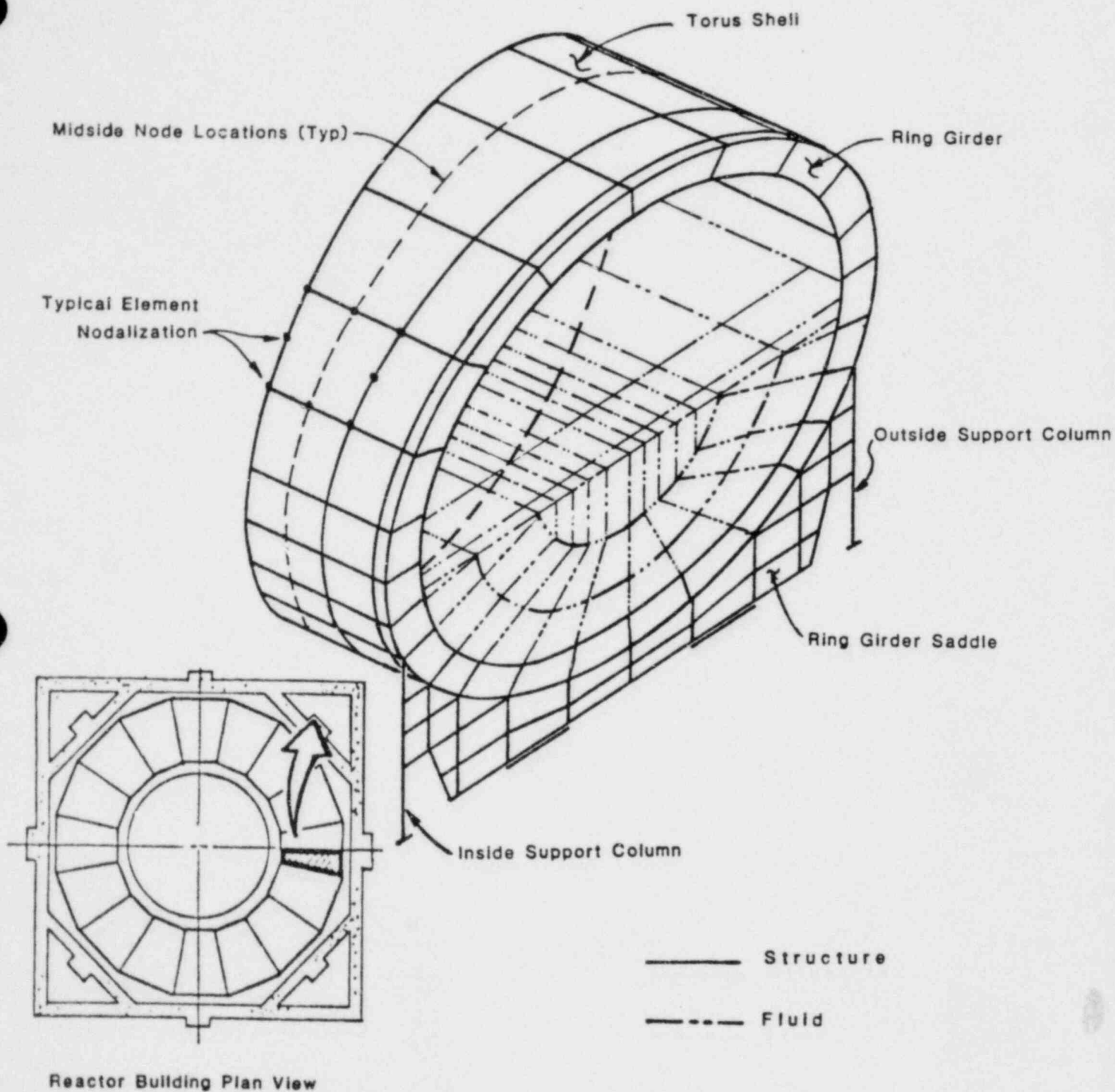


FIGURE 3.1  
1/32 SECTION TORUS MODEL

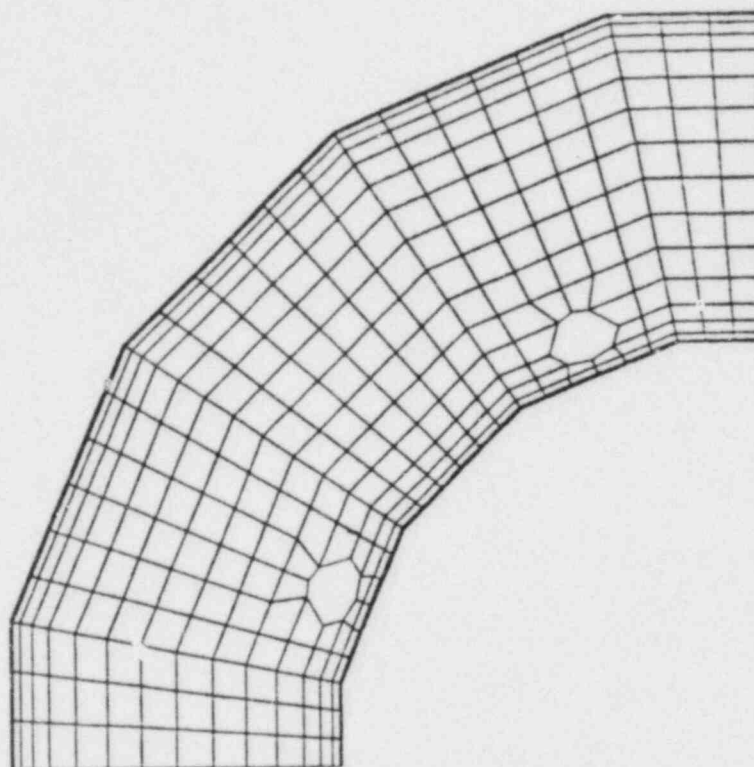


FIGURE 3.2  
90° SECTION TORUS MODEL



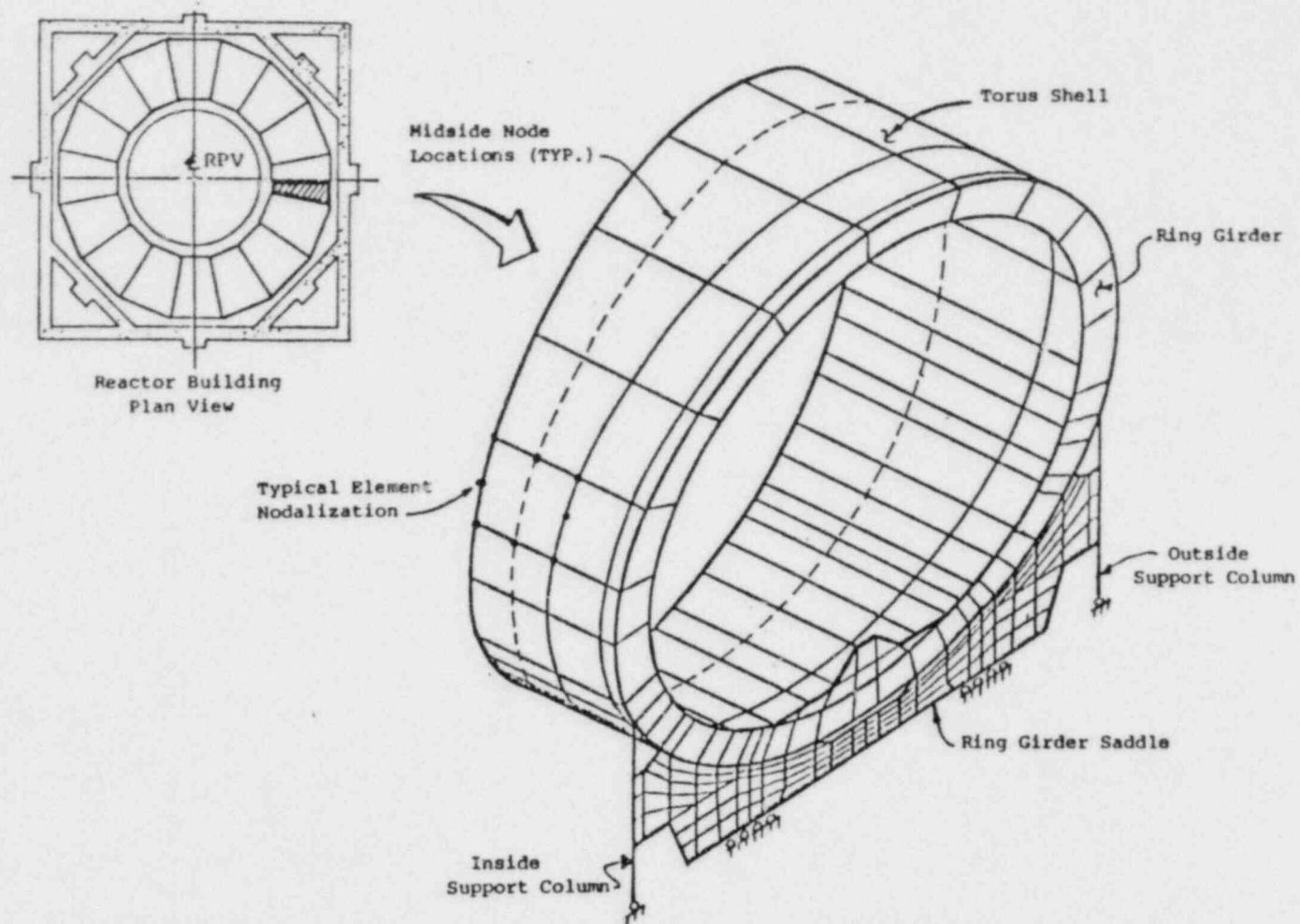
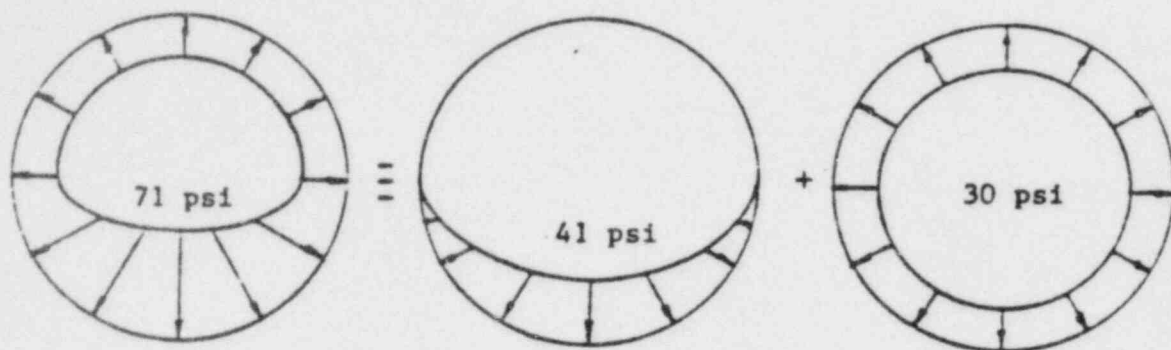
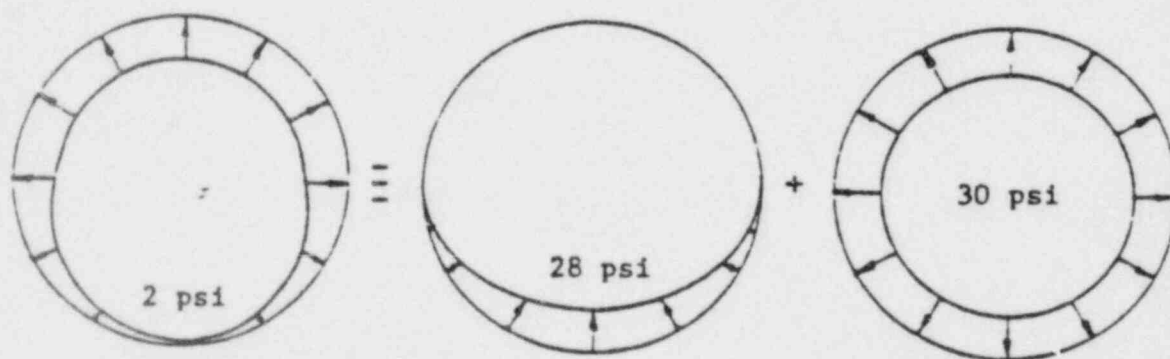


FIGURE 3.3

1/32 SECTION TORUS MODEL WITH DETAILED RING GIRDER SADDLE



Design Download



Design Upload

FIGURE 3.4

LOAD COMBINATIONS USED IN SADDLE EVALUATION

COOPER NUCLEAR STATION

PLANT UNIQUE ANALYSIS REPORT

SECTION 4

VENT SYSTEM AND SUPPORTS

#### 4.1 INTRODUCTION

This section describes the results of the structural evaluations of the vent system and associated support structures. The components included in this evaluation are the vent header, main vent, downcomers, vent header deflector, vent header support system, downcomer tiebars, main vent bellows, vent drain line, and associated penetrations and intersections on the vent system.

Descriptions of these components and modifications are provided in Section 1. The thermal-hydraulic load definitions and load combinations are described in Section 2. This section describes the design load combinations, design allowables, analysis methods and results, and code evaluations for all structural components listed above.

#### 4.2 VENT HEADER AND MAIN VENT

This subsection discusses the results of the structural evaluations of the vent header, main vent, vent header and main vent penetrations (i.e. vacuum breaker and main vent drain line penetrations), the drywell penetration, and the main vent bellows. Structural evaluations of the downcomers, downcomer/vent header intersection, and downcomer tiebars are discussed in Subsection 4.3.

##### 4.2.1 Design Load Combinations

The 27 design load combinations for the vent header and main vent are shown in Table 3.1 of Section 3. This table is taken from the PUAAG (Reference 19). ASME Code Service Limit assignments for each load combination are also indicated in the table. Of the 27 load combinations, potentially bounding load combinations were identified for the vent header and main vent evaluations. These bounding combinations are shown in Table 4.1. Combined vent

system stresses were compared against allowables for these load combinations.

#### 4.2.2 Design Allowables

The vent header and main vent are classified as Class MC components. Design allowables are taken from Subsection NE-3000 of the ASME Code.

##### 4.2.2.1 Vent Header and Main Vent

Stress intensity values are calculated using the procedure in Subsection NE-3215 of the Code. Combined stress intensity values were required to satisfy the requirements of Subsection NE-3221 for all load combinations. Fatigue evaluation of the vent system was also performed as required by Subsection NE-3221.5.

Stress intensity allowables for the vent system Class MC components are shown in Table 4.2. These allowables are based upon material allowables for SA-516 Grade 70 steel at a design temperature of 289°F corresponding to the maximum LOCA temperature along the main vent.

##### 4.2.2.2 Vent Header and Main Vent Penetrations

The vent header and main vent penetrations (i.e., penetrations at the vacuum breaker and the main vent drain line) are evaluated against the stress intensity allowables shown in Table 4.2. In accordance with the procedure in Reference 19, allowable stresses for primary local membrane ( $P_L$ ) and primary membrane plus primary bending ( $P_L + P_b$ ) stress intensities are increased by 30% at all vent header penetrations for LOCA-related loadings. Use of increased allowables for vent header stresses due to local pool swell impact pressures was not required, as Level A/B Service Limits were satisfied for pool swell loads.

#### 4.2.2.3 Drywell Penetration

The drywell penetration was evaluated against the stress intensity allowables shown in Table 4.2.

#### 4.2.2.4 Main Vent Bellows

The stress allowable for the bellows material (A240 TP304 stainless steel) is 16.6 ksi at 300°F.

#### 4.2.3 Analysis Methods and Results

This subsection describes the analyses and key results of the vent header and main vent evaluations.

The vent system structural response to the loads described in Section 2 was evaluated to demonstrate compliance with the Structural Acceptance Criteria. The vent system response was determined through the use of several analytical techniques, which were selected based upon the nature of the loads and the expected response.

To evaluate the vent system shell response to most static and dynamic loads, a 1/16 segment of the vent system was modeled using shell elements. This model was developed to predict overall vent system dynamic behavior, general shell membrane and bending stresses, and support reactions. Stresses in the region of the downcomer/vent header intersection were determined using a detailed model of the intersection region (Subsection 4.3.3.1.1). This model provides a more accurate representation of local stresses than provided by the 1/16 segment model.

For overall vent system response to non-symmetric load cases (e.g. seismic and chug synchronization), a beam model representing



a 180° segment of the vent system was used. Scale factors were then used to translate the responses from the 180° beam model into stresses in the 1/16 shell model.

For several components, such as the vent header penetrations and downcomer tie-bars (Subsection 4.3.3.3.1), hand calculations were sufficient to predict component stresses.

This subsection describes both the analysis methods and results for all vent system load cases. After a discussion of the mathematical models used in the analyses and the predicted vent system dynamic properties, the analyses for each load case identified in Section 2 are described. The application of the loads to the structural model, the analysis methods and procedures, and the important results are summarized. Finally, the simplified calculations of miscellaneous vent system components are reviewed.

#### 4.2.3.1 Vent System Mathematical Models

The analysis of the vent system for LOCA-related, S/RV discharge-related and other load cases required three structural models: (1) a shell model of a 1/16 segment of the vent system for consideration of vent system dynamics, (2) a beam model to represent non-symmetric vent system response, and (3) a detailed model of the downcomer/vent header intersection region. This subsection describes the first two models used to evaluate the vent system. The detailed model of the downcomer/vent header intersection region is described in Subsection 4.3.3.1.1.

The vent system has eight vertical planes of symmetry which divide the vent system into sixteen repetitive structural segments.\*

---

\* Asymmetry due to the presence of vacuum breakers and S/RVDL penetrations on some of the segments, is not considered significant.

Almost all vent system load cases (e.g. pool swell, thrust load, etc.) exhibit the same symmetry. Therefore, the primary finite element model of the vent system is a shell model representing a 1/16 segment spanning from the centerline of a vent bay to the centerline of an adjacent non-vent bay. Figure 4.1 shows the shell model used in the structural evaluations.

This 1/16 segment shell model employed eight node, isoparametric shell elements to represent the main vent and vent header. Equivalent spring stiffnesses were computed for the main vent penetration at the drywell liner. The program EDS-SNAP described in Appendix B was used to develop this model.

Since the downcomers have a relatively stiff cross-section when compared with the vent header cross-sectional properties, beam elements were used to represent the downcomers in the shell model. Beam elements were also used to model the vent header support columns, downcomer tiebars, and vent header deflector. Constraint equations were specified for nodes around the downcomer/vent header junction to prevent distortion of the downcomer pipe. These constraints were intended to model the stiffening effect that the relatively rigid downcomer cross-section has on the vent header.

The axial and lateral stiffnesses of the bellows are insignificant relative to the main vent stiffness and were not included in this model. However, the covering on the bellows was expected to significantly stiffen the main vent in the hoop direction and was modeled using stiff truss elements.

A consistent mass matrix formulation was employed for the vent system shell model. The inertial effects of the suppression pool were considered by taking the mass of the fluid displaced by the submerged portion of the downcomer and downcomer tiebars and "lumping" this mass on the nodes at the downcomer tips and on the

tiebars. Additionally, the downcomer submerged portions were assumed to be filled with water for all load cases. Although there is some question as to whether this assumption is valid during CO, it provides a conservative estimate of vent system CO response. The full water mass inside the downcomer was assumed to be effective. The increased mass on the submerged downcomer portions due to the combined effects of the suppression pool and the downcomer water leg is twice the mass of the water contained in the downcomer. The mass of the vacuum breaker was included in the model by adding its mass to the nodal mass of nearby nodes.

For asymmetric load cases, a larger portion of the vent system was modeled to predict the overall structural response. Beam models of the vent system were utilized to evaluate asymmetric load cases. The results obtained using the 1/16 segment shell model were then modified to include asymmetric effects.

A  $180^\circ$  segment of the vent system was modeled using three-dimensional beam elements for the main vent lines and the vent header (Figure 4.2). By specifying either symmetric or antisymmetric conditions at the boundaries of the model, the response of the full  $360^\circ$  vent system was predicted. A 1/16 segment beam model with symmetric boundary conditions was also developed to determine scale factors relating the 1/16 segment shell model stresses to the actual  $360^\circ$  vent system stresses. The program EDGAP described in Appendix B was used for these beam models.

The two beam models were used to modify shell stresses predicted by the 1/16 segment shell model to account for asymmetries in loads. Both the  $180^\circ$  segment beam model and the 1/16 beam model were analyzed for the same loads. The  $180^\circ$  segment beam model incorporated the true boundary conditions, while the 1/16 segment beam model had the same boundary conditions as the 1/16 segment shell model. By comparing beam forces and moments between the two beam models, scale factors were developed to correct the results

from the 1/16 segment shell model. These same factors were then applied to the shell stress results for the asymmetric load case considered. The modified shell stresses were then used in subsequent Code evaluations. This procedure was required for horizontal seismic (Subsection 4.2.3.2.1) and for chug synchronization (Subsection 4.2.3.2.5) analyses.

#### 4.2.3.2 Vent Header and Main Vent

This subsection describes the analysis methods and results from the vent system shell analyses. Vent system shell stresses (except for local stresses at the downcomer/vent header intersection and penetrations) and support reactions were determined using the 1/16 segment shell model. Analyses for all load cases described in Section 2 were performed using either dynamic or equivalent static solution methods. Damping was taken to be 2% of critical for all dynamic analyses.

##### 4.2.3.2.1 Static Analyses

Vent system analyses for static design loads are described in this subsection. Analysis procedures are described for gravity, seismic, internal pressure, thermal and thrust loads.

##### (1) Gravity and Seismic

The gravity and seismic load cases were evaluated by performing static analyses using both the 1/16 segment shell and 180° segment beam models. The vent system response to vertical seismic loads was determined by scaling the gravity analysis results from the 1/16 segment shell model by the peak vertical acceleration during an SSE.

The 180° segment beam model was analyzed to determine vent system response to horizontal seismic motion. The

resulting peak horizontal acceleration was used to develop scale factors which were then applied to the 1/16 segment shell model. The procedure for performing this horizontal seismic analysis is the same as that described for the chug synchronization analysis (Subsection 4.2.3.2.5). Combined responses due to vertical and horizontal seismic motions were conservatively evaluated by absolutely adding the individual responses to each direction of input motion. Results from the SSE analysis were used in all load cases involving seismic loads.

(2) Pressure Load Analysis

Following a LOCA, the vent system internal pressure increases to its maximum value within one second and then gradually decreases (Figure 4.3). The dynamic load factor (DLF) for a single degree of freedom (SDOF) system subjected to such a transient depends upon the ratio of the rise time of the load to the period of the SDOF system.

Conservatively taking the rise time as the vent clearing time (0.2561 sec), a DLF of less than 1.1 was obtained for all vent system periods. Therefore, peak pressures were statically applied to the 1/16 segment shell to evaluate vent system response to pressure loads. Concentrated loads were applied at the downcomer miter bends to account for pressures in the downcomers.

The resulting stresses from the pressure load analysis are directly combined with stresses induced by pool swell impact and drag on the vent header on the assumption that they occur simultaneously. The pressure load analysis stress results for subsequent times are scaled in accordance with the variations in Figure 4.3 to determine stresses to be combined with other LOCA event stress results.



(3) Thermal Analysis

The vent system temperatures shown in Table 4.3 were applied at the appropriate nodal points of the shell. These temperatures correspond to the saturated steam and water temperatures at the vent system pressures occurring 2.9 seconds after the vent clearing during a DBA. Temperatures at the edges of the collar plate and Y-stiffeners, support columns, vent deflector, and downcomer tie-bars were assumed to be at 80°F, the wetwell temperature at the initiation of a DBA. A linear temperature distribution was conservatively assumed between the vent header and the edges of the collar plate and Y-stiffener.

Maximum stresses were observed at the vent header miter joint and in the main vent/vent header intersection. These stresses are due to the constraint of vent header expansion by the collar plates and Y-stiffeners.

(4) Thrust Load Analysis

Vent system thrust loads (Figure 4.4) have a time variation similar to that of the pressure loads (Figure 4.3). Therefore, a static analysis of the vent system for maximum thrust loads was performed assuming a DLF of 1.0. The concentrated thrust forces defined in Subsection 2.4.2 were converted to pressure loads along the outboard side of the vent header. Concentrated loads were applied at the downcomer miter bends.

Vent system stresses due to thrust loads were typically lower than stresses for other LOCA-related load cases.



#### 4.2.3.2.2 Vent System Dynamic Properties

The frequencies and mode shapes of the vent system were determined by performing an eigensolution of the 1/16 segment shell model using the computer program EDS-SNAP. The subspace iteration method was used for this eigensolution (Reference 31).

Eighteen natural frequencies below a 50 Hz cutoff were calculated for the vent system. The modes corresponding to the first 13 frequencies are summarized in Table 4.4. The first seven modes are downcomer modes. The 8th and the 14th through 18th modes are vent header modes. The 9th, 10th, and 13th modes are vent header deflector modes, and the 11th and 12th modes are main vent modes.

The first seven downcomer sway modes predicted by the 1/16 segment shell model do not appropriately reflect the stiffness of the reinforced downcomer/vent header intersection. Recognizing that the swing mode of the downcomers is similar to that of a spring-supported pendulum, frequencies representative of the reinforced intersection were obtained by multiplying the downcomer frequencies for the unreinforced intersection by a scale factor. This scale factor is the square root of the ratio of the stiffness of the reinforced intersection to that of the unreinforced intersection. The stiffnesses of the reinforced and unreinforced intersections were determined using the detailed downcomer/vent header intersection model both with and without reinforcement. Scale factors were determined using both in-plane and out-of-plane unit loads applied at the bottom of the downcomer. The scale factors and downcomer sway mode frequencies obtained in this manner are summarized in Table 4.5.

#### 4.2.3.2.3 Pool Swell Dynamic Analysis

A dynamic time history analysis was performed on the 1/16 shell model to evaluate the vent system response to pool swell loads. The time history analysis included loadings on all vent system

components due to pool swell impact, drag, froth impingement, and froth fallback. Figure 4.5 shows the sequence and duration of pool swell loads used in the analysis of the vent system. Pool fallback loads on the downcomer tiebars occur after the major dynamic loads and were not expected to contribute significantly to vent system response. Pool swell impact and drag loads on the downcomer/vent header reinforcing gussets and froth loads on the support columns are insignificant relative to other pool swell loads.

Vent header impact and drag loads were applied as pressure loads on the shell surface. All other loads were applied as concentrated forces. Impact and drag loads on the vacuum breaker valves were converted to equivalent forces and moments at the penetration and were applied directly to the shell model.

A mode superposition analysis of the 1/16 segment shell model was performed using the program EDS-SNAP. The previously determined mode shapes and frequencies up to 50 Hz were used in the analysis. The analysis was started at the time of initial impact on the vent header deflector and was carried out for 0.65 sec. to span the significant part of the pool swell transient. The analysis required a time step size of 0.00185 sec. and 350 time steps.

A review of the resulting response time histories indicated that the peak vent system response was obtained during the 0.65 sec. analysis duration. Figure 4.6 shows the displacement time history response at an S/RVDL penetration on the main vent. Figure 4.7 shows an acceleration response spectrum at the vacuum breaker penetration. Maximum compressive membrane stresses observed in the vent system are summarized in Table 4.6.

#### 4.2.3.2.4 CO Analysis

As discussed in Subsection 2.4.4, vent system CO loads consist of two components: (1) an oscillating internal pressure used to

determine hoop stresses in the main vent, vent header, and downcomers, and (2) lateral loads on the downcomers.

For determination of hoop stresses in the vent system during CO, the oscillatory pressures were statically applied and stresses computed by hand. Static application of the loads is justifiable since the vent system modes involving radial expansion are close to or over 1000 Hz. The frequencies of the oscillating pressures were all below 50 Hz, resulting in a DLF of 1.0. The calculated hoop stresses are 0.4 ksi for the main vent and 0.3 ksi for the vent header.

The CO lateral loads on the downcomer pairs are considered as the superposition of an oscillating uniform pressure in both downcomers and an oscillating pressure differential between the downcomers. The uniform pressure component results in a net vertical force on the vent header, while the differential pressure component imposes lateral loads on the downcomers and the remainder of the vent system. Table 4.7 summarizes these pressure loads. From a review of the pressure magnitudes, DBA CO loads bounded IBA CO loads and were conservatively used to estimate both DBA and IBA responses.

Since the CO load definition for downcomer lateral loads specifies differential pressures between downcomers in a pair, it is necessary to determine which application of pressure differential on the three downcomer pairs within a 1/16 segment of the vent system produces the maximum structural response. Figure 4.8 illustrates the eight possible configurations of downcomer pressure differential. The beam model representing a 1/16 section of the vent system was subjected to all eight downcomer load configurations. From a review of these results, configuration 7 in Figure 4.8 was identified as the controlling load case.

The downcomer pressure loads were converted to equivalent concentrated loads and were applied to the 1/16 segment vent system

shell model. Loads on the downcomer tie bars were not considered significant and, therefore, were not included in this analysis. Load magnitudes were adjusted, since the higher downcomer sway frequencies were not included in the shell model. Loads were specified in the frequency domain with the frequencies selected to maximize the structural response. A frequency domain analysis was then performed using the 1/16 segment shell model to evaluate the overall vent system response to the downcomer CO loads.

Stresses in the vent system due to CO are typically bounded by the chugging-induced stresses, justifying the use of DBA CO results for IBA CO response. Stresses at the downcomer/vent header intersection due to CO loads are discussed in Subsection 4.3.4.1.

#### 4.2.3.2.5 Chugging Analysis

As with the CO load case, chugging loads consist of two components: (1) an oscillating internal pressure used for determining main vent, vent header and downcomer stresses, and (2) lateral loads on the downcomers. The chugging analysis methods and results for the downcomers are discussed in Subsections 4.3.3.1.4 and 4.3.3.2.4.

Oscillating internal chugging pressures in the vent system occur at sufficiently low frequencies that static analysis for these loads is justified. The calculated hoop stresses are 0.4 ksi for the main vent and 0.3 ksi for the vent header.

Lateral loads on downcomers due to chugging are assumed to be a result of random pressure fluctuations in the downcomer legs. Due to the random nature of the loads, the net lateral forces must be considered to act in any direction on the downcomer leg. It is possible that, at a given time during the chugging event, a number of downcomers will be loaded in the same direction. This phenomenon is termed chug synchronization. As the number of downcomers subjected to chugging loads in the same direction increases, the probability of these loads being the maximum

possible magnitude decreases. This behavior is shown in Figure 4.9. It can be seen that, for a given probability of occurrence, as the number of downcomers chugging in synchronization increases, the forces on each of those downcomers decrease. Therefore, two separate situations must be considered: 1) one situation with the maximum load on a single downcomer, and 2) one situation with the maximum net load on the entire vent system. The first situation is used to evaluate the downcomer/vent header intersection stresses and is discussed in Subsection 4.3.3.1.4. The second situation is used to evaluate the remainder of the vent system components as described below.

The NRC Acceptance Criteria recommends a non-exceedance probability of  $10^{-4}$  for determining the maximum force per downcomer. This non-exceedance probability results in a maximum resultant force on each downcomer of 0.6 kips when all 80 downcomers chug synchronously. This 0.6 kip force is based upon FSTF data and is adjusted using the procedure in Reference 27 to develop equivalent static plant unique loads for CNS.

Accordingly, the forces acting in the plane of a downcomer pair were multiplied by the factor 7.55, and the forces acting normal to the plane of a downcomer pair were multiplied by the factor 1.66. For forces acting in other directions, the load was divided into an in-plane and an out-of-plane component and then scaled by the factors mentioned above. Loads on the tiebars were not considered significant for this analysis.

The chug synchronization load is asymmetric and cannot be directly considered using a 1/16 segment model of the vent system. To allow use of the shell model for Code evaluation, scale factors were developed to account for the effect of the boundary conditions on the 1/16 segment model. These scale factors were determined by applying the actual chug synchronization loads to a  $180^\circ$  segment beam model of the vent system (Figure 4.10). A beam model of a 1/16 segment with the same boundary conditions as the shell model was then developed.



From the 180° segment model results, it was observed that the net load resisted by each of the main vents was not the same. The loads applied to the 1/16 segment beam model were therefore further amplified by a factor of 1.87, so that the main vent modeled in the 1/16 segment model carried the appropriate resultant loads (Figure 4.10).

The 1/16 segment beam model was then analyzed for these scaled loads. The differences in the beam forces and moments between the 180° segment beam model and the 1/16 segment beam model are then the effects of the 1/16 segment boundary conditions on the actual response. The ratio of the 180° segment model results to the 1/16 segment results are the scaling factors which vary from component to component. The loads applied to the 1/16 segment shell model are also the same loads applied to the 1/16 segment beam model. Resulting stresses from the shell model are then modified by the scale factors to obtain the final vent system stresses.

Chug synchronization stress results are high in many local regions along the vent header. Treatment of these high stresses is discussed in Subsection 4.2.4.2.

#### 4.2.3.2.6 S/RV Discharge Load Analysis

The vent system is loaded at the downcomer ends due to T-quencher bubble drag loads following an S/RV discharge. A review of the time histories of these loads (Figure 4.11), indicates that the forcing function can be approximated by a simple harmonic function. An equivalent static load on the downcomers was then determined by calculating a DLF based on the downcomer sway mode frequencies and scaling the maximum applied load by this DLF. Using the load magnitudes and frequency ranges in Table 4.8, the equivalent static loads on the downcomers were obtained for three S/RV discharge load cases. These are summarized in Table 4.9.



S/RV discharge bubble drag loads are defined for the downcomers in the vent bay. Since the T-quencher discharge device is located in this bay, loads on the non-vent bay downcomers will be lower. Because the loads are proportional to the square of the distance between the S/RV discharge bubble and the downcomer, reduced loads were applied to the non-vent bay downcomers.

Equivalent static analyses of the vent system for T-quencher drag loads on the downcomers were performed using the 1/16 segment shell model. Drag loads on the tie-bars were not considered in the analysis. Where asymmetric loading of the vent system occurred due to a single valve discharge, the 180° segment beam model was used to develop scale factors to account for the asymmetry. The development of these scale factors is similar to the procedure described in Subsection 4.2.3.2.5 for chug synchronization loads.

#### 4.2.3.3 Vent Header and Main Vent Penetrations

Local stresses at vent system penetrations were evaluated using the Bijlaard method for determining stresses at rectangular and circular attachments on cylindrical shells (Reference 33). The penetrations analyzed with this method were the S/RVDL penetrations on the main vent, the drywell-to-wetwell vacuum breaker and vent drain line penetrations on the main vent/vent header intersection, and the main vent penetration on the drywell liner (Subsection 4.2.3.4).

##### (1) S/RVDL Penetration

Forces and moments at the main vent S/RVDL penetrations were obtained from the S/RVDL piping analyses. These reactions included the effects of thrust loads on the piping, wetwell hydrodynamic loads on the S/RVDLs, and main vent anchor motions.

## (2) Vacuum Breaker Penetration

For evaluation of the drywell-to-wetwell vacuum breaker penetration, the vacuum breaker valve body reactions at the main vent/vent header intersection shell were determined for the governing case of pool swell loads. The pool swell acceleration response spectra at the penetration, shown in Figure 4.7, includes reactions at the shell due to impact and drag loads on the vacuum breaker valve body.

The natural frequency of the vacuum breaker valve was estimated and the corresponding spectral acceleration was used to calculate forces and moments acting on the penetration. A shear force of 25 kips and a bending moment of 490 kip-in. were predicted at each penetration due to pool swell loads. Stresses in the main vent/vent header intersection shell were calculated by modeling the reinforcing pads as rectangular attachments and using the Bijlaard procedure. Maximum membrane plus bending stress intensity due to pool swell was 53 ksi.

## (3) Vent Drain Line Penetration

The vent drain line penetration loads were estimated from the analysis of the drain line (Subsection 4.4.3).

In all penetration analyses, vent system stresses determined from the previously described vent system analyses were added to the local stresses prior to performing Code evaluations.

### 4.2.3.4 Drywell Penetration

Local stresses on the main vent penetration at the drywell were determined using reactions obtained directly from the vent system

analyses, using results from both the 1/16 segment shell model and the 180° segment beam model. The Bijlaard method for circular attachments on cylindrical shells (Reference 33) was used to evaluate the local stresses.

#### 4.2.3.5 Main Vent Bellows

Main vent bellows stresses were determined from the maximum wetwell pressure using the procedure in Reference 35. This procedure calculates circumferential and meridional membrane stresses and meridional bending stresses due to design pressures. The maximum membrane stress in the bellows for the peak wetwell pressure of 29 psi is 4.7 ksi.

Stresses in the bellows due to the relative displacements of the torus and vent system were also calculated using the procedure in Reference 35. These stresses are used only for calculating fatigue usage of the bellows. The maximum relative axial displacement is 0.35 in. primarily due to the vent system thermal expansion.

#### 4.2.4 Code Evaluation

This subsection summarizes the Code evaluations of the vent header and main vent structural components required to demonstrate compliance with the Mark I Program Structural Acceptance Criteria (Reference 19). The design load combinations and corresponding service level limits for the vent header and main vent components are summarized in Table 4.1.

In reviewing the shell stresses, distinction is made between general shell membrane and bending stresses and local shell stresses near discontinuities and penetrations. Also, checks for shell buckling and fatigue are discussed.

The primary membrane ( $P_m$ ) and primary membrane plus primary bending ( $P_L + P_b$ ) stress intensities for design load combinations were calculated by combining the stress intensities from the vent system shell model analyses described in Subsection 4.2.3. Stress intensities from separate load cases were added by absolute summation in these combinations. This procedure is more conservative than the algebraic addition of stress components, followed by the computation of stress intensities from combined stress components. Also, stress intensities from several dynamic load combinations were conservatively combined using absolute summation. The combined stresses for the vent header and main vent were evaluated away from any local discontinuities, such as penetrations or reinforcing collars.

The Code compliance checks indicate that all vent header and main vent components satisfy the requirements of the Mark I Program for the design load combinations.

#### 4.2.4.1 Main Vent

The maximum combined stress in the main vent occurs at bottom dead center of the 1/4"-thick section near the bellows location. The controlling Level B Service Load case is pool swell plus OBE, which produces a  $P_m$  of 9.4 ksi (49% of allowable) and a  $P_L + P_b$  of 10 ksi (34% of allowable). For the Level C Service load case, where stresses due to S/RV discharge drag loads are combined with pool swell and SSE loads, a  $P_m$  of 10.7 ksi (32% of allowable) and a  $P_L + P_b$  of 11.3 ksi (22% of allowable) are observed. Thermal stresses in the main vent are low, and the secondary stresses are therefore less than 20% of allowable.

#### 4.2.4.2 Vent Header

The vent header stress intensities away from the downcomer intersections are highest at the top dead center of the header at the

midpoint of the non-vent bay span. For the bounding load case of chugging plus S/RV discharge plus OBE loads, the  $P_m$  is 12.5 ksi (65% of allowable) and the  $P_L + P_b$  is 20.8 ksi (72% of allowable). Both are within Level B Service Limit allowables.

Local stresses near the vent header miter joint are high, due to the constraint of the collar plate in this region. For the bounding load case of chug synchronization and S/RV discharge, the combined stresses were slightly above allowable. Maximum  $P_L$  is 30.3 ksi (104%), and  $P_L + P_b + Q$  is 69.1 ksi (102%). Numerous conservatisms are included in these numbers. The collar plate temperature distribution is assumed to be linear, decreasing to wetwell temperature at the outer edge. This temperature distribution effect somewhat artificially constricts vent header expansion. The stress intensities due to S/RV discharge and chug synchronization are combined using absolute sum, which is conservative considering the low probabilities associated with chug synchronization loads (Subsection 4.2.3.2.5). Based on these observations, the reported miter joint stress levels are acceptable.

Vent header collar plate stresses are induced by the differential thermal expansion of the collar. These stresses are not critical and reach only 50% of the allowable value.

#### 4.2.4.3 Main Vent/Vent Header Intersection

The highest local stresses in this area are in the vicinity of the Y-shaped reinforcing collar and along the reducer section. Local membrane stresses due to chugging and S/RV discharge loads in these two areas reach 19.1 ksi (66% of allowable) and 27.6 ksi (95% of allowable), respectively. Primary plus secondary bending stresses are approximately 50% of allowable. Stresses in the Y-shaped collar due to differential thermal expansion are also within allowables.



#### 4.2.4.4 Vent Header and Main Vent Penetrations

##### 4.2.4.4.1 S/RVDL Penetration

Evaluating the reactions at the main vent S/RVDL penetrations required the combination of reactions from the drywell and wetwell portions of the S/RVDL. These reactions were combined by absolute summation, except for cases where directions could be clearly combined algebraically (e.g. thermal anchor motions). The eight drywell S/RVDL configurations were reviewed to determine maximum reactions. These reactions were combined with the appropriate reactions from the wetwell portion of the line. Typically, the shorter wetwell S/RVDL lines produced the bounding reactions. The short wetwell line reactions were combined only with the reaction from the four drywell lines which connect to the short lines.

Maximum combined local stresses are due to the S/RV discharge thrust reactions during an IBA/SBA event. These stresses were combined with the general membrane and bending stresses in the main vent. These maximum combined local stresses are below allowable limits.

##### 4.2.4.4.2 Vacuum Breaker Penetration

Pool swell impact and drag loads on the vacuum breaker body contributed to nearly 90% of the stress at the vent header penetration. The remaining stresses are due to seismic and dead weight reactions at the vent header. After reinforcement of the intersection, maximum  $P_L$  is 21.4 ksi (57% of allowable) and  $P_L + P_b + Q$  is 63.7 ksi (94% of allowable) at a location on the vent header near the edge of the reinforcing pad.

##### 4.2.4.4.3 Vent Drain Line Penetration

Pool swell and S/RV discharge loads on the main vent drain line produce maximum stresses in the header at the main vent/vent header



intersection. When combined with general membrane and bending stresses in the header for these load cases, the maximum  $P_L$  is 17.1 ksi (45% of allowable) and  $P_L + P_b + Q$  is 32.0 ksi (47% of allowable).

#### 4.2.4.5 Drywell Penetration

Maximum drywell shell stresses at the main vent penetration are caused by reactions from the main vent due to pool swell and S/RV discharge loads. The combined membrane plus bending stress intensity is 28 ksi (41% of allowable) in the reinforcing pad around the intersection, and 12 ksi (18% of allowable) in the drywell shell away from reinforcement.

#### 4.2.4.6 Main Vent Bellows

Bellows stresses were determined for relative torus-to-vent system combined displacements at the torus penetration, and for wetwell internal pressure. Stresses due to relative displacements are used only for fatigue evaluations (Subsection 4.2.4.7). The wetwell peak pressure results in a circumferential membrane stress of 4.7 ksi and a meridional bending stress of 7.3 ksi. These stresses are 28% and 44% of the allowable for the bellows material.

#### 4.2.4.7 Shell Buckling Assessment

Compressive membrane stresses in the vent system shell components were checked against ASME Code limits for buckling. The maximum compressive stresses were compared with allowables for both hoop and axial compressive stress. The allowables were determined using the procedure in subsection NE-2133 of the ASME Code. In determining the allowables, the presence of shell reinforcement at the downcomer/vent header intersection and at the collar plate near the miter joint was accounted for in reducing the effective span of the vent header.

The compressive stresses are generally within allowables except at very localized regions (near the downcomer/vent header intersection) where stresses were determined in excess of buckling allowables. These stresses are not, however, general membrane stresses for which the allowables are defined. In addition, these stresses are induced primarily by chugging lateral loads which have a peak load duration of only 5 msec. As determined in the evaluation of torus shell buckling under dynamic loads (Reference 29), such a short duration of compressive stress does not allow gross shell deformations (associated with buckling at the static buckling stress limits) to occur. For these reasons, this local exceedence of static buckling allowables is not considered a design deficiency and the current vent header configuration is acceptable with regard to shell buckling.

#### 4.2.4.8 Fatigue Evaluation

Vent system shell components were checked against fatigue as required by ASME Code rules for MC Components. Only the critical stress regions were evaluated for fatigue. These regions were generally areas of high local stresses around penetrations or the miter joint. Stress concentration factors were developed to calculate peak stresses from the primary plus secondary stress ranges determined in the analyses. The fatigue design basis is described in Subsection 2.7.7.

##### 4.2.4.8.1 Main Vent/Vent Header Intersection

Fatigue usage at the connection of the vent header and main vent shells around the Y-collar is 0.15. Since pool swell loads are not considered in evaluating fatigue (Reference 12), the vacuum breaker/vent header penetration has insignificant fatigue usage.

#### 4.2.4.8.2 Vent Header Miter Joint

Local stresses in the vicinity of the vent header miter joint and reinforcing collar produce a fatigue usage of 0.34. Chugging loads account for 83% of this total usage.

#### 4.2.4.8.3 Main Vent Bellows

Reference 35 details the procedure used in evaluating expansion bellows for fatigue. The main vent bellows has a very low fatigue usage. The cumulative usage for all stress cycles is less than 0.01.

#### 4.2.4.8.4 Main Vent S/RVDL Penetration

In evaluating fatigue usage at the main vent S/RVDL penetration, the fatigue design basis assumes 250 S/RV actuations during normal plant operation. This assumption is justifiable since the design number of 500 S/RV actuations is based on extrapolating the total number of actuations for all eight valves at CNS. The number of actuations by a particular S/RV is substantially lower. Plant operating data show that each S/RV has approximately the same number of actuations to date. For the S/RVDL penetration, the primary contributor to fatigue usage is from stresses induced by reactions of the S/RVDL. Therefore, the design basis of 250 actuations still represents a conservative estimate of the total number of actuations by any one S/RV for the 250 S/RV actuations assumed, the fatigue usage at the penetration is below 1.0. Three-quarters of this usage comes from S/RV discharge-related load cases.

### 4.3 DOWNCOMERS AND TIEBARS

This subsection discusses the results of the structural evaluations of the downcomer/vent header intersection, the downcomers, and the downcomer tiebars.

#### 4.3.1 Design Load Combinations

The 27 design load combinations for the downcomer/vent header intersection, downcomers, and tiebar are shown in Table 3.1 of Section 3. Also indicated in Table 3.1 are the ASME Code Service Level assignments for each load combination. Of these 27 load combinations, potentially bounding load combinations are shown in Table 4.10. Actual downcomer and tiebar stresses were compared against allowables for these load combinations.

#### 4.3.2 Design Allowables

The ASME Code design classifications for the downcomer/vent header intersection, the downcomers and the downcomer tiebars are provided in this subsection.

##### 4.3.2.1 Downcomer/Vent Header Intersection

The downcomer/vent header intersection is evaluated against the stress intensity allowables shown in Table 4.2. In accordance with the procedure in Reference 19, allowable stresses for primary local membrane ( $P_L$ ) and primary membrane plus primary bending ( $P_L + P_b$ ) stress intensities are increased by 30% for LOCA-related loadings.

##### 4.3.2.2 Downcomers

The downcomers are classified by the ASME Code as Class MC Components. Design allowables are taken from Subsection NE-3000 of the Code. Table 4.2 shows the stress intensity values against which the downcomers are evaluated. These allowables are based upon material allowables for SA-516 Grade 70 steel at a design temperature of 289°F. Use of increased allowables due to local impact pressures was not required, as Level A/B Service Limits were satisfied for pool swell loads.

#### 4.3.2.3 Downcomer Tiebar

The downcomer tiebar is classified as a linear component and design allowables are taken from Subsection NF-3300 of the Code. Design stress intensity allowables for the downcomer tiebars are shown in Table 4.11. These allowables are based upon material allowables for SA-53, Grade B steel at a design temperature of 200°F (corresponding to the maximum suppression pool temperature).

#### 4.3.3 Analysis Methods and Results

This subsection describes the analyses and key results of the downcomer evaluations. The downcomer structural response to the loads described in Section 2 is evaluated to demonstrate compliance with the Structural Acceptance Criteria. This response was determined through the use of several analytical techniques described in this subsection which were selected based upon the nature of the loads and the expected response.

##### 4.3.3.1 Downcomer/Vent Header Intersection

The finite element model developed to evaluate the downcomer/vent header intersection is described in this subsection, as well as the evaluations for the bounding LOCA and S/RV discharge loads.

##### 4.3.3.1.1 Mathematical Model

The geometric complexity of the downcomer/vent header intersection region after reinforcement by the gusset plate arrangement (Figure 4.12) required a more detailed model than the 1/16 segment shell model to predict the local stresses. This level of detail in the shell model would have substantially increased the model size and made the shell model impractically large for use in dynamic analyses. Therefore, a separate, detailed model of this region was developed to qualify the intersection. The model was constructed using plate elements and the program EDSGAP.



The gusset plate reinforcement and welding pads on the vent header and downcomer are included in the detailed model shown in Figure 4.13. The model is symmetric about the vertical plane containing the vent header centerline. Symmetric or anti-symmetric boundary conditions are used at the nodes on the vertical plane, depending upon the load case being considered. The nodes at the boundaries of the planes normal to the vent header are fixed. The length of the model along the vent header was selected so that the end fixity would not affect the intersection stresses.

Static analyses of this model were performed to calculate local stresses in the intersection for unit loads at the downcomer tips (three forces and three moments). These results are scaled by actual downcomer loads either specified in the load definitions or predicted by the 1/16 segment shell model to calculate intersection stresses for actual load cases. This procedure allows prediction of local stresses at the intersection, without substantial refinement of the detailed 1/16 segment shell model.

Maximum stresses in the intersection were summarized for unit loads in six directions. Table 4.12 summarizes the unit load analysis results. The highest stresses occurred on the vent header between the gusset welding pads in the circumferential and longitudinal directions.

These unit load analysis results were scaled by the actual dynamic loads resulting from the previously performed vent system analyses. Table 4.13 summarizes these loads for load cases resulting in downcomer lateral loads. The tabulated loads are the loads on one downcomer, and do not include tie-bar loads. For chugging, two cases of lateral loads are considered: (1) the load is acting in the plane of the downcomer pair, and (2) the load is acting normal to the plane of the downcomer pair. These loads were determined using the procedure in Reference 27.



The local stresses due to pressure, thrust, gravity, and seismic loads were taken to be the same as the stresses on the "clean" vent header (2 downcomer diameters away from intersection). During vent system heat-up, it is assumed that the gusset plates around the intersection have the same temperature as the vent header and downcomers, thereby producing the same thermal stresses as predicted for the clean vent header.

#### 4.3.3.1.2 Pool Swell Analysis

Table 4.13 includes the equivalent static design loads on a single untied downcomer resulting from pool swell impact and drag on the downcomer. The design load was derived by applying the impact and drag loads on the inclined portion of the downcomer. The detailed downcomer/vent header intersection model described above was then analyzed for this design pool swell load.

#### 4.3.3.1.3 CO Lateral Loads

CO lateral loads on the downcomers are produced by uneven pressure oscillations in the two downcomers in a pair as described in Subsection 4.2.3.2.4. The maximum net downcomer lateral load due to CO was 4.3 kips in the in-plane direction. The maximum vertical load on a downcomer pair was 0.7 kips. Since these loads were bounded by the chugging lateral and vertical loads no further evaluation was required.

#### 4.3.3.1.4 Chugging Lateral Loads

Two separate design conditions were evaluated for chugging lateral loads on the downcomers: (1) the maximum chug design load occurs in the critical direction on a single downcomer, and (2) the maximum probable net load occurs on the entire vent system. The first situation is used to evaluate the downcomer/vent header intersection as discussed in this subsection. The second situation is used to evaluate the remainder of the vent system components as discussed in Subsection 4.2.3.2.5.

As shown in Table 4.13, the maximum downcomer lateral load due to chugging is 9.7 kips. This load is used in the qualification of the downcomer/vent header intersection as discussed in Subsection 4.3.4.1.

#### 4.3.3.1.5 S/RV Discharge Drag Loads

S/RV discharge bubble drag loads on the downcomer ends result in stresses in the downcomer/vent header intersection. The application of these loads was previously discussed in Subsection 4.2.3.2.6.

As shown in Table 4.13, the maximum vertical downcomer S/RV discharge lateral load is 2.2 kips and the maximum out-of-plane load is 7.5 kips. These loads were converted to stresses in the downcomer/vent header intersection using the scale factors for the detailed downcomer/vent header intersection model previously discussed in Subsection 4.3.3.1.1.

#### 4.3.3.2 Downcomers

The mathematical model and analysis procedures used to qualify the downcomers for pool swell loads and internal pressure loads due to CO and chugging are described in this subsection.

##### 4.3.3.2.1 Mathematical Model

For evaluation of the downcomer stresses due to downcomer lateral loads, the detailed downcomer/vent header intersection model was utilized, as previously described in Subsection 4.3.3.1.1. Hoop stresses in the downcomers resulting from internal pressures during the CO and chugging phases were computed by hand calculations.

#### 4.3.3.2.2 Pool Swell Analysis

An equivalent static analysis of the downcomer arm was performed for the pool swell drag loads shown in Table 4.13. A DLF of two was used in this analysis. The maximum membrane plus bending stress intensity was 17.5 ksi.

#### 4.3.3.2.3 CO Analysis

The CO internal pressure loads for the downcomers are defined as oscillating internal pressure loads as shown in Table 4.14. For determination of hoop stresses in the downcomers during CO, the oscillatory pressures were statically applied and stresses computed by hand. Static application of the CO loads is justifiable since the vent system modes involving radial expansion have frequencies over 1000 Hz. The frequencies of the oscillating pressures are all below 50 Hz, resulting in a DLF of 1.0. The calculated hoop stress is 0.6 ksi in the downcomer.

#### 4.3.3.2.4 Chugging Analysis

As with the CO case, the chugging internal pressure loads for the downcomers consist of an oscillating internal pressure. The oscillating internal chugging pressure occurs at a sufficiently low frequency that static analysis is justified for this load case. Similar to the CO internal pressure, a DLF of 1.0 was used. The resulting hoop stress is 0.6 ksi in the downcomer.

Maximum membrane and membrane plus bending stress intensities due to chugging lateral loads were 3.4 ksi and 5.4 ksi, respectively. These stresses are at a location on the downcomer away from the downcomer/vent header intersection which was discussed in Subsection 4.3.3.1.

#### 4.3.3.2.5 S/RV Discharge Analysis

Maximum membrane and membrane plus bending stress intensities due to downcomer lateral loads following an S/RV discharge are 3.3 ksi and 5.2 ksi, respectively. Again, these stresses are at a location on the downcomer away from the downcomer/vent header intersection.

#### 4.3.3.3 Downcomer Tiebar

The mathematical model and analysis procedures used to qualify the downcomer tiebars for CO, chugging, S/RV discharge, and pool swell drag loads are described in this subsection.

##### 4.3.3.3.1 Mathematical Model

Downcomer tiebar forces and moments were determined from both the vent system shell model response and a separate beam model of the tiebar. The beam model was used to determine tiebar stresses resulting from submerged structure drag and pool fallback loads.

##### 4.3.3.3.2 Pool Fallback and Drag Loads

The critical tiebar loads are due to pool fallback and CO drag loads. Maximum tiebar stresses due to combined bending moments and axial forces are 9.2 ksi for CO drag loads and 6.0 ksi for pool fallback loads. All other load cases produce stresses below 5 ksi.

##### 4.3.3.3.3 Chugging Axial Loads

The NRC Acceptance Criteria, Section 2.1.2.2.2, requires consideration of tiebar stresses induced by downcomer lateral loads due to chugging. Following the procedure in the acceptance criteria, maximum tiebar stresses were below 0.5 ksi.

#### 4.3.4 Code Evaluation

This subsection describes the Code evaluation for the downcomer/vent header intersection, downcomers, and downcomer tiebars for the design load combinations summarized in Table 4.10.

##### 4.3.4.1 Downcomer/Vent Header Intersection

The downcomer/vent header intersection stresses are highest in the portion of the vent header not covered by the reinforcing pads. The critical load combination for the intersection is S/RV discharge bubble drag loads added to chugging lateral loads using the 1.1 SRSS combination method as described in Appendix D. The maximum local membrane stress intensity is below the Level B Service allowable when the 30% increase in allowable stress is considered. The maximum bending stress intensity is below the allowable for primary plus secondary stress limits.

##### 4.3.4.2 Downcomers

The highest stresses in the downcomer legs are due to pool swell impact pressures on the angled portion of the downcomers. With downcomer internal pressures added to these stresses, the combined  $P_m$  is 5.6 ksi (29% of allowable) and the  $P_L + P_b$  is 17.5 ksi (60% of allowable). Both are within Level B Service allowables. Downcomer lateral loads produce downcomer stresses well within allowables since the vent header resists nearly all reactions from these loads due to its significantly higher flexibility.

##### 4.3.4.3 Downcomer Tiebar

The downcomer tiebar stresses were determined through the analysis methods described in Subsection 4.3.3.3.2. The maximum combined stress in the tiebar for the design load combination of pool swell and S/RV discharge loads is 12.8 ksi, which is 62% of allowable.



#### 4.3.4.4 Fatigue Evaluation

The downcomers and downcomer/vent header vent system shell components were checked against fatigue as required by ASME Code rules for MC Vessels. Only the critical stress regions were evaluated for fatigue. These regions were generally local stresses around the downcomer/vent header intersection. Stress concentration factors were developed to calculate peak stresses from the primary plus secondary stress ranges determined in the analyses.

The only contributions to fatigue usage at the downcomer/vent header intersection come from chugging and S/RV discharge lateral loads on the downcomers. All other load cases produce stresses below the endurance limit for SA-516, Grade 70 steel. In determining fatigue usage due to chugging, the load histogram defined in Section 2 was used. The sectors used to define the directions of lateral loads on the downcomer end are shown in Figure 2.23 of Section 2. The number of stress cycles following an S/RV discharge was assumed to be equal to the number of significant load cycles.

Peak stresses at the intersection were determined by multiplying the maximum primary plus secondary stress intensities by a stress concentration factor of two (Reference 36). The total usage factor is 0.49. Normal operational S/RV discharge events account for 84% of the total usage.

#### 4.4 VENT DRAIN LINE

This subsection discusses the results of the vent drain line evaluations. This drain line is situated at the bottom of the main vent/vent header intersection.



#### 4.4.1 Design Load Combinations

The significant loads on the vent drain line are those due to pool swell impact and drag and S/RV discharge T-quencher bubble drag. The vent drain line was evaluated for S/RV discharge, and S/RV discharge plus CO, chugging, or pool swell loads. Service limit assignments were taken from the Class 2 and 3 piping system assignment table in the PUAAG.

#### 4.4.2 Design Allowables

The vent drain line is classified as an ASME Class 2 piping system and is qualified in accordance with Subsection NC of the Code. The stress intensity allowables for the design combinations are provided in Table 4.15.

#### 4.4.3 Analysis Methods and Results

The vent drain line was modeled using a simple beam representation. The natural frequency of the drain line was determined to convert the dynamic drag and froth impingement load definitions into equivalent static forces. The maximum bending stress in the drain line is 18.5 ksi for T-quencher air bubble drag loads.

#### 4.4.4 Code Evaluation

Moments along the vent drain line were computed to determine stresses in accordance with Class 2 piping procedures. The most critical stress in the 1-inch line is 16.4 ksi due to S/RV discharge bubble drag loads. This stress is 91% of the Level B Service allowable. Weld stresses at the connection of the drain line to the 3-inch deflector strut are 53% of allowable.

#### 4.5 VENT HEADER DEFLECTOR

Results of the structural evaluations of the vent header deflector and its supports are discussed in this subsection.

##### 4.5.1 Design Load Combinations

The significant loads on the vent header deflector and its supports are those due to pool swell impact and drag, and froth impingement.

##### 4.5.2 Design Allowables

The vent header deflector and its supports are classified as linear structural components and are qualified in accordance with Subsection NF of the Code. The 16"-diameter vent header deflector pipe is fabricated from SA-53 Grade B steel and the supports are fabricated from SA-36 steel. The stress intensity allowables for the design loads are provided in Table 4.16.

##### 4.5.3 Analysis Methods and Results

The vent header deflector and supports were qualified modeling the deflector as a linear beam and performing hand calculations in accordance with established beam theory. For the design pool swell impact load, the maximum bending moment in the deflector was observed to be 1240 kip-in. This moment results in a bending stress of 7.2 ksi. The maximum vent header support load for the design pool swell impact load was 31 kips.

##### 4.5.4 Code Evaluation

The maximum vent header deflector stress of 7.2 ksi for the pool swell impact loads is 17% of the allowable. The corresponding support load of 31 kips is 9% of the allowable.

#### 4.6 VENT HEADER SUPPORT SYSTEM

Analytical procedures and results of the vent header support system evaluations are discussed in this Subsection.

##### 4.6.1 Design Load Combinations

The design loads and load combinations for the vent header support columns are summarized in Table 4.17.

##### 4.6.2 Design Allowables

The vent header support columns are classified by the ASME Code as linear structural supports and are qualified in accordance with Subsection NF of the Code. The Level B Service stress allowable at a design temperature of 200°F are 17.0 ksi in compression and 19.1 ksi in tension.

##### 4.6.3 Analysis Methods and Results

Combined axial forces in the vent header support columns are 49 kips compression and 24 kips tension. These forces are due to either pool swell or chugging loads in combination with gravity, pressure, thermal, and seismic loads. Lateral distributed loads of 0.9 kip/ft due to froth impingement were also considered.

##### 4.6.4 Code Evaluation

The maximum stress in the support columns resulting from the 49 kips compressive load in conjunction with the 0.9 kip/ft lateral distributed load was 28% of the Level B Service allowable. All of the associated welds were stressed well within their allowable limits.

Table 4.1

DESIGN LOAD COMBINATIONS AND CORRESPONDING  
SERVICE LEVEL LIMITS FOR THE VENT HEADER AND MAIN VENT

<u>Load Combination</u>	<u>Service Level</u>
Pool Swell + OBE	B
DBA Condensation Oscillation + SSE	C
IBA/SBA Chugging + S/RV + SSE	C
Pool Swell + S/RV + SSE	C

Table 4.2

ALLOWABLE STRESS INTENSITIES FOR VENT  
SYSTEM CLASS MC COMPONENTS

Stress Intensity Type	Allowable Stress (ksi)	
	Service Level A/B	Service Level C
Primary Membrane ( $P_m$ )	19.3	33.8
Local Membrane ( $P_L$ )	29.0	50.7
Primary Membrane plus Primary Bending ( $P_L + P_b$ )	29.0	50.7
Primary plus Secondary ( $P_L + P_b + Q$ )	67.8	N/A

Notes:

- (1) Allowable stresses for SA516, Grade 70 steel at 289°F
- (2)  $P_L$  and  $P_L + P_b$  allowable stress values increased by 30% for evaluating vent header penetrations (e.g. downcomers) for Service Level A/B load combinations involving LOCA related loads.

Table 4.3

VENT SYSTEM DESIGN TEMPERATURES

<u>Component</u>	<u>Pressure (psia)</u>	<u>Temperature (°F)</u>
Main Vent	56.7	289
Main Vent/Vent Header	50.5	282
Vent Header	44.2	274
Downcomer/Vent Header Intersection	39.4	266
Downcomer	34.5	259
Wetwell Airspace	29.7	80

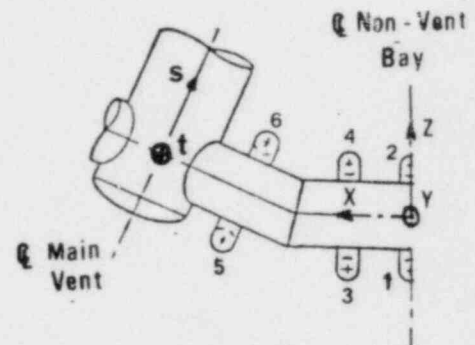
Note:

Temperatures calculated 2.9 sec after initiation of a DBA.



Table 4.4

FREQUENCIES AND MODE SHAPES  
OF 1/16 VENT SYSTEM MODEL



<u>Mode No.</u>	<u>Frequency (Hz)</u>	<u>Description of Mode Shape</u>
1	4.5	z movement of downcomers 1 and 2
2	5.9	z movement of downcomers 3 and 4
3	6.8	z movement of downcomers 5 and 6
4	13.4	x movement of 3rd downcomer
5	13.7	x movement of 4th downcomer
6	14.4	x and z movement of 6th downcomer
7	15.0	x and z movement of 5th downcomer
8	21.7	z movement of vent header
9	24.9	z movement of vent header deflector
10	30.8	y movement of vent header deflector
11	33.8	x, y, and z movement of main vent
12	34.5	s and -t movement of main vent
13	35.9	z and -z movement of vent header deflector around support columns

Table 4.5

MODIFIED DOWNCOMER SWAY MODE FREQUENCIES  
ACCOUNTING FOR GUSSET REINFORCEMENT

<u>Frequency (Hz)</u> <u>Unreinforced</u> <u>Intersection</u>	<u>Scale</u> <u>Factor</u>	<u>Frequency (Hz)</u> <u>Reinforced</u> <u>Intersection</u>	<u>Description of Mode</u>
4.5	3.71	16.7	In-plane sway - dc 1 & 2
5.9	3.71	21.9	In-plane sway - dc 3 & 4
6.7	3.71	24.9	In-plane sway - dc 3 & 4
13.4	1.45	19.4	Out-of-plane sway - dc 3
13.7	1.45	19.8	Out-of-plane sway - dc 4
14.4	1.45	20.9	Out-of-plane sway - dc 6
15.0	1.45	21.7	Out-of-plane sway - dc 5

Notes:

- (1) Unreinforced intersection frequencies determined from 1/16 shell model results.
- (2) Refer to Table 4.4 for numbering of downcomers.

Table 4.6

MAXIMUM COMPRESSIVE MEMBRANE STRESSES IN VENT SYSTEM COMPONENTS  
DUE TO POOL SWELL LOADS

<u>Location</u>	<u>Maximum Compressive Stress (ksi)</u>	
	<u>Axial</u>	<u>Hoop</u>
Main Vent	3.5	0.5
Main Vent/Vent Header Intersection	1.7	1.9
Reducer	2.3	3.5
Vent Header	2.4	0.9
Vent Header Miter Joint	2.3	4.6

Table 4.7

VENT SYSTEM DOWNCOMER LATERAL LOAD  
DUE TO CONDENSATION OSCILLATION

<u>Type</u>	<u>Pressure Amplitude (psi)</u>		<u>Frequency Range (Hz)</u>	
	<u>DBA</u>	<u>IBA</u>	<u>DBA</u>	<u>IBA</u>
Internal	<u>+3.6</u>	<u>+1.1</u>	4-8	6-10
Differential	<u>+2.9</u>	<u>+0.2</u>		
Internal	<u>+1.3</u>	<u>+0.8</u>	8-16	12-20
Differential	<u>+2.6</u>	<u>+0.2</u>		
Internal	<u>+0.6</u>	<u>+0.2</u>	12-24	18-30
Differential	<u>+1.2</u>	<u>+0.2</u>		

Table 4.8

S/RV DISCHARGE-RELATED DRAG LOADS  
ON VENT SYSTEM COMPONENTS

<u>Component</u>	<u>Event</u>	<u>Load Direction</u>	<u>Net Load (lbf)</u>	<u>Frequency Range (Hz)</u>
Downcomer	SBA/IBA	Lateral	2600	5.8-15.4
	DBA	Lateral	2430	4.5-9.4
	NOC	Lateral	2600	4.5-9.4
Downcomer Tie-Bar	SBA/IBA	Lateral	740	5.8-15.4
		Vertical	830	5.8-15.4
Main Vent Drain Line	SBA/IBA	Lateral	4	5.8-15.4

Table 4.9

EQUIVALENT STATIC LOADS ON DOWNCOMERS  
DUE TO S/RV DISCHARGE BUBBLE DRAG

<u>Event</u>	<u>Downcomer Frequency (Hz)</u>	<u>Dynamic Load</u>		<u>DLF</u>	<u>Equivalent Static Load (lbf)</u>
		<u>Magnitude (lbf)</u>	<u>Frequency (Hz)</u>		
<u>SBA/IBA</u>					
In-Plane	24.9	970	15.4	1.6	1560
Out-of-Plane	21.3	2790	15.4	2.1	5820
<u>DBA</u>					
In-Plane	24.9	890	9.4	1.2	1050
Out-of-Plane	21.3	2630	9.4	1.2	3260
<u>NOC</u>					
In-Plane	24.9	970	9.4	1.2	1130
Out-of-Plane	21.3	2790	9.4	1.2	3460

Notes:

- (1) Loads defined for downcomer pair in vent bay.
- (2) 2% damping used in calculating DLF.
- (3) In-Plane and Out-of-Plane refer to plane of downcomer pair.



Table 4.10

BOUNDING LOAD COMBINATIONS AND CORRESPONDING  
SERVICE LEVEL LIMITS FOR DOWNCOMERS AND TIEBARS

<u>Load Combination</u>	<u>Service Level</u>
Pool Swell + OBE	B
DBA Condensation Oscillation + SSE	C
IRA/SBA Chugging + S/RV + SSE	C
Pool Swell + S/RV + SSE	C

Table 4.11

DESIGN STRESS ALLOWABLES FOR DOWNCOMER TIEBARS

<u>Service Level</u>	<u>Allowable Stress (ksi)</u>		
	<u>Tension</u>	<u>Shear</u>	<u>Bending</u>
A/B	19.1	12.7	19.1
C	25.4	17.0	25.4

Table 4.12

MAXIMUM STRESSES AT THE DOWNCOMER/VENT  
HEADER INTERSECTION FOR UNIT LOAD ANALYSES

<u>Unit Load Direction</u>	$P_m$	$P_L + P_b$	$P_L + P_b$
	<u>ksi/kip</u>	(Outside Surface) <u>ksi/kip</u>	(Inside Surface) <u>ksi/kip</u>
Out-of-Plane	1.72	4.02	4.23
Vertical	0.18	0.16	0.23
In-Plane	0.62	0.50	0.90

Table 4.13

SUMMARY OF DOWNCOMER LATERAL LOADS

<u>Load Case</u>	<u>Out-Of-Plane Load (kips)</u>	<u>Vertical Load (kips)</u>	<u>In-Plane Load (kips)</u>
S/RV <sup>(1)</sup>	7.5	2.2	0
Out-Of-Plane Chugging <sup>(1) (2)</sup>	7.6	2.4	0
In-Plane Chugging <sup>(1) (2)</sup>	0	2.4	9.7
Pool Swell	0	4.3	2.5

Notes:

- (1) Drag loads on tie-bar included.
- (2) Out-of-plane and in-plane chugging loads are not combined with each other.

Table 4.14

CONDENSATION OSCILLATION PRESSURE AMPLITUDES  
IN THE DOWNCOMERS

<u>Frequency</u> <u>Range</u> <u>(Hz)</u>	<u>Amplitude</u> <sup>(1)</sup> <u>(psi)</u>	<u>Frequency</u> <u>Range</u> <u>(Hz)</u>	<u>Amplitude</u> <sup>(1)</sup> <u>(psi)</u>
0-1	0.24	25-26	0.13
1-2	0.25	26-27	0.14
2-3	0.38	27-28	0.11
3-4	0.56	28-29	0.13
4-5	1.16	29-30	0.10
5-6	2.56	30-31	0.10
6-7	0.62	31-32	0.11
7-8	0.46	32-33	0.10
8-9	0.46	33-34	0.10
9-10	0.46	34-35	0.09
10-11	0.62	35-36	0.10
11-12	0.51	36-37	0.10
12-13	0.39	37-38	0.08
13-14	0.40	38-39	0.10
14-15	0.34	39-40	0.08
15-16	0.34	40-41	0.10
16-17	0.36	41-42	0.09
17-18	0.24	42-43	0.08
18-19	0.26	43-44	0.07
19-20	0.19	44-45	0.08
20-21	0.21	45-46	0.07
21-22	0.15	46-47	0.07
22-23	0.15	47-48	0.07
23-24	0.13	48-49	0.07
24-25	0.16	49-50	0.06

Note:

(1) Half range (= 1/2 of peak to peak amplitude)

Table 4.15

STRESS INTENSITY ALLOWABLE FOR DESIGN LOAD  
COMBINATIONS FOR MAIN VENT DRAIN LINE

<u>Load Combination</u>	<u>Allowable Stress</u> <u>(ksi)</u>
S/RV	18.0
IBA/SBA Chugging + S/RV	27.0
DBA Condensation Oscillation	36.0
Pool Swell + S/RV	36.0



Table 4.16

STRESS INTENSITY ALLOWABLES FOR THE VENT  
HEADER DEFLECTOR

<u>Material</u>	<u>Service Levels</u>	<u>Allowable Stress (ksi)</u>		
		<u>Tension</u>	<u>Shear</u>	<u>Bending</u>
SA-53, Gr. B	B	21.0	14.0	23.1
	D	42.0	28.0	46.2
SA-36	B	21.6	14.4	23.8
	D	40.6	27.1	44.7

Table 4.17

DESIGN LOADS AND LOAD COMBINATIONS FOR  
VENT SYSTEM SUPPORT COLUMNS

<u>Load Combination</u>	<u>Design Load (kips)</u>	
	<u>Tension</u>	<u>Compression</u>
Pool Swell + OBE + Pressure + Thrust + Gravity + Thermal	24.0	48.0
Chugging + OBE + Pressure + Thrust + Gravity + Thermal	5.0	49.0

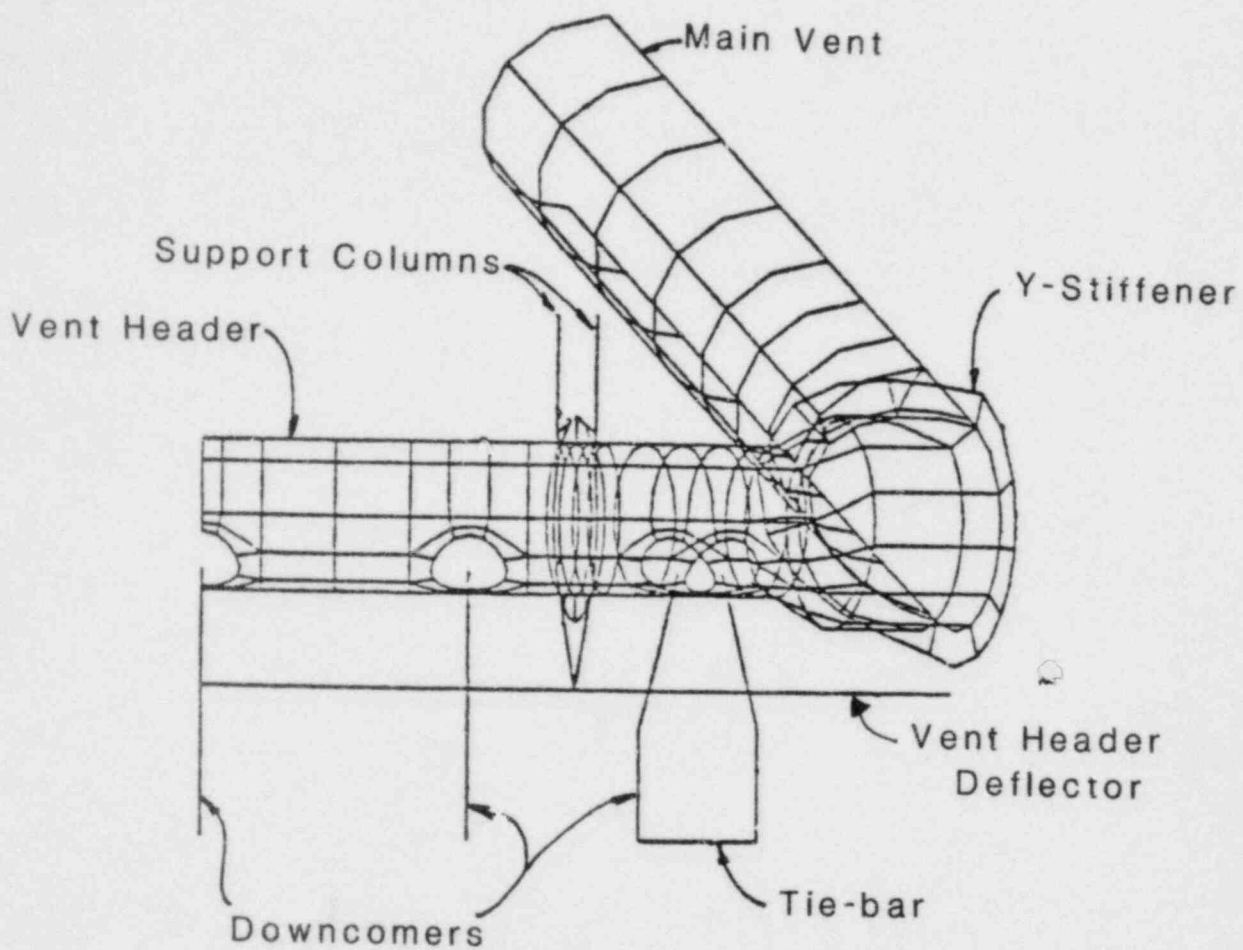


FIGURE 4.1

1/16TH FINITE ELEMENT SHELL MODEL OF VENT SYSTEM

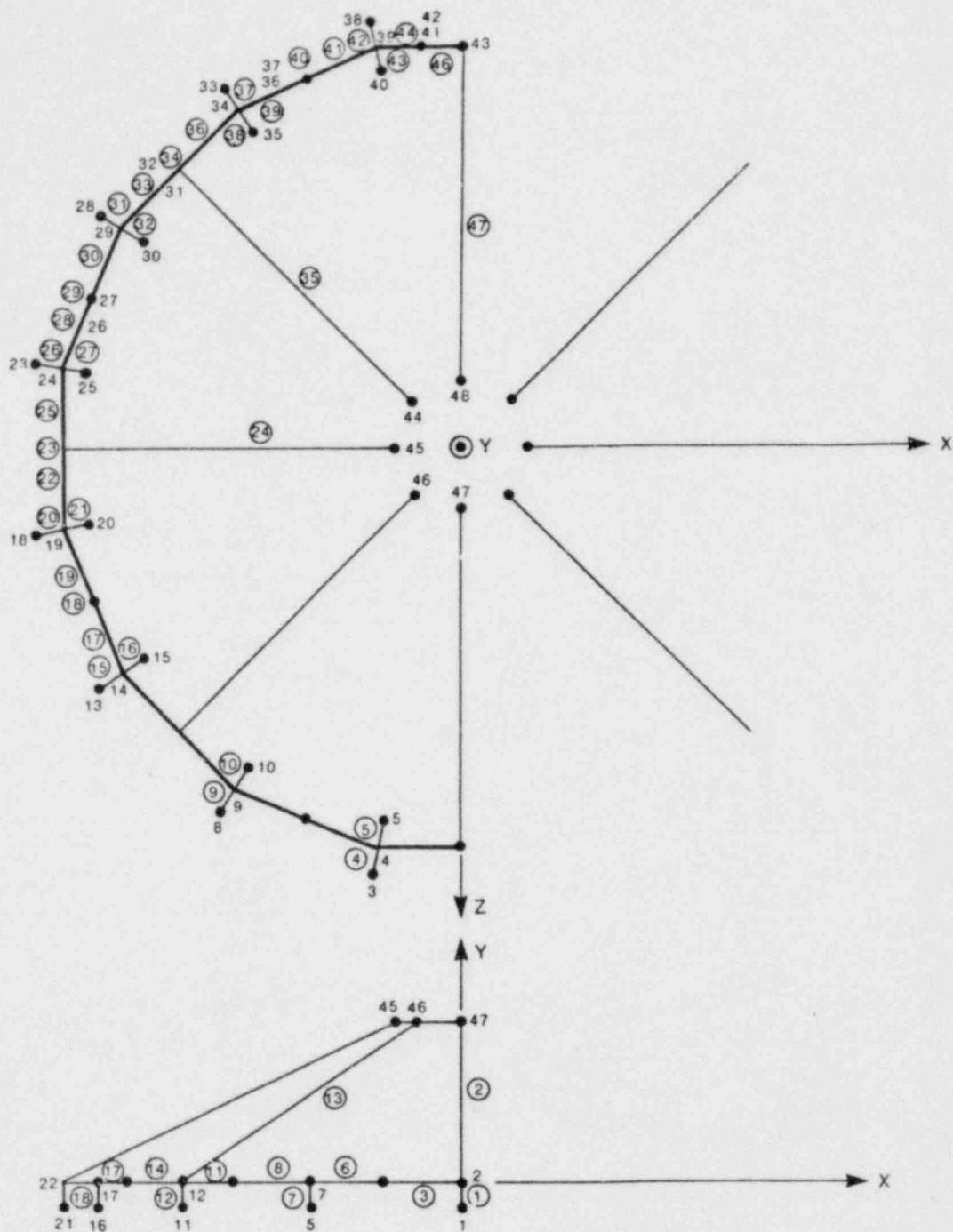


FIGURE 4.2  
180° VENT SYSTEM BEAM MODEL

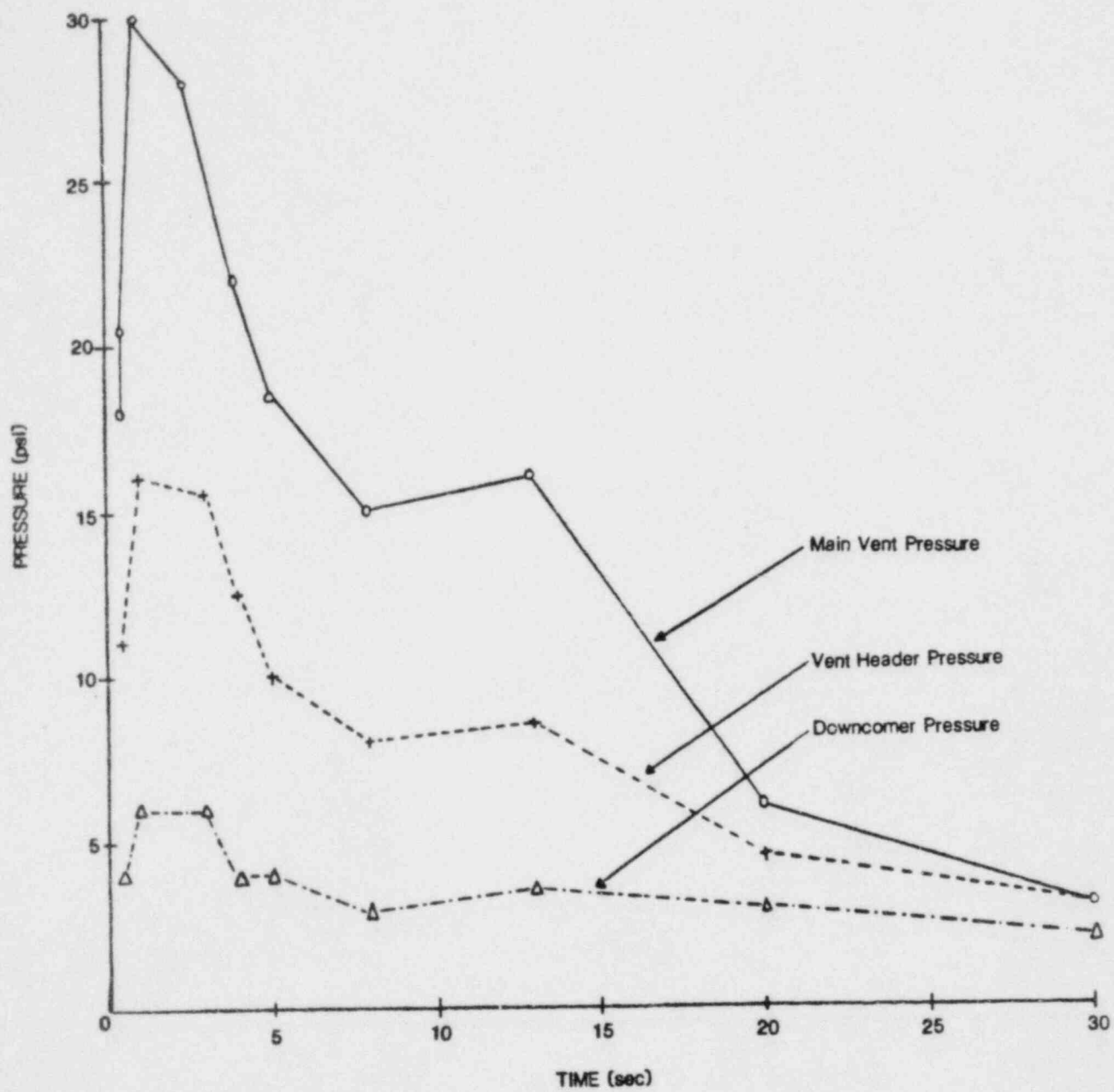


FIGURE 4.3  
VENT SYSTEM PRESSURIZATION FOLLOWING A DBA

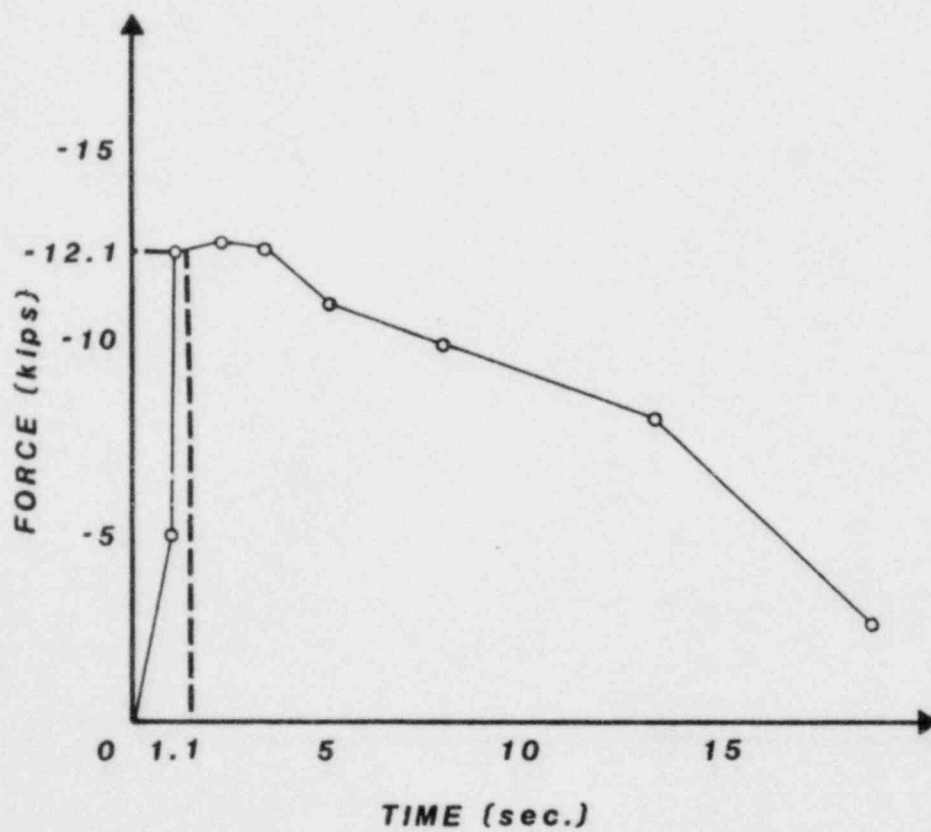
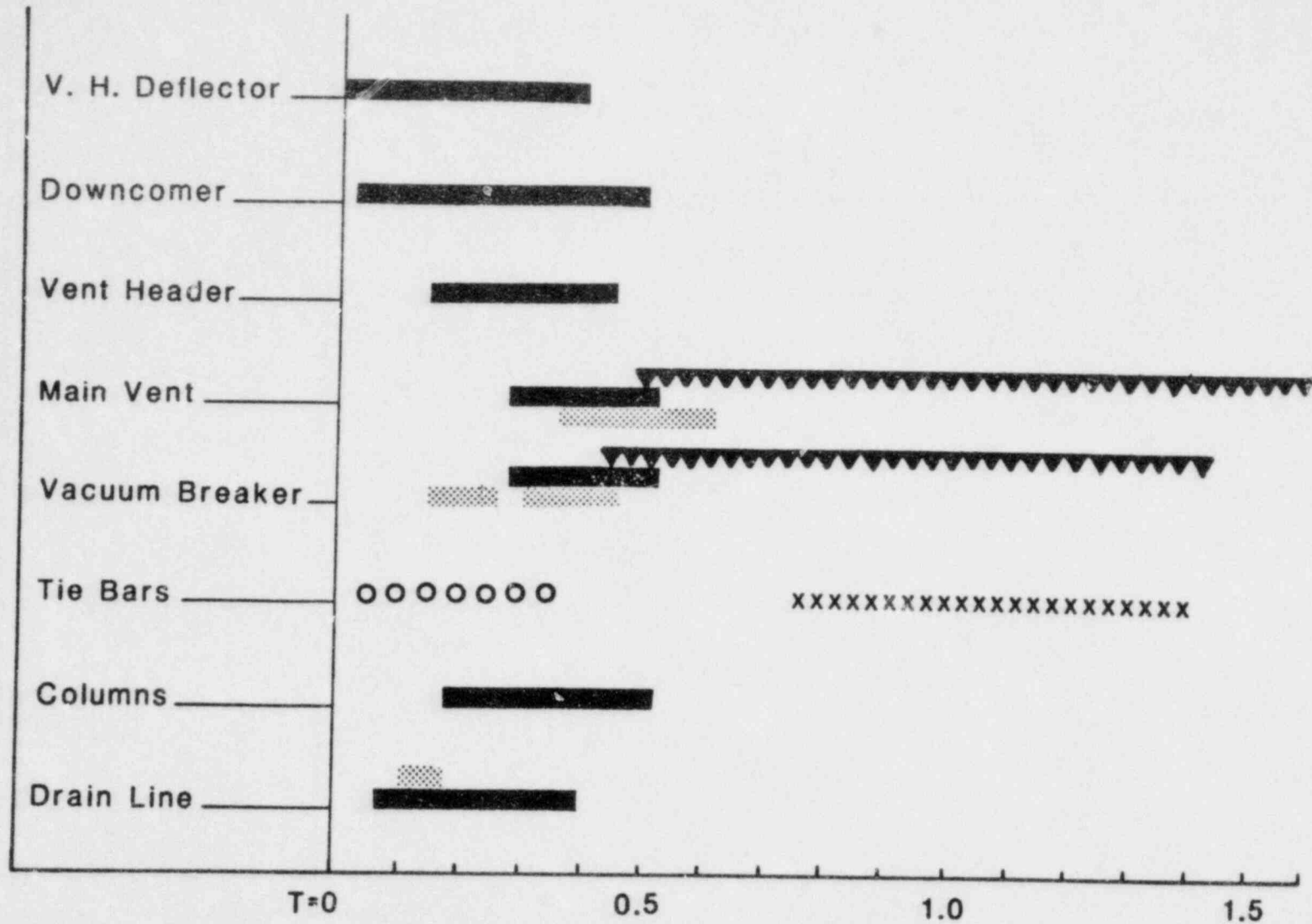


FIGURE 4.4

VERTICAL THRUST LOAD TRANSIENT ON  
MAIN VENT END CAP ( $\Delta P=0.0$ )





Note : Time T= 0 represents time at the beginning of the pool swell analysis.

Impact/Drag ■ Froth Imp'g't ▒ Froth Fallback ▼▼ Bubble Drag ○○ Pool Fallback xxx

FIGURE 4.5

SEQUENCE AND DURATION OF POOL SWELL LOAD

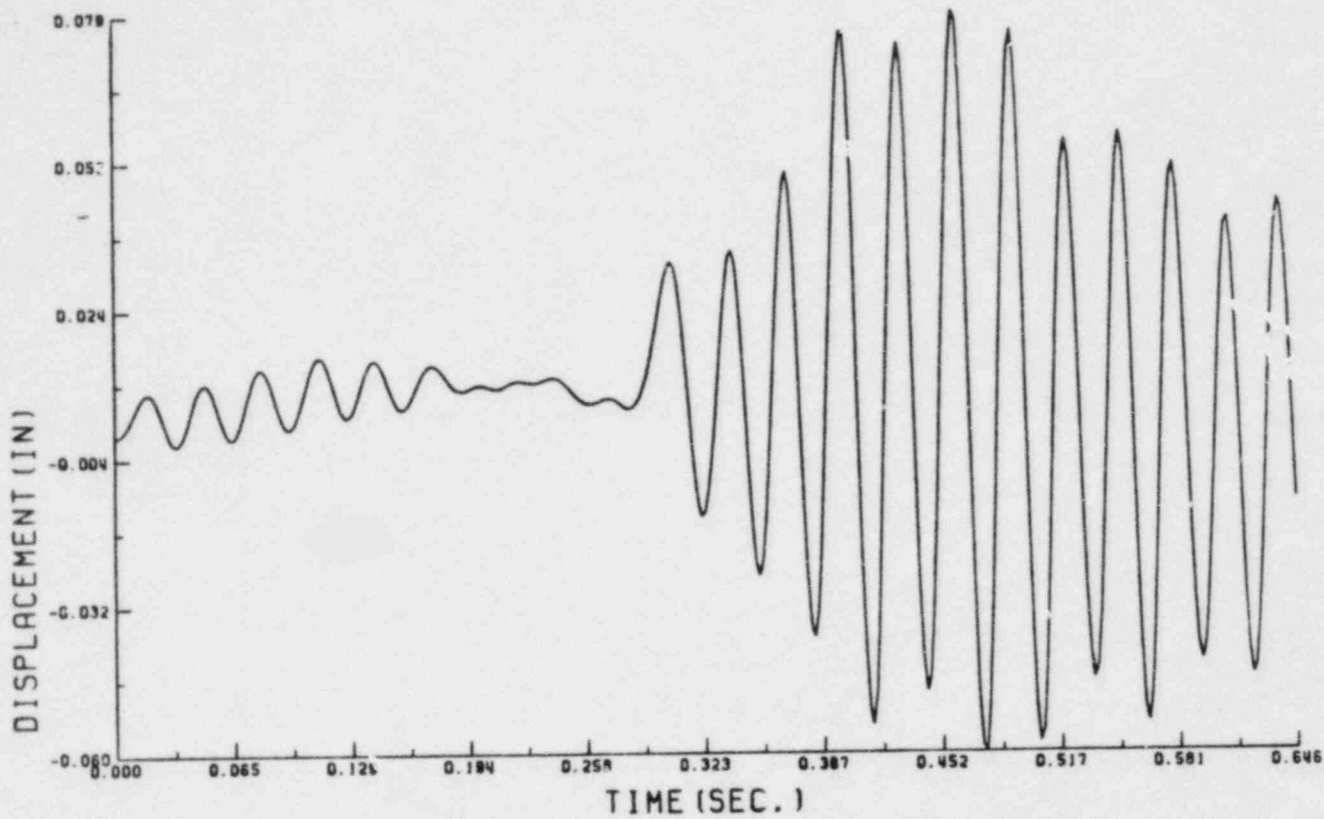


FIGURE 4.6

VERTICAL DISPLACEMENT TIME HISTORY AT  
MAIN VENT S/RVDL PENETRATION

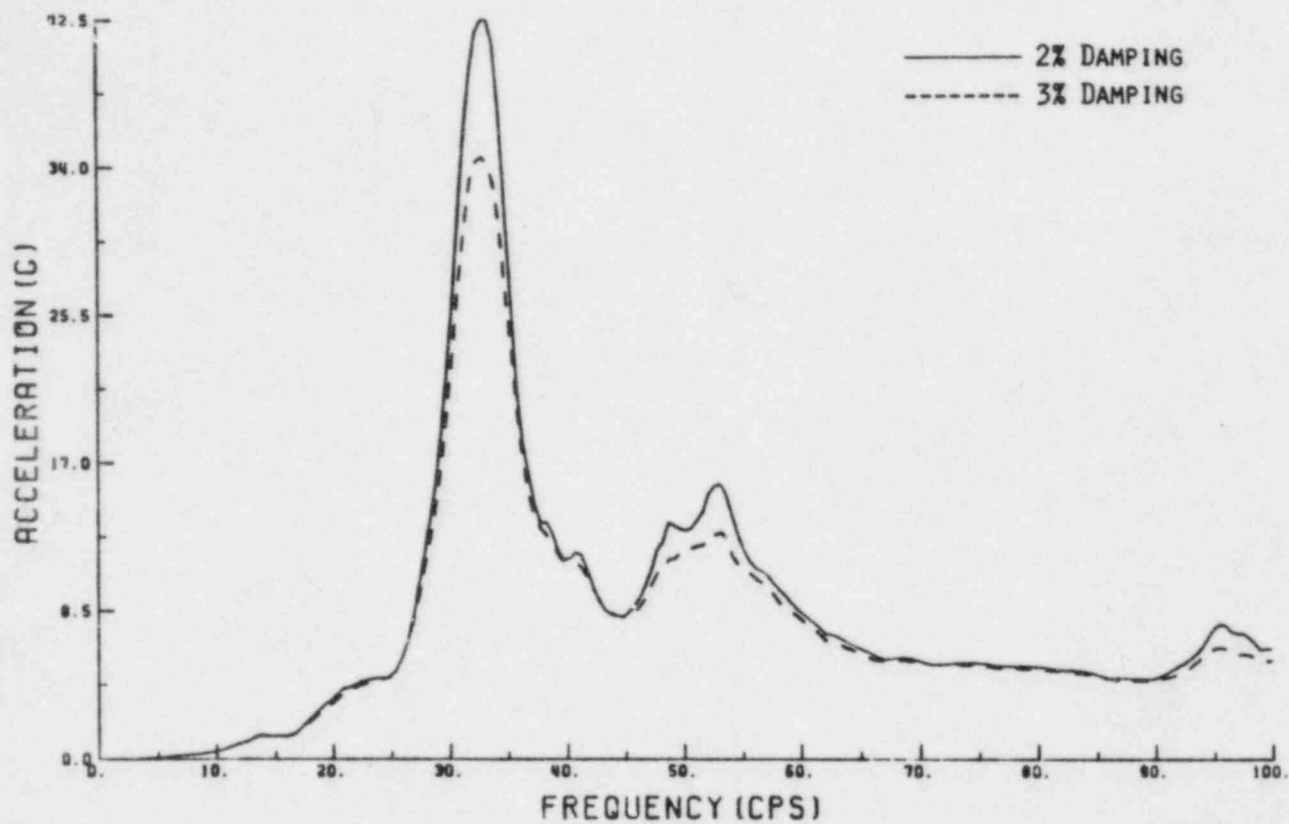
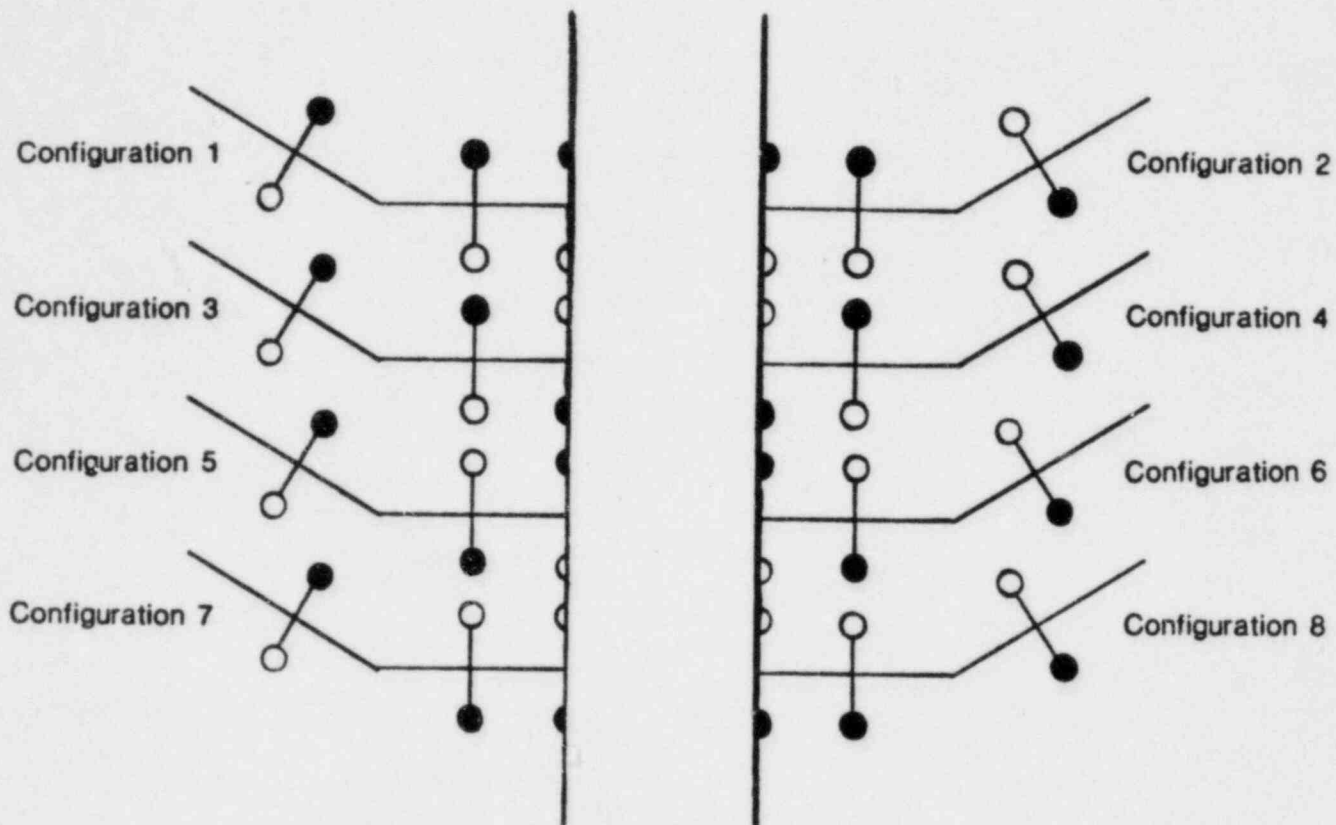


FIGURE 4.7  
VERTICAL ACCELERATION RESPONSE SPECTRUM  
AT THE VACUUM BREAKER PENETRATION



#### NOTES

Black circle indicates the downcomer with the higher pressure differential.  
Configuration 7 used in analysis.

FIGURE 4.8  
POSSIBLE CONFIGURATIONS OF DOWNCOMER PRESSURE DIFFERENTIAL  
FOR CONDENSATION OSCILLATION DOWNCOMER LATERAL LOAD

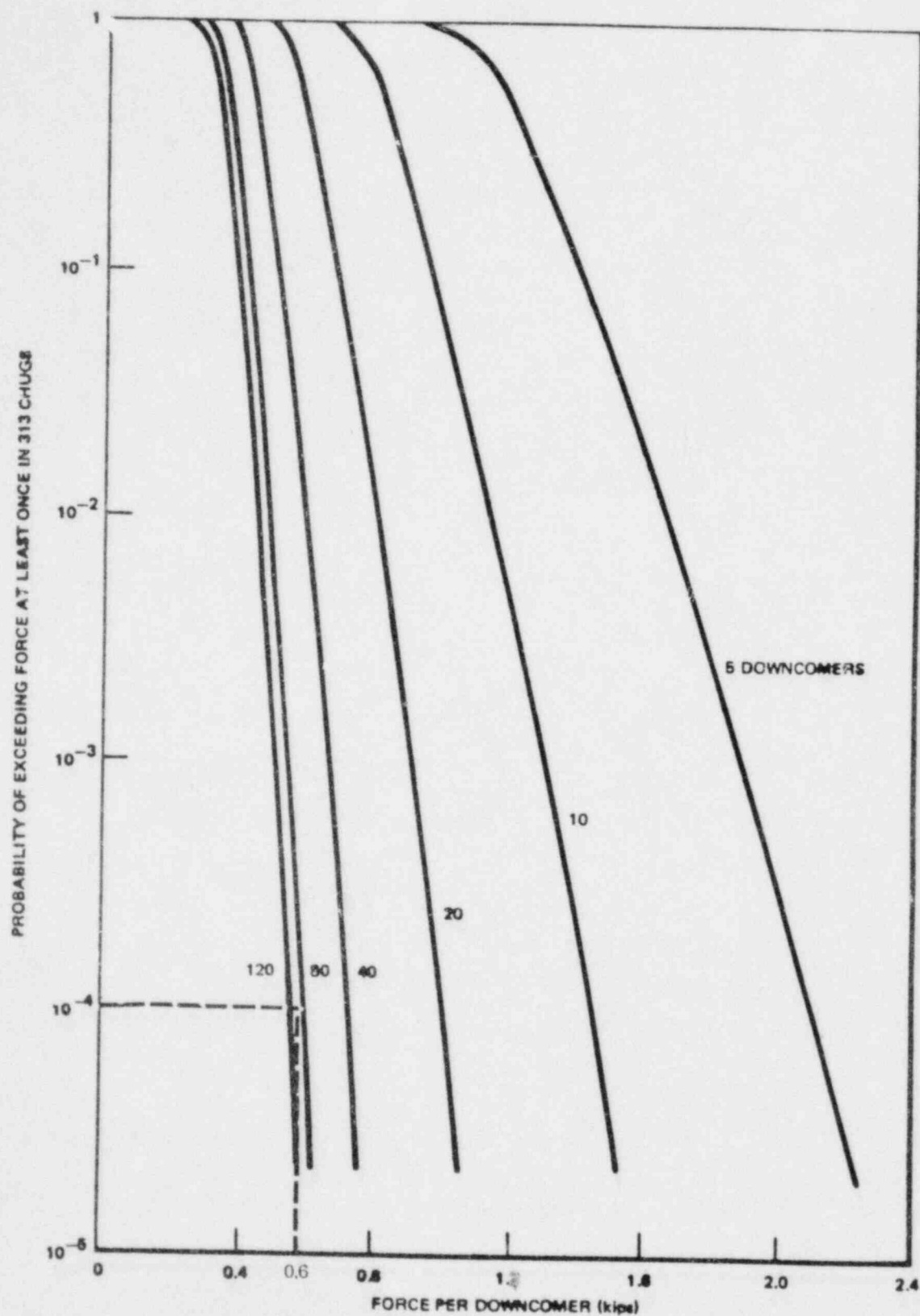
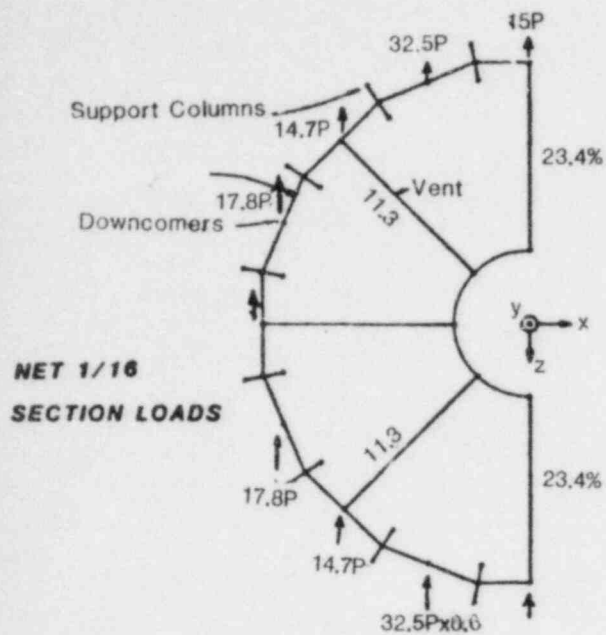
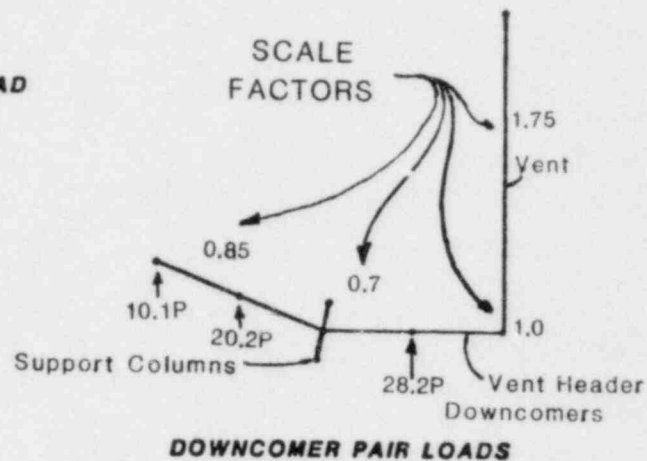


FIGURE 4.9  
CHUG SYNCHRONIZATION LOADS

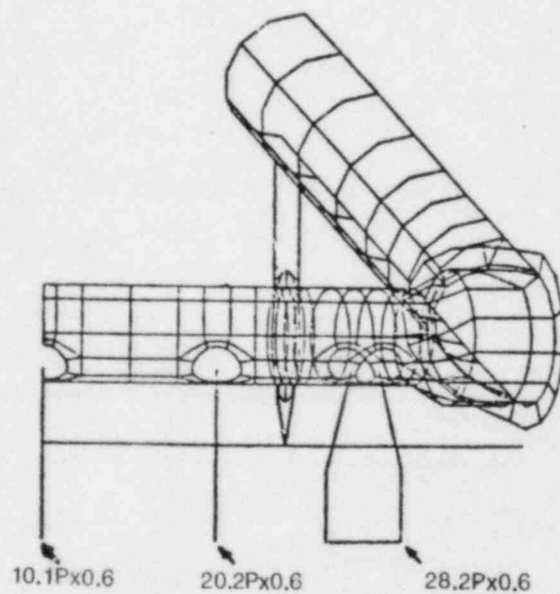


(a)  
180° BEAM MODEL

**% OF TOTAL LOAD  
CARRIED BY  
MAIN VENT**



(b)  
1/16<sup>TH</sup> BEAM MODEL



(c)  
1/16<sup>TH</sup> SHELL MODEL

FIGURE 4.10

DEVELOPMENT OF SCALE FACTORS CHUG SYNCHRONIZATION LOAD



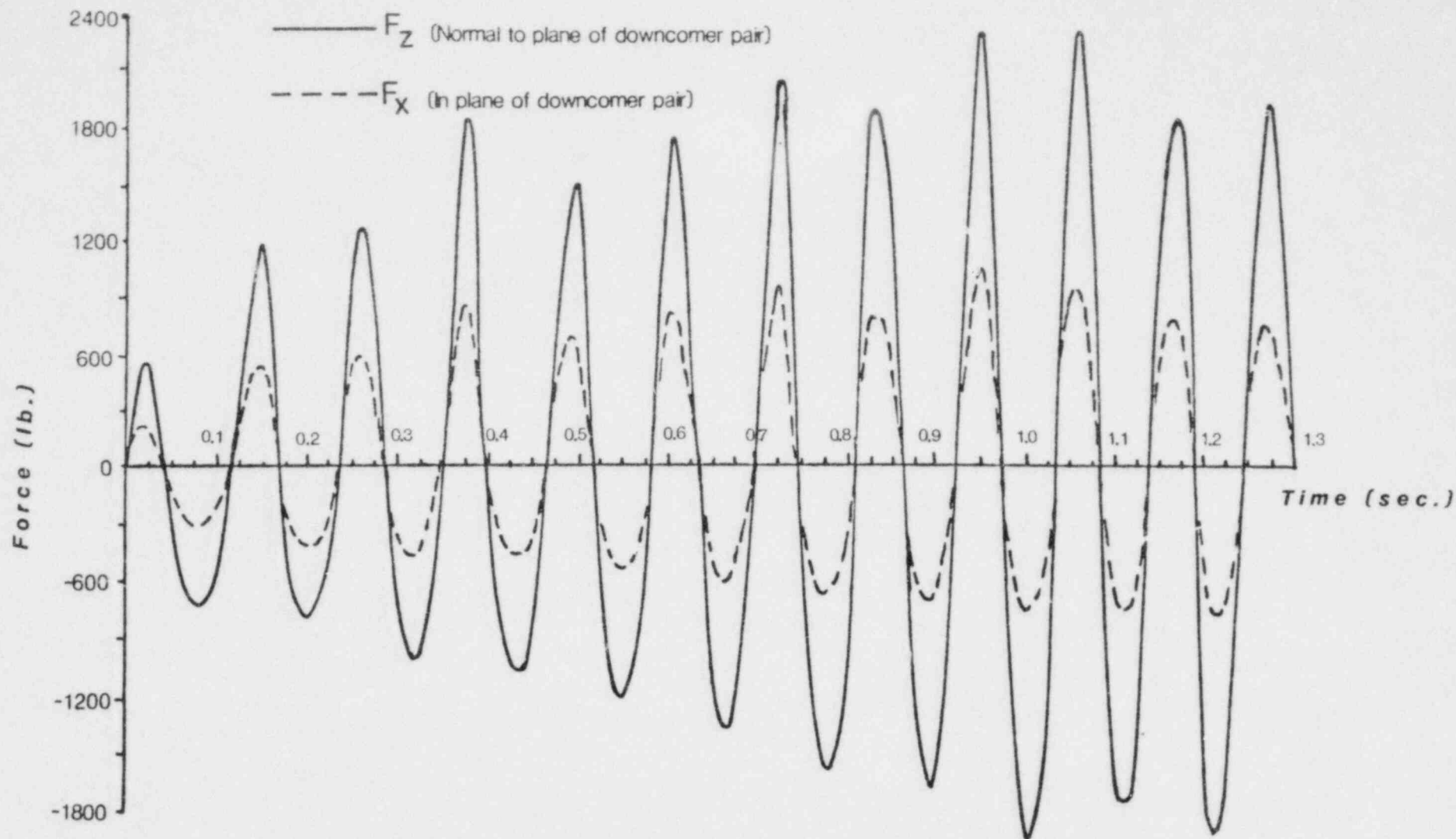


FIGURE 4.11

TYPICAL S/RV DISCHARGE DRAG LOAD TRANSIENT  
FOR SUBMERGED DOWNCOMER SEGMENT

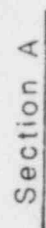
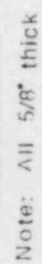


FIGURE 4.12

DOWNCOMER/VENT HEADER GUSSET REINFORCEMENT DESIGN

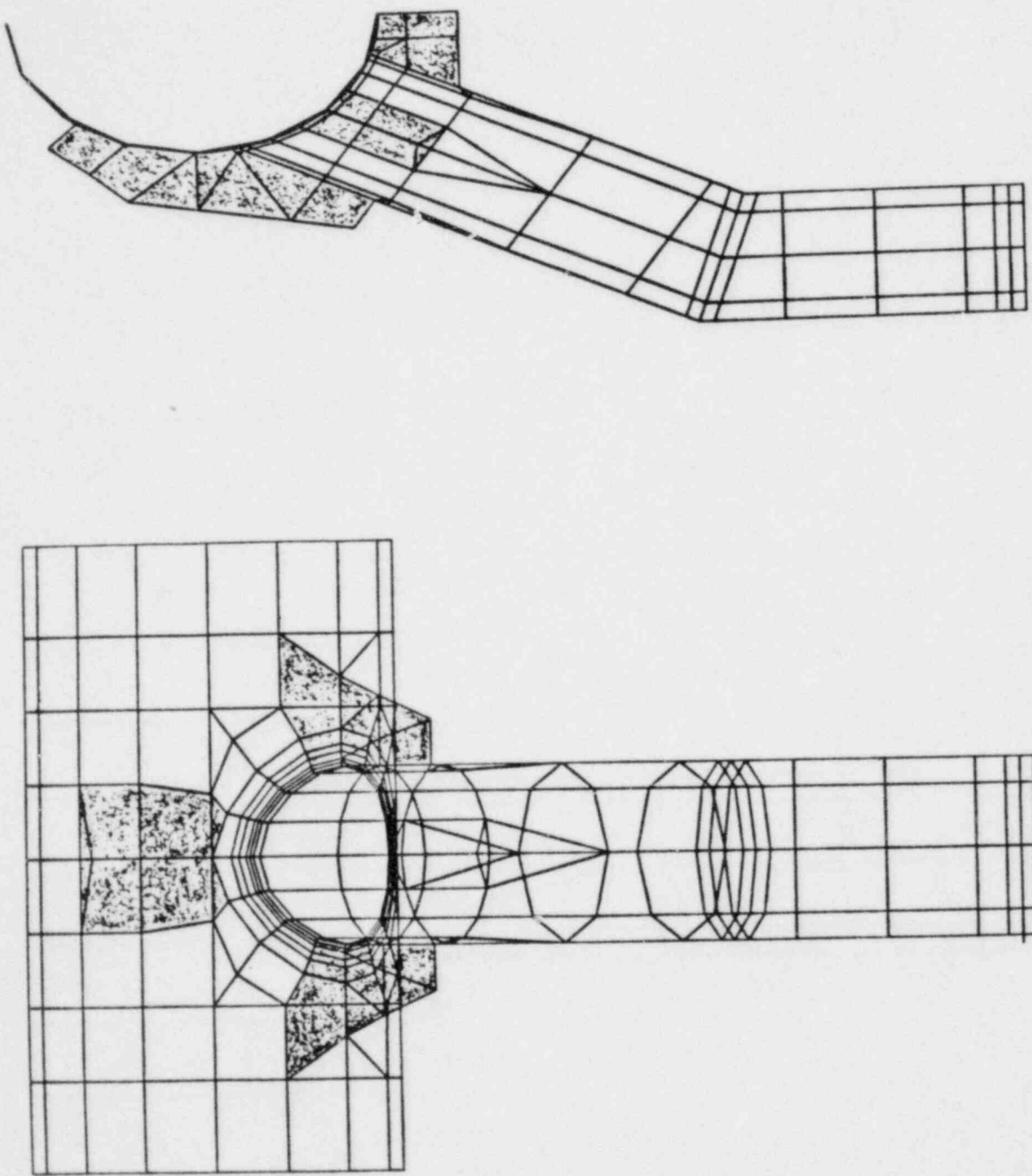


FIGURE 4.13  
DETAILED DOWNCOMER/VENT HEADER INTERSECTION MODEL  
INCLUDING GUSSET PLATE STIFFENERS

COOPER NUCLEAR STATION

PLANT UNIQUE ANALYSIS REPORT

SECTION 5

S/RV DISCHARGE PIPING

## 5.1 INTRODUCTION

This section describes the results of the evaluations performed on the CNS Safety/Relief Valve Discharge (S/RVD) piping and associated support structures. Components include the S/RV piping in both the drywell and the wetwell, piping supports on the lines, and the vacuum breakers on the drywell portion of the S/RVDL.

Descriptions of these components and their modifications are provided in Section 1 of this report. The thermal-hydraulic load definitions and load combinations are described in Section 2. For each component associated with the S/RVD piping, this section provides a description of design load combinations, design allowables, analysis methods and results, and the Code evaluation.

## 5.2 DRYWELL S/RVD PIPING

Eight S/RVs are located on the main steam lines (MSL) which discharge into the suppression pool. For each of these eight valves, a separate piping system leads from the valve, through the drywell into the main vent, and finally through the main vent into the suppression pool where the discharge device is located. Within the drywell and main vent, each of the eight S/RVDLs has a unique routing and support configuration. This section describes the evaluations of the drywell portion of the S/RVDLs; i.e., the portion of the line from the S/RV up to the main vent penetration. The remaining portion of the S/RVDL in the wetwell is discussed in Subsection 5.3.

### 5.2.1 Design Load Combinations

Table 5.1 shows the 27 design load combinations for the drywell S/RVD piping. This table is taken directly from the Mark I Structural Acceptance Criteria PUAAG (Reference 19). Service limit assignments for each event combination are also indicated in the table.

The drywell portions of the S/RVDs do not experience any direct hydrodynamic loads during a LOCA. These loads are applied indirectly through the motion of the main vent penetration. Therefore, the bounding load combinations for performing the Code evaluation on the S/RVD piping and supports in the drywell can be reduced to those shown in Table 5.2.

#### 5.2.2 Design Allowables

The S/RVD piping is classified as an essential Class 3 piping system. Design allowables are taken from Subsection ND-3600 of the ASME Boiler and Pressure Vessel Code. Similarly, all drywell piping supports are classified as Class 3 piping supports and design allowables are taken from Subsection NF-3400 of the Code.

##### 5.2.2.1 Piping Stress Allowables

The allowable stresses,  $S_h$  and  $S_c$ , for the materials used in the S/RV discharge piping were obtained from the Code, Section III, Appendix I. The stress allowables for applicable load categories and Service Limits were determined in accordance with equations 8 through 11 in Subarticle NC-3650 of the Code, and are summarized in Table 5.3 for the S/RV discharge piping at design temperature.

Those load combinations in Table 5.1 for which footnotes 3 and 4 in the Structural Acceptance Criteria (Reference 19) apply were assigned allowable stresses associated with Level C Service Limits and Level D Service Limits, respectively. The PUAAG permits allowable stresses to be increased in this manner from the values for Level B Service Limits, provided all other fatigue and operability criteria are met.

##### 5.2.2.2 Support Allowables

The allowables for the drywell S/RVD piping supports are consistent



with the PUAAG. The basic approach was to use ASME Section III, Subsection NF and Appendix XVII for all new supports and for all new parts of modified supports. Existing supports and existing members of modified supports were similarly evaluated, except that for emergency and faulted conditions (Levels C and D) only a 33% increase in normal and upset condition allowables was used. In addition to the above, and consistent with the allowance for neglecting the effects of newly defined loads which produce stresses less than 10 percent of the allowable value, a general increase of 10 percent was utilized for evaluating structural elements using original loads and those defined by the LDR.

For drywell pipe supports which are attached directly to the drywell liner, local stress intensities in the liner due to support reactions are determined using the procedure in Subsection NE-3215 of the Code. The drywell liner is classified as a Class MC component. Local stress intensities due to support reactions are considered as primary local stresses for the membrane stress intensity and secondary stresses for the surface stress intensity (as described in Code Subsection NE-3213). Allowable stresses for the combined general plus local drywell stress intensities are determined from Subsection NE-3221 of the Code.

### 5.2.3 Analysis Methods and Results

#### 5.2.3.1 S/RVD Piping Models

A separate piping model was developed for each of the eight S/RVDs in the drywell. The models extended from the MSL nozzle to the main vent penetration. The S/RV and the two 10-inch diameter vacuum breakers on each line were included in the models. Equivalent stiffnesses were provided at the main vent and MSL connections to simulate the flexibility of these points.

The piping analysis program SUPERPIPE was used to develop these models (Appendix B provides a description of SUPERPIPE). Figure 5.1 shows a representative piping model of one of the drywell lines.

#### 5.2.3.2 Piping Analysis Procedures and Results

The analyses described in this subsection were used in the qualification of the S/RVD piping and in determining support reactions and valve accelerations. All analyses were performed using the piping models discussed above. A complete set of analyses was performed for each S/RVDL configuration. All piping mode shapes up to 60 Hz were included in the dynamic analyses.

##### 5.2.3.2.1 S/RVD Thrust Loads

The pressure transient following the opening of an S/RV results in significant transient thrust loading on the S/RVD piping. A description of this transient and the development of the thrust loading on the piping is presented in Subsection 2.5.1.

The bounding S/RVD thrust load case for the drywell portion of the S/RVD piping was determined to be case A1.2 (first actuation during an IBA/SBA) based on a study comparing peak thrust forces for the longest S/RVDL for all S/RV load cases. This load case was used for detailed thrust load analyses of each of the eight S/RVDLs upstream of the main vent penetration.

For application to the S/RV discharge piping models, the transient thrust forces were defined for each of the eight S/RVDLs in the form of time-histories with total durations ranging from 0.3 to 0.5 seconds. Force time-histories were defined for each straight pipe segment between elbows and for each segment of curved pipe (excluding elbows).

The analyses were performed with SUPERPIPE using a direct integration method with an integration time step of 0.001 seconds and a total duration of 0.5 seconds. The thrust forces were applied to the model along the pipe axis at the mid-point of each segment for which the forces were defined.

The structural damping of the piping model was selected as 1% of critical, as recommended in NRC Regulatory Guide 1.61 (Reference 37). In the direct integration method, the damping matrix is defined as a linear combination of the stiffness and mass matrices of the system.

The results from the S/RVD thrust load analyses indicated that this load case was the dominating load case in terms of pipe stresses and boundary reactions for the S/RVDs upstream of the main vent penetration. A summary of the maximum pipe stresses resulting from S/RVD thrust loads for the eight S/RVDs is provided in Table 5.4.

#### 5.2.3.2.2 Vent System Motion

The S/RVDs upstream of the main vent penetration are not exposed to any direct loading from the hydrodynamic phenomena in the suppression pool. However, the S/RVDs are subjected to these loads indirectly through the dynamic motion of the downcomers, vent header and the main vents. These loads are transmitted to the S/RVDs through their penetrations at the main vents.

The dynamic motions at the S/RVD penetrations due to suppression pool hydrodynamic loadings were developed in the form of response spectra for the two typical penetration locations along the main vent. Response spectra were developed with 2% damping for the pool swell, CO, and chugging events, and with 1% damping for the bounding S/RV discharge event. The piping analyses were performed for all eight lines using the multilevel response spectral analysis methodology with single point load application at the penetration.

The directional as well as the modal combination methods used were in agreement with the recommendations in USNRC Regulatory Guide 1.92 (Reference 38). The maximum displacements of the main vent at the S/RVDL penetrations due to dynamic motion and thermal expansion were accounted for in the piping evaluations in the form of static analyses with imposed displacements at the penetrations.

#### 5.2.3.2.3 Thermal Expansion Loads

The S/RVDLs were analyzed for the effects of thermal expansion using the design temperature of 495°F. As a comparison, it was noted that the maximum S/RVDL wall temperature as determined by the RVFOR04 analyses (Subsection 2.5.1) was 468°F.

The maximum main vent penetration movements due to thermal expansion of the vent system were imposed on the S/RVDLs as anchor movements in separate static load case analyses. The maximum thermal expansion movements of the MSL at the S/RVDL connection were imposed as anchor movements as an integral part of the thermal expansion analyses of the S/RVDLs. The possible permutations of hot/cold conditions between the vent system and the S/RVDLs were evaluated to determine the maximum ranges of load effects in terms of pipe stresses and boundary reactions.

#### 5.2.3.2.4 Other Operating Loads

The S/RVDLs were also analyzed for seismic, dead weight, and internal pressure loading in accordance with the original design criteria and the FSAR (Reference 16). The seismic analyses included response spectral analyses for the OBE and SSE events, as well as static analyses simulating the relative out-of-phase displacement effects between the main vent penetration, the main steam connection point, and the intermediate rigid supports and snubbers. The results from these analyses were combined with the vent system analysis results to serve as a basis for support design evaluation and to demonstrate Code compliance.

### 5.2.3.3 Drywell Piping Support Evaluation

Drywell S/RVD piping support evaluations included evaluation of the support structures, drywell framing, reactor pedestal, and the steel liner in the drywell for the design reactions from the piping analyses.

#### 5.2.3.3.1 Pipe Support Analyses

Support load combination summaries were generated from the individual piping load case analyses for Levels A, B, C, and D Service Limits as defined by Table 5.2.

The combined reactions at each pipe support (rigid supports, snubbers, spring hangers) were determined as ranges of minimum and maximum values for each of the service limits. The support reactions from the various dynamic load cases, including inertial as well as anchor movement effects, were combined separately as applicable for each of the service limits. These unsigned quantities were then added to (or subtracted from) the maximum (or minimum values) load ranges created by the combinations of sustained loading and thermal expansion load cases.

For load combinations containing more than one dynamic load case, the two dynamic load cases producing the maximum support reactions were combined using a modified SRSS method. Any additional load cases were added by absolute summation. The modified SRSS method consists of applying a multiplier of 1.1 to the straight SRSS combination. This approach is justified for the current application by a separate study described in Appendix D.

The pool swell load case bounded other LOCA-related load cases in terms of load effects on the S/RVDs as transmitted through the main vent penetration. The effects on the S/RVDs from the S/RV discharge loading on the vent system, which is felt by the S/RVD through the motion of the main vent penetration, were bounded by the direct S/RVD thrust loads. The significant thrust effects on



the S/RVDLs occur sufficiently early following an S/RV actuation and are of sufficiently short duration to justify their decoupling from the vent motion effects.

Support structures were analyzed as linear elastic frames subject to static equivalent design loads using both hand and computer methods. Also considered were significant friction loads resulting from these design loads and self-weight. Support structures subjected to multiple pipe loads were analyzed for bounding pipe load combinations. Standard support components were evaluated by simple load rating comparisons.

Support assemblies (structures and standard components) were also checked for serviceability and functionality requirements.

#### 5.2.3.3.2 Drywell Liner Analyses

Local drywell liner stresses were determined at all locations where drywell S/RVD pipe supports were attached directly to the liner. The procedure in WRC Bulletin No. 107 (Reference 33) was used for these evaluations. Reaction loads on the drywell liner were taken from the pipe support analysis results described in the preceding subsection.

#### 5.2.3.3.3 Drywell Steel Framing Analysis

The drywell framing consists of existing W24x100 primary beams arranged in a radial pattern. These beams are braced by lateral members of lighter shapes. The overall arrangement is a typical, conventional floor grid for equipment installation and maintenance activities. There are two levels of independent framing, identified as the upper level (at a nominal elevation of 921 feet 10 inches), and the lower level (at an elevation of 901 feet 3 inches). The end connections for the radial beams are conventional beam seat brackets. The connections of the lateral beams to the radial beams are generally two-to-four bolt, bearing-type connections.



The requalification of the drywell steel was necessary due to the S/RV discharge piping support reaction loads imposed on these beams. The analysis was performed by conventional stiffness methods of structural analysis, using the computer code STRUDL. Separate analyses were performed for the upper and the lower framing levels. For each floor, the entire basic grid configuration was included in the model for completeness. In order to predict a realistic state of stresses due to torsional loadings, a three-dimensional frame was specified.

The applied loads used for the analysis were based on the following sources:

- (1) Dead load and the equipment loads were considered as documented in the original design of the drywell steel. As specified in the original design, a vertical seismic coefficient of 0.091 for the operating basis earthquake and 0.173 for the safe shutdown earthquake was used in the analysis.
- (2) The new S/RV pipe support reaction loads consisted of 290 force components applied to the upper level of the drywell framing and 264 force components applied to the lower level. The reaction loads resulted from S/RV piping reanalysis and pipe support design of 89 new or modified supports installed on the eight S/RV discharge lines.

Two basic load cases corresponding to the normal/upset (Level A/B Service Limit) and the emergency/faulted (Level C/D Service Limit) conditions were considered. These cases were identified to bound the various generic loads that formed the basis for the design of the related pipe supports. The magnitude and the application of these loads were idealized to render a significantly conservative treatment. The analysis was performed with the concurrent application of all the snubber reactions associated with each individual S/RVDL. This resulted in a total of 16 load combinations, corresponding to two combinations for each of the eight lines.

The two load combinations used for the drywell framing are as follows:

(a)  $DL + EL + PLU + OBE$

(b)  $DL + EL + PLF + SSE$

Where:

DL = Dead Load

EL = Equipment Load

PLU = Pipe Support Reaction Loads, Level A/B Service Limits

PLF = Pipe Support Reaction Loads, Level C/D Service Limits

The basis for the above bounding load combinations is documented in the "Design Specification for Requalification of Drywell Steel" (Reference 39).

#### 5.2.4 Code Evaluation

This subsection describes the Code evaluation of the drywell portion of the eight S/RVDLs for the design load combinations summarized in Table 5.2.

##### 5.2.4.1 Safety/Relief Valve Back Pressure

In order to verify that the S/RV back pressure requirements are met, the following design criteria were applied:

- (a) Under nameplate flow (ASME-rated flow) and valve inlet pressure at 103% of spring set pressure, the steady-state pipe internal pressure must be below 40% of S/RV inlet pressure, and

- (b) For 122.5% of nameplate flow and valve pressure at 103% of spring set pressure, the maximum pipe pressure must be below 550 psig.

Upon review of the S/RVDL internal pressure transients (Subsection 2.5.1), it was determined that these criteria were satisfied for all S/RVD line-clearing transients.

#### 5.2.4.2 S/RVD Piping

Maximum pipe stresses for the eight S/RVD lines upstream of the main vent penetrations were combined from the individual load case results as described by Table 5.2. The combination methods used were consistent with those used for support reactions as described in Subsection 5.2.3.3.1, with the exception that the thermal expansion and imposed displacement effects were considered separate from the primary stresses in Code equations 10 and 11.

The combined maximum stresses were checked against allowables (pipe stress allowables are defined in Subsection 5.2.2.1) in accordance with stress equations 8 through 11 in Subarticle NC-3650 of the Code. All eight S/RVD lines, including connections to the main steam lines, satisfied all applicable stress requirements of the Code as shown in Table 5.5.

#### 5.2.4.3 Drywell Pipe Supports

All drywell S/RVD piping supports (structural members, connections, component standard hardware) were qualified to the design criteria of the Mark I Structural Acceptance Criteria (PUAAG).

#### 5.2.4.4 Drywell Liner

Local drywell liner stress intensities at drywell S/RVDL pipe support attachments were added absolutely to the maximum general stress intensities for the drywell shell. These general stress intensities were taken from the original stress report for the drywell. The combined general plus local stress intensities were then compared to Code allowables (Subsection 5.2.2.2). The Code evaluation indicated that the drywell liner was qualified at all S/RVD pipe support attachments points.

#### 5.2.4.5 Drywell Steel Framing

The original design and construction of the drywell framing was based on criteria specified in the AISC Manual of Steel Construction, 6th Edition (Reference 15). Requalification of the drywell framing was based on criteria contained in the AISC Manual of Steel Construction, 7th Edition, including Specification Supplements. These design criteria are judged to be equal to or more restrictive than the criteria applied to initial design and construction.

The drywell framing analysis results were evaluated to AISC Code criteria. However, it is recognized that the AISC Code does not consider torsional stresses in a rigorous manner. Also, most public domain computer programs having AISC Code checking capability ignore the contribution of torsional effects. This limitation was eliminated by using the STRUDL computer program with Code checking in conformance with Appendix XVII of the ASME Code, Section III. The program also accounts for pure and warping stresses due to applied torsional loads. Since Appendix XVII requirements are essentially identical to the AISC Code, its use was considered appropriate for a more realistic analysis. Accordingly, the members were checked to AISC Code, but using the ASME Code Appendix XVII for the purpose of Code qualification. The ASME Code limits the allowable compressive stress to  $2/3$  of

the critical buckling stress for Level C/D Service Limits. The allowable tensile stress is specified as high as 1.88 times the yield stress, however these allowable stresses for Level C/D Service were modified by substituting limits with a value of 1.33 times the Level A/B Service Limits. This approach restricts the allowable stresses to approximately 0.9 times the yield stress of the material, which is consistent with the original design margins intended for extreme loading conditions. In essence, the above modification of ASME allowables provides a Code check per the AISC Code.

The calculated stresses were compared with the allowable stresses and combined interaction ratios conforming to Sections 1.5 through 1.9 of the AISC Code. A summary of the final interaction ratios incorporating minor framing modifications is presented in Table 5.6. The table includes the maximum interaction ratio of the most severely loaded members of the upper and lower framing levels for each of the eight S/KV lines. All members were in compliance with Code requirements.

Connections were evaluated for their load capacity in comparison with the applicable support reactions. The evaluation results indicate that the stresses in the various components of the connections, including welds, are within the allowable values.

### 5.3 WETWELL S/RVD PIPING

From the main vent penetration into the wetwell, there are two distinct piping and support configurations for the S/RVDLs. Four of the eight lines discharge in the vent bay where they enter the wetwell. This configuration is referred to as the short line or S/RVDL A. The remaining four S/RVDLs are routed to the adjacent vent bays. This configuration is referred to as the long line, or S/RVDL B. This subsection describes the evaluations of the above mentioned components including the piping, T-quencher discharge device, and associated supports.

### 5.3.1 Design Load Combinations

The 27 design load combinations and service level assignments for the wetwell S/RVD piping are shown in Table 5.1.

The wetwell portion of the S/RVDs are subjected to direct application of hydrodynamic loads during a LOCA or S/RV discharge, as well as S/RVD line-clearing transients. Table 5.7 indicates the bounding load combinations for the wetwell lines and supports. Some of the events in these load combinations (e.g. pool swell impact loading) are only applicable to the evaluation of S/RVD B, since the short line is not subjected to these loads.

### 5.3.2 Design Allowables

The wetwell portion of the S/RVD is classified as essential Class 3 piping, similar to the drywell portion of the lines. Therefore, subsections ND-3600 and NF-3400 are applicable for obtaining design allowables for the piping and supports, respectively.

#### 5.3.2.1 Piping Stress Allowables

The major portion of the S/RVD wetwell lines consist of SA-106 Grade B material, i.e., the same as for the drywell portions of the lines. The allowable stresses defined in Subsection 5.2.2.1 and Table 5.3 for SA-106 Grade B are applicable to the wetwell piping from the vent penetration to the reducer at the discharge device. The reducer consists of SA-234 WPB material with allowables as listed in Table 5.3.

#### 5.3.2.2 Support Allowables

The allowables for the wetwell S/RVD piping supports are consistent with the Mark I Structural Acceptance Criteria (PUAAG) and are based on the requirements of ASME Section III, Subsection NF and Appendix XVII.



#### 5.3.2.3 Fatigue Considerations

The wetwell portion of the S/RVDL is a Class 3 piping system; therefore, evaluation for cyclic loading is required only for thermal cycling. However, the NRC has required additional confirmation of the adequacy of this piping system for mechanical cyclic loads (Reference 40). This confirmation is being provided by the Mark I Owners Group through a generic program which will still be unresolved at the time this report is submitted. Therefore, these fatigue considerations are not addressed in the evaluations of the wetwell S/RVD piping. Fatigue due to thermal cycling was addressed as required by the Code. Should additional fatigue evaluations be required on a plant unique basis in the future, a separate submittal for CNS would be prepared.

#### 5.3.3 Analysis Methods and Results

This subsection describes the analyses of the wetwell S/RVD piping and supports.

##### 5.3.3.1 S/RVD Piping Models

A separate piping model was developed for each of the two wetwell S/RVDL configurations. The models extend from the main vent penetration to the discharge device, and include the T-quencher, T-quencher support assembly, and the 16-inch diameter support pipe (on S/RVDL B only). Equivalent stiffnesses were provided at the main vent and ring girder attachment points to simulate the flexibility of those points. The added mass effect of the suppression pool was included along the submerged length of the piping and the submerged supports, using the procedure in Reference 41. Since the peak loads in the S/RVD line-clearing transient occur after the water leg has cleared the line, the S/RVDL was modeled as empty of water during the transient. For other design load cases, the S/RVDL was modeled with water in the line up to the suppression pool high water level.

The piping analysis program SUPERPIPE was used to develop these models. Figure 5.2 shows the piping models used in the evaluation of these lines.

#### 5.3.3.2 Piping Analysis Procedures and Results

The analyses described in this subsection were used in the qualification of the wetwell S/RVD piping and supports. These analyses were also used to determine support reactions and design moments on the ramshead component of the quencher. All analyses were performed using the piping models described above. In the dynamic analyses, all modes up to 60 Hz were considered.

##### 5.3.3.2.1 S/RVD Thrust and Water-Clearing Loads

The loads addressed in this subsection are those which occur during the initial phases of the S/RV discharge transient, namely in-line pressure wave and water thrust loads, uneven water and air clearing thrust loads on the T-quencher arms, and T-quencher water jet-induced drag loads. The development of these loads is described in Subsection 2.5.1.

The in-line pressure wave thrust loads acting on the wetwell piping upstream of the initial water level in the pipe are similar to those acting on the drywell portions of the lines as described in Subsection 5.2.3.2.1. For the line segments downstream of the initial water level in the line, the significant transient loads are in the form of water thrust loads caused by the initial expulsion of the water slug in the pipe. Direct integration force time-history analyses were performed for the two S/RVDL wetwell configurations. Simultaneous pressure wave thrust forces in the air space portions of the line and water thrust forces in the submerged portions were considered. The transient thrust force analyses were performed in timesteps of 0.001 seconds for a duration of 0.25 seconds which ensured the inclusion of peak piping responses prior to termination. The structural damping was

selected to be 1% of critical (consistent with the drywell line analyses and NRC Regulatory Guide 1.61). The bounding load case used in the analysis was case A1.2 (first actuation during IBA/SBA).

The uneven air clearing loads on the T-quencher arms were bounded by the uneven water clearing loads. Two potentially bounding water clearing load cases were evaluated for each S/RVDL configuration. In one case the horizontal unbalanced forces perpendicular to the T-quencher arms were applied in the same direction to maximize the net force reactions. In the second case the same forces were applied in opposite directions for the two T-quencher arms to maximize the moment about the ramshead. In both cases the maximum net unbalanced force along the T-quencher arms was also included. The results from the two cases were then enveloped to serve as a basis for component qualification. These analyses were based on the S/RV Discharge Load Case C3.1 with stabilized water level. The analyses were performed as direct integration time-history analyses with a time step of 0.002 seconds and a duration of 0.4 seconds. The damping ratio used was 1% of critical.

The S/RVD piping is not subjected to any T-quencher water jet-induced drag loading. A portion of the 16-inch support pipe, which provides support for the lower portion of S/RVDL B, is subjected to T-quencher water jet loads. These loads were considered separately in the support evaluation.

#### 5.3.3.2.2 Pool Swell-Related Loads

Pool swell-related loads include pool swell impact, drag, and fallback loads for portions of the S/RVDLs located above the suppression pool. Also included are drag loads on the submerged portion of the S/RVDL induced by LOCA water jets or LOCA air bubbles. The source and definition of these loads are described in Subsection 2.4.3.

The airspace portion of S/RVDL A is oriented vertically and is therefore not subjected to pool swell impact, drag, fallback, or froth impingement loads. The routing of S/RVDL B includes horizontal piping which is exposed to pool swell impact, drag and fallback loads. The fallback loads were bounded by the impact and drag loads. S/RVDL B was analyzed for the impact and load drags in a direct integration force time-history analysis. The analysis was performed for the most severe impact case of  $\Delta p = 0$  in time steps of 0.0005 sec for a duration of 0.15 sec. The duration selected was sufficient to ensure that the peak response of the piping was included prior to termination. A damping ratio of 2% of critical was specified.

The induced drag loads due to LOCA water jet and LOCA air bubbles were applied as static equivalent loads on the submerged portions of both line configurations. Loads on submerged pipe support components were also included. Dynamic load factors (DLF) were determined for the water jet loads based on the piping response frequencies and the load rise time. The DLFs for the LOCA air bubble-induced drag loads were conservatively chosen as 2.0.

Certain key pipe stress results from the load case analyses discussed in this subsection are included in the S/RVD wetwell piping stress summary in Table 5.8.

#### 5.3.3.2.3 CO and Chugging Drag Loads

The loads addressed in this subsection are the oscillatory drag loads, including fluid structure interaction (FSI) and interference effects, on the submerged portions of the S/RVD piping during the CO and chugging phases of a LOCA. The development of these loads is addressed in Subsections 2.4.4.4 and 2.4.5.4.

As discussed in Subsection 2.4.4.4, two conditions were considered for CO drag loads, average and maximum source strength. S/RVD piping analysis results for each condition were enveloped for use

in the Code evaluations for CO loads. Similarly, the two post-chug load cases described in Subsection 2.4.5.4 were used to analyze the piping. Again, analysis results were enveloped for use in the Code evaluations for chugging loads.

The CO and chugging drag loadings for each case were defined in the frequency domain as force intensities for 50 load harmonics equally spaced in 1 Hz bands between 0 and 50 Hz. Assuming steady state response, DLFs were calculated for each load harmonic and for each piping response frequency. The DLF was maximized within each 1 Hz band which included a piping response frequency, by adjusting the load harmonic to produce perfect resonance with the piping mode. The damping ratio used was 2% of critical (consistent with Regulatory Guide 1.61). The DLFs provide a basis for determining the contribution from each load harmonic to the response of each piping mode of vibration. The combination of contributions from each of the 50 load harmonics results in a static equivalent force vector for each piping response mode considered. This force vector then consists of static equivalent inertia forces at the locations of masses in the piping model. The method used for combining the contributions from different load harmonics for the S/RVD piping corresponds to that used for the torus shell evaluation as described in Subsections 3.2.3.2.4 and 3.2.3.2.5. The random phasing technique for combining the contributions from the CO load harmonics was also used in the S/RVDL evaluations. Chugging load harmonics were combined using absolute summation.

The equivalent static load vectors were applied to the piping models as individual static load cases corresponding to each of the piping modes of vibration up to 50 Hz. The results from these static analyses were then combined according to the 10% grouping method for modal contributions as defined in USNRC Regulatory Guide 1.92.

Key stress results from the CO and chugging drag load analyses are included in the S/RVD wetwell piping stress summary in Table 5.8.



#### 5.3.3.2.4 T-Quencher Air Bubble Drag Loads

All submerged portions of the S/RVD piping and supports are subjected to standard and acceleration drag loads caused by the oscillations of the air-vapor bubbles expelled from the T-quenchers following an S/RV actuation. The source and development of these drag loads for application to the submerged S/RVD piping and supports are described in Subsection 2.5.5.3.

The drag loads applied to the piping models correspond to a single valve actuation during an SBA (Load Case A1.2). The submerged structure drag loads produced by this case bound those produced by any other load case. The two lines were evaluated for the drag loads caused by five different air bubble configurations, each of which was developed to maximize a particular load effect on the piping system. The results from these five analyses were then enveloped for each line to produce conservative results representing the T-quencher air bubble drag load case.

The analyses were performed with equivalent static loads representing the oscillating drag loads. The equivalent static loads were determined from the peak oscillating loads on individual pipe segments through the use of DLFs. The oscillating, driving frequency of the bubbles was conservatively selected from the possible range of 5.0 to 15.4 Hz, such that the driving frequency maximizes the DLFs. Structural damping corresponding to 2% of critical was used in these analyses.

Typical stress results from the T-quencher air bubble drag analyses are included in the S/RVD wetwell piping stress summary in Table 5.8.

#### 5.3.3.2.5 Vent System and Torus Motion

The S/RVD lines in the wetwell are subjected to dynamic vent system motion at the main vent penetrations. All other piping supports are attached to the torus ring girders, which were



considered rigid for the dynamic piping analyses. The S/RVD wetwell piping systems have no connections to the torus shell and are not affected by shell motion.

The evaluation of the wetwell S/RVD piping for dynamic motion at the main vent penetration was performed in the same manner and using the same loads as used in the drywell piping analyses described in Subsection 5.2.3.2.2. The loading obtained from the vent system analyses (Section 4) was represented by both response spectra and maximum displacements. The spectra were developed for the two typical penetration locations, with 1% damping for the bounding S/RVD event and 2% damping for LOCA-related loading.

The piping analyses were performed using a multi-level response spectral method with excitation applied at only the main vent penetration. Static analyses were performed with the corresponding maximum displacements imposed at the main vent penetration and the ring girder attachment points for the S/RVDL supports.

Maximum pipe stresses for representative main vent penetration motions are included in the S/RVD wetwell piping stress summary in Table 5.8.

#### 5.3.3.2.6 Thermal Expansion Loads

Thermal expansion analyses were performed for the two S/RVD wetwell routings based on the design temperatures of the lines. The design temperature is 370°F below high water level (HWL) and 450°F above HWL. The use of these design temperatures for the thermal expansion analyses was conservative since they exceed the maximum pipe wall temperatures predicted by RVFOR04 for the wetwell portion of the S/RVDL.

Separate thermal anchor motion piping analyses cases were performed to account for the maximum thermal movements of the main vent penetration and the attachment points of the pipe supports to the torus ring girder. The maximum range of load effects due to thermal expansion and anchor motion was then determined from the individual analyses to account for the possible hot/cold combinations between the main vent, the S/RVDLs, and the torus.

#### 5.3.3.2.7 Other Operating/Design Loads

In addition to the S/RV discharge and other hydrodynamic loadings, the S/RVD wetwell piping was also analysed for seismic (OBE and SSE), dead weight, and internal pressure in accordance with the original design criteria and the FSAR (Reference 16).

#### 5.3.3.3 T-Quencher Evaluation

The analysis of the T-quencher discharge device considers both the T-quencher arms and the ramshead component connecting the T-quencher to the S/RVDL.

##### 5.3.3.3.1 T-Quencher Arms

Bending moments along the T-quencher arms were determined from the results of the piping analyses (see Subsection 5.3.3.2). Stresses were determined based on the reduced section properties of the arms due to the discharge hole pattern. These reduced section properties were determined at several critical locations along the arm.

##### 5.3.3.3.2 Ramshead Component

The ramshead component is a nonstandard piping component which consists of two 12-inch short radius elbows welded together and reinforced by three gusset plates. The evaluation of the ramshead consisted of determining the bending moments from the piping analyses (see Subsection 5.3.3.2), determining the local stress on

the ramshead shell due to the SRV discharge blowdown loads using the finite element method, and determining the stress intensification factor for the ramshead by reviewing the available test data.

The thrust load evaluation was performed to determine the local membrane stresses in the shell due to the axial force and gusset plate reactions. A 3-dimensional finite element model was developed which included the elbow and gussets. An axial force was applied to the inlet end and the stresses were determined. The stresses from this analysis were combined with the piping stresses for the appropriate load cases. The stress intensification factor was determined by reviewing the test data (Reference 42) on the Monticello ramshead (which is geometrically similar to the CNS ramshead). The test data produced a peak stress index of 1.85. Based on the Code interpretation for the stress intensification factor ( $i = C_2 K_2 / 2$ ), a stress intensification factor of 1.0 was determined for use in the ramshead analysis.

#### 5.3.3.4 Wetwell Piping Support Evaluation

The wetwell S/RVD piping support evaluation included the evaluation of the line supports and T-quencher support assembly for the design reactions predicted by the piping analysis.

##### 5.3.3.4.1 S/RVD Piping Supports

The support reaction results from the individual piping load case analyses described in the previous subsections were combined for Level A, B, C, and D Service Limits in accordance with Table 5.7, which represents the bounding combinations from the 27 design load combinations in Table 5.1.

In the submerged portions of the S/RVD piping systems, all support structures were included in the piping models up to their ring girder connections. Inertia effects from the support structures,

as well as submerged structure drag loads, were included in the corresponding piping load case analyses. For these support structures, the support reactions (forces and moments) were combined and summarized at the pipe-to-support connection points and at the support structure welds to the ring girders.

The methodology used for the combination of the support reactions was the same as that used for supports in the drywell as described in Subsection 5.2.3.3.1.

Supports for wetwell S/RVD piping supports were analyzed as linear elastic structures subject to static equivalent design loads. The design loads used were the same as those loads used in the wetwell S/RVD piping analyses.

#### 5.3.3.4.2 T-Quencher Support Pipe

The T-quencher support assembly was included in the piping analyses of the wetwell lines. Therefore, reactions at various components and moments in the pipe due to S/RV blowdown and submerged structure drag loads were available from these analyses. These results were used to check the detailed plate components and welded connections along the support assembly. Reactions at the ring girder attachment points were considered in the analysis of the torus shell (Subsection 3.5.3).

#### 5.3.3.4.3 T-Quencher Support Bracing

The 10-inch diameter stiffening pipe located in the non-vent (non-discharge) bays was not included in the piping analyses. This component was evaluated for submerged structure drag loading using the procedures described in Subsection 6.3.3.2. Since this component has a simple geometry, all evaluations were performed using hand calculations.

#### 5.3.4 Code Evaluations

This subsection describes the Code evaluation of the wetwell portion of the S/RVDLs for the design load combinations summarized in Table 5.7.

##### 5.3.4.1 S/RVD Piping

Maximum pipe stresses for the two S/RVD routings downstream of the vent penetrations were combined from the individual load case results described in Table 5.7. The combination methods used here were consistent with those used for support reactions as described in Subsections 5.2.3.3.1 and 5.3.3.4.1, with the exception that the thermal expansion and imposed displacement effects were considered separately from the primary stresses in Code equations 10 and 11. The combined maximum stresses were checked against allowables (pipe stress allowables are defined in Subsection 5.3.2.1) in accordance with stress equations 8 through 11 in Subarticle NC-3650 of the Code. All piping components in the wetwell portions of the S/RVD lines (including the ramshead) satisfied the applicable stress requirements of the Code.

##### 5.3.4.2 T-Quencher Assembly

All stresses along the T-quencher arms are within allowables. The Code evaluation of the arms was performed using the same procedure as the remainder of the S/RVD piping (see above).

Using the stress intensification factor for the ramshead component indicated in Subsection 5.3.3.3.2 and the design forces and moments on the component the ramshead was qualified for all design load combinations.

#### 5.3.4.3 Wetwell Pipe Supports

All wetwell S/RVD piping supports (structural members, connections, component standard hardware) were qualified to the design criteria of the Mark I Structural Acceptance Criteria (PUAAG).

#### 5.3.4.4 T-Quencher Supports

Stresses in all components of the T-quencher support assembly are within allowables for the design load combinations. All welded connections in the support assembly were also shown to be within allowable design limits.

### 5.4 S/RVDL VACUUM BREAKERS

Two 10-inch diameter vacuum breakers are mounted in the drywell on each of the eight S/RV discharge lines. The valves open whenever drywell pressure exceeds that in the S/RVDL, thereby limiting the water reflood in the S/RVDL after S/RV actuation.

#### 5.4.1 Design Criteria

The S/RVDL vacuum breaker valves were evaluated for design pressure and temperature, pressure transients, gravity and seismic loadings in accordance with the applicable requirements of the ASME Boiler & Pressure Vessel Code, Section III, and ANSI B16.5-1977.

#### 5.4.2 Analysis Methods and Code Evaluation

The analysis consisted of evaluating the structural adequacy of all pressure retaining parts, the hinge arm shaft, the flange and flange bolts. In addition, the analysis included evaluation of the gasket seating force and the torsional and bending moment capacity of the component body.



The evaluation determined that the flange design pressure, evaluated in accordance with ASME B&PV Code, Section III, Paragraph ND-3658.1, is less than the rated pressure at the design service temperature of 500°. The flange bolts and pressure retaining components were within allowable stress limits. The flange gasket seating loads conformed to Code requirements. The hinge arm shaft was evaluated and shown to be within Level A Service Limits as specified in Table ND-3521.1 of ASME Section III. An additional analysis of the shaft was performed using a limit analysis method as described in NB-3228.2 of the ASME B&PV Code, Section III, which resulted in the design load being less than the lower bound collapse load.

Table 5.1

### EVENT COMBINATIONS AND SERVICE LEVELS FOR CLASS 2 and 3 PIPING

[illegible]

Table 5.2

BOUNDING LOAD CASE COMBINATIONS FOR S/RVD LINES IN THE DRYWELL

<u>Event Combination</u>	<u>EQ</u>	<u>SRV</u>	<u>SRV + EQ</u>	<u>SBA/IBA + SRV</u>	<u>SBA/IBA + SRV + EQ</u>	<u>DBA + SRV + EQ</u>	<u>DBA + SRV + EQ</u>
Type of Earthquake	O	-	S	-	S	S	S
Combination No. (1)	-	1	3	11	15	25	27
Service Level	B	B	C	C	D	D	D

Loads:

Normal	X	X	X	X	X	X	X
Thermal Expansion	X	X	X	X	X	X	X
Pipe Pressure	X	X	X	X	X	X	X
Earthquake	X	-	X	-	X	X	X

S/RVD:

Line thrust loads	-	X	X	X	X	X	X
Vent motion	-	X	X	X	X	X	X

LOCA:

Pool swell vent motion	-	-	-	-	-	X	-
CO vent motion (2)	-	-	-	X	X	-	X
Chugging vent motion (2)	-	-	-	X	X	-	X

Notes:

- (1) From Table 5.1.
- (2) The bounding combination of drag loads and vent motion loads from the CO and chugging phases, respectively, was used.

Table 5.3

S/RV DISCHARGE PIPING STRESS ALLOWABLES

ASME Material Designation	<u>ASME Code NC-3650 Stress Equations</u>					
	8 ( $S_h$ )	9B <sup>(1)</sup> ( $1.2S_h$ )	9C <sup>(1)</sup> ( $1.8S_h$ )	9D <sup>(1)</sup> ( $2.4S_h$ )	10 ( $1.25S_h$ $+0.25S_c$ )	11 ( $2.25S_h$ $+0.25S_c$ )
SA-106 Gr.B	15.0	18.0	27.0	36.0	22.5	37.5
SA-234 WPB	17.5	21.0	31.5	42.0	26.2	43.7

Notes:

- (1) B, C and D refer to Service Levels.
- (2) Stresses in ksi.
- (3) Allowable stresses given at design temperature.

Table 5.4

MAXIMUM PIPE STRESSES DUE TO S/RVD THRUST LOADING  
IN DRYWELL ROUTING OF S/RVDLs

<u>S/RVD Line Number</u>	<u>Maximum Stress (1) (ksi)</u>	<u>Component Type and Location (2)</u>
71A	11.1	Elbow #9
71B	10.9	Elbow #9
71C	9.6	Butt weld at MS Tee
71D	11.4	Butt weld at MS Tee
71E	10.8	Elbow #7
71F	8.7	Vacuum Breaker Tee
71G	10.4	Elbow #9
71H	11.1	Elbow #2

Notes:

- (1) Stresses presented as:  $S = 0.75 \times i \times M_R / Z$ .
- (2) Elbows are counted sequentially from the mainsteam connection.

Table 5.5

S/RVDLs IN THE DRYWELLMAXIMUM STRESS AS A PERCENTAGE OF ALLOWABLE FOR  
BOUNDING LOAD COMBINATION

<u>S/RVD Line Number</u>	<u>ASME Code NC-3650 Stress Equation</u>				
	<u>8</u>	<u>9B(1)</u>	<u>9C(1)</u>	<u>9D(1)</u>	<u>11(2)</u>
71A	33	95	65	67	70
71B	33	91	72	61	66
71C	33	72	52	48	46
71D	32	92	67	79	34
71E	34	87	61	65	54
71F	39	78	54	54	52
71G	33	90	76	59	75
71H	36	96	74	66	68

Notes:

- (1) B, C, and D refer to Service Levels for stresses caused by occasional loads.
- (2) Compliance is shown with equation 11, in lieu of equation 10, as per subparagraph NC-3652.3 of the Code.



Table 5.6

RESULTS OF CODE EVALUATIONMAXIMUM INTERACTION RATIOS

L I N E	M E M B E R	Axial	<u>Flexural</u>		Comb.	Service Level	Beam Azimuth (Degrees)
			$\frac{f_a}{F_a}$	$\frac{f_{by}}{F_{by}}$			
U							
P	A	16	0.02	0.28	0.34	0.64	A/B Rad. At 120
P	B	118	0.02	0.50	0.51	1.03	A/B Lat. Bet. 81 & 98
E	C	62	0.04	0.36	0.43	0.83	A/B Lat. Bet. 148 & 171
R	D	24	0.00	0.00	0.66	0.66	A/B Rad. At 171
	E	65	0.00	0.36	0.32	0.68	A/B Lat. Bet. 189 & 212
L	F	79	0.00	0.42	0.55	1.07	A/B Rad. At 189
E	G	32	0.03	0.10	0.49	0.62	D Rad. At 240
V	H	106	0.06	0.41	0.27	0.74	D Rad. At 240
E	H	67	0.06	0.59	0.36	1.01	D Lat. Bet. 212 & 240
L							
L							
O	A	108	0.07	0.06	0.36	0.49	A/B Lat. Bet. 15 & 51
W	B	108	0.05	0.18	0.18	0.41	A/B Lat. Bet. 15 & 51
E	C	213	0.01	0.04	0.34	0.39	A/B Lat. Bet. 148 & 171
R	D	46	0.00	0.02	0.21	0.23	A/B Rad. At 171
	E	247	0.01	0.51	0.23	0.75	A/B Lat. Bet. 189 & 212
L	F	250	0.01	0.18	0.13	0.32	D Lat. Bet. 189 & 212
E	G	284	0.00	0.26	0.25	0.51	A/B Lat. Bet. 238 & 260
V	H	95	0.02	0.01	0.41	0.44	A/B Rad. At 328
E							
L							

Table 5.7

BOUNDING LOAD COMBINATION FOR S/RVD LINES IN THE WETWELL

Event Combination	EQ	SRV	SRV + EQ	SBA/IBA + SRV	SBA/IBA + SRV + EQ	DBA + SRV + EQ	DBA + SRV + EQ
Type of Earthquake	O	-	S	-	S	S	S
Combination No. (1)	-	1	3	11	15	25	27
Service Level	B	B	C	C	D	D	D

Loads:

Normal	X	X	X	X	X	X	X
Thermal Expansion	X	X	X	X	X	X	X
Pipe Pressure	X	X	X	X	X	X	X
Earthquake	X	-	X	-	X	X	X
S/RVD:							
Air Bubble Drag	-	X	X	X	X	X	X
Vent motion	-	X	X	X	X	X	X
Line Thrust Loads	-	X	X	X	X	X	X
Uneven Water Clearing	-	X	X	X	X	X	X

LOCA:

Pool Swell Impact/Drag	-	-	-	-	-	X	-
Froth Impingement	-	-	-	-	-	X	-
Pool Swell Vent Motion	-	-	-	-	-	X	-
Water Jet	-	-	-	-	-	X	-
Air Bubble Drag	-	-	-	-	-	X	-
CO Drag Loads (2)	-	-	-	X	X	-	X
CO Vent Motion (2)	-	-	-	X	X	-	X
Chugging Drag Loads (2)	-	-	-	X	X	-	X
Chugging Vent Motion (2)	-	-	-	X	X	-	X

Notes:

(1) From Table 5.1.

(2) The bounding combination of drag loads and vent motion loads from the CO and Chugging phase, respectively, was used.

Table 5.8

REPRESENTATIVE MAXIMUM PIPE STRESS FOR  
THE WETWELL ROUTING OF THE S/RVD LINES

<u>Load Case</u>	<u>Routing A Maximum Stress (ksi)</u>	<u>Routing B Maximum Stress (ksi)</u>
S/RVD:		
Air Bubble Drag Loads	4.4	6.3
Line Thrust Loads	5.3	7.1
Uneven Water Clearing	2.2	1.3
LOCA:		
Pool Swell Impact & Drag	N/A	5.5
Pool Swell Vent Motion	4.2	5.5
Air Bubble Drag Loads	0.6	1.3
CO Drag Loads	9.4	18.7
CO Vent Motion	0.8	1.4
Chugging Drag Loads	8.9	20.8

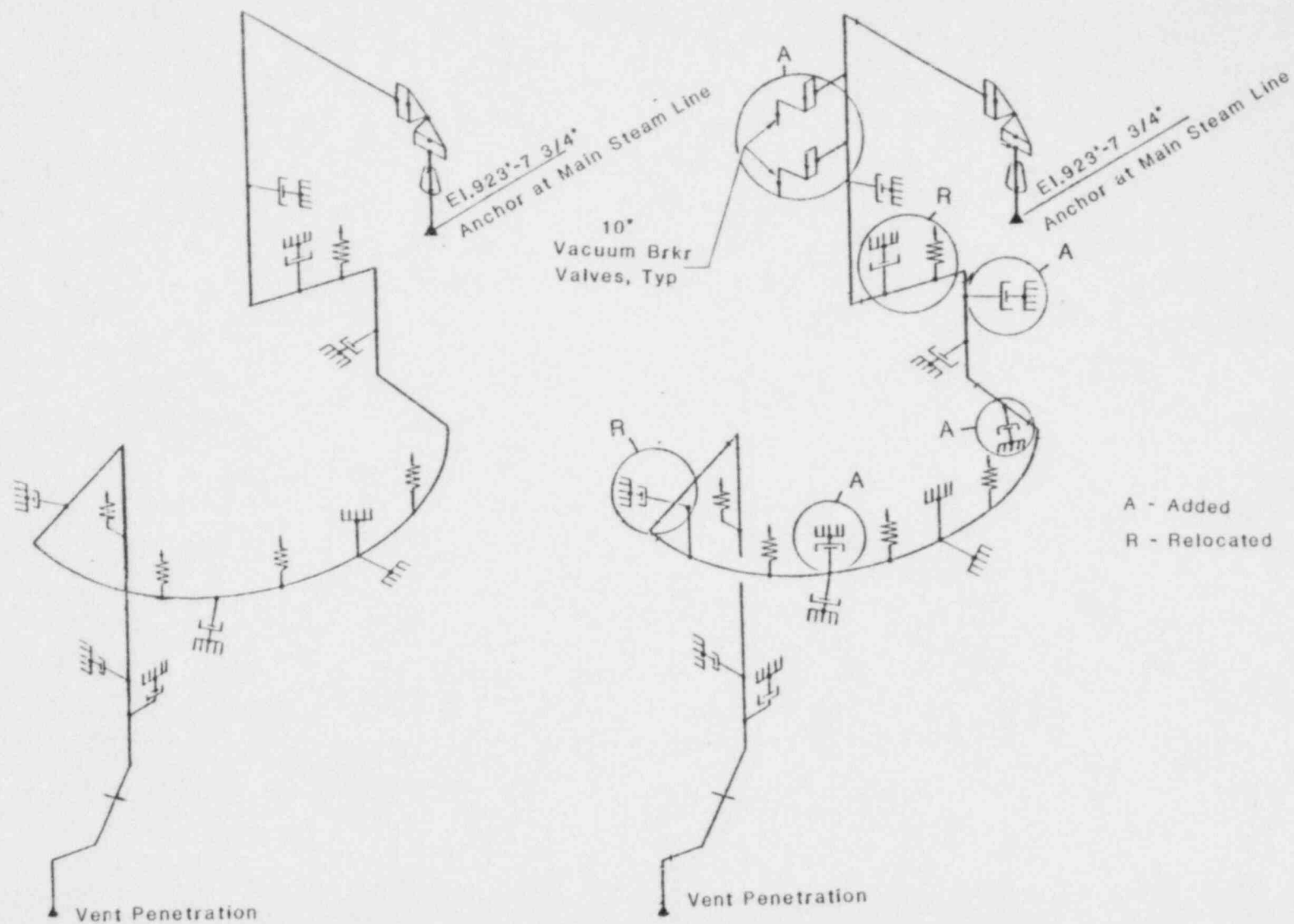
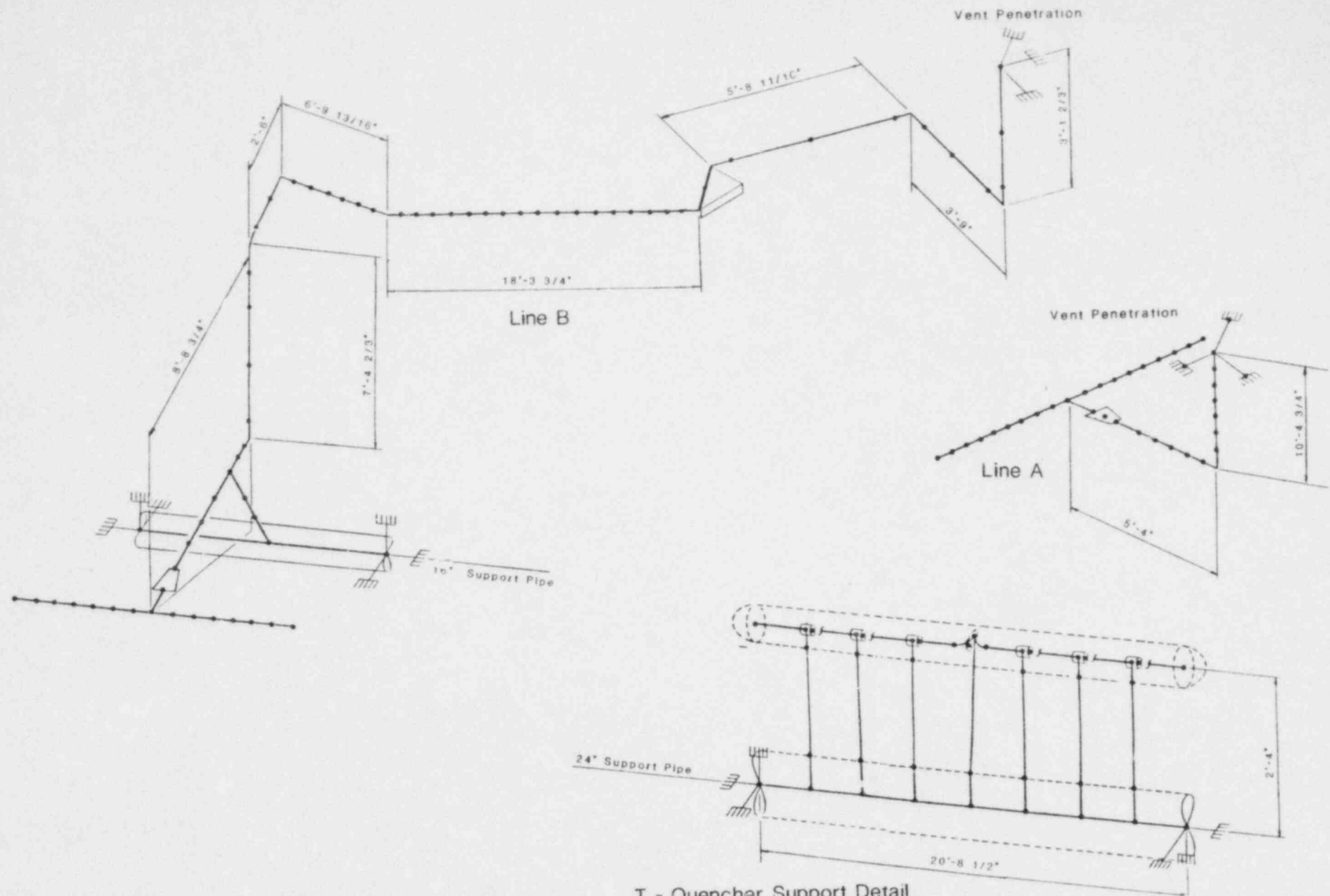


FIGURE 5.1

REPRESENTATIVE DRYWELL S/RVD LINE MODEL (LINE 71G)  
BEFORE AND AFTER MODIFICATIONS



T - Quencher Support Detail

FIGURE 5.2

S/RVD LINE MODELS (WETWELL ROUTING)

COOPER NUCLEAR STATION

PLANT UNIQUE ANALYSIS REPORT

SECTION 6

TORUS ATTACHED PIPING AND  
TORUS INTERNAL STRUCTURES



## 6.1 INTRODUCTION

This section describes the results of the evaluations performed on the CNS piping systems which have an attachment point on the torus shell boundary. The majority of these piping systems are ECCS-related. Most of the systems considered have a segment both external to the torus pressure boundary and a segment inside the wetwell. Since the design loads and analyses requirements differ depending on whether the segment is inside or outside of the wetwell, a separate description is provided for each. Components included in these evaluations are the piping and piping supports, valves and branch lines along the piping system, and the pump and turbine nozzles at the end of some of the lines. Also included in this discussion are the evaluations of the non-essential structures located in the wetwell, including the monorail beam and platform system. These non-essential structures are subjected to the same loadings as the piping inside the wetwell and typically follow a similar analysis procedure.

Descriptions of the components evaluated in this section are provided in Section 1 of this report. The thermal-hydraulic load definitions and load combinations are described in Section 2. For each component evaluated, this section provides a description of design load combinations, design allowables, analysis methods and results, and the Code evaluation.

## 6.2 PIPING SYSTEMS EXTERNAL TO TORUS

Cooper Nuclear Station has a number of piping systems which are connected to penetrations on the torus shell boundary. A summary of the attached piping systems is provided in Section 1 of this report. A number of supports and active components (including valves and pumps) are located on most of these systems. This subsection describes the evaluation of these piping systems and components for the new containment load definitions.

For piping systems external to the torus, effects due to Mark I hydrodynamic loads are induced by the motion of the torus shell boundary. This motion is determined from the torus shell analyses (Section 3) and differs in magnitude and nature depending on the torus load case. In evaluating external piping systems, distinction is made between large-bore lines (torus penetration diameter of 6" or greater) and small-bore lines (torus penetration diameter under 6"). The primary distinction is the manner in which torus shell dynamic motions are considered.

#### 6.2.1 Design Load Combinations

Table 5.1 shows the 27 design load combinations for the torus attached piping. This table is taken directly from the PUAAG (Reference 19). Service limit assignments for each event combination are also indicated in the table.

The external torus attached piping does not experience any direct hydrodynamic loads during a LOCA or S/RV discharge. These loads are applied indirectly through the motion of the torus shell penetration. Therefore, the bounding load combinations for performing the Code evaluation on the torus attached piping and supports outside of the torus can be reduced to those shown in Table 6.1.

#### 6.2.2 Design Allowables

The majority of the torus attached piping is classified as essential Class 2 piping systems. Design allowables are taken from Subsection NC-3600 of the Code. Similarly, all external torus attached piping supports are classified as Class 2 piping supports, and design allowables are taken from Subsection NF-3000 of the Code.

##### 6.2.2.1 Piping Stress Allowables

The base stress allowables,  $S_h$  and  $S_c$ , for the piping external to the torus were taken from Appendix I of the Code. The stress

allowables for applicable load categories and service limits were determined in accordance with equations 8, 9, 10, and 11 in Subarticle NC-3650 of the Code. These allowable stresses are summarized in Table 6.2 for SA-106 Grade B material. In the case of load combinations from Table 5.1 for which footnotes 3 and 4 in the Structural Acceptance Criteria apply, the allowable stresses for Level C ( $1.8 S_h$ ) and Level D ( $2.4 S_h$ ) Service Limits were used.

Service limits for valves are specified in the PUAAG. As stated in Subsection 5.5.1 of the PUAAG, requirements for valve operability are satisfied by meeting Level B Service Limit stress allowables for all postulated event combinations. Therefore, Level B Service Limit stress allowables were used for all events to satisfy operability criteria for all valves.

Stress allowables for pressure retaining parts of the valves are given in Table I.7 of the ASME Code. Stress allowables for non-pressure retaining parts are obtained using the rules of Appendix XVII and stress allowables from Table I.7.

The pump and turbine nozzles are classified as Class 2 or Class 3 components. Their allowable stresses are those given by the Code, Section III, Subsections NC-3400 and ND-3400. Allowable stresses for all load cases are elastic stresses.

Pump operability is considered to be the ability of the pump to provide adequate fluid delivery during and after a LOCA. During such an event, the pump shaft displacement should not constrain movement of the impeller to the extent that fluid flow is impeded. The loading on the pump due to the Mark I hydrodynamic loads is transmitted to the pump only through the suction and discharge nozzles. Because of the relative stiffness of the pump nozzle to the pump casings significant levels of nozzle deformation would have to exist before any significant loading would be seen

by the pump shaft and the impeller. Thus if the nozzles do not exhibit large deformations, no significant deformations will occur at the shaft due to hydrodynamic loads. Significant displacements of the shaft can then only be induced by seismic loading. Because the design seismic loading has not changed, no inertia effects will be considered for pump operability.

#### 6.2.2.2 Support Allowables

The allowables for the torus attached piping supports are consistent with the Mark I Structural Acceptance Criteria. The basic approach was to use Code Subsection NF and Appendix XVII. Existing pipe support component hardware did not have load capacity data consistent with ASME Subsection NF. Allowable load increases of 33% for the Level C and D Service Limits were used. In addition to these increases, the pipe support design loads due to Mark I hydrodynamic loads plus original design loads were compared with the original pipe support design loads. If the new design load did not exceed the original design load by more than 10%, the support was considered acceptable.

#### 6.2.2.3 Fatigue Considerations

All torus attached piping systems are classified as Class 2 or 3 systems and, therefore, evaluation for cyclic loading is required only for thermal cycling. However, the NRC has required additional confirmation of the adequacy of these piping systems for mechanical cyclic loads (Reference 40). This confirmation is being provided by the Mark I Owners Group through a generic program which will still be unresolved at the time this report is submitted. Therefore, these fatigue considerations are not addressed in the evaluations of the torus attached piping. Fatigue due to thermal cycling was addressed as required by the Code. Should additional fatigue evaluations become required on a plant unique basis, a separate submittal for CNS will be prepared at that time.

### 6.2.3 Analysis Methods and Results

This subsection describes the analyses of the external torus attached piping, and the evaluations of associated supports and active components.

#### 6.2.3.1 Piping Models

All torus attached piping of diameter greater than one inch was modeled using the piping analysis program SUPERPIPE (described in Appendix B). Piping systems with a diameter of one inch or less were modeled such that each geometric configuration and typical torus attachment location was covered. This procedure was acceptable since a number of these small pipes distributed around the torus were identical. Table 6.3 summarizes all torus attached piping by torus penetration number and defines the associated piping models.

Each piping model external to the torus was modeled from the torus shell connection point to a point along the pipe beyond which the load effects from the torus excitation were no longer significant. This model termination point was either an anchor, or in cases where extending the model to an anchor would lead to unnecessarily excessive model sizes, a point at which the torus excitation effects had attenuated to negligible values. The acceptability of model termination points other than anchors was confirmed in the piping analysis phase by verifying that the combined load effects (pipe stresses) from torus excitation had attenuated below 10% of the design allowables for an extended length of piping before the termination point.

As described in Subsection 6.2.3.2, the coupled response of torus shell and attached piping was determined for all torus attached piping systems with a diameter greater than 6 inches. The torus vent purge and drain lines, although having diameters greater than 6 inches, were analyzed using uncoupled torus motion. The piping



model used to determine the coupled response included the internal as well as the external portion of the line and supports. The location of the torus penetration in this model was left unrestrained while the eigenvectors and eigenvalues were determined for all modes up to 50 Hz. This eigensolution provided the piping dynamic characteristics used as input for determining the coupled response.

For the load case analysis of each piping system two models were used. These models differed from each other only in the definition of the boundary conditions at the torus penetration point:

- (1) For evaluation of the piping due to coupled torus/piping excitation, the torus penetration point was modeled as a rigid anchor, since the torus shell flexibility was accounted for in the coupled response definition.
- (2) For evaluation of all other load cases, the torus penetration point was modeled with finite stiffness values in the 6 degrees of freedom (dof) as obtained from a static analysis of the torus shell model.

The stiffness properties of pipe support components were evaluated separately and incorporated in the piping model. Valves were included in the piping models as rigid components and were evaluated separately in detail as described in Subsection 6.2.3.6.

Branch lines connected to the torus attached piping having nominal ratios of branch line diameter to main pipe diameter greater than 1:4 were included as integral parts of the main piping models. Smaller branch lines were considered to have negligible effect on the response of the main pipe and were included only by lumped mass points in the models. The acceptability of these smaller branches under loading transmitted from the main pipe was evaluated separately as described in Subsection 6.2.3.5.



All large bore piping models were based on documentation from the as-built verification program performed during 1979. As-built information for small bore piping and supports were obtained and documented for the Mark I Containment Program during 1981.

#### 6.2.3.2 Coupling of Torus and Piping System

In determining the response of the torus shell at an attached piping penetration, the effect of the piping system can modify the response predicted by the torus shell analyses. A methodology was developed to account for these effects (Reference 43). The methodology modifies acceleration time histories from the torus shell analyses (referred to as uncoupled time histories) to account for the stiffness and mass effects of the piping.

The procedure used to modify uncoupled torus acceleration time histories and account for coupling with the attached piping was as follows:

- (1) Perform uncoupled torus shell response analysis to obtain acceleration time histories at all attachment points. These analyses are described in Section 3.
- (2) Determine the modal response of the torus shell to an externally applied force at all attachment points. Use the results from a complete frequency and mode shape analysis of the torus for all modes below 50 Hz. This eigensolution is also described in Section 3.
- (3) Determine modal response characteristics of each uncoupled piping model subjected to an applied unit force at each attachment dof. This requires an eigensolution of the piping model with the attachment dof unrestrained. The piping models described in Subsection 6.2.3.1 were used in this step. These models include both the internal and external portion of the attached piping system.

- (4) Input into the coupling program the uncoupled torus shell acceleration response time histories at the piping attachment points for each dof to be considered in the coupling analysis (from Step 1), the uncoupled torus modal response characteristics (from Step 2), and the uncoupled piping modal response characteristics (from Step 3). The output of the program is the coupled acceleration response time history at the piping attachment points for all dofs where coupling effects between the piping and torus are considered.
- (5) Use the response spectra of the coupled acceleration response time histories (with specified damping) at the piping attachment point as input to an uncoupled piping analysis. The resultant piping response includes the effect of coupling between the structure and piping.

The details of this procedure can be found in Reference 43.

Coupled response spectra for all torus shell dynamic analyses (as described in Section 3) were generated in this manner. For loads defined in the frequency domain (CO and chugging), equivalent acceleration time histories resulting in the same acceleration levels predicted by the torus analyses were generated. These generated time histories are based on the frequency components of the torus response from 0 to 50 Hz. Coupled torus shell response spectra were generated only at the large-bore torus attached piping penetrations. For the small-bore lines, where the effect of the piping on the torus is likely to be minimal, uncoupled response spectra were generated directly from the torus acceleration response time histories.

Torus shell displacements at all penetrations for all static and dynamic load cases were also provided as input to the piping analysis.

#### 6.2.3.3 Analysis Procedures and Results

The analyses described in this subsection were used in the qualification of the external torus attached piping, torus penetrations (Section 3), piping supports, and active components. A complete set of analyses was performed for each large-bore line. For the small-bore lines, a reduction in the number of analysis cases was possible due to similarity in the piping configuration and design loads.

All dynamic piping analyses were performed using damping values consistent with the guidelines in NRC Regulatory Guide 1.61 (Reference 37). For dynamic load cases included in Level B Service load combinations, the damping values were 1% and 2% of critical for pipe sizes  $\leq 12$  inches and  $> 12$  inches, respectively. The damping values for load cases included in Level C and D Service load combinations were 2% and 3% of critical damping depending on the pipe size category. All dynamic piping analyses for LOCA and S/RV discharge related loads were performed using the multi-level response spectral method. The frequency cut-off for torus excitation load cases was 50 Hz. The spatial and modal combination methods used were consistent with the guidelines in NRC Regulatory Guide 1.92 (Reference 38). Thus, the SRSS method was used for combining directions of excitation and the 10% grouping method was used for the modal combination. The rigid body acceleration effects and, more generally, the high frequency piping response beyond the modal cut-off frequency, were taken into account in the piping analyses by the missing mass correction methodology used in SUPERPIPE.

##### 6.2.3.3.1 Torus Shell Motion

The development of the dynamic torus shell motion at piping penetrations is addressed in Subsection 6.2.3.2. The torus shell motion applied to the piping models was defined as acceleration response spectra in three orthogonal translational directions at

the penetration. The piping models were subjected to the simultaneous motion of these three excitation directions in a multi-level response spectral analysis for each load case considered. For this application each torus penetration point was defined as one excitation level while all other pipe supports were associated with a zero-excitation level. In cases where more than one torus penetration was included in the same piping model, the load effects from the different penetrations were combined by absolute summation, which conservatively represents out-of-phase motion. Consistency with the coupled torus/pipe response definition required that the torus penetration be considered as a rigid anchor for these load cases.

The quasi-static displacement effect at the torus penetrations were decoupled from the inertial effects in the analyses and were considered as separate static load cases. These analyses were imposed displacement load cases. The piping response to each directional component of the imposed displacements was evaluated separately, followed by an SRSS combination of directional response consistent with NRC Regulatory Guide 1.92.

A total of three potentially bounding LOCA-related torus motion load cases were considered in the piping analysis: pool swell, DBA CO, and chugging. Representative maximum stress results for these load cases are summarized for the large bore torus attached piping systems in Table 6.4. A total of nine S/RV discharge-related torus motion load cases were considered in the piping evaluations as summarized in Table 6.5. One SVA case and one MVA case were selected out of the nine for explicit piping analysis. The results for the remaining seven cases were generated by applying scale factors to the two explicit cases. The scale factors, which are also included in Table 6.5, correspond to the ratios between maximum torus shell pressures for the different S/RV discharge load cases. Representative maximum pipe stresses corresponding to S/RVD loading are also summarized in Table 6.4.

#### 6.2.3.3.2 Other Piping Loads

In addition to the dynamic torus shell motion load cases described above, the following load cases were considered in the piping analyses:

- (1) Seismic inertia and anchor movements (OBE and SSE).
- (2) Thermal expansion of the piping systems at maximum operating temperature.
- (3) Thermal anchor movements; notably torus movements at maximum suppression pool temperature.
- (4) Imposed displacements at torus penetration due to torus pressurization.
- (5) Internal pipe pressure.
- (6) Dead weight.

The seismic analyses were performed as response spectral analyses consistent with the original design criteria in the FSAR (Reference 16). The thermal expansion, internal pressure, and dead weight analyses were also performed as specified by the original design criteria.

The quasi-static torus movement cases due to suppression pool heatup and torus pressurization were obtained from the torus evaluation described in Section 3. The piping anchor movement analysis results from the imposed torus thermal movements were combined with the piping thermal expansion results to produce the maximum possible thermal range for each individual component in the piping system.



The dead weight analysis was performed using the actual as-built load settings for constant force and spring hanger supports. These load settings were applied as pre-loads on the corresponding support components in the model.

#### 6.2.3.4 External Piping Support Evaluation

Support load combinations were generated from the piping analyses for Levels A, B, C and D Service load combinations as defined by Table 6.1. The combined reactions at each pipe support (rigid support, snubber, or spring hanger) were determined as a maximum range in each supported direction. The support reactions from the various dynamic load cases, including inertial as well as anchor movement effects, were combined separately as applicable for each of the level service limits whereupon these unsigned quantities were added to (or subtracted from) the maximum (or minimum) values of the load ranges created by the combination of dead weight and thermal expansion load cases.

For load combinations containing more than one dynamic load case, a maximum of two dynamic cases were combined using a modified SRSS approach. To this result any additional dynamic load cases were added by absolute summation. The modified SRSS approach consists of a multiplier of 1.1 applied to a straight SRSS combination. This approach is further justified for the current application by a separate study described in Appendix D.

The support load combinations described above were generated for the reevaluation of all existing support components on the torus attached piping systems as well as for all new or modified supports required to qualify the piping to the new hydrodynamic loadings.

Support structures were analyzed as linear elastic structures and checked for serviceability and functionality. The support components evaluated include welded pipe attachments, component standard



hardware, pipe support structural members, connections, and the building structures to which the supports attach.

#### 6.2.3.5 Branch Line Evaluations

As mentioned in Subsection 6.2.3.1, branch lines connected to the torus attached piping systems with branch-to-run diameter ratios less than 1:4 were excluded from the main piping model based on their negligible impact on the response of the main pipe. This subsection describes the methodology that was used to evaluate these branch lines under loading transmitted from the main pipe through the branch connection point. A total of 114 branch lines were excluded from the main piping analysis models and were subsequently considered using separate, simplified evaluations as described below.

The branches were initially screened and grouped into two major categories: (1) 69 branches were simple unsupported cantilever-type vent and drain lines, and (2) the remaining 45 branches were supported.

The cantilever-type branches were subjected only to inertial loading caused by the accelerations of the main pipe at the branch connection point. In addition, self-weight and internal pressure were considered. An equivalent static calculation was used to evaluate the stresses in these branches (including the branch connection). The dynamic response of the cantilevers was characterized by the DLF, which was determined based on the dominating driving frequencies of the main pipe at the branch connections and the fundamental frequencies of the cantilevering branches. The load case combinations and acceptance criteria for the branch line evaluations were the same as for the torus attached main piping, although the number of explicit load case combinations was reduced by the use of worst case enveloping procedures.

The second major group of branch lines (i.e. the supported lines) were in addition evaluated for imposed displacements at the branch connection point as well as thermal expansion effects of the branch itself. A group of six branch lines, which due to their geometric complexity and/or high load magnitude were unsuited for evaluation by the hand calculation methods, were modeled for detailed analyses using the SUPERPIPE program.

#### 6.2.3.6 Torus Attached Piping Valve Evaluations

The valves on the torus attached piping were evaluated to demonstrate that the valves are qualified for all postulated events in Table 5.1. The valves were divided into groups of identical valves and an evaluation was performed for each group. The maximum piping acceleration for each group was used to calculate stress levels in the valve being evaluated. As described in Subsection 6.2.2.1, allowable stresses were determined in accordance with the requirements of the PUAAG. The piping acceleration of non-rigid valves was increased by a factor of 1.5 prior to the calculation of stresses. This factor accounts for any amplification of the piping acceleration which may be caused by the dynamic response of the valve structure, and is specified in IEEE 344-1975 (Reference 44) and Standard Review Plan 3.7.2 (Reference 45). The steps followed in the valve evaluations are summarized below:

- (1) Divide the valves on torus attached piping into groups of identical valves.
- (2) Determine the maximum piping acceleration for the valves in each group.
- (3) Calculate stresses in the critical sections of each valve (i.e. yoke legs, flange bolting) for the maximum three-dimensional resultant piping acceleration, including the 1.5 factor whenever appropriate, in each of three orthogonal directions.

- (4) Combine operational stresses with the stresses resulting from the most severe of the three load cases described in (3) above.
- (5) Compare calculated stresses to allowable stresses.
- (6) Verify that the valve complies with established standards:
  - ANSI B16.34-1977, minimum wall thickness and temperature pressure rating.
  - ASME NC-3521, ratio of valve body section modulus and allowable stress to pipe section modulus and allowable stress.
  - ASME Appendix XVII, valve flanges.

#### 6.2.3.7 ECCS Pump and Turbine End Load Evaluations

The ECCS pumps and turbines were qualified for the torus attached piping loads by evaluating: (1) nozzle and casing stresses, (2) flange loads, and (3) anchor bolt loads.

Stresses at the nozzle/casing crotch were calculated using the Code Subsection NB-3500, and were compared with the ASME Code allowable stresses. The nozzles were evaluated as Class 2 or 3 piping.

For several turbines, the piping was connected to the turbine by pipe flanges instead of pipe nozzles. Flange loads were evaluated using Code Subsections NC/ND-3100, -3300, and -3600 and compared to allowable loads given in ANSI B16.6-1977 (Reference 46).

For the baseplate and baseframe anchor bolts, tensile and shear stresses were evaluated using Code Subsection NF-3100 and Appendix XVII. The anchor bolt embedments were evaluated using the ACI-349-76 Code, Appendix B (Reference 47).

#### 6.2.4 Code Evaluation

This Subsection describes the Code evaluation of the external torus attached piping components for the design load combinations summarized in Table 6.1.

##### 6.2.4.1 External Piping

The maximum pipe stresses, as defined by equations 8 through 11 in Subsection NC-3650 of the Code, resulting from the bounding load combinations in Table 6.1 were all shown to be within the corresponding Code allowables. A summary of the maximum stress to allowable ratios for the torus attached piping external to the torus is provided in Table 6.6.

For the Code stress verifications, an SRSS combination increased by a factor of 1.1 was used to calculate combined pipe stresses for a maximum of two dynamic load cases in any combination. Any additional dynamic load cases included in the same load combination were added by absolute summation.

The allowable stresses for those load combinations from Table 6.1 for which footnotes 3 and 4 in the Structural Acceptance Criteria apply, were taken to be those for Level C ( $1.8 S_h$ ) and D ( $2.4 S_h$ ), respectively. By these footnotes, the Structural Acceptance Criteria permits the allowable stresses to be increased in this manner from the value for Service Level B ( $1.2 S_h$ ), provided all other fatigue and operability criteria are met. The fatigue considerations are discussed in Subsection 6.2.2.3. The operability considerations are addressed in Subsections 6.2.4.4 and 6.2.4.5.

##### 6.2.4.2 External Piping Supports

All pipe support components (i.e. welded pipe attachments, component standard hardware, pipe support structural members, connections, and the building structures to which the supports attach) were qualified to meet the design criteria.

#### 6.2.4.3 Branch Lines

The small bore branch lines connected to the torus attached piping systems were evaluated separately in a conservative, enveloping manner consistent with the main pipe approach described in Subsection 6.2.4.1. This evaluation verified that all branch lines within the range of torus excitation influence satisfy all applicable code stress criteria.

#### 6.2.4.4 Torus Attached Piping Valves

All valves were analyzed or mechanically supported to meet stress and operability requirements for all load conditions specified by the PUAAG.

#### 6.2.4.5 ECCS Pumps and Turbines

The ECCS pumps and turbines satisfy the appropriate stress criteria from the Code Subsections NB, NC, and NF.

Pump operability has been satisfied for two reasons: First, the only load applied to the pumps due to Mark I program considerations are through suction and discharge nozzles. Since it has been assured that these nozzles do not yield and hence, do not exhibit significant deformation, the pump shaft and impeller cannot be impacted by them. Further, seismic design loads have remained unchanged and thus, will not impact pump operability. No other Mark I loads affect pump operability.

### 6.3 PIPING SYSTEMS INTERNAL TO TORUS

A number of ECCS-related piping systems have segments inside the torus shell boundary. These piping systems generally function as intakes to or discharges from the ECCS pumps and turbines. Several of these lines are supported from the ring girder or torus shell.

For these internal piping systems, direct application of the Mark I hydrodynamic loads is required. In addition, the torus shell motion at the penetration and at any support attached to the torus is considered. This subsection describes the evaluations of these internal piping systems.

#### 6.3.1 Design Load Combinations

The 27 design load combinations and service limit assignments for the internal torus attached piping are shown in Table 5.1.

The internal portions of the torus attached piping are subjected to direct application of hydrodynamic loads during a LOCA or S/RV discharge, as well as torus shell dynamic motion. Table 6.7 indicates the bounding load combinations of the piping and supports. Some of the events in these load combinations (e.g. pool swell impact loading) are only applicable to the evaluation of certain lines depending on location in the suppression chamber.

#### 6.3.2 Design Allowables

The torus internal piping is primarily classified as essential Class 2 piping, similar to the external piping. Thus, Subsection NC-3600 and NF-3000 are applicable for obtaining the design allowables for the piping and supports, respectively.

##### 6.3.2.1 Piping Stress Allowables

The piping stress allowables for the internal portions of the torus attached piping are the same as those for the external portions of the same piping systems as described in Subsection 6.2.2.1 and Table 6.2.



#### 6.3.2.2 Support Allowables

Supports for the torus internal piping were designed to meet the requirements of ASME Code Subsection NF and Appendix XVII.

#### 6.3.2.3 Fatigue Considerations

Fatigue considerations for the torus internal piping are the same as for the external piping (Subsection 6.2.2.3). Fatigue analysis for mechanical cyclic loads is therefore not addressed at this time.

#### 6.3.3 Analysis Methods and Results

This Subsection describes the analysis of the torus internal piping and supports.

##### 6.3.3.1 Piping Models

The internal portions of the torus attached piping were included in integrated internal/external piping models for purposes of generating coupled torus/pipe response at the torus shell boundaries as discussed in Subsections 6.2.3.1 and 6.2.3.2. For the load case analyses and pipe stress evaluations, internal pipe portions were modeled and analyzed separately since the majority of the load cases affecting the internal piping are unique to the wetwell region.

The torus internal piping systems are listed by function and penetration number in Table 6.8.

With the exception of the containment spray header, which extends around the top of the torus and penetrates the torus at two locations, the torus internal piping consists exclusively of short, submerged suction strainers and partially submerged discharge pipes.

With the exception of the T-shaped suction strainers, which are identified in Table 6.8, the torus internal piping systems were modeled using the program SUPERPIPE (described in Appendix B). The modeling methodology for the internal piping was identical to that for the external piping (Subsection 6.2.3.1), with the exception of the modeling of submerged piping. In order for the model to realistically simulate the dynamic characteristics and response of submerged pipe segments, an artificial added mass was distributed along these segments. The added mass consisted of the mass of the displaced fluid in accordance with Reference 41. In addition, the mass of the fluid contained inside submerged piping was included in the models.

For load cases represented by coupled torus/pipe response spectra at the torus shell boundary, the pipe attachment points were modeled as rigid anchors at the boundary to be consistent with the development of these loads (described in Subsection 6.2.3.2). Rigid anchors were located at the torus penetration point as well as at locations where pipe supports were attached to the torus shell. Structural steel members connecting the pipe to the torus shell boundary were included in the piping models with their actual stiffness properties.

For analyses of load cases other than coupled torus/pipe dynamic response, the boundary condition at the torus shell was modeled using the actual shell stiffness obtained from the torus analysis model (Section 3).

#### 6.3.3.2 Analysis Procedures and Results

The analyses described in this subsection were used in the qualification of the torus internal piping, torus penetrations (Section 3), and piping supports. A complete set of analyses was performed for each piping system.

The dynamic piping analyses were performed using damping values recommended in NRC Regulatory Guide 1.61 as described for torus external piping in Subsection 6.2.3.3. Directional and modal combination methods used were in accordance with NRC Regulatory Guide 1.92 as described in Subsection 6.2.3.3 for external piping.

Modal analyses were performed for hydrodynamic loading up to a cut-off frequency of 50 Hz. Higher mode response or rigid body acceleration effects were accounted for in response spectral analyses by the missing mass correction methodology in SUPERPIPE. Several of the torus internal piping systems, notably the short T-shaped suction strainers, have fundamental response frequencies in excess of 50 Hz. In these cases, and for other simple cantilever configurations, the dynamic analyses were performed by equivalent static methods including the zero period acceleration effects.

#### 6.3.3.2.1 Pool Swell-Related Loads

The loads addressed in the Subsection are pool swell impact, drag, and fallback loads, froth impingement loads, LOCA bubble drag loads, and LOCA water jet loads. The source and development of these loads for application to torus internal piping systems are defined in Subsections 2.4.3.3. through 2.4.3.6. The torus internal piping subjected to these loads are identified in Tables 2.5 and 2.6.

Equivalent static analyses were performed for the affected piping systems. The dynamic load factor used was conservatively taken as two. With the exception of the containment spray header piping, for which the froth impingement effects were significant, the effects on the torus internal piping from pool swell-related loads were found to be relatively minor. This was primarily due to small exposed areas, routing close to the torus shell, and stiff piping configurations.

#### 6.3.3.2.2 CO and Chugging Drag Loads

The loads addressed in this subsection are the oscillatory drag loads, including fluid structure interaction (FSI) and interference effects, on submerged piping during the CO and chugging phases of a LOCA. The development of these loads is addressed in Subsections 2.4.4.4 and 2.4.5.4.

The analysis methods and the consideration of the different CO and chugging load cases were the same methods used for the S/RVDLs. A description of these methods can be found in Subsection 5.3.3.2.3.

#### 6.3.3.2.3 S/RV Discharge Drag Loads

The loads addressed in this subsection are the T-quencher water jet loads and T-quencher air bubble-induced drag loads as experienced by the torus internal piping.

All submerged segments of the torus internal piping systems are subjected to T-quencher air bubble-induced drag loads, while only two lines, the RCIC and HPCI pump suction strainers, are subjected to T-quencher water jet loads. The T-quencher water jet loads on these two strainers are bounded by the T-quencher air bubble drag loads, which immediately follow in the event sequence.

The T-quencher air bubble drag loads act on the submerged piping as harmonic drag forces oscillating within the range of 5 to 15 Hz. All torus internal piping systems listed in Table 6.8, with the exception of containment spray piping which has no submerged portions, were analyzed for T-quencher air bubble drag loads. The analyses were performed with equivalent static loadings determined from the peak oscillating load, defined for each individual pipe and support segment, multiplied by a DLF. The driving frequencies from the oscillating bubbles were selected from the possible range of 5 to 15 Hz, such that the DLFs were maximized. Since all submerged piping have their first mode frequencies above 15 Hz, a

driving frequency of 15 Hz was chosen for all cases. The damping values used for these analyses were 1% and 2% of critical for piping diameters  $\leq 12"$  and  $> 12"$  respectively.

#### 6.3.3.2.4 Torus Shell Motion

The dynamic torus shell motion effects on attached internal piping were evaluated in the same manner as for the external piping, as described in Subsection 6.2.3.3.1. The analyses were performed as multilevel response spectral analyses with loading applied independently at each penetration attachment point and support to the torus shell. For piping configurations with multiple shell attachment points (penetration plus one or more supports), the results obtained from excitation applied at individual levels were combined by absolute summation, conservatively simulating out-of-phase motion. The torus attachment points were modeled as rigid anchors for these analyses to ensure consistency with the development of the coupled torus/pipe response. The load cases considered were the same as those considered for the external piping as described in Subsection 6.2.3.3.1. Damping values, as well as directional and modal combination methods, used were also identical to the corresponding items for external piping evaluations. The dynamic, relative displacement effects between the penetration and other restrained boundaries of the piping systems were evaluated separately as static load cases. The results from these static analyses were added to the inertial effects for support evaluations, but were evaluated separately from the inertial effects in the Code piping stress verifications.

#### 6.3.3.2.5 Containment Piping and Thermal Operating Loads

As with the external piping systems (Subsection 6.2.3.3.2), each internal piping system was evaluated under a complete set of design and operating loads. Thus, in addition to the hydrodynamic loads discussed above, piping analyses were performed for dead weight, internal pressure, seismic (OBE and SSE), thermal expansion and



thermal anchor movements. These analyses were based on the original load definitions and the FSAR.

The results from these analyses were combined with the hydrodynamic suppression pool-related load effects for evaluation of torus penetrations, pipe stresses, and pipe supports.

#### 6.3.3.3 Internal Piping Support Evaluation

Support load combinations were generated from the individual piping load case analyses for Level A, B, C, and D Service Limits as defined in Table 6.7. The majority of the torus internal piping systems are short, unsupported cantilevers transmitting all loads directly to the torus shell penetrations. Lines having additional supports to the ring girders or the torus shell are the HPCI and RCIC turbine exhaust and condensate drain lines, the RHR pump test lines, and the containment spray header.

The support load combinations were performed in a manner similar to those for the external piping described in Subsection 6.2.3.4. Thus, the modified SRSS method was used for combining a maximum of two load cases, with any additional dynamic cases in the same combination being added by absolute summation. The submerged structure drag loads were combined with the corresponding applicable torus motion load cases.

As a conservative measure for the support design evaluation, no distinction was made in the load combinations between primary and secondary (imposed displacement) loads. The support reactions due to thermal expansion and thermal anchor displacements were included in the combinations for all service limits, and the displacement effects caused by dynamic load cases were included with the corresponding primary inertia load effects in Levels B, C, and D Service Limit combinations.



Supports for torus internal piping were analyzed as linear elastic structures subject to static equivalent design loads. The design loads included piping loads in addition to LOCA pool swell impact, drag, and fallback loads on the support structures above the high water line. Below the high water line, supports were evaluated for submerged structure drag loads.

Reactions at the support attachment points to the ring girder and torus shell were considered in the torus shell evaluations (Subsections 3.1 and 3.5).

#### 6.3.4 Code Evaluation

This Subsection describes the Code evaluation of the torus internal piping and supports for the design load combinations summarized in Table 6.7.

##### 6.3.4.1 Internal Piping

The piping stress results were combined in accordance with the bounding load combinations in Table 6.7. Comparisons were made between actual maximum pipe stresses for these combinations and applicable Code allowables for Level A through D Service Limits as per stress equations 8 through 11 in Subarticle NC-3650 of the Code. The stress allowables are addressed separately in Subsection 6.3.2.1. Table 6.2 provides as an example the allowable stresses for material specification SA-106 Grade B.

With the exception of the demineralized water inlet pipe, which is discussed below, all torus internal piping was shown to satisfy the Code stress requirements as referenced in the previous paragraph.

The demineralized water inlet pipe (penetration X-228) is not used and is therefore capped immediately outside the torus shell. The internal portion of this pipe was subjected to a complete set of load case analyses as discussed in Subsection 6.3.3. The maximum

stresses for this pipe under Level A, C, and D Service loadings were within Code allowables. For Level B Service loading, one location remote from the torus penetration had a maximum stress exceeding the Service Level B allowable by 24%. This stress level was below the Service Level C allowable and was well below the yield strength. Assurance against gross failure has therefore been demonstrated. Since the pipe has no pressure-retaining function, this local Level B Service Limit overstress is considered acceptable.

The load case combination methods used for the Code stress evaluation of the torus internal piping correspond directly to those used for the external piping as described in Subsection 6.2.4.1.

#### 6.3.4.2 Internal Piping Supports

All existing pipe support components were qualified to the design criteria.

### 6.4 TORUS INTERNAL STRUCTURES

This subsection describes the evaluations of the non-essential structural components located in the wetwell. These structures are the monorail beam and the platform system. Although these systems serve no containment safety function, evaluation is required to ensure that they do not damage other safety-related components.

#### 6.4.1 Design Load Combinations

Table 3.1 shows the 27 design load combinations for torus internal structures and the appropriate service limits. This table is taken directly from the PUAAG. The number of design load combinations can be reduced due to the configuration of the internal structures in the torus.

#### 6.4.1.1 Platform System

The platform system consists of framing, grating, handrails, and ladders located above the pool surface, as well as support columns extending either into the suppression pool or, in a few locations, to the top of the torus. For portions of the platform above the high water level, the only design loads are pool swell-related loads and platform dead weight, for which Level E Service limits are specified in the PUAAG. For the support columns, the design load cases are shown in Table 6.9.

#### 6.4.1.2 Monorail Beam

The monorail beam is only subjected to froth impingement loads. Evaluations are performed for this load plus monorail dead weight. Level E Service limits are specified in the PUAAG for this combination.

#### 6.4.2 Design Allowables

The torus internal structures are classified as component supports governed by Subsection NF-3000 of the Code. Allowable stresses are evaluated using Appendix XVII of the Code.

The special non-Code Level E Service limit defined in the Structural Acceptance Criteria has not been explicitly applied to any torus internal structure. Any structural member that becomes a missile in the torus could damage some of the relatively thin-walled safety-related systems, such as the downcomers. Thus, in the design of non-safety-related structures, Level D Service limits are applied to ensure that the structure has adequate strength to remain integral throughout the postulated accident. Use of Level D Service Limits provides a more restrictive design criteria than use of the special Level E Service Limit. Therefore, Level D Service Limits were specified for all Level E Service load combinations.

### 6.4.3 Analysis Methods and Results

This subsection discusses the analysis methods for the non-essential torus internal structures. Since these structures are not safety-related, their functionality may be impaired during a LOCA. For evaluating the dynamic nonlinear response of these structures, the ductility was included in calculating the DLF. This procedure for calculating a DLF for a single dof nonlinear structure is described in Reference 48. A ductility ratio of three was used in all equivalent static analyses.

#### 6.4.3.1 Platform System

Platform system components were separated into horizontal members (grating, framing, handrails, and ladders) and support members. Reactions from the platform system on the torus shell ring girder were considered in the evaluation of the ring girder (Section 3).

##### 6.4.3.1.1 Horizontal Members

Loads acting on the horizontal members of the platform framing system are caused by pool swell impact, followed by drag, pool fallback, and froth impingement, as described in Section 2.

Equivalent static design loads were applied to each individual member of the platform. Natural frequencies of each structure were evaluated, including the effect of added mass (Reference 41), to account for fluid mass moving past the structure. In addition, 5% of the prescribed vertical load was applied in the horizontal direction in order to approximately account for the horizontal load component.

##### 6.4.3.1.2 Support Columns

Platform support columns were analyzed for design loads using equivalent static analyses. Evaluations were performed using the

procedures described in Subsection 6.3.3 of this section. Design loads included submerged structure drag loads for the submerged portion of the columns and froth impingement loads for the columns located in the torus airspace. The added mass effect of column submergence was included in estimating the column natural frequencies.

#### 6.4.3.2 Monorail Beam

Equivalent static analyses were performed on the monorail beam, considering uniform froth impingement loading in both the horizontal and vertical directions. Reactions at the monorail support attachments to the torus shell were considered in the torus shell evaluations (Section 3).

#### 6.4.4 Code Evaluation

This Subsection describes the Code evaluation for the platform system and monorail beam for the design load combinations summarized in Subsection 6.4.2.

##### 6.4.4.1 Platform System

The platform framing members and support columns were designed in accordance with the Limit Analysis Design rules of the Code Appendices XVII and F. A Level D Service load factor of 1.1 has been used in compliance with the provisions of Appendix F. The support columns were assumed not to yield in performing this limit analysis. All beam-column connections are detailed to develop full ductility of the members. (Inclined struts are also considered columns.)

All structural components of the platform system are therefore within design allowables. The columns have a minimum stress margin of 15%.

#### 6.4.4.2 Monorail Beam

Stresses at all locations in the monorail beam were found to be within allowables. Stresses were checked in the beam, the bolted connections, and in the monorail supports.



Table 6.1

BOUNDING LOAD CASE COMBINATIONS FOR TORUS ATTACHED EXTERNAL PIPING

Event Combination	EQ	SRV	SRV + EQ	SBA/IBA + SRV	SBA/IBA + SRV + EQ	DBA + SRV + EQ	DBA + SRV + EQ
Type of Earthquake	O	-	S	-	S	S	S
Combination No. (5)	-	1	3	11	15	25	27
Service Level	B	B	C	C	D	D	D
<hr/>							
Loads:							
Normal	X	X	X	X	X	X	X
Thermal Exp.	X	X	X	X	X	X	X
Pipe Pressure	X	X	X	X	X	X	X
Earthquake	X	-	X	-	X	X	X
S/RVD	-	X(1)	X(2)	X(2)	X(2)	X(3)	X
LOCA:							
Pool Swell	-	-	-	-	-	X	-
CO	-	-	-	X(4)	X(4)	-	X(4)
Chugging	-	-	-	X(4)	X(4)	-	X(4)

Notes:

- (1) S/RVD case bounding A1.1 and C3.1 is used.
- (2) S/RVD case bounding A1.2, A2.2, A3.2, C3.2, and C3.3 is used.
- (3) S/RVD case A1.3.
- (4) When CO and Chugging are included in the same combination, the bounding case is used.
- (5) From Table 5.1.

Table 6.2

TORUS ATTACHED PIPING STRESS ALLOWABLES

ASME Subsection NC-3650 <u>Stress Equations</u>	<u>Stress Limit</u>	<u>Allowable Stress (ksi) (2)</u>
8	$S_h$	15.0
9B	$1.2S_h$	18.0
9C	$1.8S_h$	27.0
9D	$2.4S_h$	36.0
10	$1.25S_h + 0.25S_c$	22.5
11	$2.25S_h + 0.25S_c$	37.5

Notes:

- (1) B, C, and D refer to Service Levels
- (2) Allowable stresses for SA-106 Grade B steel at design temperature

Table 6.3

TORUS PIPE PENETRATIONS AND ASSOCIATED  
ANALYSIS MODELS FOR EXTERNAL PIPING

Penetration Number	Piping Model Number	Line Size (in.)	Description	Notes
X-203A	1	1	Oxygen Analyzer	(1)
X-203B	2	1	Oxygen Analyzer	(1)
X-205	3	20	Vacuum Relief from Bldg. and Vent Purge Inlet	(1)
X-206A	4	1	Liquid Level Indicator	(2)
X-206B	4	1	Liquid Level Indicator	(2)
X-206C	5	1	Liquid Level Indicator	(2)
X-206D	5	1	Liquid Level Indicator	(2)
X-209A	6	1	Air and Water Temperature	(3)
X-209B	6	1	Air and Water Temperature	(3)
X-209C	6	1	Air and Water Temperature	(3)
X-209D	6	1	Air and Water Temperature	(3)
X-210A	7	18	RHR Pump Test Line	(2)
X-210B	8	18	RHR Pump Test Line	(2)
X-211A	7	6	Containment Cooling to Spray Header	(2)
X-211B	8	6	Containment Cooling to Spray Header	(2)
X-212	9	12	RCIC Turbine Exhaust	(1)
X-213A	10	8	Torus Drain	(1)
X-213B	11	8	Torus Drain	(1)
X-214	12	24	HPCI Turbine Exhaust	(1)
X-215	13	1	Atmospheric Pressure Instrumentation	(1)
X-220	14	16	Vent Purge Outlet	(1)
X-221	15	2	RCIC Condensate Drain	(1)
X-222	16	2	HPCI Condensate Drain	(1)
X-223A	17	10	Core Spray System Pump Test Line	(1)
X-223B	18	10	Core Spray System Pump Test Line	(1)
X-224	19	6	RCIC Pump Suction	(1)
X-225A	20	20	RHR Pump Suction	(2)
X-225B	20	20	RHR Pump Suction	(2)
X-225C	21	20	RHR Pump Suction	(2)
X-225D	21	20	RHR Pump Suction	(2)
X-226	22	16	HPCI Pump Suction	(1)
X-227A	23	16	Core Spray Pump Suction	(2)
X-227B	23	16	Core Spray Pump Suction	(2)
X-228	-	10	Demineralized Water Inlet	(4)

Table 6.3 (Continued)

TORUS PIPE PENETRATIONS AND ASSOCIATED  
ANALYSIS MODELS FOR EXTERNAL PIPING

Penetration Number	Piping Model Number	Line Size (in.)	Description	Notes
X-229A	24	1	Vacuum Breaker Actuating Air	(2), (3)
X-229B	24	1	Vacuum Breaker Actuating Air	(2), (3)
X-229C	24	1	Vacuum Breaker Actuating Air	(2), (3)
X-229D	24	1	Vacuum Breaker Actuating Air	(2), (3)
X-229E	24	1	Vacuum Breaker Actuating Air	(2), (3)
X-229F	24	1	Vacuum Breaker Actuating Air	(2), (3)
X-229G	24	1	Vacuum Breaker Actuating Air	(2), (3)
X-229H	24	1	Vacuum Breaker Actuating Air	(2), (3)
X-229J	24	1	Vacuum Breaker Actuating Air	(2), (3)
X-229K	24	1	Vacuum Breaker Actuating Air	(2), (3)
X-229L	25	1	Vacuum Breaker Actuating Air	(2), (3)
X-229M	25	1	Vacuum Breaker Actuating Air	(2), (3)

Notes:

- (1) Torus pipe penetration associated with unique piping model.
- (2) Piping associated with two or more penetrations interconnected in the same piping model.
- (3) Similar piping configurations associated with two or more penetrations represented by generic model.
- (4) Pipe is capped immediately outside torus shell; no analysis performed for external piping.

Table 6.4

LARGE BORE TORUS ATTACHED EXTERNAL PIPING  
REPRESENTATIVE MAXIMUM STRESSES

Penetration No.	Maximum stress (ksi) for torus motion load cases (1)				
	S/RVD (2)		DBA LOCA		
	<u>A1.1</u>	<u>A2.2</u>	<u>Pool Swell</u>	<u>CO</u>	<u>Chugging</u>
X-205	1.1	1.6	(3)	2.2	1.6
X-210A/-211A	3.0	9.7	1.4	11.6	5.0
X-210B/-211B	5.1	10.1	2.6	15.4	7.0
X-212	13.9	6.6	5.0	10.7	8.6
X-214	4.1	2.7	2.4	6.2	2.3
X-220	4.8	5.6	2.3	10.7	5.1
X-223A	12.5	11.8	6.3	26.6	8.5
X-223B	4.8	7.1	1.5	8.5	4.6
X-224	6.1	6.6	2.8	9.5	2.8
X-225A/B	5.3	4.9	1.5	6.2	3.5
X-225C/D	11.2	10.9	4.1	10.3	4.2
X-226	1.6	4.7	1.1	2.1	1.4
X-227A/B	8.3	10.9	3.5	12.7	20.9

Notes:

- (1) The stress results refer to the dynamic, inertia portion of the torus motion.
- (2) Stress results for other S/RVD cases obtained by scaling of cases A1.1 and A2.2 (see Table 6.5).
- (3) This load case was not explicitly analyzed. Bounding DBA-LOCA case was conservatively used in the code compliance verification.

Table 6.5

SCALE FACTORS TO BE USED ON COUPLED S/RV  
RESPONSES TO OBTAIN ALL S/RV LOAD CASES

Load	Event	No. of Valves	Actuation	Load Case	Scale Factor	Base Load Case
1	NOC	8	CVA	C3.1	1.41	6ADS
2	NOC	1	FVA	A1.1	1.09	SVA
3	IBA/SBA	8	CVA	C3.2	1.41	6ADS
4	IBA/SBA	6 (ADS)	FVA	A2.2	1.0	6ADS
5	DBA	1	FVA	A1.3	1.0	SVA
6	IBA/SBA (1)	1	FVA	A1.2	use load 2	
7	NOC (1)	8	FVA	A3.1	use load 1	
8	IBA/SBA (1)	8	FVA	A3.2	use load 3	
9	IBA/SBA (2)	8	CVA	C3.3	0.0	N/A

Notes:

- (1) Loads for these cases have not been specifically evaluated. Bounding loads for these cases are provided.
- (2) For load case C3.3 (steam in S/RVDL), zero torus shell pressure loads are assumed.



Table 6.6

LARGE BORE TORUS ATTACHED EXTERNAL PIPING  
MAXIMUM STRESS AS A PERCENTAGE OF ALLOWABLES  
FOR BOUNDING LOAD COMBINATIONS

<u>Penetration Number</u>	<u>ASME Code NC-3650 Stress Equations</u>				
	<u>8</u>	<u>9B<sup>(1)</sup></u>	<u>9C<sup>(1)</sup></u>	<u>9D<sup>(1)</sup></u>	<u>11<sup>(2)</sup></u>
X-205	10	66	92	70	73
X-210A/-211A	31	76	61	55	99
X-210B/-211B	44	68	55	53	36
X-212	23	83	64	67	26
X-214	44	57	46	38	77
X-220	10	72	99	87	5
X-223A	35	78	60	60	91
X-223B	39	59	56	57	59
X-224	19	67	97	68	59
X-225A/B	19	45	42	38	93
X-225C/D	32	83	99	91	63
X-226	18	45	59	46	82
X-227A/B	22	90	98	90	50

Notes:

- (1) B, C, and D refer to Service Levels for stresses caused by occasional loads.
- (2) As allowed by Subparagraph NC-3652.3, the requirements of equation 11 were in lieu of equation 10 requirements.

Table 6.7

BOUNDING LOAD COMBINATION FOR TORUS ATTACHED INTERNAL PIPING

Event Combination	EQ	SRV	SRV + EQ	SBA/IBA + SRV	SBA/IBA + SRV + EQ	DBA + SRV + EQ	DBA + SRV + EQ
Type of Earthquake	O	-	S	-	S	S	S
Combination No. (1)	-	1	3	11	15	25	27
Service Level	B	B	C	C	D	D	D
<hr/>							
<u>Loads:</u>							
Normal	X	X	X	X	X	X	X
Thermal Exp.	X	X	X	X	X	X	X
Pipe Pressure	X	X	X	X	X	X	X
Earthquake	X	-	X	-	X	X	X
<u>S/RVD:</u>							
Air Bubble Drag	-	X	X	X	X	X	X
Torus Motion	-	X	X	X	X	X	X
<u>LOCA:</u>							
Pool Swell							
Impact/Drag	-	-	-	-	-	X	-
Froth Impingement	-	-	-	-	-	X	-
Pool Swell							
Torus Motion	-	-	-	-	-	X	-
Water Jet	-	-	-	-	-	X	-
Air Bubble Drag	-	-	-	-	-	X	-
CO Drag Loads (2)	-	-	-	X	X	-	X
CO Torus Motion (2)	-	-	-	X	X	-	X
Chugging Drag							
Loads (2)	-	-	-	X	X	-	X
Chugging Vent							
Motion (2)	-	-	-	X	X	-	X

Notes:

(1) From Table 5.1.

(2) The bounding combination of drag loads and torus motion loads from the CO and chugging phases, respectively, was used.

Table 6.8

TORUS PIPE PENETRATIONS AND ASSOCIATED  
ANALYSIS MODELS FOR INTERNAL PIPING

Penetration Number	Piping Model Category (1)	Line Size (in.)	Description
X-210A	2	18	RHR Pump Test Line
X-210B	2	18	RHR Pump Test Line
X-211A	4	6	Containment Cooling to Spray Header
X-211B	4	6	Containment Cooling to Spray Header
X-212	3	12	RCIC Turbine Exhaust
X-214	3	24	HPCI Turbine Exhaust
X-221	2	2	RCIC Condensate Drain
X-222	2	2	HPCI Condensate Drain
X-223A	2	10	Core Spray System Pump Test Line
X-223B	2	10	Core Spray System Pump Test Line
X-224	1	6	RCIC Pump Suction
X-225A	1	20	RHR Pump Suction
X-225B	1	20	RHR Pump Suction
X-225C	1	20	RHR Pump Suction
X-225D	1	20	RHR Pump Suction
X-226	1	16	HPCI Pump Suction
X-227A	1	16	Core Spray Pump Suction
X-227B	1	16	Core Spray Pump Suction
X-228	2	10	Demineralized Water Inlet (2)

Notes:

- (1) For analysis purposes, the lines were grouped in four categories:
- (1) T-shaped suction strainers
  - (2) Partially submerged discharge piping
  - (3) Turbine exhaust spargers
  - (4) Containment spray header.
- (2) The demineralized water inlet pipe is not used; it is capped immediately outside the torus shell.

Table 6.9

DESIGN LOAD CASES FOR PLATFORM SUPPORT COLUMNS

<u>Load Cases</u>	<u>Service Level</u>
T-quencher Bubble Drag	A
DBA CO	E
Chugging + T-quencher Bubble Drag	E
LOCA Bubble Drag + T-quencher Bubble Drag	E

COOPER NUCLEAR STATION

PLANT UNIQUE ANALYSIS REPORT

SECTION 7

POOL TEMPERATURE EVALUATION

## 7.1 INTRODUCTION

Cooper Nuclear Station takes advantage of the large thermal capacitance of the suppression pool during plant transients requiring S/RV actuation. Steam is discharged from the main steam lines, through the S/RVs and S/RVDLs, and into the suppression pool where it is condensed. This condensation results in an increase in the temperature of the suppression pool water. Although stable steam condensation is expected at all pool temperatures, the NRC has imposed a local temperature limit of 200°F in the vicinity of the T-quencher discharge devices (Reference 11). The NRC has also imposed design requirements for a suppression pool temperature monitoring system to ensure that plant Technical Specification requirements are met.

This section describes the plant unique transient analyses for suppression pool temperature to demonstrate satisfaction of the 200°F limit. This section also describes the pool temperature monitoring system design as it pertains to the NRC requirements.

## 7.2 DESIGN TRANSIENTS AND INITIAL CONDITIONS

In order to demonstrate that the 200°F temperature limit imposed by the NRC is satisfied, the Commission has required that the following events be analyzed for local pool temperature response (Reference 49):

- (1) Stuck-open S/RV during power operation assuming reactor scram at 10 minutes after the suppression pool reaches a bulk pool temperature of 110°F and all pool-cooling systems are operable.
- (2) Same events as in (1) above, with only one RHR train operable.



- (3) Stuck-open S/RV during hot standby, assuming an initial 120°F bulk pool temperature and only one pool-cooling train operable.
- (4) Automatic Depressurization System (ADS) activated following a small line break, assuming an initial 120°F bulk pool temperature and only one pool-cooling train operable.
- (5) Primary system is isolated and depressurized at a rate of 100°F per hour with an initial 120°F bulk pool temperature and only one pool-cooling train operable.

NPPD's current licensing basis for transient analysis is to assume no single failure other than the single equipment malfunction or operator error which initiated the event. Therefore, the failure of one RHR loop, as requested in NRC events 2, 3, and 5 above, is beyond the currently accepted licensing basis for anticipated operational transients. Even though these events exceed the currently accepted licensing bases, to address the NRC request for such events with single failures, seven transient events have been identified. These seven transient events are summarized in Table 7.1. One of these seven events is expected to result in the maximum long-term suppression pool temperature.

The following initial conditions were used in the analyses:

- Feactor operation at 104% of rated thermal power (2486 MWt).
- Suppression pool temperature at the normal power operation Technical Specification limit (95°F).
- Minimum Technical Specification suppression pool water volume (87,650 ft<sup>3</sup>).

- The suppression pool has no initial velocity.
- Wetwell and drywell airspaces are at nominal operating conditions.

### 7.3 MODEL DESCRIPTION

In order to properly model each of the seven transients and evaluate the local pool temperature, two computer codes were used in the analyses.

#### 7.3.1 Coupled Reactor and Suppression Pool Model

The first computer code uses a coupled RPV and suppression pool thermodynamics model, which is utilized to calculate the transient response of the suppression pool during long-term events which add heat to the pool. This model performs fluid mass and energy balances in the reactor primary system and the suppression pool, and calculates the reactor vessel water level, pressure, and the long-term response of the suppression pool bulk temperature. The various modes of operations of all important auxiliary systems, such as the S/RVs, MSIVs, ECCS, RHR system, and feedwater, are modeled. To simulate a specified reactor cooldown rate or depressurization rate, a rate of change of temperature or pressure may be imposed onto the reactor vessel. In addition, the model also simulates system set points (automatic and manual), and specified operator actions.

#### 7.3.2 Local Pool Temperature Model

The second computer code was used to calculate the water temperature in the vicinity of the quencher during S/RV discharge events which add heat to the pool. Results from the previous code, such as the mass and energy added to and removed from the pool during each transient (i.e., RHR and S/RV flows), were input into this code, along with pool geometry, submerged structures geometries, and pool initial conditions.

The overall local temperature analysis consists of two major coupled components: a momentum balance to solve for the bulk pool velocity and a two-dimensional energy model which superimposes the local recirculation on the bulk velocity to determine the temperature distribution in the pool.

The code calculations include the temperature in the bay(s) of discharge downstream of the quencher device, on the bay centerline, at elevations above and below the quencher device.

The local temperature is the average of the temperatures calculated in the vicinity of (above and below) the T-quencher in the downstream portion of the bay. The reported local temperatures correspond to the bay with the highest temperature calculated in this manner.

#### 7.4 POOL TEMPERATURE EVALUATION RESULTS

Long-term S/RV discharge transients have been analyzed assuming an initial pool temperature of 95°F (Technical Specification limit). Pool temperature results for the seven transients analyzed are presented in Table 7.1. Details of these analyses are contained in References 50 and 51.

The analysis of Case 2C (a demonstration case, i.e., normal depressurization at isolated hot shutdown) shows a maximum local pool temperature of 188°F. This demonstrates that with no system failures and in the event of a non-mechanistic scram, depressurizing the RPV with S/RVs at 100°F/hr results in local pool temperatures that are well below the condensation stability limit set by the NRC ( $T_{\text{local}} = 200^{\circ}\text{F}$ ).

Case 1A (stuck-open relief valve (SORV) at power with one RHR loop available) and case 2A (reactor rapid depressurization after isolation with one RHR loop available) resulted in maximum local pool temperatures of 196°F and 198°F, respectively. High local

temperatures are present in this case due to reduced mixing when the available RHR system is assumed to be switched to a non-pool-cooling mode.

The maximum local pool temperatures of all other cases also remained below 200°F throughout the transient. In general, local-to-bulk temperature differences at the time of maximum temperatures are about 12°F for cases where two RHRs are assumed available, and about 20°F for cases where one RHR is assumed available. Thus, bulk pool circulation induced by RHRs leads to good thermal mixing, which effectively lowers the local pool temperatures in the vicinity of quencher devices.

Additional analyses show that long-term pool temperatures following a LOCA and Net Positive Suction Head (NPSH) available for the standby cooling pumps are well within required limits.

#### 7.5 POOL TEMPERATURE MONITORING SYSTEM

The NRC Regulatory Guide 1.97 gives specific requirements for torus temperature monitoring of plants under construction. However, operating plants are directed to follow the requirements of NUREG-0737 (i.e. TMI action plan requirements). The issue of torus temperature monitoring is not addressed by NUREG-0737; however, the CNS system has been designed to comply with the basic intent of Reg. Guide 1.97.

The requirements of the SER (Reference 11) were also met by the pool temperature monitoring system. Satisfaction of these requirements is summarized below:

- (1) Redundant pool temperature monitors are located on the torus shell at each quencher. This placement meets the SER requirements for demonstrating a sufficient number and distribution of pool temperature sensors. The Technical Specification limits will be derived from the calculated

bulk pool temperature difference transient. This calculation will be performed by the future plant process computer to be installed by NPPD. Provisions for computer input signals are included in the system design.

- (2) Temperature sensors are located five feet below the minimum suppression pool water level to assure proper pool temperature monitoring.
- (3) An indicating recorder is provided in the control room. The determination of bulk pool temperature is dependent on the development of computer software for the future plant process computer.
- (4) Alarm set points are established by NPPD consistent with the Technical Specification pool temperature limits.
- (5) All sensors are designed to Seismic Category I, Quality Group B. The thermowells are provided in accordance with the GE Quality Assurance Program described in topical report NEDO 11209-04A. The sockolets are provided in accordance with the requirements of ASME Section III Articles NE-2311(D) and NE-2121(C). Seismic and environmental qualification tests were conducted by the RTD manufacturer. The system is energized from onsite emergency power supplies.

The environmental design requirements for the Reactor Building are summarized in Table 7.2. Any cable or equipment related to the pool temperature monitoring system meets these requirements.

Table 7.1

SUMMARY OF RESULTS  
COOPER POOL TEMPERATURE RESPONSE (1)

<u>Case No.</u>	<u>Event</u>	<u>Number of S/RVs Manually Opened</u>	<u>Maximum Cooldown Rate (°F/hr)</u>	<u>Maximum Bulk Pool Temperature (°F)</u>	<u>Maximum Local Pool Temperature (°F)</u>
1A	SORV at Power, 1 RHR Loop	2	995 (2)	167	196
1B	SORV at Power, Spurious Isolation, 2 RHR Loops	1	503	179	198
2A	Rapid Depressurization at Isolated Hot Shutdown, 1 RHR Loop	5	900	172	198
2B	SORV at Isolated Hot Shutdown, 2 RHR Loops	1	503	161	181
2C	Normal Depressurization at Isolated Hot Shutdown, 2 RHR Loops	5	100	171	188
3A	SBA - Accident Mode, 1 RHR Loop	6 (ADS)	4,500	171	195
3B	SBA - Failure of Shutdown Cooling Mode, 2 RHR Loops	5	100	170	180

Notes:

(1) Initial pool temperature = 95°F.

(2) When the main condenser is available.



Table 7.2

ENVIRONMENTAL REQUIREMENTS FOR DEVICES TO BE  
MOUNTED IN HARSH ENVIRONMENTS

<u>Environmental Conditions</u>	<u>Design Requirements Reactor Building, Auxiliary Building</u>
<u>TEMPERATURE</u>	
Normal	40°F Minimum 120°F Normal 150°F Maximum for one day per year Duration: For Equipment Qualified Life
Abnormal	235°F for 6 hours 135°F for next 24 hours 120°F for next 99 days
<u>STATIC PRESSURE</u>	
Normal	$\pm 2$ psig
Abnormal	+ 5 psig for 6 hours followed by + 2 psig for 24 hours
<u>RELATIVE HUMIDITY</u>	
Normal	20% Minimum 50% Normal 90% Maximum
Abnormal	Steam for 6 hours followed by 100% for 24 hours
<u>RADIATION</u>	
Normal	$1 \times 10^5$ Rad total integrated dose, gamma accumulated in a 40-year life
Abnormal	$3 \times 10^7$ Rad total integrated dose, gamma

COOPER NUCLEAR STATION

PLANT UNIQUE ANALYSIS REPORT

SECTION 8

APPENDICES AND REFERENCES

## APPENDIX A

### ADAPTATION OF THE SRSS METHOD FOR COMBINED TORUS SHELL PRESSURES FOLLOWING MULTIPLE S/RV ACTUATIONS

#### A.1 INTRODUCTION

Following the actuation of a Safety/Relief Valve (S/RV), the discharging air forms an oscillating and rising bubble within the suppression pool. As a result of this phenomenon, periodic positive and negative pressure loads are induced on the wetted portion of the torus shell. These pressure transients decay both in time and in distance (i.e., attenuate longitudinally and circumferentially along the torus). In the case of single valve actuation, the pressure transient is determined using the semi-empirical computer code QBUBSO2. For the case of multiple valve actuation, a suitable method of combining the individual pressure waves must be established. For the peak torus shell pressures, two different methods of calculation are considered. With the first method, the peak pressure is determined by taking the square root of the sum of the squares of the participating pressure peaks (SRSS method). With the second method, the peak is determined by linearly adding the participating pressure waves (Linear Addition method)\*. Although the two methods do not yield the same result, a general pattern can be expected with regard to relative magnitudes of the peaks calculated by SRSS and Linear Addition. The purpose of this study is to determine the form of this pattern and to assess the conservatism in using SRSS methodology for combining the peak torus shell

---

\* A special form of Linear Addition assumes that all the component waves are in phase, and combines the peaks of the component waves by linear superposition. This method is called the absolute sum (ABSS) method. Although this is a conservative approach, it is unrealistic due to the fact that in-phase bubble formation is extremely unlikely. In this study, the ABSS method is implicitly contained in the method of Linear Addition.

pressures during multiple valve actuations. Since the problem involves variables of a random nature, a statistical approach has been followed. Details of the analysis are presented in this appendix.

## A.2 COMBINED TORUS SHELL PRESSURE

The combined torus shell pressure at a particular location is due to the contribution of individual pressure waves originating from varying distances and having different waveforms. The CNS suppression pool geometry under consideration is shown in Figure A.1. A typical pressure wave is illustrated in Figure A.2. Up to eight of these waves (with different amplitude, frequency, and phase) can exist in the suppression pool during a multiple S/RV discharge event. The determination of combined peak pressure due to these waves is discussed in the following subsections.

### A.2.1 SRSS Method

With the SRSS method, the combined peak pressure due to multiple S/RV discharge is calculated as:

$$P_{srss} = \pm \sqrt{\sum_{i=1}^N (\alpha_i P_{oi})^2} \quad (1)$$

where:

- $P_{srss}$  = combined peak torus shell pressure at a given location using SRSS
- $P_{oi}$  = peak pressure at the torus bottom dead center under the T-quencher arm for valve "i"
- $N$  = number of valves actuating (equal to the number of pressure waves)
- $i$  = valve index
- $\alpha_i$  = spatial attenuation coefficient

With this method, the phase difference and time decay of individual pressure waves are not considered (i.e., all the waves are assumed to be in phase). Combined peak positive and peak negative pressures are determined by substituting the corresponding amplitudes into Equation 1 above.

### A.2.2 Linear Addition

With this method, individual pressure waves due to each actuating valve are added algebraically to yield the combined pressure wave due to multiple S/RV discharge. The equation in its general form is

$$P = \sum_{i=1}^N \alpha_i P_i(t) \quad (1a)$$

The method of Linear Addition is physically the correct procedure for combining the pressures due to multiple sources of disturbances. This is a consequence of the linearity of the phenomena which allows direct superposition of the individual effects. The difficulty in applying the method lies in the fact that, for problems of the kind considered here, the bubble oscillation frequencies and the phasing of different waves can not be known a priori. Thus, approximate alternatives (such as the SRSS method) which do not require such knowledge are preferred. The statistical procedure followed in this study, however, will allow valid conclusions to be drawn regarding the method of Linear Addition. Assuming that the component waves are sinusoidal in form and considering the time decay and phasing for each wave, Equation 1a has been approximated as:

$$P = \sum_{i=1}^N \alpha_i B_i(n) P_{oi} \sin \omega_i (t - \phi_i) \quad (2)$$

where:

$n$  = cycle number

$B_i$  = time decay coefficient for the  $n^{\text{th}}$  cycle of wave "i"

$\alpha_i$  = angular frequency

$t$  = time

$\phi_i$  = phase angle

The combined peak positive and peak negative pressures are determined by choosing the maximum and minimum, respectively, of the combined pressure wave as given by Equation 2 above. As can be

seen, the phase shift and time decay effects have been considered with this method.

A special form of Linear Addition assumes that all the participating pressure waves oscillate in-phase. This form is called the ABSS method. The combined peak pressure is found by linearly superimposing the peaks of the participating pressure waves. This method, in essence, amounts to assuming an identical frequency of oscillation for different bubbles and zero phase shift between waveforms (Equation 2). Since in this study both the angular frequency,  $\omega_i$ , and the phase angle,  $\phi_i$ , are treated as random variables, it is logical to assume that the method of ABSS is implicitly contained in the method of Linear Addition.

### A.3 PRESSURE WAVE CHARACTERISTICS AND STATISTICAL DATA

The analysis requires assembly of the data that describe the pressure wave characteristics for each S/RV discharge line. In general, each wave can be uniquely defined in terms of:

#### (1) Pressure Wave Characteristics

- First peak positive/negative amplitudes
- Frequency
- Time decay

#### (2) Pressure Arrival Time - time from the initiation of the event to the moment the pressure disturbance is felt at the suppression pool boundary.

For a given line geometry and initial conditions (e.g., pressure and temperature of the suppression pool), the pressure wave characteristics are all determined by the valve opening time. The pressure arrival time is further dependent on the reactor pressure rise rate, valve set point, and water clearing time (time from the S/RV actuation to the moment the pressure disturbance is felt at



the suppression pool). A schematic definition of these quantities is given in Figure A.3.

#### A.3.1 Pressure Wave Characteristics

Pressure wave characteristics for the S/RV discharge lines were determined for LOCA-SBA (Small Break Accident) first valve actuation conditions. Previous studies indicated that SBA conditions resulted in the most severe loading on the torus shell. Furthermore, the S/RV discharge lines were categorized into three groups according to the similarities in the pressure wave characteristics (refer to Figure A.1). A typical line was then chosen for each group and the wave characteristics were determined, using the computer codes QBUBSO2 and RVFORO4.

#### A.3.2 Statistical Test Data

Due to the random nature of the reactor pressure rise rate, valve set point variation, and total valve opening time, statistical test data were needed for realistic simulation of these variables.

##### A.3.2.1 Reactor Pressure Rise Rate

The pressure rise rate distribution for CNS (a BWR 4 plant) is shown in Figure A.4 (Reference 52). This distribution represents the probability density function for pressure rise rates for events opening more than 2/3 of the S/RV's, weighted by the relative occurrence of the events, and averaged over all reactor conditions anticipated during the last 40 percent of an operating cycle. The pressure rise rate for the SBA event is generally smaller than the data represented by Figure A.4 (Reference 53). Since higher pressure rise rates are more likely to produce higher combined peak pressures by Linear Addition (due to smaller phase shift), use of this data is conservative for the purpose of this study. The data of Figure A.4 has been used for all cases studied except for the ADS actuations, where the valves are considered to open simultaneously.

#### A.3.2.2 Valve Set Point Variation

The valve opening time, defined as the time from the valve actuation to the moment of maximum lift, has a normal distribution with a range of 5 to 90 msec (Reference 54). Since 0.998 of the population in a normal distribution is contained within six standard deviations, the valve opening time has been simulated by:

$$\text{mean} \quad (5+90)/2 = 47.5 \text{ msec}$$

$$\text{standard deviation} = (90-5)/6 = 14.2 \text{ msec}$$

#### A.4 ANALYSIS PROCEDURE

With the combined torus shell pressure as defined in Subsection A.2 and the pressure wave characteristics established in Subsection A.3, five different cases were studied and the results were compared. The cases considered are:

- (1) Eight multiple valve actuations (MVA)
- (2) Three adjacent MVA (S/RVs 71F, 71G, and 71H)
- (3) Three MVA with minimum phase difference (S/RVs 71A, 71E, and 71G)
- (4) Six valve ADS (Automatic Depressurization System) actuation
- (5) Three valve ADS actuation (with minimum phase difference, i.e., S/RVs 71A, 71E, and 71G).

The analyses were performed with a computer program utilizing a Monte Carlo method for the simulation of the random variables. This program calculates the combined peak torus shell pressure using SRSS and Linear Addition methods. Each case involved 400 trials, and during each trial random numbers were utilized to determine:

- (1) Reactor pressure rise rate (one for each trial)
- (2) Valve set point (one for each valve)
- (3) Total valve opening time (one for each valve)

The pressure wave characteristics were then determined using the relation discussed in Subsection A.3. The pressure arrival time was determined from:

$$t_a = (P_v - P_{ref}) / PRR + t_{wc} \quad (3)$$

where:

$t_a$  = pressure arrival time  
 $P_v$  = pressure at valve opening (randomly chosen)  
 $P_{ref}$  = reference pressure (taken as the minimum pressure at valve opening)  
 $PRR$  = reactor pressure rise rate  
 $t_{wc}$  = water clearing time (function of randomly chosen total valve opening time)

The combined peak pressures (both positive and negative) are calculated using Equation 1 for the SRSS method and Equation 2 for the Linear Addition method. For the Linear Addition method, the combined pressure wave is calculated so that at least one full cycle of each pressure wave is included. The combined pressure is calculated under the T-quencher arm of S/RVDL 71G where the maximum pressure was expected to occur. The results of the calculations were statistically analyzed to determine the distribution function and bounding factors.

#### A.5 RESULTS AND CONCLUSIONS

The results of the study corresponding to the five different cases analyzed are summarized in Table A.1. Each case was evaluated by the percentage of failures, where a failure is defined as the pressure calculated by Linear Addition being greater than the pressure calculated by SRSS (for negative pressures, absolute

values are compared). The corresponding 90 percent confidence intervals are also indicated in Table A.1. The results indicate that except for the case of six valve ADS actuation, the combined peak torus shell pressure is generally bounded by the Linear Addition method. To establish a general trend, the frequency (probability density) distributions of the peak pressure ratios (Linear Addition/SRSS) were also generated for the eight MVA case. These distributions are given in Figure A.5 for the positive and negative peaks. The corresponding mean and standard deviations are indicated on the respective graphs. The data were also examined for the phasing of the pressure waves, and it was found that:

- (1) The case of eight MVA produced the highest peak pressures.
- (2) With 90 percent confidence level, the SRSS method bounded 50 percent of the peak pressures for the eight MVA case.
- (3) The probability of having multiple valve actuation with in-phase pressure waves is extremely low.
- (4) The peak positive pressures are always greater than the peak negative pressures (absolute value)
- (5) The peak pressures calculated by Linear Addition have a wider range of variation.

Further examination of the results indicated that the SRSS method, with a multiplier of 1.2 applied to the peak pressures calculated by Equation 1, bound approximately 90 percent of the peak pressures (see Figure A.5). Thus, with Equation 1, modified as

$$P_{srss} = \pm 1.2 \sqrt{\sum_{i=1}^N (\alpha_i P_{oi})^2} \quad (3)$$

the analysis was repeated and it was found that:

With a 90 percent confidence level, the SRSS method bounds 85 percent of the peak pressures for the eight MVA case, and 97 percent for all the remaining four cases.

Since the eight-MVA case produces the highest torus shell pressure, the following conclusion, based on the eight MVA case, is reached:

- A multiplier of 1.2 is to be applied to the method of SRSS in determining the combined peak torus shell pressures. The result thus obtained is expected to bound 85 percent of the peak pressures calculated by Linear Addition. In the event that the calculated pressure exceeds the value determined by the LDR methodology, the lower value can be taken.

It was pointed out in Subsection A.3.1 that the study was based on the SBA first valve actuation event which produced the highest torus pressure loads. All the other cases are expected to produce lower peak pressures. Examination of Eqs. 1 and 2 indicate that any reduction in the peak pressure,  $P_{oi}$ , will be reflected in the combined pressure of Linear Addition by the same magnitude. The same reduction, however, will have a comparatively smaller effect on the combined pressure by SRSS due to the summation under the square root. Therefore, the ratio

$$k = \frac{\text{Combined Peak Pressure by Linear Addition}}{\text{Combined Peak Pressure by SRSS}}$$

is expected to remain nearly the same, with a tendency to drop. Thus, the results are conclusive in a general and conservative manner.

Table A.1

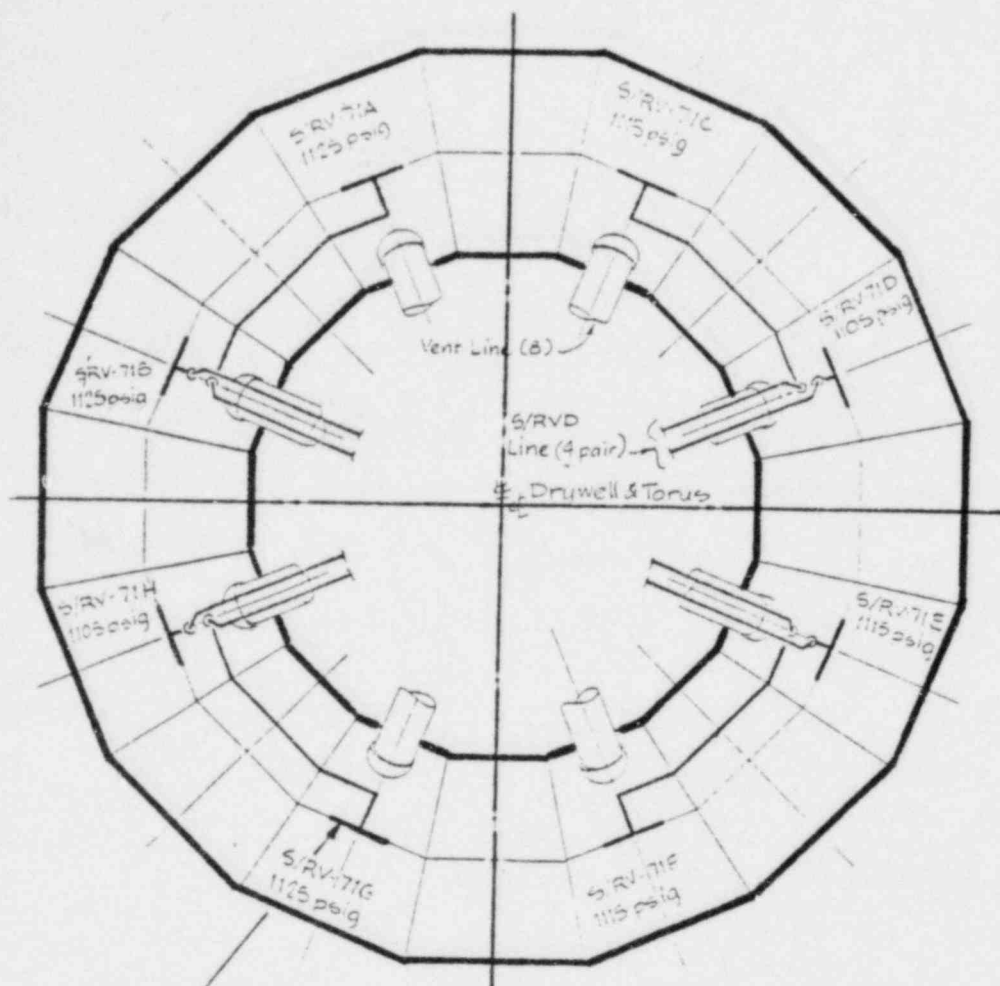
## SUMMARY OF PEAK PRESSURE COMPARISON

CASE	PERCENT FAILURE*			90 % CONFIDENCE LIMITS	
	Positive Peaks	Negative Peaks	Combined**	Lower Limit	Upper Limit
8 MVA	51	43	54	50	58
3 MVA (Lines F,G,H) -All Adjacent	49	42	52	48	52
3 MVA (Lines A,E,G)	48	51	57	53	61
6 ADS (Lines A,B,C,E,G,H)	1	3	3	2	4
3 ADS (Lines A,E,G)	96	78	96	94	98

\* A failure is defined as the combined peak pressure calculated by linear addition being greater than the combined peak pressure calculated by SRSS method.

\*\* Combined failure means failure of either the positive or the negative peak

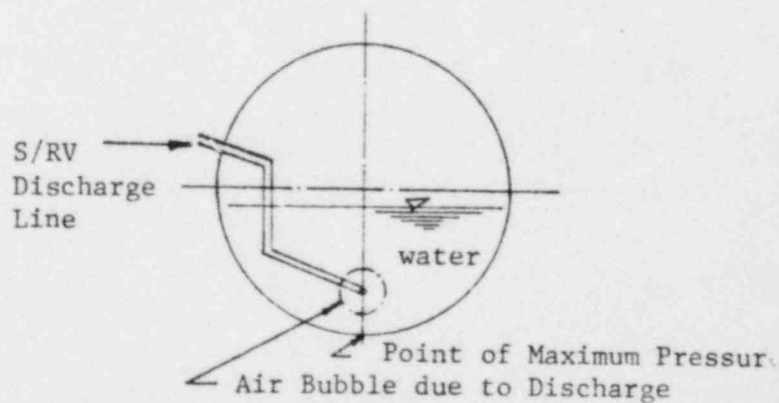




point of maximum pressure  
(See the sectional view below)

#### LINE GROUPS:

- Group 1: S/RV - 71D  
S/RV - 71E  
S/RV - 71F
- Group 2: S/RV - 71B  
S/RV - 71C  
S/RV - 71H
- Group 3: S/RV - 71A  
S/RV - 71G



Section View of the Torus

FIGURE A.1

SUPPRESSION POOL GEOMETRY AND S/RV DISCHARGE LINES

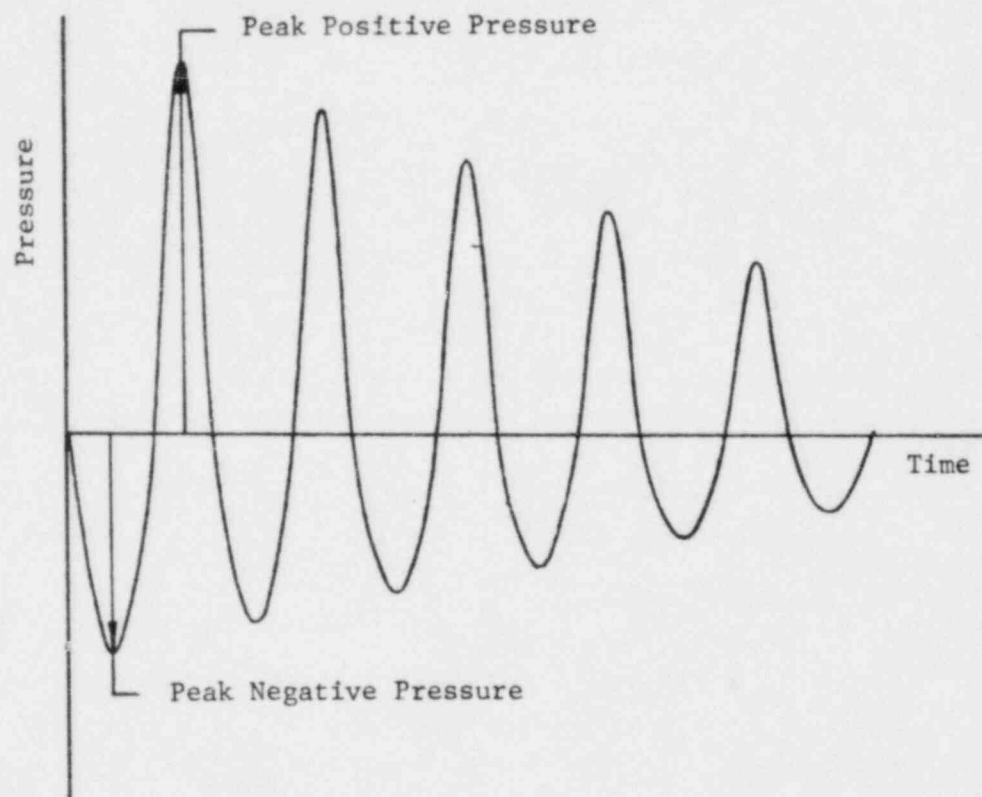


FIGURE A.2  
TYPICAL PRESSURE WAVE

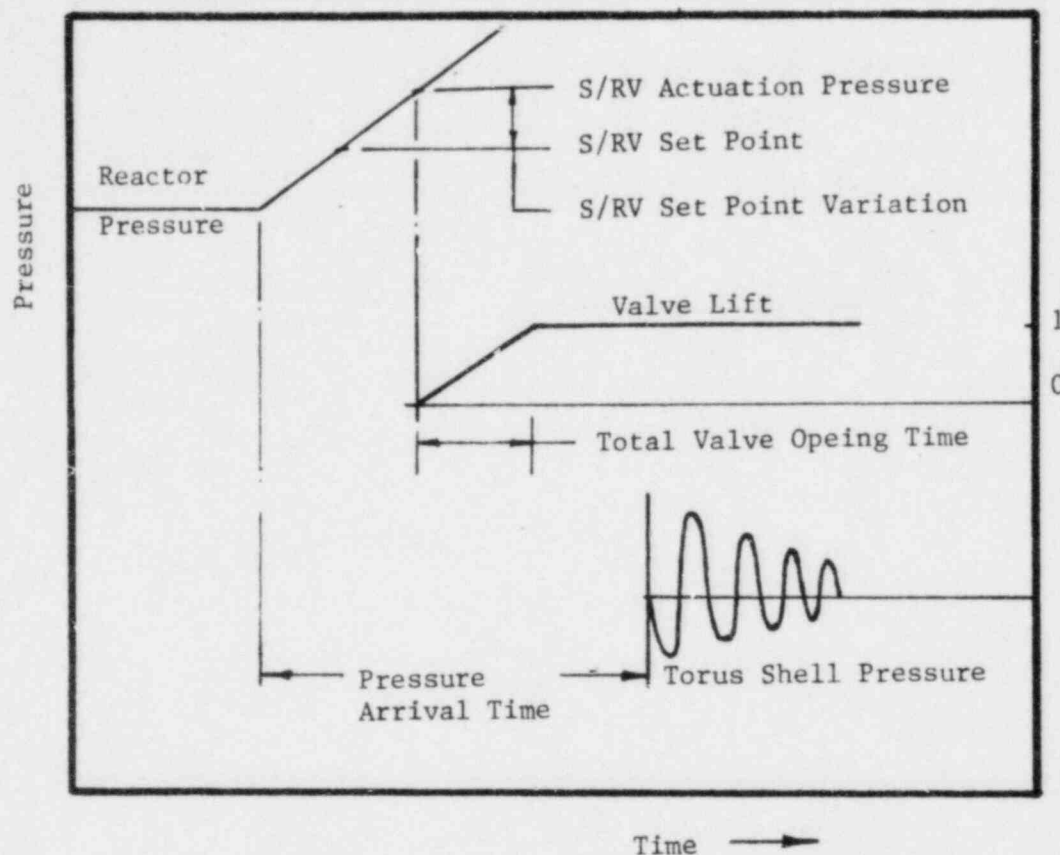


FIGURE A.3

SEQUENCE OF S/RV DISCHARGE EVENTS

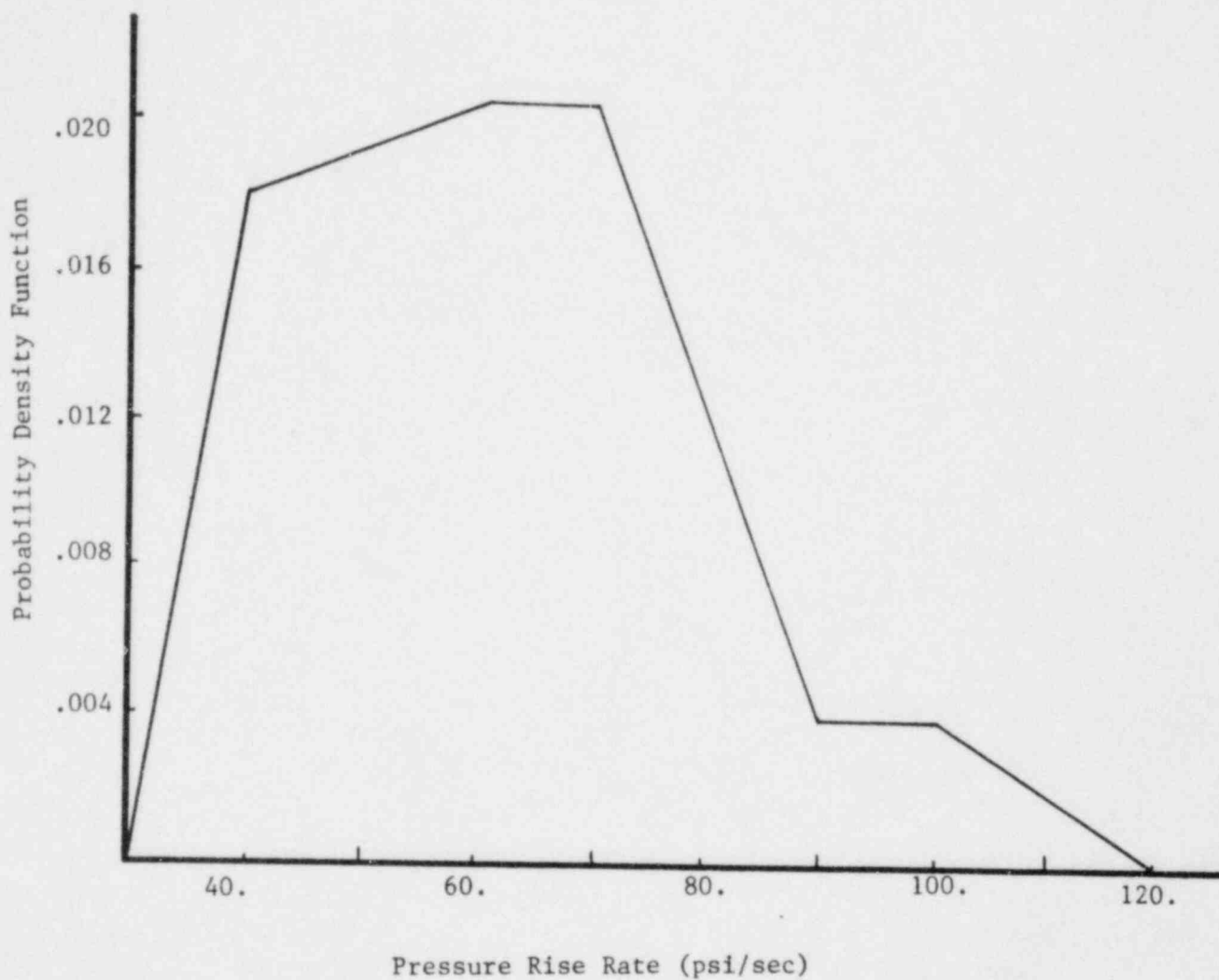
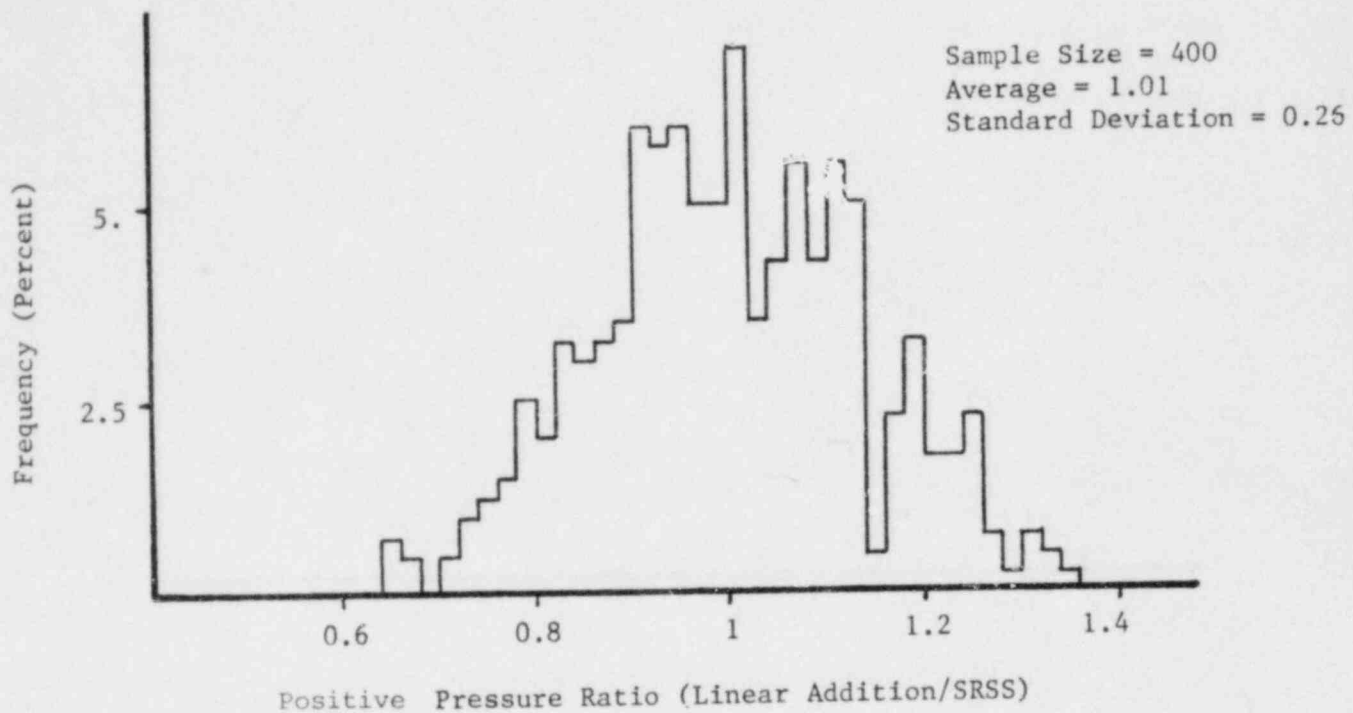
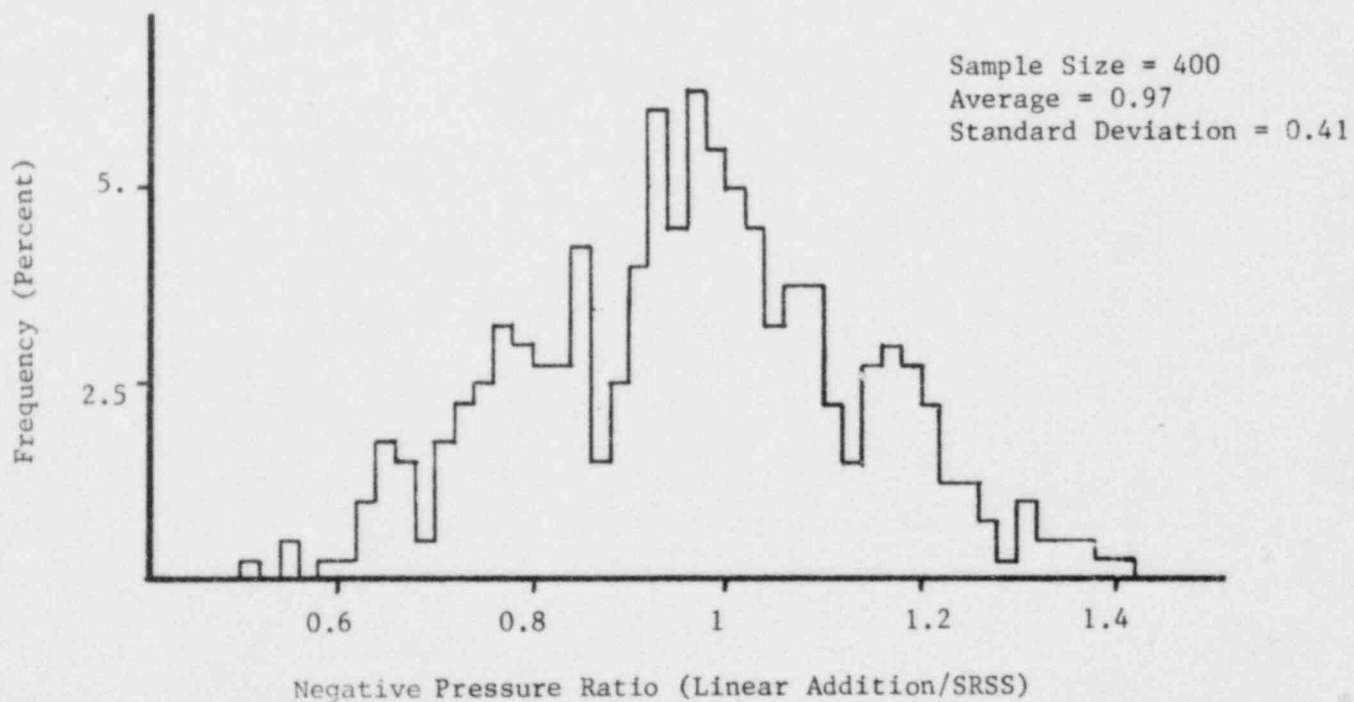


FIGURE A.4  
PROBABILITY DENSITY DISTRIBUTION FOR THE  
REACTOR PRESSURE RISE RATE



(a)



(b)

FIGURE A.5

FREQUENCY DISTRIBUTION OF COMBINED PEAK  
PRESSURE RATIOS - 8 MVA

## APPENDIX B

### DESCRIPTIONS OF MAJOR COMPUTER PROGRAMS

#### B.1 EDSGAP

EDS Nuclear Inc. Program EDSGAP is a general purpose finite element program for linear elastic analyses of arbitrary structural or piping systems. EDSGAP is based on the Program SAP developed by Professor E. L. Wilson at the University of California, Berkeley, and includes improvements and features of his later version SAP IV. In addition to input and output options added by EDS for user convenience, considerable effort has gone into increasing the speed and storage capabilities, debugging the various subroutines, and adding analysis features.

The program contains such element types as general beam, truss, two- and three-dimensional solid, shell and plate, translational/rotational spring, and fluid. These element types may be used both singly and in compatible combinations. The program includes static and dynamic options. Out-of-core storage may be utilized for solution of the equations of equilibrium, storage of problem data, and/or solution results.

Static analyses are performed using the direct stiffness method, in which element stiffness matrices are formed according to virtual work principles and assembled to form a global stiffness matrix for the system relating external forces and moments to joint displacements and rotations. Applied static loads may be specified as combinations of concentrated forces, thermal expansion loads, pressure forces, and inertial (body) forces.

The equations of equilibrium of the system are solved for joint displacements and rotations by Gaussian reduction techniques.



Dynamic options within the program include:

- (1) Frequency calculations only, by either the Rayleigh Ritz Method, or the Generalized Eigenvalue Method.
- (2) Frequency calculations followed by response history analysis using mode superposition.
- (3) Frequency calculations followed by response spectrum analysis.
- (4) Response history analysis by direct integration.

Dynamic loadings may be specified as acceleration spectra or combinations of arbitrary applied force and moment time histories and three independent orthogonal component time histories of acceleration.

The basis for EDSGAP is the program SAP which is an accepted, standard program in the public domain. Nevertheless, EDSGAP has been verified for a comprehensive set of example problems in accordance with EDS Nuclear Inc. quality assurance procedures. Extensive and complete verification, with detailed descriptions of the example problems and comparison results from standard programs or from hand calculations, have been preformed and documented in accordance with established EDS Nuclear Quality Assurance procedures.

## P.2 EDS-SNAP

EDS Nuclear Program EDS-SNAP (Structural Nonlinear Analysis Program) is a general purpose program for nonlinear static and dynamic finite element analysis. It is based on the program ADINA developed at MIT under Professor K. J. Bathe. ADINA was developed from the programs NONSAP and SAP IV developed at the University of California, Berkeley, under Professor E. L. Wilson. Considerable

effort has gone into increasing analysis features and input/output options.

EDS-SNAP was used in EDS' asymmetric LOCA load studies for PWR plants. EDS-SNAP has also been used extensively in EDS' previous evaluations of fluid-structure interaction problems involving BWR containment systems.

#### Elements and Material Types

The structural systems that can be analyzed using EDS-SNAP can be composed of combinations of a number of different finite elements. The program presently contains the following element types:

- (1) three-dimensional truss element
- (2) two-dimensional plane stress and plane strain elements
- (3) three-dimensional plane stress element
- (4) axisymmetric shell or solid elements
- (5) three-dimensional solid or thick shell elements
- (6) three-dimensional thin shell element
- (7) three-dimensional beam element
- (8) two and three-dimensional compressible fluid elements

A pressure-based 3/D added mass element is available which can be used to model incompressible fluid effects in a fluid-structural system.

Nonlinearities due to large displacements, large strains, and nonlinear material behavior can be represented. The material descriptions presently available are:

Truss Element

- (1) linear elastic
- (2) nonlinear elastic
- (3) thermo-elastic
- (4) elastic-plastic (isotropic and kinematic hardening)
- (5) thermo-elastic-plastic and creep

Two and Three-Dimensional Elements

- (1) isotropic linear elastic
- (2) orthotropic linear elastic
- (3) isotropic thermo-elastic
- (4) curve description model; volumetric strain-dependent material properties with tension cracking
- (5) concrete model with cracking and crushing, stress-dependent material properties, and thermal effects
- (6) elastic-plastic (Drucker Prager model, isotropic and kinematic hardening)
- (7) thermo-elastic-plastic-creep

#### Beam Element

- (1) linear elastic
- (2) elastic-plastic, isotropic hardening

#### Shell Element

- (1) linear elastic
- (2) elastic-plastic, isotropic hardening

#### Fluid Elements

- (1) inviscid, constant bulk modulus

Program EDS-SNAP uses an out-of-core solver, i.e., the equilibrium equations are processed in blocks, and very large finite element systems can be considered. Also, all structure matrices are stored in compacted form, i.e., only nonzero elements are processed, resulting in maximum system capacity and solution efficiency.

#### Solution Schemes

EDS-SNAP is capable of static and dynamic, linear and nonlinear analysis of a finite element system response. In dynamic analysis implicit time integration (the Newmark or Wilson methods), explicit time integration (central difference method), mode superposition analysis, or frequency domain analysis can be employed. In nonlinear analysis, an incremental solution of the equilibrium equations are used. Equilibrium iteration on these equations is possible to insure the accuracy and stability of the solution. To allow the user to specify an effective and efficient nonlinear solution scheme, either a modified Newton iteration or a quasi-Newton iteration (BFGS method) may be used and a new stiffness matrix may be formed at user-specified solution steps.

EDS-SNAP is also capable of evaluating the natural frequencies and mode shapes of a structural system through either the determinant search or the subspace iteration method.

### B.3 SUPERPIPE

SUPERPIPE, developed by EDS Nuclear Inc., is a general-purpose piping program which performs comprehensive structural analysis of linear elastic piping systems for dead weight, thermal expansion, seismic time history or response spectra, arbitrary force time history, and other loading conditions. Analyses are performed to ASME requirements for Class 1, 2, and 3 systems.

The program has a number of automatic features for user ease in defining the piping system. These include automatic generation of node coordinates and curved segments or elbows, automatic cartesian/polar coordinate transformation, built-in data libraries for standard material properties, stress indices, and piping schedules. Various plotting capabilities and extensive diagnostic error and warning messages aid in checking the model.

The program has a number of element types which may be used in any combination. These include:

- Straight pipe
- Curved pipe
- Valve
- General Beam
- Flexible coupling
- Arbitrary stiffness matrix

In addition to the basic capabilities for performing dead weight, thermal expansion, seismic response spectrum, and anchor movement analyses, SUPERPIPE offers a number of more sophisticated features for specialized piping analyses. These include:

- (1) Analysis with multiple response spectra for piping supported at different levels within a building and, therefore, subjected to independent loading (different spectra) at each level.
- (2) Modal superposition or direct-integration techniques of time-history analysis for shock loads associated with steam hammer and water hammer effects in piping systems, or other arbitrary force time-history loadings.
- (3) Analysis with multiple acceleration time-history for situations in which a piping system is subjected to independent motions at each support, and in which the effect of phase relationships between these motions is important.

Static or dynamic equilibrium equations are formulated using the direct stiffness method, in which the element stiffness matrices are formed according to virtual work principles and assembled to form a global stiffness matrix for the system, relating external forces and moments to joint displacements and rotations. Six degrees of freedom may be specified at each joint of the global system for both static and dynamic analyses.

Static equilibrium equations are solved using Gaussian reduction techniques on the compacted stiffness matrix. For dynamic problems, the equilibrium equations may be solved using either step-by-step direct integrations of the coupled equations of motion, or by first calculating natural frequencies and mode shapes and transforming the system into a set of uncoupled equations of motion. The eigensolution is performed using the subspace iteration method or, optionally, the Householder-QR method.

For ease in reviewing results, the output of SUPERPIPE is arranged in stress report format with special summaries for Code compliance, support loads, break location evaluation, maximum stresses, welded attachment point stresses, flexible connection deformation, displacements, etc.



The program has been thoroughly tested and verified for a comprehensive set of sample problems, including extensive comparisons with several publicly available programs. The program has further been benchmarked against the ASME as well as the NRC benchmark problems. All verification analyses have been documented in accordance with established EDS Nuclear Quality Assurance procedures.

## APPENDIX C

### MODELING OF FLUID STRUCTURE INTERACTION EFFECTS USING EDS-SNAP

#### C.1 INTRODUCTION

In predicting the response of structures which either contain a large volume of fluid or are submerged in fluid, it is often necessary to consider the effects of fluid structure interaction (FSI) on these structures. One very good indication of the significance of FSI effects is the influence of the fluid on the natural frequencies of the structure. It is known that the presence of fluid alters the natural frequencies of a "dry" structure. The accuracy with which the natural frequencies are predicted depends very much on the accuracy of the method by which the fluid effects are included in the finite element model of the structure.

A number of alternative modeling techniques, of varying degrees of accuracy are available for the modeling of fluid effects. The most simple approach that has been used consists of lumping a portion of the fluid mass into the structural mass matrix. The magnitude of mass to be lumped at a particular structural node is based on the tributary area around that node. Accordingly, this method had been referred to as the tributary mass matrix (TMM) approach. This method, though simple to implement, is not accurate because it does not account for the coupling between the structural response of adjacent points in the structure, both in the circumferential and longitudinal directions. This method generally predicts frequencies which are lower than the actual frequencies of the structure.

A second approach to the fluid modeling problem consists of modeling the fluid region with a finite element mesh. The fluid elements allow consideration of fluid compressibility and generally

assume inviscid behavior. Although this approach is appropriate for many applications, the introduction of a fluid finite element mesh results in a dynamic model of very large size, for which the computational costs can become impractical. Although techniques exist for reducing the dynamic degrees of freedom before extracting the model frequencies, the amount of engineering judgment involved in these techniques can make it difficult to determine the accuracy of the results.

Recognizing the approximate nature of the TMM approach and the high computer cost associated with a compressible fluid finite element approach, an alternative method had been developed which provides good accuracy at a relatively low cost in applications where the fluid can be considered to be incompressible. This method, termed the added mass approach, had been incorporated into the program EDS-SNAP. Some of the important features of this method are described below.

## C.2 THEORETICAL CONSIDERATIONS

The basic approach used in the added mass formulation is to treat the fluid as a pressure boundary condition acting on the structure. This then eliminates the need to solve the complete fluid flow history, since the fluid region is represented by the fluid-structure boundary in the final set of finite element equations. The pressure boundary condition is a force required to accelerate the fluid to allow the structure to displace. Since this force is proportional to the structural acceleration, it is considered an "added mass" on the structure and can be completely accounted for in the structural mass matrix.

The added mass formulation models the fluid as inviscid and incompressible. The effect of the fluid on the structure is initially considered as an additional forcing term in the structural finite element equations:

$$\underline{M} \ddot{\underline{U}} + \underline{C} \dot{\underline{U}} + \underline{K} \underline{U} = \underline{R} + \underline{R}_p \quad (1)$$

when  $\underline{M}$ ,  $\underline{C}$ , and  $\underline{K}$  are the structure mass, damping, and stiffness matrices respectively;  $\underline{U}$ ,  $\dot{\underline{U}}$ , and  $\ddot{\underline{U}}$  are the vectors of structural displacement, velocity, and acceleration respectively;  $\underline{R}$  is the time-dependent external load vector; and  $\underline{R}_p$  is the load on the structure induced by the fluid. The FSI-induced load is related to the fluid pressure  $p$  by a direction matrix  $\underline{B}$ :

$$\underline{R}_p = \underline{B}^t p \quad (2)$$

The added mass formulation involves the development of a relationship between the fluid pressures and the acceleration of the structure boundary. The fluid region is discretized into nodal points and elements where each nodal point has one variable specified: fluid pressure. Free surface ( $p = 0$ ) boundary conditions are specified and the pressures along the fluid structure interface are related to the structural boundary accelerations,  $\ddot{\underline{U}}$ , by:

$$p = - \rho_F \underline{B} \ddot{\underline{U}} \quad (3)$$

where  $\rho_F$  is the fluid density, and  $\underline{B}$  is the same direction matrix used in Equation 2. By coupling the fluid equation for pressure with the structural equation through the boundary accelerations, the FSI load  $\underline{R}_p$  can be expressed in terms of the structural accelerations. Therefore, this term can be summed with the structural mass matrix on the left-hand side of Equation 1 to give:

$$(\underline{M} + \underline{m}) \ddot{\underline{U}} + \underline{C} \dot{\underline{U}} + \underline{K} \underline{U} = \underline{R} \quad (4)$$

where  $\underline{m}$  is now the added mass matrix. Equation 4 is then solved using conventional finite element equation solvers, with the combined fluid-structural mass matrix in the solution.

This added mass procedure is an attractive solution approach because once the fluid added mass,  $\underline{m}$ , is derived and added to the structure mass, the remainder of the solution does not entail significant additional computational cost for solving the structure

alone, i.e., without fluid. Yet the results are comparable to the more expensive explicit fluid-structure solution using fluid finite elements. The added mass approach does require that the fluid behavior be incompressible over the frequency range of interest.

In addition to the accuracy of the method, it was also determined that the finite element discretization required for accurate results with the incompressible fluid element is much coarser than would be needed with conventional fluid finite elements. This gives the method the added advantage of being computationally efficient.

### C.3 IMPLEMENTATION

A self-contained computer module CONMASS was coded to calculate the added mass as developed above. The input to this module is the appropriately discretized specific geometry for the fluid region of interest. The module generates the added mass matrix,  $\underline{m}$ , whose elements are added to the masses at the wetted structural degrees of freedom. The matrix exhibits mass coupling between adjacent nodes and is therefore a non-diagonal mass matrix.

The module CONMASS was linked to an appropriate structural computer code. The major step in this linkage is to appropriately add the added mass,  $\underline{m}$ , to the structure mass matrix,  $\underline{M}$ .

The structural code used for this purpose is the finite element program EDS-SNAP. Program EDS-SNAP is based upon the ADINA program, which was developed at the Massachusetts Institute of Technology for general finite element linear and nonlinear analysis.

The EDS-SNAP code is a very well-structured general purpose finite element code which easily allowed incorporation of the CONMASS module. The EDS-SNAP code contains truss, beam, continuum, and structural finite elements, and also has a non-diagonal mass matrix capability which is required for the added mass approach.

## APPENDIX D

### COMBINATION OF DYNAMIC STRUCTURAL RESPONSES

#### D.1 INTRODUCTION

The structural evaluation of the Mark I containment system for Cooper Nuclear Station (CNS) involved the determination of dynamic structural responses of the Mark I torus, torus support system, vent system, S/RV discharge lines, torus attached piping, and torus internal structures to LOCA and S/RV discharge loads. These dynamic responses had then to be combined in accordance with feasible event combinations, as enumerated in the Mark I Containment Program Structural Acceptance Criteria. The procedure for combining any two dynamic responses in the CNS evaluations is described in this appendix, and the basis for the procedure is presented and justified.

The combined response from the two dynamic events mentioned above was obtained for CNS by taking the Square Root of the Sum of Squares (SRSS) of the peak responses from the individual events, and then scaling this result upward by an additional 10%. This procedure, which will be referred to as a 1.1 SRSS combination, is based on the randomness in the time interval between the initiation of a postulated LOCA and the initiation of a S/RV discharge. It follows that the maximum responses resulting from the two events will combine in a random manner. For this type of combination, an SRSS method is typically used instead of the unnecessarily conservative absolute sum (ASUM) combination of the peak responses. Based on a statistical analysis of structural response data applicable to CNS, the 1.1 SRSS combination was determined to have a higher confidence level than the generally accepted confidence level typically applied to justify an SRSS combination. Therefore, the 1.1 SRSS combination, which is more conservative than the standard SRSS combination, was used.



A procedure that is used for justifying an SRSS combination of dynamic responses is to take a number of pairs of dynamic responses and compute cumulative distribution functions (CDFs) for the random combination of each pair. From these CDFs, the probability of non-exceedance (PNE) of the value of response obtained by an SRSS combination can be determined. The SRSS combination is considered of acceptable conservatism if the statistical evaluation of the data indicates that the SRSS value has a PNE of 0.84 or greater. This approach was the basis for justification of the SRSS combination of pairs of dynamic structural responses in the Mark II containment evaluations. The statistical data for this justification is reported in GE Report NEDE-24010-P (Reference 55).

This appendix provides the results of a statistical study using the same technical approach as in the Mark II study, but with Mark I data applicable to CNS. Using comparable criteria, it is shown that a 1.1 SRSS combination is appropriate in this case.

The 1.1 SRSS combination approach was chosen because it is a convenient indirect means of attaining a PNE of 0.84, whereas the direct computation of CDFs on a case-by-case basis to justify the combination would have been computationally formidable. The basis for the 1.1 SRSS method is still, however, the CDF combination method allowed by the Mark I Structural Acceptance Criteria.

The following sections of this appendix discuss the types of dynamic loads for which the 1.1 SRSS combination was applied, and describes the computational procedure for obtaining CDFs. The data that was analyzed is then reviewed, and the statistical results are presented to justify the combination procedure.

## D.2 DYNAMIC LOADS

The dynamic loads that were relevant for consideration in the combination procedure fall into the categories of LOCA and S/RV discharge loads.

The LOCA loads which occur consist of the pool swell (PS), condensation oscillation (CO), and chugging (CH) loads. The S/RV discharge loads may either be due to a single-valve actuation (SVA), multiple valve actuations (MVA), or by activation of the six CNS S/RVs forming the Automatic Depressurization System (6ADS).

### D.3 COMPUTATION OF CDF

The CDF for the combination of any two time histories of response is the relationship between the random variable representing the value of combined response and its probability of non-exceedance (PNE). For each pair of time histories, the positive CDF is generated by selecting the maximum positive value for the combined response, and the negative CDF is generated in an identical manner by selecting the maximum negative value.

The CDF for a pair of time histories of response  $R_1$  of duration  $T_1$  and  $R_2$  of duration  $T_2$  (for an example, see the top right of Figure D.1) is computed according to the following procedure:

- (1) The two time histories are positioned end-to-end, so that the end-time of  $R_1$  coincides with the start-time of  $R_2$  (as shown in the top left diagram of Figure D.1).
- (2) The time  $T_1$  is divided into a desired number of time-steps  $n_1$ . Using the same time interval, the time  $T_2$  is divided into  $n_2$  steps.
- (3) Keeping  $R_2$  fixed in time,  $R_1$  is stepped successively forward relative to  $R_2$ , one time-step at a time, until  $R_1$  has completely "passed through"  $R_2$  and the start-time of  $R_1$  coincides with the end-time of  $R_2$ . To reach this point,  $R_1$  will have been shifted forward through  $n_1+n_2-1$  steps. This process is illustrated in the sequence of diagrams on the left in Figure D.1.

- (4) For each position of  $R_1$ , the maximum positive and negative algebraic sum of the two responses is determined and stored in ascending order.
- (5) The CDF is a plot of each of the maximum values computed versus the ratio of the number of maximum values less than it, to the total number ( $n_1+n_2-1$ ) of maximum values. This ratio is the NEP of the particular maximum value being considered. Schematic CDF curves are shown at the bottom right of Figure D.1.

As illustrated in Figure D.1, the Absolute Sum, and the NEPs associated with the SRSS and the 1.1 SRSS values of the combined response (or for that matter any other value of the combined response) can be readily read-off.

#### D.4 DATA BASES AND RESULTS

The data set that was utilized to develop results applicable to CNS was a set of 39 CDFs for Mark I torus responses and a set of 72 CDFs for torus attached piping systems. These were developed for a generic Mark I study, the results of which are reported in GE Report NEDE-24632 (Reference 56). Figure D.2 shows an example of a time history pair and the corresponding CDF.

The statistical characteristics of the Mark I data, in the form of NEP for SRSS combinations, are presented in Table D.1. This data is compared with the results for the 582 CDFs reported in Reference 55 for various components for Mark II plants. Comparison of these results indicates that there is remarkable consistency between the Mark I data and the considerably larger sample used for the Mark II SRSS combination justification.

Using the complete set of Mark I data from Reference 56, the 1.1 SRSS combination demonstrated a 0.84 NEP with a confidence level significantly in excess of 90%. Comparing this result with those presented in Table D.1, where for an SRSS combination the 0.84 NEP

is attained with approximately 55% confidence level for both the Mark I and Mark II data, the enhanced conservatism of using the 1.1 SRSS combination is clearly demonstrated.

Additionally, a limited number of time-history response data that were available from the Cooper Station analyses for applicable pairs of dynamic load combinations, were examined. Computation of CDFs for these time history pairs showed that using the 1.1 SRSS combination the 0.84 NEP was not attained for the PS + SVA loading combination at torus support columns, but that for the rest of the applicable data the confidence level of 0.84 NEP is comparable to that of the larger Mark I data base. The PS + SVA case represents a combination of two loads of significantly differing predominant periods and therefore in this case it was felt that the CDF based SRSS combination approach is inappropriate. Therefore, for the CNS torus support column stress qualification an absolute sum combination was used for the dynamic response from PS and SVA load cases. For other dynamic load combinations on torus supports and for all other structural components such as the torus shell, vent system, S/RV discharge lines, torus attached piping, and torus internal structures, a 1.1 SRSS combination was used.

#### D.5 CONCLUSION

A statistical review of Mark I and CNS dynamic response was performed on the basis of CDF data for combined response. Based on this review, it has been shown that the use of a 1.1 SRSS combination satisfies the criterion of 0.84 NEP with more than a 90% confidence level. It is, therefore, a conservative combination rule for CNS dynamic response.

Table D.1

NON-EXCEEDANCE PROBABILITIES

	<u>Mark I</u>		<u>Mark II</u>
	<u>Torus SRSS</u>	<u>Piping SRSS</u>	<u>SRSS</u>
Mean	0.85	0.87	0.86
Standard Deviation	0.09	0.06	0.12
90% Confidence	0.69	0.78	0.67
98.4% Confidence	0.58	0.72	0.50

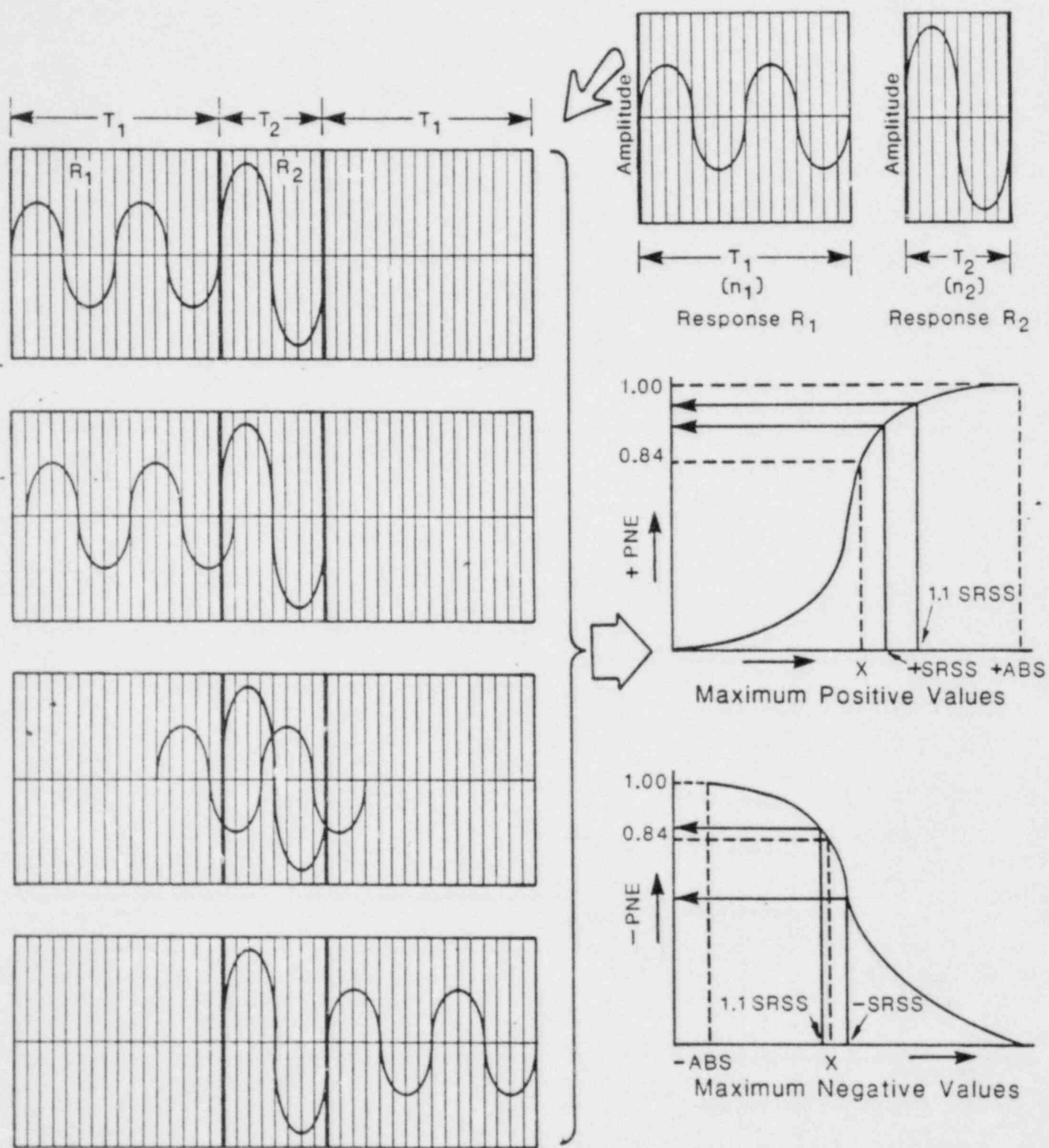
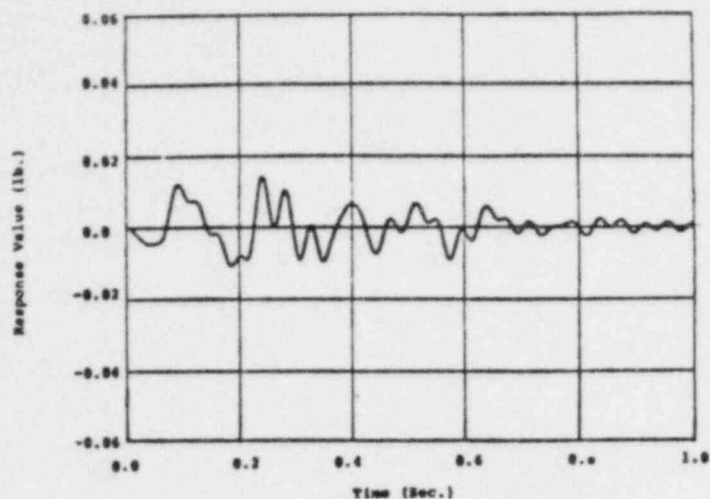


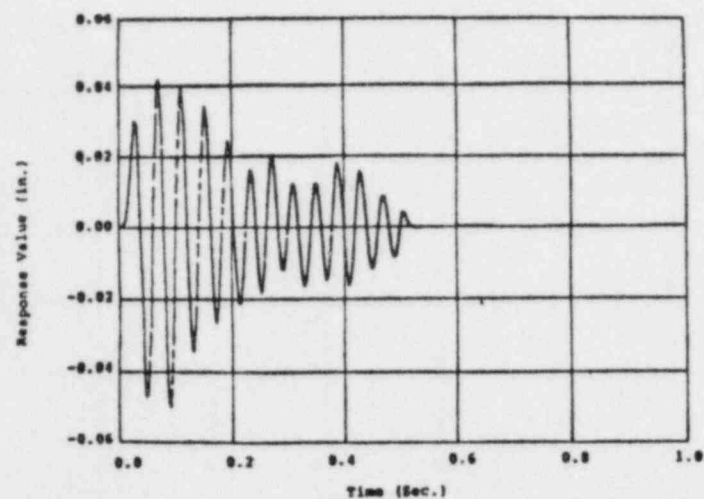
FIGURE D.1

ILLUSTRATION OF CDF COMPUTATION

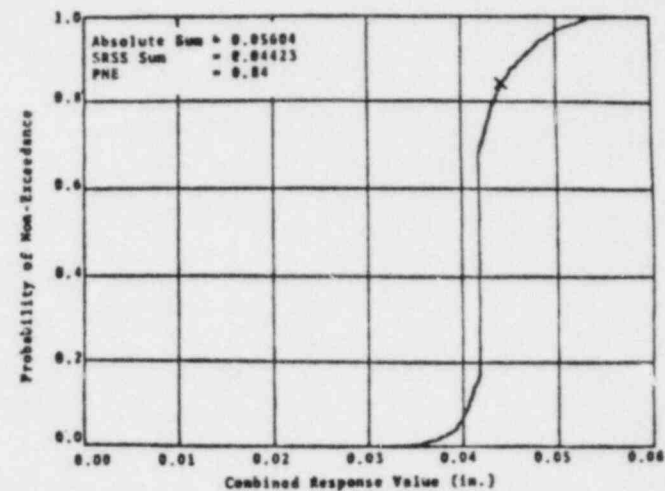




RESPONSE 1 FOR CDF 2  
HIGH PRESSURE CORE INJECTION LINE Y DISPLACEMENT AT NODE 5A  
DUE TO S/RV



RESPONSE 2 FOR CDF 2  
HIGH PRESSURE CORE INJECTION LINE Y DISPLACEMENT  
DUE TO CHUGGING



CUMULATIVE DISTRIBUTION FUNCTION 2  
HIGH PRESSURE CORE INJECTION LINE Y DISPLACEMENT  
DUE TO S/RV + CHUGGING

FIGURE D.2  
TYPICAL CDF FOR MARK I DATA

## REFERENCES

1. U.S. Nuclear Regulatory Commission Letter (D.L. Ziemann) to NPPD (J.M. Pilant), February 14, 1975.
2. U.S. Nuclear Regulatory Commission Letter (D.L. Ziemann) to NPPD (J.M. Pilant), April 19, 1975.
3. "Mark I Containment Evaluation, Short Term Program Final Report, Volume I-V", NEDC-20989, General Electric Company, September, 1975.
4. "Mark I Containment Evaluation, Short Term Program Final Report, Addendum 1", NEDC-20989, General Electric Company, November, 1975.
5. General Electric Company Letter (L.J. Sobon) to the NRC (V. Stello), "Mark I Short Term Program Report Questions", September 9, 1976.
6. "Description of Short Term Program Plant Unique Torus Support Systems and Attached Piping Analyses", NUTECH Report MK I-02-012, including Rev. 1, May 1976, and Rev. 2, June 1976.
7. "Mark I Containment Evaluation, Short Term Program Final Report, Addendum 2", NEDC-20989, General Electric Company, June 1976.
8. "Mark I Containment Evaluation, Short Term Program Final Report, Addendum 3", NEDC-20989, General Electric Company, August 1976.
9. "Mark I Containment Evaluation, Short Term Program Plant Unique Analysis, Torus Support System and Attached Piping", Nebraska Public Power District, August 1976.
10. "Mark I Containment Short Term Program, Safety Evaluation Report", NUREG-0408, U.S. Nuclear Regulatory Commission, December 1977.
11. "Safety Evaluation Report -- Mark I Containment Long-Term Program (Resolution of Generic Technical Activity A-7)," NUREG-0661, U.S. Nuclear Regulatory Commission, July 1980.
12. ASME Boiler and Pressure Vessel Code, Section III, Division 1, Nuclear Power Plant Components (edition as noted in text).
13. "Power Piping", USAS B31.1.0, 1967.
14. "Nuclear Power Piping", USAS B31.7, 1968.

15. Manual of Steel Construction, American Institute of Steel Construction, Chicago (edition as noted in text).
16. "Final Safety Analysis Report, Cooper Nuclear Station, Amendment #77, March 4, 1982.
17. "Mark I Containment Program Load Definition Report", NEDO-21888, General Electric Company, Rev. 2, November 1981.
18. U.S. Nuclear Regulatory Commission, "NRC Acceptance Criteria for the Mark I Containment Long Term Program", Revision 1, February 1980.
19. Mark I Containment Program Structural Acceptance Criteria Plant Unique Analysis Applications Guide", NEDO-24583-1, Rev. 1, October 1979.
20. Nebraska Public Power District Letter (J. Pilant) to U.S. NRC (T. Ippolito), "Summary of Technical Decisions, Mark I Containment Modification and Analysis Approach, Cooper Nuclear Station", dated October 26, 1981.
21. "Evaluation of Mark I S/RV Load Cases C3.1, C3.2, and C3.3 for the Cooper Nuclear Station," NEDC-24359, General Electric Company, August 1981.
22. "Mark I Containment Program, Plant Unique Load Definition, Cooper Nuclear Station", NEDO-24573, General Electric Company, Rev. 1, June 1981.
23. "Mark I Containment Program - Analysis of Full Scale Test Facility for Condensation Oscillation Loading", NEDE-24645-P, General Electric Company, prepared by Bechtel Corp., July 1979.
24. "Mark I Containment Program - Full Scale Test Program - Evaluation of Supplemental Tests - Task 8.4", NEDE-24539-P, Supplement No. 1, General Electric Company, prepared by Continuum Dynamics Inc., July 1981.
25. "Mark I Containment Program - Analysis of FSTF Vent System for Condensation Oscillation Loads, Downcomer Frequencies, and Damping - Task 9.5.1", NEDE-24838, General Electric Company, prepared by Bechtel Corp., August 1981.
26. "Mark I FSI-Induced Submerged Structure Loads for the Cooper Plant", Technical Notes No. 81-9, prepared by Continuum Dynamics Inc., Princeton, New Jersey, May 1981.
27. "Mark I Containment Long Term Program - Development of Downcomer Lateral Loads from Full Scale Test Facility Data - Task Number 7.3.2", NEDE-24537-P, General Electric Company, prepared by EDS Nuclear Inc., May 1979.

28. Wheeler, A. J., "Mark I Containment Program Analytical Model for Computing Transient Pressures and Forces in the Safety-Relief Valve Discharge Line", NEDE-23749-P, General Electric Company, Feb. 1978.
29. "Mark I Containment Program, Buckling Evaluation of a Mark I Torus," WE8109.31, General Electric Company, prepared by Bechtel Corporation, EDS Nuclear Inc., and Anamet Laboratories, Inc., January 1982.
30. Rush, R.H., and Jackson, J.E., "Treatment of Hydrodynamic Effects for Toroidal Containment Vessels," Tennessee Valley Authority, Knoxville, Tennessee, December 1978.
31. Bathe, K.J., and Wilson, E.L., Numerical Methods in Finite Element Analysis, Prentice-Hall Inc., New Jersey, 1976.
32. Kennedy, R.P., Short, S.A., and Tong, W.H., "Harmonic Phasing for Mark I Torus Shell Condensation Oscillation Loads," SMA 12101.02.R001, Structural Mechanics Associates, Newport Beach, California, July 1980.
33. Wichman, K.R., Hopper, A.G., and Mershon, J.L., "Local Stresses in Spherical and Cylindrical Shells Due to External Loadings", WRC Bulletin No. 107, March 1979.
34. Timoshenko, S., and Krieger, S.W., Theory of Plates and Shells, 2nd Edition, McGraw-Hill, 1959.
35. "Standards of the Expansion Joint Manufacturers Association", Section C, Issue 1, Expansion Joint Manufacturers Association, Inc.
36. Rodabaugh, E.C., "Review of Data Relevant to the Design of Tubular Joints for Use in Fixed Offshore Platforms", WRC Bulletin No. 256, 1978.
37. U. S. Nuclear Regulatory Commission, Regulatory Guide 1.61, "Damping Values for Seismic Design of Nuclear Power Plants", October 1973.
38. U. S. Nuclear Regulatory Commission, Regulatory Guide 1.92, "Combining Modal Responses and Spatial Components in Seismic Response Analysis", Rev. 1, February 1976.
39. "Analysis and Design of Drywell Steel Framing", Kaiser Engineers, Inc., Calculation No. 80154-027-01, Revision 0, January 8, 1982.
40. General Electric Company Letter to Mark I Utilities, "Mark I Containment Program - Conference Report - Resolution of NRC Concerns on Containment Piping Fatigue Evaluation - September 24, 1981", October 8, 1981.

41. Dong, R.G., "Effective Mass and Damping of Submerged Structures", Report No. UCRL-52342, Lawrence Livermore Laboratory, April 1978.
42. General Electric Company Letter (B.W. Smith) to Mark I Utilities, "Mark I Containment Program - Task 6.2.1 - Monticello T-quencher Stress Report", July 20, 1978.
43. Kennedy, R.P., and Kincaid, R.H., "CMDOF - A Computer Program to Couple the Response of Structures and Supported Equipment for Multiple Degrees of Coupling Using the Results from Uncoupled Structure and Equipment Analysis", SMA 12101.03.R001, Structural Mechanics Associates, Newport Beach, California, November 1980.
44. IEEE Recommended Practices for Seismic Qualification of Class 1E Equipment for Nuclear Power Generating Stations, ANSI/IEEE 344-1975, The Institute of Electrical & Electronics Engineers, Inc., 1975.
45. U. S. Nuclear Regulatory Commission Standard Review Plan, Section 3.7.2, Seismic System Analysis, July 1981.
46. American National Standard for Steel Valves, ANSI B16.34-1977, The American Society of Mechanical Engineers, 1977.
47. "Code Requirements for Nuclear-Related Concrete Structures", American Concrete Institute Standard 349-76.
48. Biggs, J.M., Introduction to Structural Dynamics, McGraw-Hill, 1964.
49. Letter from NRC to Mark I Utilities, Docket No. 50-220, December 12, 1977.
50. "Cooper Nuclear Station, Suppression Pool Temperature Response", NEDC-24360-P, General Electric Company, August 1981.
51. General Electric Company Letter (R.H. Lube) to NPPD (T.E. Hoeman), "Transmittal of Final Report for Suppression Pool Temperature Response, Cooper Nuclear Station", March 15, 1982.
52. "Mark II BWR 4/5 Methodology for Containment Forcing Functions from Multiple Safety Relief Valve Actuations", WEDO-25060, General Electric Company, Sept. 1979.
53. "Mark I Containment Pressure and Temperature Response to Small Break Accident (SBA)", EDS Report No. AAD-78-013, Rev. 0, EDS Nuclear, San Francisco, November 1978.



54. General Electric Company Letter (B.P. Brooks to R.S. Vij), "Safety Relief Valve Data for Relief Valve Loads Task Force Information Needs", June 5, 1979.
55. "Technical Bases for the Use of the Square Root of the Sum of the Squares (SRSS) Method for Combining Dynamic Loads for Mark II Plants", NEDE-24010-P, General Electric Company, July 1977.
56. "Mark I Containment Program, Cumulative Distribution Functions for Typical Dynamic Responses of a Mark I Torus and Attached Piping Systems", NEDE-24632, General Electric Company, December 1980.